THE JOURNAL
OF
CHEMICAL PHYSICS

VOLUME 19, NUMBER 1 JANUARY, 1951

The Vibrational Spectra of Diborane and Some of its Isotopic Derivatives*

R. C. LORD AND E. NIELSEN†
Spectroscopy Laboratory and Department of Chemistry, Massachusetts Institute of Technology, Cambridge 39, Massachusetts
(Received October 16, 1950)

The infrared spectra of ordinary diborane, of $B_2^{10}H_6$, and of $B_2^{10}D_6$ have been determined in the vapor state over the spectral range 250–3800 cm^{-1}. The Raman spectra of ordinary diborane and $B_2^{10}D_6$ have been measured in the liquid at −130°C. Qualitative depolarization measurements have been made on nearly all observed Raman lines. The vibrational spectra have been interpreted with the help of the various selection rules and the product rule for isotope shifts. The fundamental frequencies obtained from this interpretation differ considerably from those previously published, but are in agreement with a large amount of spectroscopic data, including much not hitherto available. It is concluded that the nonplanar bridge model (D_{2h} symmetry) fits the spectroscopic data best, although the unsymmetrical C_{2h} form cannot be definitely excluded. The theoretical and observed vapor heat capacities agree satisfactorily over the temperature range 100–300°K.

IT was first shown by Price[1] that the contours of the infrared absorption bands of diborane lend strong support to the bridged structure of this molecule. A considerable amount of recent spectroscopic work[2–4] has confirmed Price's study, and, by extension of the investigation to both infrared and Raman spectra of the deuterium derivative, has enabled a tentative interpretation of the spectra. The present investigation was undertaken prior to the publication of references 2 and 3, with the same general objectives. However, it seemed to us worthwhile to free the infrared spectra of the complications associated with the presence of three species of molecules arising from the naturally occurring B^{10} and B^{11} isotopes. Inasmuch as B^{10} is available in a form from which diborane can be readily synthesized, the additional effort needed to make essentially pure B^{10} modifications of B_2H_6 and B_2D_6 is small and is amply repaid by the simplification of the spectra. Our spectroscopic results and interpretation differ somewhat from those of previous workers primarily because of the study of the B^{10} modifications. In addition, our infrared work has some new features, and the Raman spectra include extensive, although only qualitative, polarization studies, hitherto unreported, on the deuterium derivative.

EXPERIMENTAL DETAILS

Preparation and Purification of Materials

Diborane containing the natural mixture of boron isotopes (hereafter called "ordinary diborane"), $B_2^{10}H_6$, and $B_2^{10}D_6$ have been prepared and purified in quantities sufficient for Raman work (up to 15 ml of liquid) by a modification of the procedure of Finholt, Bond, and Schlesinger.[5] Working with millimole quantities, they showed that the reaction between boron trichloride and lithium aluminum hydride in an ether solution gave diborane in very high yields.

Preliminary preparations were tried first by the modification suggested by them that the trichloride etherate be prepared first and then added to the ether

* The work here reported has been aided greatly by support from the ONR under Project NR-019-103 of Contract N5ori-07810. The isotopes boron-10 and deuterium were supplied on allocation from the Isotopes Branch of the AEC, to whom we are grateful for cooperation.

† This paper is based on material contained in a thesis submitted by E. Nielsen to the Graduate School of the Massachusetts Institute of Technology in partial fulfillment of the requirements for the degree of Doctor of Philosophy, January, 1950. Detailed accounts of the preparative procedures for the diboranes are given in the thesis.

[1] W. C. Price, J. Chem. Phys. **16**, 894 (1948).

[2] Webb, Neu, and Pitzer, J. Chem. Phys. **17**, 1007 (1949).

[3] W. E. Anderson and E. F. Barker, J. Chem. Phys. **18**, 698 (1950).

[4] B. Rice, ONR Contractor's Progress Report XXXIV-13, Contract N6ori-020, Task Order X, University of Chicago. We are much indebted to Dr. Rice for sending us this preliminary report of his work, from which the values listed in column 1 of Table IV were obtained.

[5] Finholt, Bond, and Schlesinger, J. Am. Chem. Soc. **69**, 1199 (1947).

TABLE I. Infrared bands of B_2H_6 and $B_2{}^{10}H_6$ (cm^{-1}).

B_2H_6 Stitt (reference 6)	B_2H_6 Price (reference 1)	B_2H_6 This research	$B_2{}^{10}H_6$ This research	D_{2h} assignment
393, 412 s, 431	*ca* 430 m	368 s	368 s	ν_{10}
673, 685 w				
	811 vw	812 vvw	787 vvw	$\nu_{17}-\nu_4$
831 w	831 vw, 849 vw	829 vw	829 vw	ν_5
981 s	974 s	973 s (type C)	977 s (type C)	ν_{14}
1154, 1178 vs, 1197	1175 vs	1177 vs (type A)	1181 vs (type A)	ν_{18}
1274, 1311 m	1267, 1302 fw	1287 w (type A)?	1298 w (type A)?	$\nu_{10}+\nu_{12}$
1377 m	1377 fw	1374 w (type C)	1374 w (type C)	$\nu_{10}+\nu_{15}$
1405 m	*ca* 1405 vw			
1587, 1608 vs, 1626	1604 vs	1602 vvs (type A)	1606 vvs (type A)	ν_{17}
1722 w				
1852, 1874 s	1850, 1870 s	1860 ms (type B)	1869 ms (type B)	$\nu_5+\nu_7$
		1882 m (type C)	1887 m (type C)	ν_{13}
1993 m	1984 w	1992 w (type C)	1999 w (type C)	$\nu_9+\nu_{15}$
	2088			
2134 vw	2124, 2143, 2200 vw	2142 vvw	2151 vvw	$\nu_3+\nu_{14}$
2217 vw	2215, 2230 vw	2228 vvw	2242 vvw	
2353 s	2345 m	2347 m (type A)	2359 m (type A)	$\nu_3+\nu_{18}$
		2394 vw	2412 w (type A)	$\nu_4+\nu_{17}$
2558 s	2522 s	2525 vs (type A)	2528 vs (type A)	ν_{16}
2625 s	2614 s	2612 vs (type B)	2625 vs (type B)	ν_8
		2787 vw (type A)?	2795 vw (type A)?	$\nu_3+\nu_{17}$?
		2869 vw?	2876 vw (type B)?	
3135 vw	3135 vw			
3670 s	3600–3700 s	3638, 3650, 3668, 3705 s	3641, 3662, 3673, 3712 s	$\nu_3+\nu_{16}$, $\nu_2+\nu_{17}$, etc.

w = weak; m = medium; s = strong; v = very; f = fairly. Bands marked "vvw" are barely detectable at 600-mm pressure. Question marks (?) note what might be impurities.

TABLE II. Infrared bands of B_2D_6 and $B_2{}^{10}D_6$ (cm^{-1}).

B_2D_6 Webb, Neu, and Pitzer (reference 2)	$B_2{}^{10}D_6$ This research	D_{2h} assignment
	262	ν_{10}
	592 vvw	ν_5
707 m		
722 s	728 s (type C)	ν_{14}
794 m		
876 s	881 vs (type A)	ν_{18}
914 m		
	981, 989, 997 w	$\nu_{10}+\nu_{12}$, $\nu_{10}+\nu_{15}$
1075 w		
1203 vvs	1205 vvs (type A)	ν_{17}
	1283 vvw	?
	1322 m (type A)	$\nu_5+\nu_{15}$
	1406 w (type C)	$\nu_9+\nu_{15}$
1461 s	1459 ms (type B)	$\nu_5+\nu_7$
	1491 m (type C)	ν_{13}
1705 m		
	1799 s (type A)	$\nu_3+\nu_{18}$
1850 s	1857 vs (type A)	ν_{16}
1994 s	1999 vs (type B)	ν_8
	2134 w (type A)	$\nu_3+\nu_{17}$
	2219 w (type B)	$\nu_2+\nu_9$
2506 w		
2596 w		
	2704 m (type A)	$\nu_2+\nu_{17}$
	2759 vw (type A)	$\nu_3+\nu_{16}$
2768 s		
2902 m		
3132 m		
3372 m		

solution of lithium aluminum hydride, and were tried then with commercial boron trifluoride etherate in place of the boron trichloride. The $B_2{}^{10}H_6$ and $B_2{}^{10}D_6$ were prepared by making $B^{10}F_3$ from calcium fluoborate ($CaF_2 \cdot B^{10}F_3$), forming the boron trifluoride etherate and then causing the etherate to react with an ether solution of lithium aluminum hydride and lithium aluminum deuteride, respectively. The purity of the diborane product was checked after preparation and during purification by means of its infrared spectrum. In addition to a little ether, which is easily removed by passage through a trap held at −130 to −150°, there were other impurities. These were identified from their infrared absorption bands as silane and silicon tetrafluoride. The silane was removed by trap-to-trap distillation and the silicon tetrafluoride by bubbling the

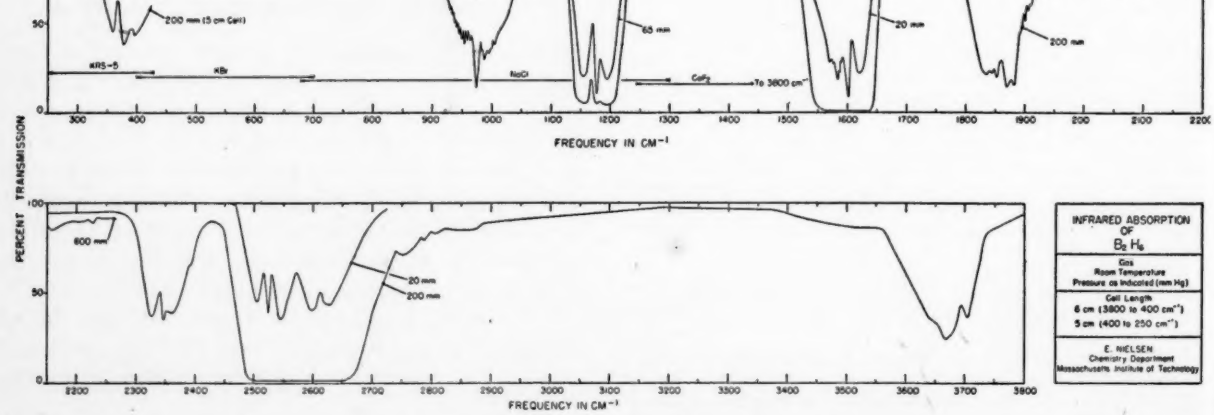

FIG. 1. Infrared absorption spectrum of ordinary diborane.

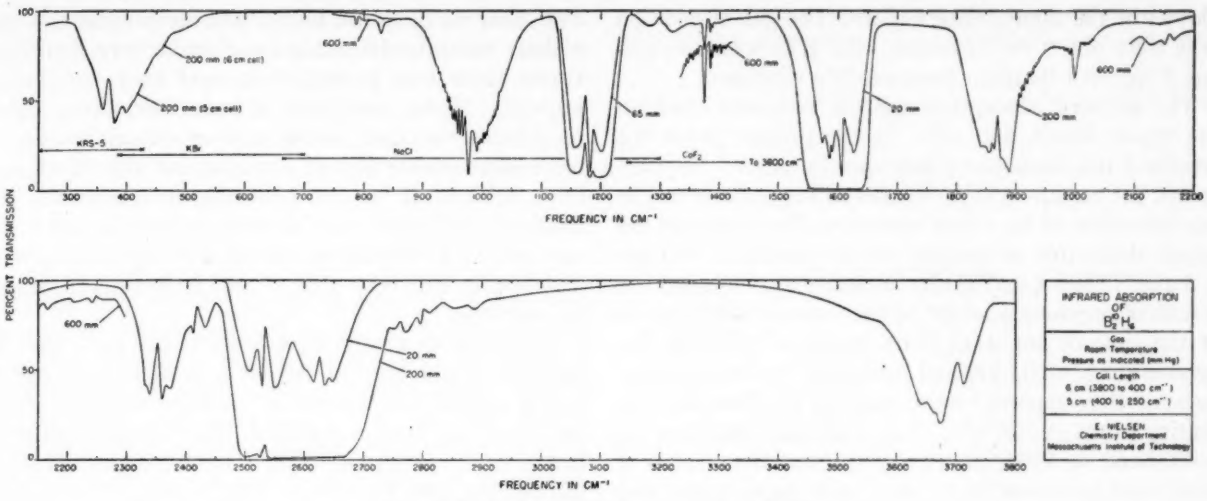

FIG. 2. Infrared absorption spectrum of $B_2{}^{10}H_6$.

diborane through an ether solution of lithium aluminum hydride or deuteride, first at dry-ice temperature and then at room temperature.

Except that the $B^{10}F_3$-etherate was formed first, the preparation of $B_2{}^{10}H_6$ and $B_2{}^{10}D_6$ was the same as that used for ordinary diborane. The $B_2{}^{10}D_6$ obtained from lithium aluminum deuteride and $B^{10}F_3$-etherate is of much higher isotopic purity with respect to deuterium than a sample of the deuterated diborane obtained from six successive exchanges between diborane and deuterium.[2] Only a few weak infrared bands in the region of 1600 to 1720 cm^{-1} and a band at 2590 cm^{-1} that could be attributed to partially deuterated diborane were detectable with a 6-cm cell at 600-mm pressure. Two exchanges, each of a month's duration, using a molar ratio of $B_2{}^{10}D_6$ to deuterium of one to seven further enhanced the isotopic purity to the point where the infrared bands attributed to partially deuterated diborane were barely detectable at 600-mm pressure and were not detectable at 200-mm pressure in a 6-cm cell.

Infrared Spectra

The infrared absorption spectra were measured over the range 250–3800 cm^{-1} by means of a modified Perkin-Elmer 12B spectrometer. The most significant modification was the addition of a housing for the instrument so that it could be swept out with dry nitrogen. In this way the water-vapor absorption could be reduced so drastically that its effect on the spectrum was negligible. In the low frequency region (250–450 cm^{-1}) a thallium bromo-iodide prism was used, and scattered light was minimized by reflection of the source radiation from two plane-grating filters (1000 and 3200 lines/inch, respectively) in series. The resolution achieved was more or less uniform throughout the spectrum, amounting to about 3 cm^{-1} except at the highest frequencies. The band maxima and minima were measured with a precision of about 2 cm^{-1}, again except at the highest frequencies, where it may be as much as 4 cm^{-1}. Prisms of potassium bromide, rock salt, and fluorite were em-

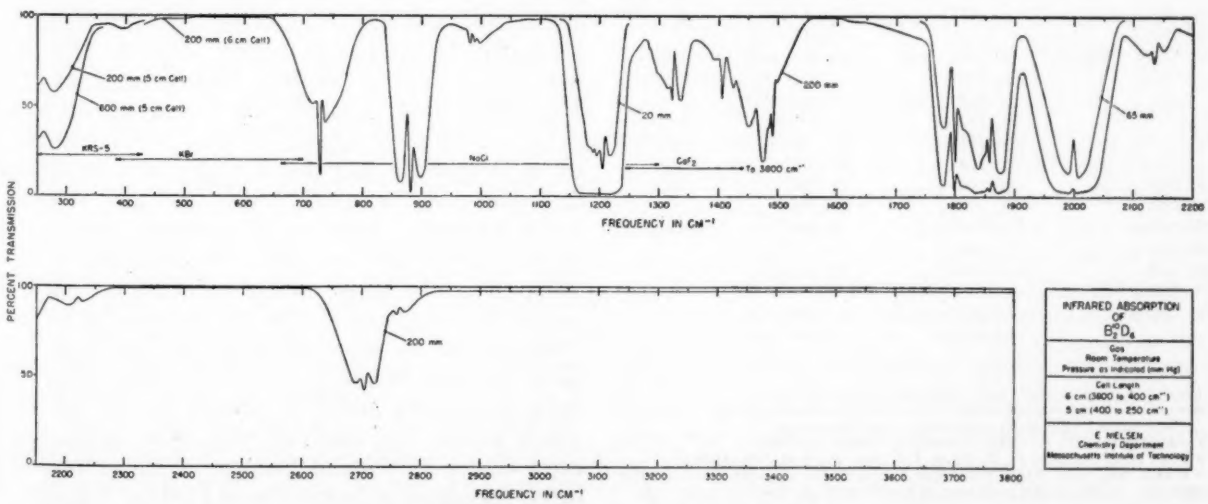

FIG. 3. Infrared absorption spectrum of $B_2{}^{10}D_6$.

ployed in the appropriate regions. The gas absorption cells were one 6 cm in length with KBr windows and one 5 cm with thallium bromo-iodide windows.

The infrared absorption spectra were measured on the vapor, liquid, and solid. In the present paper the results of the condensed-phase spectra will not be given except for certain specific details of importance to the interpretation of the vapor spectrum. The results of the vapor absorption measurements are presented in Figs. 1–3 and Tables I and II. In the latter are included the results of previous workers[1,2,6] that were available to us at the time of our work. The results of the high dispersion study of Barker and Anderson[3] are not included because they reported data only on the five high intensity bands at 368, 973, 1173, 2520, and 2609 and the weak band at 1990. The low dispersion frequencies of Price and ourselves for these bands agree quite well with the grating values. With one or two exceptions, our results are presented in terms of the measured positions of the band centers. These centers are maxima for type A and type C bands, and minima for type B bands.

At this point we wish to discuss certain minor discrepancies between previous work and ours. In Table I bands are listed for Stitt[6] and Price[1] at about 1405 and 3135 that we have not found. The former shows a suspicious intensity difference (medium *vs* very weak) between these two investigators, and may well be an impurity. Under conditions of less water vapor, higher resolution, and comparable pressure-×-cell length, we have been unable to find any trace of this band, and have rejected it as not belonging to diborane. The band at 3135, called very weak by both Stitt and Price, may well be a diborane band, but is so high in frequency and low in intensity that if real it is unquestionably an overtone.

Price reports a very weak band at 849 cm^{-1} that we have not found. Since it has not appeared on our curves under comparable conditions to those used by Price, we regard the band as doubtful. Stitt has reported weak bands at 673, 685, and 1722 that Price and ourselves did not confirm. To be sure, Stitt worked at somewhat higher effective pressures, but the region around 680 on our curves is quite free of absorption, and at 1722 Stitt presumably had trouble with water vapor. We have not attempted to interpret any of these bands.

Of the bands reported by us in Table I and not previously reported by others, the most significant is the type C band at 1882 cm^{-1} in ordinary diborane and at 1887 in $B_2{}^{10}H_6$. The good resolution afforded by the fluorite prism in this region, together with the virtual absence of water-vapor absorption, enables the clear discernment (See Figs. 1 and 2) of a type C band partially fused with the strong type B band at 1860 in B_2H_6 and at 1869 in $B_2{}^{10}H_6$. This band is of primary importance in the vibrational assignment, as will be seen later.

In addition we have found two very weak bands in ordinary diborane at 2787 and 2869, and 2795 and 2876 in $B_2{}^{10}H_6$. The isotopic frequency shift in both cases is about right, but we question whether they belong to diborane, because they were not reported by Price, who studied this region with an LiF prism.

Comparison of the infrared spectrum of $B_2{}^{10}D_6$ reported by us in Table II with that of B_2D_6 reported by Webb, Neu, and Pitzer[2] indicates that our material had a considerably higher deuterium content. The bands they report at 707, 794, 914, 1075, 1705, 2506, 2596, 2768, 2902, 3132, and 3372 cm^{-1}, some of which they have assigned to vibrations of B_2D_6, were not observed by us, despite the fact that our spectra were obtained at higher pressure-×-cell length, and with somewhat better resolution. They should probably, therefore, be attributed to partially deuterated diborane, of which Webb, Neu, and Pitzer estimate about 9 percent to be present in their sample. The bands reported by us in Table II and not reported by Webb, Neu, and Pitzer lie at 262, 592, 981–997, 1283, 1322, 1406, 1491, 1799, 2134, 2219, 2704, and 2759. Except for the 262 band, which cannot be observed with KBr optics, these extra bands were found because of higher pressures, better resolution of fluorite above 1300 cm^{-1}, absence of water vapor, and absence of interfering bands from

TABLE III. Raman spectrum of B_2H_6 (cm^{-1}).

Anderson and Burg[a]	Webb, Neu, and Pitzer (reference 2)	This research	D_{2h} assignment
(9) 2101 *k*			
(3) 2527 *l*			
(3) 2102 *i*			
	(vw) 606 *e*		
	(vvw) 617 ? *e*		
	(vw) 794 *g*	(0) 796 *g* (*p*)	
	(vw) 811 *g*	(0) 808 *g* (*p*)	
	(vw) 820 *g*		
	(w) 795 *f*	(3) 793 *f* (*p*)	
(10) 2523 *k*			
	(s) 764 *e* (812 *f*)	(6) 759 *e p*	$2\nu_{10}$
(5) 793 *e*	(vs) 792 *e* $\bar{p}$	(vs) 794 *e p*	$\nu_4(B^{11}-B^{11})$
(4) 806 *e*	(vs) 808 *e* $\bar{p}$	(s) 807 *e p*	$\nu_4(B^{11}-B^{10})$
(3) 821 *e*	(s) 821 *e*	(2) 820 *e*	$\nu_4(B^{10}-B^{10})$
(4) 2523 *i*		(2) 2523 *i p*	
(2*d*) 2775 *k* (1008 *e*)	(s) 1013 *e ndp*	(5*d*) 1011 *e dp*	ν_{15}
	(w) 1108 *e*[b]		
	(s) 1180 *e ndp*	(7) 1180 *e dp* ?	ν_3
	(w) 1321 *e*	(1) 1320 *e p*	$\nu_9+\nu_{10}$
	(w) 1745 *e*	(1*d*) 1747 *e* (*dp*)	ν_6
	(w) 1784 *e*	(1*d*) 1788 *e* (*dp*)	$\nu_5+\nu_9$
(3) 2106 *g*	(s) 2105 *g*	(5) 2007 *e p*	$2\nu_{15}$
(1) 2101 *f*	(s) 2102 *f*	(5) 2103 *f p*	
(10) 2102 *e*	(vs) 2097 *e* $\bar{p}$	(vs) 2104 *e p*	ν_2
(0) 2522 *g*	(s) 2523 *g*	(3) 2525 *g p*	
(0) 2521 *f*	(vs) 2522 *f*	(8) 2523 *f p*	
(3) 2489 *e* (4256 *k*)			
(8) 2522 *e*	(vvs) 2523 *e* $\bar{p}$	(vs) 2524 *e p*	ν_1
	(s) 2591 *e*	(9) 2591 *e dp*	ν_{11}

$\bar{p}$ = definitely polarized; *ndp* = not definitely polarized.
p = polarized, *dp* = depolarized by densitometer measurement.
(*p*) = polarized, (*dp*) = depolarized by visual estimate.
e = 4358; *f* = 4347; *g* = 4339; *i* = 4077; *k* = 4047; *l* = 3984.
[a] T. F. Anderson and A. B. Burg, J. Chem. Phys. 6, 586 (1938).
[b] Webb, Neu, and Pitzer (reference 2) report the absolute wave number of this line, without interpretation as to the exciting line.

[6] F. Stitt, J. Chem. Phys. 9, 780 (1941).

the partially deuterated compounds. The resolution achieved under these favorable circumstances enabled identification of the band types of all the major absorption bands, and thus simplified greatly the comparison with the spectra of the nondeuterated compounds and the assignment of frequencies to the normal vibrations of the molecule.

Raman Spectra

The Raman spectra were photographed in the liquid state. The low temperature experimental arrangement has been described elsewhere,[7] but for purposes of comparison with the results of other workers, we will mention here that our spectra were obtained with a Zeiss three-prism spectrograph giving a dispersion in the blue of about 0.04 mm to the angstrom. Refrigeration of the 4-ml Raman tube was obtained with cold nitrogen gas, by means of which the tube was kept at about −130°C. Exposure times were three hours for ordinary spectra and from 14 to 24 hours for polarization measurements. Hg-4358 was used throughout; and saturated sodium nitrite (1 cm) and 0.01 percent duPont Rhodamine 5GDN extra (1 cm) solutions were used to reduce, respectively, the intensity of the mercury violet lines and the continuous background in the blue-green. As an index of the resolution achieved, it may be mentioned that the ordinary diborane isotopic triplet at 796–807–820 cm^{-1} was resolved without difficulty. The wave number precision is 2–3 cm^{-1}.

The polarization measurements were made by a single-exposure method with the use of a split piece of Polaroid sheet that passed the parallel and perpendicular components one above the other on the slit. The very strong polarization of the spectrograph optics was compensated by insertion of a half-wave plate of cellophane behind the piece of Polaroid passing the parallel component. Because of incomplete correction or partial attenuation of the parallel component by the half-wave plate, for a depolarized line the intensity ratio, $I_\perp/I_\parallel$, of perpendicular to parallel component was not the theoretical 6/7, but was very slightly larger than unity over the spectral range involved (4500–4900A). Thus, if a given Raman line showed a value equal to or less than unity for $I_\perp/I_\parallel$, the line was definitely polarized, while if $I_\perp$ was larger than $I_\parallel$, the line was depolarized or at most very slightly polarized. The important point concerning this qualitative procedure is that error is made only in the direction of measuring a slightly polarized line to be depolarized, and not vice versa. As will be seen later, such a procedure is sufficient to make definite statements about previous doubtful or unmeasured depolarization factors and to require changes in the vibrational assignment.

The Raman data are listed in Tables III and IV, along with those of previous investigators. The agreement in Table III is very good, but one or two differences need comment. We have been unable to find three very weak lines reported by Webb, Neu, and Pitzer[2] at 606, 617, and 1108 cm^{-1}. These authors question 617 themselves, and do not assign the 1108 line to its origin of excitation but simply report its wave number value 21830.2. Their line at 606 may be real, inasmuch as their spectra were obtained on a larger quantity of diborane (30 *vs* 4 ml) than ours. However, we have been unsuccessful in finding any trace of the line and believe that if it is real, it is a difference tone (possibly $\nu_9-\nu_{10}$). Arguments against the assignment of this line to ν_{12}, as suggested by them, are given below. One further difference concerns the assignment of excitation for the line reported by Webb, Neu, and Pitzer at 20,934.6 cm^{-1}. If this line is ascribed to excitation by Hg-4339, as was done by them, it can be readily interpreted as the 2104 Raman line. However, it is too strong for this, being in fact slightly stronger than the corresponding 2104 line excited by Hg-4348. Since we have always found that lines excited by Hg-4339 are markedly weaker than those by Hg-4348, we feel that the line at 20,934.6 should be assigned to Hg-4358 as a distinct Raman line at 2004 (our value is 2007).

TABLE IV. Raman spectra of B_2D_6 and $B_2{}^{10}D_6$ (cm^{-1}).

B_2D_6: Rice[a]	$B_2{}^{10}D_6$: This research	D_{2h} assignment
	(0) 726 *g*	
	(2) 725 *f p*	
vs 710 *e*	(vs) 726 *e p*	ν_4
	(4*d*) 730 *e* (*dp*)	ν_{15}
	(0) 928 *f* (*p*)	
s 905 *e*		
m 915 *e*		
	(8) 929 *e p*	ν_3
vw 966 ? *e*	(0) 967 *e*	$\nu_9+\nu_{10}$
	(0) 984 *e*	Source ?
m 1269 *e*	(2) 1273 *e dp*	ν_6
	(1) 1394 *e p*	CO_2−?
	(3) 1513 *g p*	
	(3) 1435 *e p*	$2\nu_{15}$
	(7) 1511 *f p*	
(vs) 1509 *e*	(vs) 1510 *e p*	ν_2
	(0) 1750 *e* (*p*)	$2\nu_{18}$
	(5) 1834 *f p*	
	(7?) 1882 *f*	
	(s) 1833 *e p*	$2\nu_3$
(vs) 1860 *e*	(vs) 1880 *e p*	ν_1
(s) 1870 *e*		
(s) 1956 *e*	(9) 1975 *e dp*	ν_{11}
	(5) 2000 *e dp*	$\nu_6+\nu_{15}$

[a] See reference 4.

Table IV lists our results for $B_2{}^{10}D_6$ along with preliminary values of Rice[4] for ordinary B_2D_6. It will be seen that the change from the natural mixture of boron isotopes to the pure B^{10} compound makes several striking differences. The doublet 905–915 in ordinary B_2D_6 changes to the single line 929 in $B_2{}^{10}D_6$. The 1860–1870 doublet changes to 1833–1880 and reverses in intensity from vs-s to s-vs. The interpretation of this change will be discussed later.

At one stage in the handling of the $B_2{}^{10}D_6$ the material became contaminated with a small amount of

[7] R. C. Lord and E. Nielsen, J. Opt. Soc. Am. **40**, 655 (1950).

TABLE V. Symmetry species of vibrations of nonplanar D_{2h} and C_{2h} models.

Symmetrical bridge (D_{2h})			Unsymmetrical bridge (C_{2h})		
Species of vibrations	Number of vibrations	Activity	Species of vibrations	Number of vibrations	Activity
A_g	4	R., pol.	A_g	6	R., pol.
A_u	1	Inactive	A_u	4	I.
B_{1g}	2	R., dep.	B_g	3	R., dep.
B_{1u}	3	I., type B	B_u	5	I.
B_{2g}	2	R., dep.			
B_{2u}	2	I., type C			
B_{3g}	1	R., dep.			
B_{3u}	3	I., type A			

CO_2, as was shown by the infrared spectrum. It is believed that the weak Raman line reported at 1394 originated from this dissolved CO_2. The weaker companion CO_2 line at 1285 would probably be obscured by the rather fuzzy $B_2{}^{10}D_6$ line at 1273.

INTERPRETATION OF THE SPECTRA

Our intention at the beginning of this work was to examine the spectroscopic data in terms of as many different symmetries of diborane as were compatible with its empirical formula. We have done this, but have found that most structures can be ruled out readily on the basis of the gross features of the spectra and do not need special discussion. For example, any structure with a threefold, or higher, symmetry axis, e.g., ethane-like structures (D_{3d} or D_{3h}) or 4-proton-bridge structures (D_{4h} or D_{2d}), can be eliminated, as was first shown by Price,[1] on the ground that the rotational structures of the infrared absorption bands indicate an asymmetrical-top type of structure. There are equally strong arguments (for example, the obvious presence of a center of symmetry) against the other types of structures except for the planar and nonplanar forms of the symmetrical (D_{2h}) and unsymmetrical (C_{2h}) two-proton-bridge model.

A decision between the planar and nonplanar forms is best made from the rotational envelopes of certain infrared bands. The Raman spectrum is of no use because only one Raman-active vibration changes symmetry species on passing from the planar to nonplanar model, and the selection rules and expected location of frequencies are the same for both structures. The product rule does not help, because the assignment of Raman-active frequencies made on the basis of either structure fits the corresponding set of product rules equally well.

On the other hand, two infrared-active vibrations trade symmetry species in the two models. One of these is the puckering vibration of the bridge ring, which belongs to a species producing a band of type C structure (see below) in the planar model and type B in the nonplanar. The other is an unsymmetrical stretching of the bridge bonds and its infrared band would have a type B envelope in the planar and type C in the nonplanar model. The puckering vibration is expected to be at a low frequency and the stretching at a high value. As will be seen below, the former has been rather surely identified with the lowest infrared band at 368 cm^{-1}, but the location of the latter is ambiguous. In the expected bridge stretching region there are two bands of comparable intensity, one of type B and the other of type C. These lie at 1860 and 1882, respectively, in ordinary diborane and at 1459 and 1491 in $B_2{}^{10}D_6$. Since either of these bands could be equally well assigned to the bridge stretching vibration in the light and heavy compounds, their band types cannot be used to decide the question of planarity.

The decision therefore rests exclusively with the type of the 368 cm^{-1} band. On the basis of our work it is difficult to decide between a type B and a type C with washed-out rotational structure. However, the high resolution work of Anderson and Barker[8] has shown unequivocally that the band is of type B, and that therefore the planar structure is ruled out.‡

We are thus left with a choice between the nonplanar symmetrical two-proton-bridge model (D_{2h}) and the unsymmetrical form (C_{2h}). In the former all four bridge bonds are identical, while in the latter each bridge hydrogen has two different bonds. The normal vibrations of the D_{2h} model have been worked out, insofar as symmetry allows, by Bell and Longuet-Higgins[8] and their enumeration of the vibrations, adopted by references 1, 2, and 4, will be used here. Approximate normal vibrations for the C_{2h} model can be sketched from those of the D_{2h} model by removal of the appropriate symmetry elements. The selection rules for the two models are given in Table V. The infrared-active frequencies that have the vibrating electric moment along the least, middle, and greatest moment of inertia occur respectively in species B_{3u}, B_{1u}, and B_{2u}, and give rise to bands of type A, B, and C.[9] In the nonplanar D_{2h} model the axis through the boron atoms is that of least inertia and through the bridge hydrogens that of greatest.

The major difference between the spectra expected of the two models is in the number of Raman-active fundamentals that are depolarized, three for the C_{2h} model and five for the D_{2h} model. The Raman spectra of the B_2H_6 and $B_2{}^{10}D_6$ give only the following possi-

‡ There appears to be an inconsistency in Anderson and Barker's paper in this connection. On p. 704 they have used the type B character of the 368 band as an argument for the nonplanarity of the molecule, stating, "If the bridge hydrogens were in the same plane as the four terminal hydrogens, the out-of-plane bending vibration involving the bridge hydrogens would cause variation of the electric moment along the greatest axis of inertia. A type C band would then be expected for the lowest frequency band." Earlier (p. 700) they had, however, assigned the 368 band to a terminal hydrogen wagging vibration by analogy to ethylene. This latter vibration (ν_{14} in their notation, ν_9 in the present paper) would give rise to a type B band in either the planar or nonplanar structure.

[8] R. P. Bell and H. C. Longuet-Higgins, Proc. Roy. Soc. (London) A183, 357 (1945); these vibrations are also shown by Price (reference 1) and Anderson and Barker (reference 3).

[9] Compare G. Herzberg, *Infrared and Raman Spectra* (D. Van Nostrand Company, Inc., 1945), pp. 460 ff.

bilities for depolarized lines: B_2H_6: 1012, 1180, 1747, 1788, 2591; $B_2{}^{10}D_6$: 730, 1273, 1975, 2000.

Of these lines the 1180 cm^{-1} of B_2H_6 is the only possible analog of the definitely polarized 929 cm^{-1} of $B_2{}^{10}D_6$ and must therefore be considered to be slightly polarized. The very weak pair 1747 cm^{-1} and 1788 cm^{-1} is interpreted as an example of strong Fermi resonance between a fundamental and a combination band, with 1273 cm^{-1} being the corresponding single fundamental frequency of the $B_2{}^{10}D_6$. The line at 2000 cm^{-1} in $B_2{}^{10}D_6$ is likewise interpreted as an overtone borrowing enough intensity from the fundamental 1975 cm^{-1} to be observable. The 730-cm^{-1} line of $B_2{}^{10}D_6$ is too close to the strong 726 line to determine its depolarization but is the only possible analog of the 1012 cm^{-1} line in the B_2H_6. We are left then with only three depolarized lines: B_2H_6: 1012, 1765§, 2591; $B_2{}^{10}D_6$: 730, 1273, 1984.

The observation of only three depolarized Raman lines might be taken as evidence for the C_{2h} model. However, it is not possible to assign them all to the vibrational species B_g, to which depolarized lines for this model must belong. There are three of these, one a terminal B—H stretching vibration and the other two anti-rotation vibrations analogous to the B_{2g} and B_{3g} vibrations of the D_{2h} model. The 2591 line can be readily assigned to the stretching vibration, and the 1012 line to one of the remaining two. However, a frequency of 1765 is considerably too high for either of the latter. One would expect, in fact, that the 1765 line comes from some form of vibration involving a stretching of the bridge bonds, none of which on the C_{2h} model should give rise to a depolarized line.

A companion objection comes from the application of the product rule to the B_g species. The value of the product-rule ratio for this species in any reasonable C_{2h} nonplanar structure of diborane should be within 2 percent of 2.37. The observed product ratio is 2.49, which not only is in definite disagreement but disagrees in the wrong direction, since the anharmonicity correction nearly always makes the observed ratio smaller than the theoretical for species containing stretching vibrations.[10]

In order for these discrepancies to be reconciled with C_{2h} symmetry, one must make some special assumptions. It is conceivable that the 1747–1788 doublet in B_2H_6 and the 1273 line in $B_2{}^{10}D_6$ are combination frequencies belonging to species B_g. However, this is highly improbable in view of their intensities and the absence of nearby depolarized fundamentals from which they could borrow intensity. It could also be supposed that the lines are actually slightly polarized but, because of our inability to distinguish such lines from depolarized ones, are not recognized as totally symmetrical. Such a situation could easily arise if the C_{2h} model does not deviate much from D_{2h} symmetry. Since the evidence is not compelling, however, we tentatively reject the C_{2h} structure and will proceed with an interpretation on the basis of the D_{2h} model.

§ Estimated position of fundamental corrected for resonance shift.

[10] F. Halverson, Revs. Modern Phys. 19, 94 (1947).

VIBRATIONAL ASSIGNMENT FOR NONPLANAR D_{2h} MODEL

Assignments of the observed infrared and Raman spectra to the vibrations of nonplanar D_{2h} model have been made by taking into consideration the infrared band types and the polarization of the Raman lines as well as the Teller-Redlich product rule. These are summarized in Tables V and VI. The frequency numbering scheme is that of Bell and Longuet-Higgins.[8] Assignment of combination tones is indicated in Tables I–IV and Tables VII and VIII.

As has been shown by various workers,[1–3] there seems to be little question about the assignments of the infrared-active fundamentals except for ν_9 and ν_{13}, when one considers band type, expected location in the spectrum, and the product rule where it is applicable. The assignments to the Raman-active totally symmetrical vibrations also appear to be quite certain, especially in view of the assignments for $B_2{}^{10}D_6$, which are in good agreement with the product rule.

The remaining assignments, with the exception of ν_7 and ν_{12}, are pretty definitely required by the experimental results obtained in this investigation and in addition explain bands for which prior assignments either could not account or are invalidated by our results. The arguments presented below will be given mainly in terms of the frequencies observed for ordinary diborane and hold equally well for those of the isotopic molecules.

TABLE VI. Fundamental frequencies of diborane.

Species	Vib'n. No.[a,b]	Frequency in cm^{-1} $B_2{}^{11}H_6$	$B_2{}^{10}H_6$	$B_2{}^{10}D_6$	C_2H_4[c]	Product rule Obs.	Theor.
Ag	1	2524	···	1860*	3019	2.63	2.695
	2	2104	···	1511	···		
	3	1180	···	929	1342		
	4	794	820	726	1623		
Au	5	829	729	592	1027	1.40	1.414
B_{1g}	6	1768*	···	1273	···	1.65	1.659
	7	(1035)	(1044)	(870)	943		
B_{1u}	8	2612	2625	1999	3106	2.47	2.520
	9	(950)	···	(705)	810		
	10	368	368	262	···		
B_{2g}	11	2591	···	1980*	3075	1.63	1.627
	12	(920)	(930)	(740)	1236		
B_{2u}	13	1915*	1920*	1465*	···	1.75	1.782
	14	973	977	728	949		
B_{3g}	15	1012	···	730	···	1.39	1.414
B_{3u}	16	2525	2528	1845*	2990	2.43	2.520
	17	1602	1606	1205	···		
	18	1177	1181	881	1444		

[a] See reference 1.
[b] See reference 8.
[c] See reference 11.
* Frequencies thus marked have been corrected for a presumed shift due to Fermi resonance.
The product rule values, both theoretical and observed, have been calculated for the pair $B_2{}^{11}H_6-B_2{}^{10}D_6$.
Frequencies enclosed in parentheses have been evaluated only from overtones.

Raman Assignments

Observed Fundamentals

The previous assignment to the nontotally symmetrical vibrations (species B_{1g}, B_{2g}, and B_{3g}) is changed by the polarization data. The lines at 1321 cm^{-1} and 764 cm^{-1} previously assigned to ν_{15} and ν_{12}, respectively, are polarized, and therefore cannot be assigned as fundamentals.

The assignment of the line at 2591 cm^{-1} is without question. It is in the region for the terminal B—H stretching vibration and must therefore be assigned to ν_{11}. The Teller-Redlich product rule will not permit either of the other depolarized lines (1765 cm^{-1} and 1011 cm^{-1}) to be in this same species (B_{2g}), leaving ν_{12} as unobserved. Of the remaining normal modes (ν_6, ν_7, and ν_{15}), only ν_6 seems to be of the type to which the 1765 cm^{-1} can be assigned. While ν_6 involves stretching of the bridging bonds and would be expected to be in the region of 1600 to 2100 cm^{-1}, ν_7 and ν_{15} involve only twisting or bending of bond angles and by analogy with ethylene[11] are expected to lie in the neighborhood of 1000 cm^{-1} or lower.

With 1765 cm^{-1} assigned to ν_6, 1011 cm^{-1} cannot be assigned to ν_7 on the basis of the product rule and must be assigned to ν_{15}, for which the product rule is satisfied. It is thus ν_7 and ν_{12} that are weak in the Raman effect, which is also observed for the corresponding vibrations in ethylene.

TABLE VII. Infrared combination and difference tones of B_2H_6 and $B_2{}^{10}D_6$ (cm^{-1}).

Assignment	B_2H_6 Calc.	B_2H_6 Obs.	$B_2{}^{10}D_6$ Calc.	$B_2{}^{10}D_6$ Obs.	Remarks
$\nu_{17}-\nu_4$	808	812 vvw	479	···	Shift to 787 in $B_2{}^{10}H_6$ dictates this assignment.
$\nu_{10}+\nu_{12}$	(1288)	1287 w	(1002)	*ca* 998 w	Overlapping weak bands in $B_2{}^{10}D_6$.
$\nu_{10}+\nu_{15}$	1380	1374 w	(992)	*ca* 988 w	Overlapping weak bands in $B_2{}^{10}D_6$.
$\nu_5+\nu_{11}$	1841	···	(1322)	1322 m	Band in B_2H_6 would be hidden by 1860 band.
$\nu_5+\nu_7$	(1864)	1860 ms	(1462)	1459 ms	
$\nu_9+\nu_{13}$	(1962)	1992 w	(1435)	1406 w	Bands shifted by Fermi resonance with ν_{13}.
$\nu_3+\nu_{14}$	2153	2142 vvw 2228 vvw	1657	···	Not expected in $B_2{}^{10}D_6$ owing to smaller anharmonicity.
$\nu_3+\nu_{13}$	2357	2347 m	1810	1799 s	Fermi resonance with ν_{16}.
$\nu_4+\nu_{17}$	2396	2394 vw	1931	···	Would be hidden by ν_3 in $B_2{}^{10}D_6$.
$\nu_3+\nu_{17}$	2782	2787 vw?	2134	2134 w	2787 in B_2H_6 considered impurity since not reported by Price (reference 1). Intensity difficult to determine owing to closeness of ν_3 and lower resolution in this area.
$\nu_3+\nu_{19}$	3054	···	2216	2219 w	Resonance with ν_3 causes appearance in $B_2{}^{10}D_6$.
$\nu_3+\nu_{17}$	3706	3700	2716	2704 m	
$\nu_3+\nu_{16}$	3705	3700	2774	2759 vw	

Calculated frequencies enclosed in parentheses were used in the evaluation of one of the fundamentals involved.

[11] R. L. Arnett and B. L. Crawford, Jr., J. Chem. Phys. 18, 118 (1950).

Infrared Assignments

Observed Fundamentals

As noted earlier, there is a new type C band observed with its "Q" maximum at approximately 1882 cm^{-1}, partly under the R branch of the relatively strong type B band at 1860 cm^{-1}. Because of its intensity relative to the other type C band at 1992 cm^{-1}, the 1882-cm^{-1} band is preferred as the fundamental ν_{13}, which is in Fermi resonance with the other band. In the deuterated compound the analogous bands are reversed, with the more intense one at 1491 cm^{-1} and the combination band at 1406 cm^{-1}. It is also probable, though not detectable with our instrument, that the combination band in ordinary diborane analogous to the type A band in $B_2{}^{10}D_6$ at 1322 cm^{-1} is hidden under the P branch of the type B band at 1860 cm^{-1}.

Unobserved Fundamentals

The locations of the unobserved fundamentals ν_5, ν_7, ν_9, and ν_{12} are obtained by consideration of the overtone and combination bands observed in both Raman and infrared spectra. The use of the infrared combination bands for this purpose is made much less arbitrary by the stringent requirements of band type, product rule, and selection rules that a given interpretation must satisfy.

The interpretation is best begun by a consideration of ν_9. This vibration has previously[1,2] been assigned to the weak band at 1287 sandwiched in between the strong type A band at 1177 and the type C band at 1374 cm^{-1}. There are several objections to this assignment. The frequency is rather high for this kind of vibration, which lies at 810 in ethylene,[11] where it of very low intensity. The product rule places ν_9 at 950 cm^{-1} in $B_2{}^{10}D_6$ if 1287 is correct for $B_2{}^{11}H_6$, whereas no band is observed within 30–40 wave numbers of this point, and in particular there is no band at 914 cm^{-1}, which Webb, Neu, and Pitzer used as the B_2D_6 value for ν_9. Finally, it should be mentioned that the band type of the 1287 band is not clear-cut. It could be a type B band, but because its structure differs noticeably from that of the 368 and 2620 bands, it is possibly a superposition of two overtone bands of different types. A high resolution study of the region 1200–1400 cm^{-1} in $B_2{}^{10}H_6$ and 900–1100 in $B_2{}^{10}D_6$, where the corresponding bands should fall, would be well worthwhile.

To locate ν_9 we make use of the fact that there is no combination of the already assigned fundamentals that can account for a type C band at 1992 cm^{-1} (1406 in $B_2{}^{10}D_6$), and of the few possibilities involving the unassigned fundamentals, all but $\nu_9+\nu_{15}$ can be excluded either as giving unreasonably high values for the unobserved fundamentals or as leading to a conflict with the product rule. If we assume that in the absence of Fermi resonance with the type C fundamental at about 1915 cm^{-1} (1465 in $B_2{}^{10}D_6$), the over-

tone would lie at approximately 1955 (1435 in $B_2{}^{10}D_6$), we obtain (with the help of the previously assigned values of ν_{15}) values of about 943 in diborane and 705 in $B_2{}^{10}D_6$.

The reason for the failure to observe ν_9 in the vapor seems to be that strong broad type C bands occur at both 973 in diborane and at 728 in $B_2{}^{10}D_6$, thereby obliterating the resumably much weaker ν_9. It is of interest to note that in the infrared spectra of solid diborane and $B_2{}^{10}D_6$ there are bands at 938 and 703 cm^{-1}, respectively, that show up when the rotational envelope of the type C band (ν_{14}) is eliminated by condensation.

Next, let us consider the interpretation of the type A band at 1322 cm^{-1} in $B_2{}^{10}D_6$, for which no analog is observed in B_2H_6. If we assume that this band is a strong combination band in its own right or that it appears strong because of resonance with ν_{17} at 1205 cm^{-1}, there is in either case no combination band except $\nu_5+\nu_{15}$ that will satisfactorily explain the absence of this band in ordinary diborane. We obtain from this assignment a value of 592 cm^{-1} for ν_5 of the deuterated compound, and from the product rule a value of 828 cm^{-1} for ordinary diborane. The corresponding summation band in ordinary diborane would then occur at 1840 cm^{-1}, where it would be hidden by the P branch of the type B band at 1860 cm^{-1}. It is to be expected that the summation band in ordinary diborane will be weak because part of the intensity in the deuterated compound can be accounted for on the basis of resonance with ν_{17}.

There is a very weak band in the vapor spectrum of ordinary diborane at 829 cm^{-1} which shows no isotope shift on passing to $B_2{}^{10}H_6$. An analogous band is found in $B_2{}^{10}D_6$ at 592 cm^{-1}. It is remarkable that a band showing these properties, which are to be expected only of ν_5 and the already-assigned ν_{15}, should appear at the place in the spectrum where ν_5 is located on the basis of overtone interpretation. ν_5 is, of course, forbidden, and one's first reaction is to try to explain the band as a difference tone. This is a very difficult task purely on numerical grounds, but when one imposes the additional requirements that the band show no B^{10}–B^{11} isotope shift and a shift of 1.40 from $B_2{}^{10}H_6$ to $B_2{}^{10}D_6$, and that the difference tone be an allowed infrared transition, the task becomes impossible.

One is thus impelled to review reasons for ν_5 to appear in the vapor spectrum. One possibility has been suggested earlier by Herzberg[12] in the case of ethylene, that of interaction between the A_u vibration and those of species B_{1u}, B_{2u}, and B_{3u} produced by Coriolis forces. Since there are vibrations with frequencies not too far removed from 829 and 592 cm^{-1} in each of these species in ordinary diborane and $B_2{}^{10}D_6$, respectively, the appearance of the A_u vibration in both molecules can be understood on this basis.

[12] G. Herzberg, reference 9, p. 467 and earlier discussion cited there.

TABLE VIII. Raman overtones, combination and difference tones of B_2H_6 and $B_2{}^{10}D_6$.

Assignment	B_2H_6 Calc	B_2H_6 Obs	$B_2{}^{10}D_6$ Calc	$B_2{}^{10}D_6$ Obs	Remarks
$2\nu_{10}$	736	759	524	···	Resonance with ν_4 explains presence in B_2H_6. See text.
$\nu_9+\nu_{10}$	1330	1321	972	967	See text concerning ν_{10}.
				984	Source ?
$\nu_5+\nu_9$	1799	1788	1300		Exact resonance with ν_6 in B_2H_6.
$2\nu_{15}$	2024	2007	1460	1436	Resonance with ν_2.
$2\nu_{18}$	2354		1762	1750	Resonance with ν_1 in $B_2{}^{10}D_6$.
$2\nu_3$	2360		1858	1833	Resonance with ν_1 in $B_2{}^{10}D_6$.
$\nu_6+\nu_{15}$	2780		2003	2000	Resonance with ν_{11} in $B_2{}^{10}D_6$.

Another possibility is a diborane structure of C_{2h} symmetry that deviates only slightly from D_{2h}. The most significant change to be expected in the infrared spectrum of such a model from the D_{2h} form is the appearance of ν_5 as a weak but allowed fundamental. As was mentioned earlier, there is also a possibility of explaining the small number of depolarized Raman lines on the basis of a C_{2h} structure that approximates D_{2h}. In view of several *ad hoc* assumptions that would have to be made to do this, we prefer the alternative explanation of the appearance of ν_5 in the spectrum. It would appear that a determination of the type of 828 band might decide between these two explanations. If Coriolis interaction between ν_5 and ν_{14} is responsible for the former's appearance, the band type should be C. If C_{2h} symmetry is the reason, the band ought to be type B.

The most prominent band in the spectrum not assigned to a fundamental is the type B band at 1860 cm^{-1} in ordinary diborane that shifts to 1459 in $B_2{}^{10}D_6$. An explanation of these bands is essential because of their intensity. The fact that they are unequivocally type B means that they must be overtones, since all the type B fundamentals have been assigned. In agreement with this is the fact that the bands do not fit the B_{1u} product rule if the type B bands at 2612 and 368 (1999 and 262 in $B_2{}^{10}D_6$) are taken as the other fundamentals.

There are only two reasonable overtone assignments for these bands, $\nu_5+\nu_7$ and $\nu_{12}+\nu_{18}$. The first assignment puts ν_7 at about 1035 and 870 in light and heavy diborane, and the second gives ν_{12} as 690 and 580, respectively. The former interpretation fits the product rule well and places ν_7 at a very reasonable location. The latter makes ν_{12} rather low, and disagrees with the product rule by 4 percent. This disagreement is not as significant as it might be in view of the correction for Fermi resonance that has to be made in the value of ν_{11} in $B_2{}^{10}D_6$ and the unknown amount of anharmonicity in $\nu_{12}+\nu_{18}$. However, no such objections hold for the former interpretation and we shall adopt it.

The evaluation of ν_{12} is more difficult because there are no unassigned depolarized Raman lines to which it could be assigned. The line at 606 used by Webb, Neu,

and Pitzer[2] for ν_{12} has not been found on our plates. Moreover, this value does not appear in any combination tone that can be unequivocally said to involve ν_{12}, and 606 seems quite low for a vibration whose analog in ethylene has been assigned[11] a value of 1236. One possibility is that the overtone at 1287 (or one of its components) might belong to type A instead of type B. In this event, there are few combination tones that can explain it. The most acceptable of these is $\nu_{10}+\nu_{12}$, which would place ν_{12} at about 920 cm^{-1}. In $B_2{}^{10}D_6$ there is a band at 997 cm^{-1} which is part of a complex set of peaks belonging to at least two overtones. If we assign this band to $\nu_{10}+\nu_{12}$, we obtain a value of ν_{12} in $B_2{}^{10}D_6$ of about 740 cm^{-1}. This value is in precise accordance with the product rule, although the close agreement is not significant in view of the difficulty of estimating the effects of anharmonicity on the overtone frequency as well as the possible effect of Fermi resonance with the fundamentals at 1177 in ordinary diborane and at 881 in $B_2{}^{10}D_6$.

Having thus completed a set of fundamentals, we are now in a position to consider the interpretation of the overtones. Most of them, especially those whose symmetry species can be determined from band envelopes or depolarization factors, can be given reliable interpretation. In view of the relative stringency of the selection rules, the ease and completeness with which the overtones in the spectra of all the isotopic forms can be explained is evidence of the essential correctness of the vibrational assignments.

The overtones and their suggested interpretations are listed in Tables VII and VIII. Since pertinent comments on the overtones are included in the tables, we will not discuss them further except $2\nu_{10}$ as observed at 759 cm^{-1} in the Raman effect in ordinary diborane. Since ν_{10} lies at 368 cm^{-1} in the vapor phase, its first overtone should occur at 736 except for anharmonicity. It would require a rather large positive anharmonicity to change the latter figure to 759, and an even larger anharmonicity if the 759 value includes the depressing effect of Fermi resonance with ν_4 at 794 cm^{-1}. On the other hand, if ν_{10} changes its value upward on passing from vapor to liquid, the correction need not be so large and might even change sign.

We have investigated the infrared spectra of liquid and solid diborane in preliminary fashion, and have found that the 368 vapor band definitely shifts its position upward in the liquid to 380 cm^{-1}. Since the Raman spectra were observed in the liquid, this value should be used in calculating the position of the harmonic first overtone. The combined effect of Fermi resonance and anharmonicity then gives the resultant frequency of 759 cm^{-1}. The overtone $2\nu_{10}$ should be much weaker, if present at all, in $B_2{}^{10}D_6$, because it shifts to a place 200 cm^{-1} removed from ν_4.

Finally, it should be mentioned that the set of fundamental frequencies here reported, while differing somewhat from those of Webb, Neu, and Pitzer,[2] give about the same calculated values for the heat capacity of the vapor over the temperature range where it has been measured by Stitt.[13] The new set of frequencies will give somewhat different values of the thermodynamic functions from those previously reported;[2] but in view of the rather minor nature of the differences, it has appeared not worthwhile to calculate new values until further evidence with respect to the present assignment accumulates.

Confirmation of this assignment awaits additional work of various kinds. It would be desirable to look for the Raman-allowed fundamentals ν_7 and ν_{12} in liquid diborane by different excitation (e.g., Hg-4047) and with longer exposures than have hitherto been used.‖ Study of the liquid and solid infrared spectra will also be helpful. As was mentioned above, we have found evidence for the presence of ν_9 at the expected places in B_2H_6 and $B_2{}^{10}D_6$ in the solid spectrum. When accurate values of the entropy and heat capacity of the vapor over wide temperature ranges become available, these should also serve as a check on the assignment. Finally, it is apparent that there is needed a normal-coordinate treatment of the vibrations of diborane on the basis of a more general potential function than the simplified one of Bell and Longuet-Higgins.[8]

[13] F. Stitt, J. Chem. Phys. 8, 981 (1940).

‖ Compare the recent success of Rank, Shull, and Axford, J. Chem. Phys. 18, 116 (1950), in finding the ethylene frequency analogous to ν_{12} in diborane at the position predicted by Arnett and Crawford (reference 11) from an analysis of the infrared combination bands.

The Mass Spectra of C_1–C_4 Monodeutero Paraffins

D. P. STEVENSON AND C. D. WAGNER
Shell Development Company, Emeryville, California

August 28, 1950

The magnetically scanned mass spectra of methane-*d*, ethane-*d*, propane-1-*d*, propane-2-*d*, *n*-butane-1-*d*, *n*-butane-2-*d*, *i*-butane-1-*d*, and *i*-butane-2-*d*, characteristic of 75-volt ionizing electrons and 75°C are given and compared with the mass spectra of the corresponding hydrocarbons.

A qualitative account of the origin of the isotope effects in mass spectra is given. It is shown that in a molecule containing equivalent isotopic species, the molecule-ion formed by electron impact will preferentially dissociate the lighter isotope and that the mass spectra of symmetrically substituted isotopic species (*A'BA'*) will be more like the mass spectra of the isotopically pure species (*ABA*) than are those of the unsymmetrically substituted isotopic species (*ABA'*). It is further shown that the equality (or lack thereof) of parent ion sensitivities of different isotopic preparations to the parent ion sensitivity of the natural substance is not a criterion of the purity (or lack thereof) of the preparations. Attention is called to the close relation between isotope effects in mass spectra and temperature effects in mass spectra.

The two-parameter empirical theory of isotope effects proposed by Evans, Bauer, and Beach is applied to the mass spectra of the methanes and ethanes and found to be inadequate for the prediction of mass spectra for accurate analysis of isotopic mixtures. It is found, however, that for certain electron impact induced processes, such as $RH+\epsilon^- \rightarrow R^+ + H + 2\epsilon^-$, the effective values of the parameters, Γ and π, are essentially equal for the monodeutero C_1 through C_4 paraffins.

It is shown that for the process, $RH+\epsilon^- \rightarrow R^+ + H + 2\epsilon^-$, the specific dissociation probability of secondary hydrogens is greater than that of primary hydrogens by a factor of 4 for propane and 10 for *n*-butane, while in isobutane the specific dissociation probability of the tertiary hydrogen is 30 times that of a primary hydrogen.

It is found that in certain states of the paraffin molecule-ions the hydrogens are sufficiently mobile that they undergo very extensive intramolecular redistribution in the short life of the molecule ion (half-life <0.1–1.0 microseconds) before they dissociate. Such states are of less common occurrence among paraffins than among olefins.

INTRODUCTION

THE preparation and purification of the eight monodeutero paraffins, C_1 through C_4, were described in papers published elsewhere;[1] methods for purity determination were also given. It is the purpose of this paper to describe the mass spectra of these substances and to discuss the relation of these mass spectra to the mass spectra of the corresponding hydroparaffins as measured with a commonly used type of sector field mass spectrometer. The discussion includes a qualitative account of the origin of the isotope effects which are observed.

Mass spectra of some of the substances herein considered have been previously published.[2–4] However, these previous measurements were made with a different type of mass spectrometer employing a different scanning technique, and as a result are not directly comparable with our mass spectra. In order to present a consistent discussion of the quantitative aspects of the mass spectra of the monodeutero paraffins, our results on previously investigated substances are included.

EXPERIMENTAL

All mass spectra reported in this paper were measured with a Westinghouse type LV Mass Spectrometer. Magnetic scanning was employed, the positive ion accelerating potential being 1000 volts and the positive ion drawing out potential being 5.0 volts (corresponding to a field of 12.9 volts/cm). The ionizing electron current from a 0.005-inch wolfram cathode was 5.0 microamperes, while the total emission from the cathode was in the range 15–20 microamperes. All mass spectra reported are those characteristic of 75-volt ionizing electrons. The effective temperature of the gas entering the ionization chamber of the mass spectrometer tube was 75±3°C as measured by the thermocouple attached to "Plate 7" of the mass spectrometer tube.

The gas enters the mass spectrometer through a Consolidated Engineering Corporation "Leak," which has an effusive speed of 8.4 cc/min as measured with methane. The leak is connected to the mass spectrometer tube by 30 cm of 14-mm i.d. tubing. The gas flowing into the mass spectrometer is stored in the standard, 2-liter, jacketed reservoir supplied by Westinghouse, at an initial pressure of approximately 0.1-mm Hg pressure.

In order that the pumping speed of the mass spectrometer tube exhaust system should be essentially independent of fluctuations in the pumping speed of the mercury diffusion pumps as well as the surface temperatures of traps, the "liquid nitrogen trap" supplied by the manufacturer was eliminated and a section of tubing was used to connect the mass spectrometer tube to the "mercury return trap" in order that the pumping speed at the mass spectrometer tube be geometrically controlled at *ca* 1 liter/sec.

The mass spectra were recorded with a Consolidated Engineering Corporation Recording Oscillograph, Type 5-104. The Recording Oscillograph is coupled in the usual manner to the third stage of a dc amplifier de-

[1] C. D. Wagner and D. P. Stevenson, J. Am. Chem. Soc. (to be published).
[2] Evans, Bauer, and Beach, J. Chem. Phys. 14, 701 (1946), CH_3D.
[3] Turkevich, *et al.*, J. Am. Chem. Soc. 70, 2638 (1948), CH_3D, C_2H_5D, *n*- and *i*-C_3H_7D.
[4] R. E. Honig, Phys. Rev. 75, 1319 (1949).

TABLE I. Mass spectra of methanes and ethanes, 75-ev 75°C magnetic scan., 1000-volt positive ion acceleration.

	CH_4	CH_3D	C_2H_6	C_2H_5D
S volts/cm	1.77	2.01	1.30	1.30
m/q				
12	0.0080	0.0063	0.0024	0.0024
13	0.0265	0.0131	0.0056	0.0044
14	0.0680	0.0289	0.032	0.015
15	0.733	0.111	0.041	0.038
16	1.000	0.624		0.024
17		1.000		
24			0.013	0.012
25			0.084	0.056
26			0.566	0.319
27			0.894	0.599
28			3.04	1.330
29			0.676	2.47
30			1.000	0.608
31				1.000

signed and constructed in these Laboratories.[5] The input resistance to the first stage of this amplifier is a Victoreen 10,800-megohms resistor. The sensitivity of the positive ion detection system is 4 meters/volt as measured by the deflection of the oscillograph G-1 on the recorder paper.

The mass spectra are tabulated as intensities of the various ion fragments relative to the intensity of the "parent ion" equal to unity (1.000), all ion intensities having been corrected for contributions of naturally occurring C^{13} containing species. These C^{13} corrections were made by means of the formula,

$$S_m^c=[S_m^0-n'\rho S^0_{m-1}+\tfrac{1}{2}(n'+1)(n'+2)\rho^2 S^0_{m-2}]/(1-\rho)^n, \quad (1)$$

where S_m^0, S_{m-1}^0, etc., are the observed intensities of the ions of $m/q=m$, $m-1$, etc., S_m^c is the C^{13} corrected intensity of the ion of $m/q=m$, n' is the number of carbon atoms in the ions $m/q=m$, $m-1$, etc., and ρ is the natural relative abundance of $C^{13}(C^{13}/C^{12})$. From measurements on CO_2 prepared from a number of pure hydrocarbons as well as E. K. Company, white label, ethyl bromide and *n*-propyl bromide, the value of ρ is 0.0102.

The mass spectra of the methanes and ethanes are given in Table I, those of the propanes in Table II, and those of the butanes in Table III. The H^+, D^+, H_2^+, and HD^+ ions were not measured. Ions of nonintegral m/q, which arise from the delayed dissociation of metastable ion states with half-lives greater than *ca* one microsecond are not tabulated;[6] nor are the intensities of doubly charged ions and weaker ions in the mass spectra.

Prior to correcting the mass spectra for their natural C^{13} content, the mass spectra of the various deutero paraffins were corrected for their C_nH_{2n+2} content determined as described elsewhere.[1]

Throughout this paper, unless otherwise explicitly stated, we will use the word "sensitivity" to denote the specific intensity of the parent ion, $C_n{}^{12}H_{2n+2}{}^+$ or $C_n{}^{12}H_{2n+1}D^+$. The value of the sensitivities given in Tables I, II, and III are in volts (across 10,800 megohms) per cm Hg pressure of $C_n{}^{12}H_{2n+2}$ or $C_n{}^{12}H_{2n+1}D$ in the 2-liter reservoir from which the gas flows through the leak to the mass spectrometer tube.

DISCUSSION

Before we enter into a detailed discussion of the mass spectra of the various isotopic substances, it appears desirable to give a short general discussion of the origin of the isotope effects in mass spectra and enumerate the theoretical conclusions which can be easily reached. The theory of the difference to be expected in the mass spectra of isotopic species of diatomic molecules appears to be in satisfactory form.[7,8] The agreement between the calculated and observed ratios of the dissociation probabilities of H_2^+ and D_2^+ formed by electron impact is well within the experimental uncertainty.[8,9] The general conclusion concerning the mass spectra of isotopic diatomic molecules is that by virtue of their greater amplitude of oscillation a larger fraction of the "light" isotopic species will have internuclear distances such that "Franck-Condon" transitions to energy levels above the dissociation limit of the molecule-ion may take place. Thus, the relative intensity of atomic ions in the mass spectra of the "light" isotopic species will be greater than in the "heavy" species. This conclusion has a hitherto unpublished corollary given in the following paragraph.

TABLE II. Mass spectra of propanes, 75-ev 75°C magnetic scan., 1000-volt positive ion acceleration.

	C_3H_8	C_3H_8-1-*d*	C_3H_8-2-*d*
S volts/cm	1.80	1.77	1.71
m/q			
14	0.0072		
15	0.0263	0.0172	0.0215
16	···	0.0144	0.0081
25	0.0083	0.0073	0.0058
26	0.109	0.0826	0.0622
27	0.631	0.427	0.348
28	1.213	0.945	0.635
29	1.986	1.488	1.337
30	···	1.106	2.005
36	0.0107	0.0098	0.0092
37	0.0696	0.0500	0.0522
38	0.112	0.0791	0.0831
39	0.375	0.214	0.251
40	0.0455	0.208	0.178
41	0.348	0.109	0.144
42	0.132	0.290	0.237
43	0.768	0.127	0.199
44	1.000	0.804	0.618
45		1.000	1.000

[5] The design and construction of this dc amplifier, which employs Victoreen electrometric tubes (VX-41) in both the first and second stages, was carried out under the direction of Mr. W. H. Thurston.

[6] For a discussion of the measurement of the lives of metastable ions formed by electron impact, see J. A. Hipple, Phys. Rev. **71**, 594 (1947).

[7] Bleakney, Condon, and Smith, J. Phys. Chem. **41**, 197 (1937).

[8] D. P. Stevenson, J. Chem. Phys. **15**, 409 (1947).

[9] N. Bauer and J. Y. Beach, J. Chem. Phys. **15**, 150 (1947).

The electronic energy of molecules is to a high approximation independent of the mass of the nuclei.[10] Thus, the probability of ionization by electron impact will be equal for all isotopic species to this same approximation; and for all other conditions equal, the total number of molecule-ions formed will be independent of the isotopic species. Since a larger fraction of the light isotopic species will result in molecule-ions which dissociate (see above), the specific intensity, i.e., the sensitivity, of the "parent-ion" of the light isotopic species will be smaller than that of the "heavy" species.

In polyatomic molecules, the smaller average amplitudes of oscillation of "heavy" isotopic species will also result in a smaller fraction of the "heavy" molecules than of the "lighter" molecules having configurations which permit transitions to levels above dissociation limits of the molecule-ions. Polyatomic molecules differ from diatomic molecules in several important respects that together are sufficient to reverse the sign of the isotope effects in the mass spectra of the polyatomic molecules. The most important difference between diatomic and polyatomic molecules is that alternate dissociation fragments differ in zero-point energy. If we consider, for example, the electron impact induced process of the molecule ABA,

$$ABA+\epsilon^-\rightarrow A+BA^++2\epsilon^-, \tag{2}$$

proceeding through, $ABA+\epsilon^-\rightarrow ABA^++2\epsilon^-$, followed by dissociation, there are two alternate, identical, dissociation paths if both A are the same isotope. If we consider the isotopic molecule, ABA', where A' is a "heavier" isotope of A, then the process

$$ABA'+\epsilon^-\rightarrow A+BA'^+2\epsilon^- \tag{3}$$

will be more probable than

$$ABA'+\epsilon^-\rightarrow A'+AB^++2\epsilon^- \tag{4}$$

by virtue of the lower zero-point energy of BA'^+ than of AB^+; and thus the intensity of BA'^+ in the mass spectrum of ABA' will be greater than that of AB^+. Depending on the magnitude of the isotope effect on the amplitudes of oscillation in the ground state, the intensity of BA'^+ in the mass spectrum of ABA' may be greater than, equal to, or less than one-half that of AB^+ in the mass spectrum of ABA. The intensity of AB^+ in the mass spectrum of ABA' will always be less than one-half that of AB^+ in the mass spectrum of ABA.

In the case of hydrocarbons a greater fraction of the molecules have configurations that result in electron impact-induced dissociation than do diatomic molecules.[11] Thus, the effects of changes in amplitude in the molecule are probably less important in determining dissociation probabilities than the effects of changes in zero-point energy of the dissociation products brought about by isotopic substitution. However, the fact that the changes in amplitude associated with rather small temperature changes markedly affect the degree of dissociation of molecule-ions formed by electron impact,[11] indicates the *a priori* evaluation of the relative importance of ground-state energies and fragment energies is not possible.

TABLE III. Mass spectra of butanes, 75-ev 75°C magnetic scan., 1000-volt positive ion acceleration.

	n-C_4H_{10}	n-C_4H_{10}-1-d	n-C_4H_{10}-2-d	i-C_4H_{10}	i-C_4H_{10}-1-d	i-C_4H_{10}-2-d
S volts/cm	1.50	1.52	1.47	0.465	0.452	0.420
m/q						
14				0.022		
15	0.0274	0.0189	0.0222	0.122	0.087	0.114
16		0.0128	0.0077		0.049	0.038
26	0.121	0.093	0.089	0.171	0.136	0.135
27	0.870	0.621	0.591	2.46	1.718	1.838
28	0.905	0.825	0.866	0.167	0.922	1.336
29	1.247	0.933	1.060	0.660	0.370	0.536
30		0.673	0.659		0.322	0.253
39	0.391	0.272	0.223	1.90	1.24	1.37
40	0.0400	0.148	0.202	0.221	0.856	1.022
41	1.132	0.619	0.366	5.64	2.70	2.00
42	0.555	0.825	0.905	6.16	5.57	4.86
43	4.30	2.29	0.649	16.24	9.01	7.31
44		2.44	4.42		11.96	19.42
55	0.0488	0.0250	0.0162	0.0836	0.0221	0.042
56	0.0374	0.0420	0.0424	0.0770	0.0764	0.101
57	0.138	0.0368	0.0382	0.669	0.0644	0.422
58	1.000	0.146	0.117	1.000	0.712	0.0568
59		1.000	1.000		1.000	1.000

The complete absence of knowledge concerning the nature of the potential energy surfaces of polyatomic molecule-ions precludes the *a priori* evaluation of the relative importance of the effects described above. However, the origin of the mass spectral isotope effects, named by Evans, Bauer, and Beach,[2] the π- and Γ-effects, is explained.

The argument given above indicates that the dissociation probability of various isotopic species may be expected to be different. Referring to our discussion of the relative sensitivities of isotopic diatomic molecules, we conclude that different isotopic species may have different sensitivities, and thus that equality of the apparent sensitivities of isotopic species is not a criterion of purity of isotopic preparations.

One further qualitative conclusion can be reached. Considering again the process,

$$ABA+\epsilon^-\rightarrow A+BA^++2\epsilon^-, \tag{5}$$

and that in the second isotopic species, $A'BA'$. The lower zero-point energy of the again equivalent dissociation fragments, BA'^+, will compensate for the smaller amplitude of oscillation of the heavier species, $A'BA'$; and thus we expect the mass spectrum of $A'BA'$, to be much more like that of ABA than will be that of the unsymmetrical ABA'.

Among isotopic hydrocarbons, the simplest set is the group of acetylenes: acetylene, acetylene-d_1 and acetylene-d_2. The mass spectra of these acetylenes have been measured with a Consolidated mass spec-

[10] G. Herzberg, *Atomic Spectra and Atomic Structure* (Prentice-Hall, Inc., New York, 1937), Chapter V.

[11] For the temperatures which commonly obtain in mass spectrometer tubes, 75–250°C, over 50 percent of the paraffin ions formed by electron impact (20- to 100-volt electrons) dissociate; see, for instance, D. P. Stevenson, J. Chem. Phys. **17**, 101 (1949). Only 2 percent of the hydrogen molecule-ions formed by electron impact dissociate, see reference 9.

TABLE IV. Application of Eq. (10) to the mass spectrum of methyl deuteride.

m/q	$\sigma_m{}^H$	$\sigma_{m-1}{}^D$	$\delta S_m\left(\begin{smallmatrix}\pi=1\\ \Gamma=1\end{smallmatrix}\right)$	$\delta S_m\left(\begin{smallmatrix}\pi=0.45\\ \Gamma=1.13\end{smallmatrix}\right)$
17	...	1	(0.0)	(0.0)
16	...	$\frac{1}{2}$	−11.9	−0.6
15	$\frac{1}{4}$	$\frac{1}{2}$	+95.5	+13.5
14	$\frac{1}{2}$	$\frac{1}{4}$	+40.5	−6.9
13	$\frac{1}{2}$	...	+51.3	−13.0
12	1	...	+27.0	−17.4

trometer.[12] It is found that the specific probability of the processes,

$$C_2H_2+\epsilon^-\rightarrow C_2H^++H+2\epsilon^-, \quad (6)$$

$$C_2HD+\epsilon^-\rightarrow C_2H^++D+2\epsilon^-, \quad (7)$$

$$C_2D_2+\epsilon^-\rightarrow C_2D^++D+2\epsilon^-, \quad (8)$$

are in the ratio, 1:0.6:0.9, while the specific probability of the process

$$C_2HD+\epsilon^-\rightarrow C_2D^++H+2\epsilon^- \quad (9)$$

on the same scale is 1.2. We see that the decrease in amplitude in the heavy acetylenes is more important than the lowering of the zero-point energy of C_2D^+ in determining the mass spectra, since the decrease in the specific probability of $C_2HD^+\rightarrow C_2H^++D$ is greater than the increase in that of $C_2HD^+\rightarrow C_2D^++H$ and the process $C_2D_2^+\rightarrow C_2D^++D$ is less probable than $C_2H_2^+\rightarrow C_2H^++H$. This is not out of line with the discussion above, since between 75 and 300°C only about 20 percent of the $C_2H_2^+$ ions dissociate.[11]

The absence of a quantitative character to the theory of mass spectral isotope effects discussed above is quite serious from the analytical point of view. A casual survey of Tables I, II, and III immediately reveals that quantitative analysis of isotopic mixtures of hydrocarbons is not possible unless the mass spectra of all isotopic species that may be in the mixture are known.[13] Thus, in order that tracer studies of the reactions of hydrocarbons may realize their complete potential, a means of estimating reasonably accurately the mass spectra of unavailable isotopic species is needed.[14] At present the empirical approach suggested by Delfosse and Hipple[15] and modified by Evans, Bauer, and Beach[2] appears to be the most practical one to the problem of predicting the mass spectrum of a given deutero-paraffin from the mass spectrum of the paraffin. With a slight modification, the method consists of assigning values to two "isotope parameters," π and Γ, which measure the decrease in the probability of the process, $C_nH_{2n+1}D^+\rightarrow C_nH_{2n+1}{}^++D(\pi)$, and the increase in the probability of the process, $C_nH_{2n+1}D^+\rightarrow C_nH_{2n}D^++H(\Gamma)$, with respect to the probability of the process $C_nH_{2n+2}{}^+\rightarrow C_nH_{2n+1}{}^++H$, and assuming the value of Γ to be applicable to all H's in the molecule.[16] In this notation the relative intensity at any m/q in the C_n portion of the mass spectra of $C_nH_{2n+1}D$ is written

$$S_m=\sigma_m{}^H\Gamma^n\pi\rho_m+\sigma_{m-1}{}^D\Gamma^{n+2}\rho_{m-1}, \quad (10)$$

where Γ and π have been defined, n is the number of hydrogens that must be removed from C_nH_{2n+2} to give the ion m/q, ρ_m and ρ_{m-1} are the relative intensities of the ions m/q and $(m-1)/q$ in the mass spectrum of C_nH_{2n+2}, and $\sigma_m{}^H$ and $\sigma_{m-1}{}^D$ are statistical weights equal to the ratio of the number of ways the two ions m/q can be formed from $C_nH_{2n+1}D$ to the number of ways the corresponding ions can be formed from C_nH_{2n+2}. For instance, the two ions of $m/q=15$ in the CH_3D mass spectrum are CH_3^+ and CHD^+. For $m/q=15$ of the mass spectrum of CH_3D, $\sigma_{15}{}^H=1/4$ and $\sigma_{14}{}^D=3/6$, corresponding, respectively, to the one way CH_3^+ can be formed from CH_3D and the four ways CH_3^+ can be formed from CH_4, and the three ways CHD^+ can be formed from CH_3D and the six ways of forming CH_2^+ from CH_4. By evaluating the parameters π and Γ by means of the intensities of a pair of appropriate ions in the mass spectra of the monodeuteride and the ordinary hydrocarbon, the remainder of the "parent region" mass spectrum of the deuteride is calculable from that of the ordinary hydrocarbon. To the extent the parameters π and Γ are general ones, it should be possible to predict the mass spectra of other hydrocarbons.

As might be expected from the qualitative theory described above, it turns out that the specific effects in each hydrocarbon are too complex to be represented by but two parameters. This is illustrated in Tables IV and V, where the results of the application of Eq. (10) to the mass spectra of the methyl and ethyl deuterides, respectively, are shown. In these tables there are tabulated for the ions $12\leqslant m/q\leqslant 16$ of methyl deuteride and $24\leqslant m/q\leqslant 30$ of ethyl deuteride, the values of $\sigma_m{}^H$ and $\sigma_{m-1}{}^D$ and the quantities

$$\delta S_m=[(S_{\text{calc}}-S_{\text{obs}})/S_{\text{obs}}]\times 100$$

for $\pi=\Gamma=1$ and $\pi=0.45$ and $\Gamma=1.13$. The first pair of values of π and Γ correspond to no isotope effect. In the case of the second pair the value, $\Gamma=1.13$, was chosen to fit S_{16} of the methyl deuteride mass spectrum and the value $\pi=0.45$ is the average of the values that fit S_{15} ($\pi=0.37$) and S_{13} ($\pi=0.52$) of this mass spectrum. In the evaluation of the σ for ethane, it was assumed

[12] F. L. Mohler and V. H. Dibeler, Phys. Rev. **72**, 158 (1947). The results of Mohler and Dibeler have been confirmed in these Laboratories with a Consolidated mass spectrometer, and furthermore there is good agreement between Westinghouse and Consolidated mass spectra (these Laboratories).

[13] Qualitative distinction of certain species is possible in some cases as has been noted by Turkevich, *et al.* (reference 3).

[14] For examples of the large variety of species which can arise, see Wagner, Beeck, Otvos, and Stevenson, J. Chem. Phys. **17**, 419 (1949), on the reactions of monodeutero paraffins in the presence of an aluminum chloride-alumina catalyst.

[15] J. Delfosse and J. A. Hipple, Phys. Rev. **54**, 1060 (1938).

[16] We will from this point onward restrict our discussion to the relation between the mass spectra of deutero-paraffins.

that the ions $C_2H_4^+$, $C_2H_3^+$, and $C_2H_2^+$ have the ethylene, vinyl, and acetylene structures as is suggested by the appearance potentials of these ions in the mass spectra of ethane.[17]

It is apparent from the calculations summarized in Tables IV and V that a simple two parameter equation like Eq. (10) cannot represent the mass spectrum of a single monodeuteride. However, in view of the complex nature of the phenomenon that Eq. (10) attempts to represent, it is surprising that the two parameters chosen for the methyl deuteride mass spectrum do as well as they do in representing the ethyl deuteride mass spectrum. Furthermore, contrary to the opinion expressed by Turkevich, *et al.*,[3] a better representation of the mass spectrum of the monodeuterides is obtained with $\pi<1$ and $\Gamma>1$ than when it is assumed that there are no isotope effects; i.e., $\pi=\Gamma=1$.

Comparison of the individual S_m (1, 1) and S_m (0.45, 1.13) indicates that in all cases the probability of breaking a C—D bond in a particular manner is less than that of breaking an equivalent C—H bond, i.e., $\pi<1$, and that the probability of breaking a particular C—H bond in the deuteride is always greater than that of breaking an equivalent C—H bond in the ordinary hydrocarbons, i.e., $\Gamma>1$. These two observations are in complete agreement with the qualitative theory outlined above.

Calculations similar to those for methyl and ethyl deuteride have been made for the propyl and butyl deuterides and with similar results. For brevity only a few of the more interesting results will be presented here.

From the facts that $S_{44}(C_3H_8\text{-}2\text{-}d)<S_{43}(C_3H_8\text{-}d_0)<S_{44}(C_3H_8\text{-}1\text{-}d)$ and $S_{58}(n\text{-}C_4H_{10}\text{-}2\text{-}d)<S_{57}(n\text{-}C_4H_{10}\text{-}d_0)<S_{58}(n\text{-}C_4H_{10}\text{-}1\text{-}d)$, it is apparent that in the processes

$$C_3H_8+\epsilon^-\rightarrow C_3H_7^++H+2\epsilon^- \qquad (11)$$

$$n\text{-}C_4H_{10}+\epsilon^-\rightarrow C_4H_9^++H+2\epsilon^- \qquad (12)$$

the ions $C_3H_7^+$ and $C_4H_9^+$ are most often formed through the loss of a secondary hydrogen atom. Similarly, since $S_{58}(i\text{-}C_4H_{10}\text{-}2\text{-}d)<S_{57}(i\text{-}C_4H_{10}\text{-}d_0)<S_{58}(i\text{-}C_4H_{10}\text{-}1\text{-}d)$, it can be concluded that in the process

$$i\text{-}C_4H_{10}+\epsilon^-\rightarrow C_4H_9^++H+2\epsilon^- \qquad (13)$$

the ion $C_4H_9^+$ is most often formed through the loss of a tertiary hydrogen.

If we represent by p, s, and t the probabilities of dissociation of primary, secondary, and tertiary hydrogens in such processes as Eqs. (11), (12), and (13), we may write for the relative intensities of $C_3H_7^+$ in the propane-d_0 mass spectrum and of $C_3H_6D^+$ in the propane-d mass spectra the equation

$$\begin{aligned}&\rho_{43}=6p_3+2s_3;\quad C_3H_8\text{-}d_0\\ &S_{44}=\Gamma(5p_3+2s_3);\quad C_3H_8\text{-}1\text{-}d\\ &S_{44}=\Gamma(6p_3+s_3);\quad C_3H_8\text{-}2\text{-}d\end{aligned} \qquad (14)$$

[17] J. A. Hipple, Phys. Rev. **53**, 530 (1938). D. P. Stevenson and J. A. Hipple, J. Am. Chem. Soc. **64**, 1588 (1942).

TABLE V. Application of Eq. (10) to the mass spectrum of ethyl deuteride.

m/q	σ_m^H	σ_{m-1}^D	$\delta S_m\left(\begin{smallmatrix}\pi=1\\ \Gamma=1\end{smallmatrix}\right)$	$\delta S_m\left(\begin{smallmatrix}\pi=0.45\\ \Gamma=1.13\end{smallmatrix}\right)$
31	...	1	(0.0)	(0.0)
30	...	$\frac{5}{6}$	−7.4	+4.6
29	$\frac{1}{6}$	$\frac{2}{3}$	−13.4	+6.5
28	$\frac{1}{3}$	$\frac{1}{2}$	+9.8	−12.9
27	$\frac{1}{2}$	$\frac{1}{3}$	+6.0	−5.9
26	$\frac{2}{3}$	$\frac{1}{6}$	+22.9	−15.0
25	$\frac{5}{6}$	...	+25.0	−8.9
24	1	...	+8.3	−8.3

and similar equations for ρ_{57} and S_{58} of the various butane mass spectra. Solutions of such equations for the data given in Tables II and III yield:

$$\begin{aligned}&\text{propane,}\quad p_1/s_3=0.25,\quad \Gamma_3=1.13;\\ &n\text{-butane,}\quad p_{n4}/s_{n4}=0.10,\quad \Gamma_{n4}=1.08;\\ &i\text{-butane,}\quad p_{i4}/t_{i4}=0.030,\quad \Gamma_{i4}=1.09.\end{aligned}$$

We note that the values of Γ for the dissociation of a single hydrogen by the propyl and butyl deuteride molecule-ions are about equal to those for the corresponding processes in methyl deuteride ($\Gamma_1=1.13$) and ethyl deuteride ($\Gamma_2=1.08$). Thus, it appears that for the process,

$$C_nH_{2n+1}D+\epsilon^-\rightarrow C_nH_{2n}D^++H+2\epsilon^- \qquad (15)$$

in the monodeutero paraffins, the specific probability of the dissociation of an hydrogen atom is about 10 percent greater than in the corresponding ordinary paraffin.

The relative probabilities of dissociating primary and secondary or primary and tertiary hydrogens calculated from Eqs. (14) and the data of Tables II and III are in agreement with the general concept that the strength of carbon hydrogen bonds decrease in the order, primary>secondary>tertiary. In terms of the qualitative model of the isotope effect described above, the difference in the specific probability of the dissociation of equivalent C—D and C—H bonds by a given molecule-ion arises from the difference in the zero-point energies of the fragments produced; and the ratio of these dissociation probabilities is π/Γ for the molecule. The different dissociation probabilities for primary, secondary, and tertiary C—H bonds arise in a similar manner; and thus to the extent that π/Γ measures the difference in the energy levels of two dissociation paths of a single energy surface, the ratios p/s and p/t should likewise be measures of the difference in the energy levels of the alternate paths by which a molecule-ion can dissociate either a primary or a secondary or a primary or a tertiary hydrogen. However, our ignorance of how these differences in energy levels quantitatively affect alternative dissociation probabilities is the glaring weakness of the theory outlined above; and thus it is not apparent how differences in dissociation energies can be deduced from the ratio of dissociation probabilities.

The intensities of the ions of $m/q=30$ in the mass spectra of the propane-*d*'s and those of the ions of $m/q=44$ in the mass spectra of the butane-*d*'s are of considerable interest. This arises from the fact that energetic considerations[18] suggest that such processes as,

$$RCH_3^+ \rightarrow R^+ + CH_3, \qquad (16)$$

which give rise to these ions are of the simple type represented by Eqs. (2), (3), and (4). We find that the intensities $m/q=30$ (propane-1-*d*) and $m/q=44$ (*n*-butane-1-*d*) are 11.4 percent and 13.5 percent greater, respectively, than one-half those of $m/q=29$ (propane-d_0) and $m/q=43$ (*n*-butane-d_0) and that the intensity of $m/q=44$ (*i*-butane-1-*d*) is 10.4 percent greater than two-thirds that of $m/q=43$ (*i*-butane-d_0). These greater intensities of the "heavy isotopic species" cannot be due to a rearrangement of atoms prior to dissociation, as has recently been suggested,[4] since we also find the intensity of $m/q=30$ (propane-2-*d*) to be one percent greater than that of $m/q=29$ (propane-d_0), and the intensities of $m/q=44$ (*n*-butane-2-*d* and *i*-butane-2-*d*) to be 2.8 percent and 19.6 percent greater, respectively, than those of $m/q=43$ (*n*-butane-d_0 and *i*-butane-d_0). In terms of the qualitative discussion given above, this indicates the differences in zero-point energy of the alternate dissociation paths on the surfaces of the molecule-ion to be of greater importance in determining the relative dissociation probabilities of isotopic species than changes in amplitude in the ground state. The close equality of the isotope effects on such processes as Eq. (16) in propane-1-C^{13} and propane-1-*d*, *n*-butane-1-C^{13} and *n*-butane-1-*d*, etc.,[19] is in accord with the simple theory of the phenomenon.

That in certain states of molecule-ions extensive rearrangements of the hydrogens precede the dissociation process is apparent when the quite significant intensity of the ion $m/q=16(CH_2D^+)$ in the mass spectra of propane-2-*d*, *n*-butane-2-*d*, and *i*-butane-2-*d* is noted. The nature of the mass spectra of these samples is such that there is no possibility that the intensity of the CH_2D^+ ion in their mass spectra might be due to contamination by isomeric isotopic species.[20] It is not clear whether these rearrangements are isomerizations in the chemical sense, i.e., whether they indicate the presence of several minima on the potential energy hypersurface of the ion-state or simply the result of the failure of the concept of directed valence in highly energized states because of amplitudes of oscillation becoming comparable in magnitude with interatomic separations. In this regard it is probably significant that the appearance potentials of such ions as CH_3^+ in the propane and butane mass spectra and $C_2H_5^+$ in the isobutane mass spectrum[17,21] are significantly (2–10 ev) greater than the energies required for the simplest reactions which may be written.

It was indicated above that it would be expected that there should be isotope effects on the sensitivity (parent ion) as well as on the relative probability of forming particular fragments. In Tables I and II we find all possible cases: the parent ion sensitivities of monodeutero paraffins less than, equal to, and greater than those of the corresponding hydroparaffins. Only one case requires special mention, namely, that of methane and methyl deuteride. The discrimination in the ion-source of the Westinghouse mass spectrometer is such that for $m/q>22$–24 the fraction of the ions lost during acceleration is proportional to $(V)^{-\frac{1}{2}}$, where V is the positive ion accelerating potential. The origin of this loss has been discussed for an idealized ion source by Coggeshall.[22] Owing to the use of a small magnetic field (*ca* 150 gauss) across the ion source to align the ionizing electron beam, the fraction of the ions lost during acceleration is proportional to $(MV)^{-\frac{1}{2}}$ for $m/q(M)<22$–24. Thus, when magnetic scanning of mass spectra is employed, the efficiency of collection of ions $CH_3D^+(m/q=17)$ is greater than that of ions $CH_4^+(m/q=16)$. The magnitude of this effect in our Westinghouse mass spectrometer is such that the efficiency of collection of CH_3D^+ is *ca* 10 percent greater than that of CH_4^+ ions. It should be noted that this discrimination effect distorts only the apparent relative sensitivities of CH_3D and CH_4, not the comparison of relative intensities in the mass spectra of the two methanes. This latter fact results from a cancellation of the discrimination effects when the ratio of the intensities of two ions in the mass spectrum of a single substance is computed.

When allowance has been made for the effects of ion discrimination, the sensitivity of CH_3D is but 2–3 percent rather than 12–13 percent greater than that of CH_4. This difference corresponds closely to the difference in the fraction the respective parent ions contribute to the mass spectra of these compounds; that is the dissociation probabilities of CH_3D^+ ions formed by 75-volt electron impact are 2–3 percent smaller than those of similarly formed CH_4^+ ions.

ACKNOWLEDGMENT

The authors wish to express their indebtedness to their colleagues, particularly Dr. O. Beeck and Dr. J. W. Otvos for stimulating discussions during the course of this work.

[18] D. P. Stevenson, J. Chem. Phys. **10**, 291 (1942).
[19] D. P. Stevenson, J. Chem. Phys. **19**, 17 (1951).
[20] Propane-2-*d* is unique in that the infrared absorption at 13.3–13.7μ permits an absolute upper limit of 4 percent to be set to the contamination by propane-1-*d*. See reference 1.
[21] M. B. Koffel and R. A. Lad, J. Chem. Phys. **16**, 420 (1948). J. J. Mitchell and F. F. Coleman, *ibid.* **17**, 44 (1949).
[22] N. D. Coggeshall, J. Chem. Phys. **12**, 19 (1944).

On the Mass Spectra of Propanes and Butanes Containing C^{13}

D. P. STEVENSON
Shell Development Company, Emeryville, California

(Received August 28, 1950)

A mass spectrometric method of analysis of C^{13} enriched samples of paraffins, both with respect to the gross concentrations of $-C_0^{13}$, $-C_1^{13}$, and $-C_2^{13}$ species and the concentration of C^{13} isomeric species is described, with particular reference to samples of propane-1$-C^{13}$, propane-2$-C^{13}$, *n*-butane-1$-C^{13}$, *n*-butane-2$-C^{13}$, *i*-butane-1$-C^{13}$, and *i*-butane-2$-C^{13}$ prepared in connection with tracer studies of certain paraffin reactions. With respect to the analysis, the necessary *a priori* assumptions and *a posteriori* checks of the assumptions are described.

The relative intensities of certain C_1 and C_2 ion fragments characteristic of the 75-ev mass spectra of propane$-C_0^{13}$, propane-1$-C_1^{13}$, and propane-2$-C_1^{13}$, and certain C_1, C_2, and C_3 ion fragments characteristic of the 75-ev mass spectra of the six similar butanes are tabulated. The isotope effects on the dissociation probabilities of certain states of the propane and butane molecule-ions are discussed in terms of a simple qualitative model.

Of particular interest is the observation that in the states of $C_3H_8^+$ which dissociate into C_1 ion fragments, and the states of i-$C_4H_{10}^+$ which dissociate into C_1 or C_2 ion fragments the carbon atoms become essentially indistinguishable, and the mass spectra of the isomeric C_1^{13} compounds become essentially identical as far as the relative intensities of these fragments are concerned.

INTRODUCTION

In this paper there are described the isotopic analyses and the mass spectra of certain propanes and butanes "labeled" in one position with C^{13} that have been prepared in the Laboratories in connection with fundamental studies of certain paraffin reactions.[1–3] Since pure specimens of C^{12} or C^{13} are not as yet available, C^{13} labeled compounds necessarily only exist as mixtures of several isotopic compounds, differing from the particular compound of interest both in the relative number of C^{12} and C^{13} atoms in the molecule and in the positions of the C^{12} and C^{13}. The determination of the complete composition of a preparation of a C^{13} labeled compound from its mass spectrum involves a number of points which to the author's knowledge have not been discussed previously.

The mass spectra of the various C^{13} labeled substances are of interest in several connections. The existence of isotope effects in the mass spectra (i.e., changes in the dissociation probability of molecule-ions formed by electron impact) provides a basis for understanding what have previously been thought to be anomalous intensities in the mass spectra of ordinary hydrocarbons. Furthermore, the magnitude of the isotope effects in the mass spectra reveals the necessity of having authentic specimens of all isotopic species available prior to undertaking quantitative analyses in connection with tracer studies involving the use of C^{13} labeled substances.[4] The distribution of intensities among certain ion fragments of the electron impact induced ionization and dissociation process provides interesting information on the nature and molecular structure of some of the states of molecule-ions.

[1] Beeck, Otvos, Stevenson, and Wagner, J. Chem. Phys. **16**, 255 (1948).
[2] Otvos, Stevenson, Wagner, and Beeck, **16**, 745 (1948).
[3] Stevenson, Wagner, Beeck, and Otvos, J. Chem. Phys. **16**, 993 (1948).
[4] See also Evans, Bauer, and Beach, J. Chem. Phys. **14**, 701 (1946) on the analysis of mixed deuteromethanes.

EXPERIMENTAL

The preparation and purification of the various C^{13} labeled propanes and butanes discussed in this paper have been described elsewhere.[5] Similarly the modifications and operational details of the Westinghouse Type LV mass spectrometer have been described.[6] All mass spectra described here were recorded with magnetic scanning of the ions and are those characteristic of 75-volt ionizing electrons. The gas enters the ionization chamber of the mass spectrometer at approximately 75°C.

DISCUSSION

Isotopic Analysis

As has been indicated in the introduction, C^{13} labeled hydrocarbons are not available as pure specimens. In addition to the isotopic compound of primary interest, there are important concentrations of other isotopic species and isotopic isomers which arise in the synthesis from the natural C^{13} content of the "natural" reagents as well as the C^{12} content of the enriched reagent. Thus, in the preparation of propane-1$-C^{13}$ starting with the reaction of potassium cyanide (*ca* 50 percent C^{13}) with natural ethyl bromide[7] there are obtained in addition to *ca* 50 percent propane-1$-C^{13}$, and 48 percent$-C_0^{13}$, *ca* 0.5 percent each of propane-2$-C^{13}$, propane-1,2$-C_2^{13}$, and propane-1,3$-C_2^{13}$. Hence, the first step in the interpretation of the mass spectrum of a C^{13} labeled preparation is the determination of the concentrations of the isotopic species.

In order to determine the isotopic species composition of a sample from its mass spectrum, two assumptions

[5] See references 1 and 2 and C. D. Wagner, J. Am. Chem. Soc. (to be published).
[6] D. P. Stevenson and C. D. Wagner, J. Chem. Phys. **18**, 11 (1950).
[7] See references 1 and 5 for reaction sequence.

TABLE I. Propane−C^{13} samples—analyses.

	Propane-1 −C^{13}	Propane-2 −C^{13} [c]
Σ^0 %[a]	99.6±0.7	98.8±0.5
δ43%[b]	0.0	+0.7
δ42%	−0.7	+0.5
δ41%	−0.8	+0.5
δ40%	+0.9	+1.4
δ39%	−0.5	+0.1
$-C_0^{13}$%	45.7±0.5	45.3±0.5
$-1-C_1^{13}$%	52.7±0.5	35.8±0.4
$-2-C_1^{13}$%	0.53±0.01	17.9±0.2
$-C_2^{13}$%	1.12±0.02	1.13±0.02
η	0.533	—

[a] $\Sigma^0 = C_3H_8 - C_0^{13} + C_3H_8 - C_1^{13} + C_3H_8 - C_2^{13}$ unnormalized original sum.
[b] $\delta_m = \frac{S_m(\text{obs.}) - S_m(\text{calc.})}{S_m(\text{obs.})} \times 100$.
[c] This material from propane-1 −C^{13} by isomerization over Al_2Br_6. See reference 1 for evidence of attainment of equilibrium.

TABLE II. Analysis of butane−C^{13} samples.

	n-butane-1 −C^{13}	*n*-butane-2 −C^{13} [b]	*i*-butane-1 −C^{13}	*i*-butane-2 −C^{13}
Σ^0% [a]	99.2±1.0	98.9±1.0	98.4±0.3	98.2±1.2
δ57%	+0.8	+0.1	−0.8	+0.7
δ56%	+1.6	−2.0	+1.7	+2.0
δ55%	+0.4	−0.8	+1.0	+0.3
$-C_0^{13}$%	81.0±0.3	81.0±0.3	50.3±0.3	81.5±0.3
$-1-C_1^{13}$%	16.8±0.2	9.22±0.2	47.7±0.5	2.47±0.02
$-2-C_1^{13}$%	1.64±0.02	9.22±0.2	0.51±0.01	15.5±0.2
$-C_2^{13}$%	0.52±0.02	0.56±0.02	1.44±0.02	0.49±0.02
η	0.165	—	0.482	0.160

[a] $\Sigma^0 = C_4H_{10} - C_0^{13} + C_4H_{10} - C_0^{13} + C_4H_{10} - C_0^{13}$ unnormalized original sum.
[b] This material from *n*-butane-1 −C^{13} by isomerization over Al_2Br_6. See reference 2 for evidence of attainment of equilibrium.

must be made that are subject to partial *a posteriori* confirmation. These assumptions are: (1) that the parent ion sensitivities of the various C^{13} isotopic species are equal[8] and (2) that the probabilities of the various carbon-isotopic molecule-ions losing one or more hydrogen atoms or molecules to form "stripped" ions are equal. These two assumptions, in combination with a knowledge of the monoisotopic mass spectrum of the hydrocarbon and the intensity of three ions in the mass spectrum of the labeled specimen, suffice to determine the concentration of the $-C_0^{13}$, $-C_1^{13}$, and $-C_2^{13}$ species of the specimen.[9] Since in the mass spectra of paraffins there are present many more than three ions, the quality of assumption (2) may be tested by comparing the mass spectrum calculated from the so-determined concentrations with that observed. If such calculations verify assumption (2), then the degree to which the sum of the concentrations of the $-C_0^{13}$, $-C_1^{13}$, and $-C_2^{13}$ species add to 100 percent is a measure of the accuracy of assumption (1).

The calculations outlined in the preceding paragraph presuppose a knowledge of the mass spectrum of the $-C_0^{13}$ hydrocarbon. This may be calculated from the mass spectrum of an ordinary hydrocarbon[10] in the following manner. The specific intensity (sensitivity coefficient) of a singly charged ion, m/q in the mass spectrum of a $C_n{}^{12}H_m$ ($m=2n+2$, $2n$, $2n-2$, etc.) hydrocarbon is related to the observed specific intensities of the ions in the mass spectrum of the ordinary hydrocarbon by the formula

$$S_m{}^c = \left[S_m{}^0 - n'\rho S_{m-1}{}^0 + \frac{(n'+1)(n'+2)}{2}\rho^2 S_{m-2}{}^0 \right] / (1-\rho)^n, \quad (1)$$

where the S^c and S^0 are the specific intensities of the $C_n{}^{12}H_m$ and ordinary C_nH_m mass spectra, respectively, n' is the number of carbon atoms in the singly charged ions, m/q, $m-1/q$, $m-2/q$, and ρ is the natural ratio of C^{13} to C^{12}.[11] The formula (1) only corrects for the natural C^{13} content of the hydrocarbon, giving the spectrum of $C_n{}^{12}H_m$ uncorrected for natural deuterium. Since deuterium is present in its natural concentration (*ca* 0.02 percent) in the labeled C^{13} preparations, this neglect of deuterium will tend to cancel in the comparison of the mass spectra of the various carbon isotopic species. The formula (1) neglects possible isotope effects on the dissociation probability of the molecule-ions. However, this can only introduce small errors since the magnitude of the "carbon isotope effects" are of the order of five to ten percent at most and for the ions of interest the corrections are only of the order of five percent.

For the isotopic species analyses of C^{13} labeled propanes and butanes, the three ions used are those corresponding to the parent ions of the three isotopic species, $-C_0^{13}$, $-C_1^{13}$, and $-C_2^{13}$, i.e., $m/q=44$, 45, and 46 for propane and $m/q=58$, 59, and 60 for the butanes. In the case of the propane mass spectrum, the intensities of the ions corresponding to the removal of one to five hydrogens are sufficient that all may be used in checking the validity of assumption (2). For the butanes the intensities of the ions formed by the removal of two or more hydrogens are all so weak that only the calculation of the intensity of $m/q=57$ provides a reasonable test of the validity of assumption (2) for the butanes. However, since the intensities of the hydrogen stripped ions formed from the butanes are low, the accuracy of assumption (2) has relatively little effect on the accuracy of the isotopic analysis.

The results of analyses as described above of two propane−C^{13} samples are summarized in Table I and those of four butane−C^{13} samples are shown in Table II.

[8] It has been shown that for certain monodeuteroparaffins this is not true; see reference 6.
[9] Although it is present, the concentration of $-C_2^{13}$ hydrocarbon is negligibly small in all cases of interest herein.
[10] Phillips certified propane (99.9+ percent), *n*-butane (99.7+ percent), and isobutane (99.8+ percent) were used as reference compounds in this investigation.
[11] For the Phillips hydrocarbons as well as Eastman Kodak Company White Label C_2H_5Br and *n*-C_3H_7Br, ρ as measured with our mass spectrometer = 0.0102±0.0001. This value of ρ was obtained from measurements of the 45/44 ratio of carbon dioxide (corrected for natural O^{17}) prepared by the complete combustion of the various substances.

In the case of the propanes and *n*-butanes the small difference between calculated and observed intensities of the hydrogen stripped ions and the accuracy to which the sum of the $-C_0^{13}$, $-C_1^{13}$, and $-C_2^{13}$ species add to 100 percent indicate both assumptions (1) and (2) to be valid for these substances. In the case of the isobutanes, assumption (2) appears to be sufficiently valid, but the low value of the sums of $-C_0^{13}$, $-C_1^{13}$, and $-C_2^{13}$ indicate that the parent ion sensitivity of both isobutane-1$-C^{13}$ and isobutane-2$-C^{13}$ may be of the order of two to four percent less than that of isobutane$-C_0^{13}$. However, the magnitude of the apparent error in assumption (1) for the isobutanes is sufficiently small that it may be neglected for the purposes of this paper.[12]

Given the relative concentrations of the $-C_0^{13}$, $-C_1^{13}$, and $-C_2^{13}$ species in a hydrocarbon preparation and the method of synthesis it is possible to calculate the relative quantities of the various isotopic isomers provided there is no significant preferential reactivity of the various isotopic reagents. This calculation is most easily made in terms of the C^{13} content of the enriched reagent which we designate by η (in mole fraction units). This parameter, η, is related to the $-C_0^{13}$ content of the labeled propane or butane by the formula

$$-C_0^{13}=(1-\eta)(1-0.0101)^{n-1} \text{ for } C_nH_{2n+2}, \qquad (2)$$

where the mole fraction of natural C^{13} is 0.0101. The values of η for the various isotopic preparations are given in Tables I and II. The formulas for the concentration of the various isotopic isomers, in terms of the respective η, for the propane-1$-C_1^{13}$, *n*-butane-1$-C_1^{13}$, isobutane-1$-C_1^{13}$, and isobutane-2$-C_1^{13}$, are given in Table III. Formulas are not given for propane-2$-C_1^{13}$ or *n*-butane-2$-C_1^{13}$ since the samples containing useful concentrations of these species were obtained from the samples of propane-1$-C^{13}$ and *n*-butane-1$-C^{13}$, respectively, by isomerization.[1,2] The concentrations of the isotopic isomers present in the various samples are shown in Tables I and II. The formulas of Table III were used for the propane-1$-C^{13}$, *n*-butane-1$-C^{13}$, *i*-butane-1$-C^{13}$, and *i*-butane-2$-C^{13}$. The concentrations of the various species in the cases of propane-2$-C^{13}$ and *n*-butane-2$-C^{13}$ were calculated from the compositions of the propane-1$-C^{13}$ and *n*-butane-1$-C^{13}$ samples, respectively, with the aid of the assumption that the aluminum bromide treatment resulted in intramolecular equilibration and no intermolecular redistribution.[13]

THE MASS SPECTRA

Once the concentrations of the isotopic isomers of a preparation have been established as described above, the calculation of the mass spectrum[14] of the labeled isomer from the mass spectrum of the preparation follows a simple pattern. The observed mass spectrum is corrected for the contributions of the $-C_0^{13}$ compound using the mass spectrum of this substance calculated from Eq. (1). It is then corrected for the contributions of the $-C_2^{13}$ species and the minor $-C_1^{13}$ isomer assuming the mass spectra of these substances to be calculable from the mass spectrum of the $-C_0^{13}$ species by simple statistics. The residue is the mass spectrum of the substance of interest. This method was used to determine the relative intensities of C_1 and C_2 ion fragments in the mass spectrum of propane-1$-C^{12}$ and of the C_1, C_2, and C_3 ion fragments in the mass spectra of *n*-butane-1$-C_1^{13}$, *i*-butane-1$-C^{13}$, and *i*-butane-2$-C_1^{13}$. In the equilibrated propane$-C_1^{13}$ and *n*-butane$-C_1^{13}$ samples the concentrations of the -1$-C_1^{13}$ species were greater than or equal to the concentration of the species of interest, -2$-C_1^{13}$. In deducing the mass spectra of the propane-2$-C^{13}$ and *n*-butane-2$-C^{13}$, the previously de-

TABLE III. Species concentrations of C^{13} enriched propane and butanes.

Species	Propane-1$-C^{13}$	*n*-butane-1$-C^{13}$	*i*-butane-1$-C^{13}$	*i*-butane-2$-C^{13}$
C_0^{13}	$(1-\eta)(1-r)^2$	$(1-\eta)(1-r)^3$	$(1-\eta)(1-r)^3$	$(1-\eta)(1-r)^3$
-1$-C_1^{13}$	$\eta(1-r)^2+r(1-r)(1-\eta)$	$\eta(1-r)^3+r(1-r)^2(1-\eta)$	$(1-r)^3+2r(1-r)^2(1-\eta)$	$3r(1-r)^2(1-\eta)$
-2$-C_1^{13}$	$r(1-r)(1-\eta)$	$2r(1-r)^2(1-\eta)$	$r(1-r)^2(1-\eta)$	$\eta(1-r)^3$
1,2$-C_2^{13}$	$r(1-r)\eta+r^2(1-\eta)$	$\eta r(1-r)^2+r^2(1-r)(1-\eta)$	$r(1-r)^2\eta+2r^2(1-r)(1-\eta)$	$3r(1-r)^2\eta$
1,3$-C_2^{13}$	$r(1-r)\eta$	$r(1-r)^2\eta+r^2(1-r)(1-\eta)$	—[a]	—[a]
1,4$-C_2^{13}$	—[a]	$r(1-r)^2\eta$	—[a]	—[a]
2,3$-C_2^{13}$	—[a]	$r^2(1-r)(1-\eta)$	—[a]	—[a]
1,1$-C_2^{13}$	—[a]	—[a]	$2r(1-r)^2\eta+r^2(1-r)(1-\eta)$	$3r^2(1-r)(1-\eta)$
C_3^{13}	$r^2\eta$	$r^3(1-\eta)+3r^2(1-r)\eta$	$r^3(1-\eta)+3r^2(1-r)\eta$	$r^3(1-\eta)+3r^2(1-r)\eta$
C_4^{14}	—[a]	$r^3\eta$	$r^3\eta$	$r^3\eta$

Note.—η = abundance of C^{13} in enriched starting material. r = natural abundance of C^{12} in ordinary starting material, =0.0101, η and r in mole fraction units.

[a] Species does not exist.

[12] The possible effects of isotopic substitution on the parent ion sensitivity of substances is discussed elsewhere, reference 6.

[13] See reference 5 for the evidence that these samples to represent intramolecular equilibration. The equilibrium constants of the various intramolecular rearrangement reactions were assumed to be

$$\text{propane-1}-C^{13}/\text{propane-2}-C^{13}=2/1 \qquad n\text{-butane-1}-C^{13}/n\text{-butane-2}-C^{13}=1/1 \text{ etc.},$$

i.e., possible isotope effects on the relative free energy of isotopic isomers were neglected.

[14] We refer to those portions of the mass spectrum of the labeled species which have not been assumed, i.e., to the relative intensities of the ion fragments formed through the breaking of one or more carbon-carbon bonds as well as carbon-hydrogen bonds.

TABLE IV. Relative intensities of C_2 and C_1 ion fragments in the mass spectra of propane$-C_0^{13}$, -1$-C_1^{13}$, and -2$-C_2^{13}$.

m/q	$C_3H_8-C_0^{13}$	C_3H_8-1$-C^{13}$	C_3H_8-2$-C^{13}$
45		1.000	1.000
44	1.000[a]		
30		1.088	1.97
29	1.986	1.536	1.21
28	1.213	0.896	0.69
27	0.631	0.338	0.18
26	0.109	0.059	0.021
25	0.0083	0.0057	0.002
16		0.0127	0.0042
15	0.0263	0.0178	0.0253
14	0.0072	0.0052	0.0070
13	0.0022	0.0019	0.002

[a] Sensitivity relative to $m/q=58$ of n-$C_4H_{10}-C_0^{13}$ (equal to unity) is 1.20.

termined mass spectra of propane-1$-C_1^{13}$ and n-butane-1$-C_1^{13}$, respectively, were used in making corrections. Otherwise the above outlined procedure was followed.

The relative intensities of the C_1 and C_2 ion fragments in the mass spectra of propane-1$-C^{13}$ and propane-2$-C^{13}$ are compared with those of propane$-C_0^{13}$ mass spectrum in Table IV, while the relative intensities of the C_1, C_2, and C_3 ion fragments in the mass spectra of the six butanes, n- and i- $-C_0^{13}$, n- and i- 1$-C_1^{13}$, and n- and i- 2$-C_1^{13}$, are given in Table V.

Studies of the appearance potentials of $C_2H_5^+$ in the propane mass spectrum and of $C_3H_7^+$ in the butane mass spectra[15] led to the conclusion that these electron-induced processes are simple ones and that for these processes the methyl and methylene groups can be treated as units. Thus according to the model described in reference 6 we should expect the $C_2H_5^+$ of $m/q=30$ to be more intense in the propane-1$-C^{13}$ mass spectrum than the one of $m/q=29$, the $C_3H_7^+$ of $m/q=44$ to be more intense in the n-butane-1$-C^{13}$ mass spectrum than the one of $m/q=43$, and the $C_3H_7^+$ of $m/q=44$ in the i-butane-1$-C^{13}$ mass spectrum to be more than twice as intense as the one of $m/q=43$. That these expectations are fulfilled may be readily deduced from the data in Tables IV and V, as we will show in the following paragraph.

If there were no isotope effect on the dissociation probabilities of the propane or butane molecule-ions we should expect the following relations to hold between the mass spectra of the $-C_0^{13}$ and -1$-C_1^{13}$ species:

$$C_3H_8;\ S_{30}(\text{-}1-C^{13})=\tfrac{1}{2}S_{29}(-C_0^{13}) = 0.993$$
$$C_3H_8;\ S_{29}(\text{-}1-C^{13})=\tfrac{1}{2}[S_{29}(-C_0^{13})+S_{28}(-C_0^{13})] = 1.600$$
$$n\text{-}C_4H_{10};\ S_{44}(\text{-}1-C^{13})=\tfrac{1}{2}S_{43}(-C_0^{13}) = 2.16$$
$$n\text{-}C_4H_{10};\ S_{43}(\text{-}1-C^{13})=\tfrac{1}{2}[S_{43}(-C_0^{13})+S_{42}(-C^{13})] = 2.44$$
$$i\text{-}C_4H_{10};\ S_{44}(\text{-}1-C^{13})=\tfrac{2}{3}S_{43}(-C_0^{13}) = 10.7$$
$$i\text{-}C_4H_{10};\ S_{43}(\text{-}1-C^{13})=\tfrac{1}{3}S_{43}(-C_1^{13})+\tfrac{2}{3}S_{42}(-C_0^{13}) = 9.5$$

[15] D. P. Stevenson, J. Chem. Phys. **10**, 291 (1942).

where the numerical values are obtained from the $-C_0^{13}$ spectra of Tables IV and V.

We find in each case that the observed intensity of the heavy ion is greater than the calculated intensity and the calculated intensity of the light ion is greater than the observed intensity, and thus for propane-1$-C^{13}$ $C_2H_5^+$ (30)$>C_2H_5^+$ (29), for n-butane-1$-C^{13}$ $C_3H_7^+$ (44)$>C_3H_7^+$ (43), and for i-butane-1$-C^{13}$ $C_3H_7^+$ (44)$>2\times C_3H_7^+$ (43). We further note that in each case the decrease in zero-point energy of the heavy ion fragment increases its probability of formation more with respect to the corresponding dissociation process in the $-C_0^{13}$ species than the decrease in amplitude in the ground state decreases the total dissociation probability.

If we assume that the processes[16]

$$C_3H_8\text{-}1-C^{13}+\epsilon^-\rightarrow C_2H_4^+\ (29)+CH_4+2\epsilon^-$$
$$n\text{-}C_4H_{10}\text{-}1-C^{13}+\epsilon^-\rightarrow C_3H_6^+\ (43)+CH_4+2\epsilon^-$$
$$i\text{-}C_4H_{10}\text{-}1-C^{13}+\epsilon^-\rightarrow C_3H_6^+\ (43)+CH_4+2\epsilon^-$$

have their probability increased by the same factors that the formations of $C_2H_5^+$ (30) and $C_3H_7^+$ (44) have their probabilities increased, we may calculate the intensities of $C_2H_5^+$ (29) and $C_3H_7^+$ (43) as follows:

$$C_3H_8\text{-}1\text{-}C^{13}\ \ C_2H_5(29) = 1.536-\frac{1.088}{0.993}\times\frac{1.213}{2}=0.871$$

$$n\text{-}C_4H_{10}\text{-}1\text{-}C^{13}\ \ C_3H_7^+(43)=2.24-\frac{2.34}{2.16}\times\frac{0.564}{2}=1.93$$

$$i\text{-}C_4H_{10}\text{-}1\text{-}C^{13}\ \ C_3H_7^+(43)=9.2\ -\frac{11.0}{10.7}\times\frac{2}{3}6.16=5.0.$$

Comparing the sums, $C_2H_5^+$ (29)$+C_2H_5^+$ (30) of propane-1$-C^{13}$, and $C_3H_7^+$ (43)$+C_2H_7^+$ (44) of the butane-1$-C^{13}$'s with the intensities of the corresponding ions in the mass spectra of the $-C_0^{13}$ species we find the effect of the decreased amplitude in the ground state of the -1$-C^{13}$ species decreases the probability of the dissociation process by as much or slightly more than the decrease in the zero-point energy of one of the alternate ion fragments increases the dissociation probability. The magnitude of the net decreases of the probability of the processes are, for propane-1$-C^{13}$ 1.4 percent, for n-butane-1$-C^{13}$ 1.2 percent, and for i-butane-1$-C^{13}$ 0.6 percent.

For the three centrally substituted substances corresponding to $AB'A$ of the model,[6] we find that the three possible combinations of the two isotope effects are represented. In propane-2$-C^{13}$ the decreased amplitude in the ground state outweighs the decreased zero-point energy of the ion fragments and $C_2H_5^+$ (30)

[16] For proof that these are the correct representations of these processes, see Phys. Rev. **56**, 256 (1939) and J. Am. Chem. Soc. **64**, 2769 (1942) for propane, and J. Am. Chem. Soc. **64**, 1588 (1942) for the butanes.

is 0.5 percent less intense than $C_2H_5^+$ (29) in the mass spectrum of propane$-C_0^{13}$. In *n*-butane-2$-C^{13}$ the two effects cancel one another and $C_3H_7^+$ (44) of the -2$-C^{13}$ mass spectrum equals $C_3H_7^+$ (43) of the $-C_0^{13}$ spectrum to within the experimental error. In *i*-butane-2$-C^{13}$ the decreased zero-point energy of the ion fragment outweighs the decreased amplitude in the ground state and $C_3H_7^+$ (44) is six percent more intense in the -2$-C^{13}$ mass spectrum than is $C_3H_7^+$ (43) in the $-C_0^{13}$ mass spectrum.[17]

It may be noted that the absence of complimentariness of the relative intensities in the mass spectra of the isomeric pairs, $m/q=30$ in propane-1$-C^{13}$ and propane-2$-C^{13}$, $m/q=44$ in *n*-butane-1$-C^{13}$ and *n*-butane-2$-C^{13}$ and *i*-butane-1$-C^{13}$ and *i*-butane-2$-C^{13}$, conclusively proves this to be an isotope effect on the dissociation probabilities, not a rearrangement phenomenon as suggested by Honig.[18]

We note that these isotope effects on the probability of the processes $C_3H_8+\epsilon^-\rightarrow C_2H_5^++CH_3+2\epsilon^-$ and $C_4H_{10}+\epsilon^-\rightarrow C_3H_7^++CH_3+2\epsilon^-$ are such that the intensities of the ions, $m/q=30$ of ordinary propane and $m/q=44$ of ordinary butanes, due to the natural abundance of C^{13} (1.0 percent) should be greater than would be calculated by Eq. (1). That such is the case has long been known to those engaged in the mass spectrometric analysis of hydrocarbons. These isotope effects account completely (within experimental error) for the difference found to exist between the observed intensities ($m/q=30$ in propane, $m/q=44$ in butanes) and those calculated by Eq. (1). Thus, it is possible to conclude that within the present accuracy of measurement such processes as $C_3H_8+\epsilon^-\rightarrow C_2H_6^++?+2\epsilon^-$, or $C_4H_{10}+\epsilon^-\rightarrow C_3H_8^++?+2\epsilon^-$ are not brought about by impact with low energy (<100-volt) electrons.

Contrary to expectations based on its structure, propane-2$-C^{13}$ gives an ion, $m/q=16$, $C^{13}H_3^+$, whose intensity is about one-third that of the intensity of the ion in the mass spectrum of propane-1$-C^{13}$. This behavior of propane-2$-C^{13}$ is like that observed[6] in propane-2-*d* that gives CH_2D^+ of about the same intensity. This indicates that in the state of $C_3H_8^+$ which dissociates to give CH_3^+ the carbon atoms tend to lose their identity. This behavior of certain states of the first-formed molecule-ions is even more pronounced in the case of *i*-butane. The relative intensities of both C_1 and C_2 ions in the mass spectra of *i*-butane-1$-C^{13}$ and -2$-C^{13}$ are equal within the experimental error. Thus, in the states of *i*-$C_4H_{10}^+$ which dissociate into C_1 and C_2 ion fragments the carbon atoms completely lose their identity. Whether the necessary rearrangements of the atoms take place in the dissociation step or whether the dissociation is preceded by a series of rearrangements cannot be determined from the available data. Ions with half-lives in the range 1 to 10^4 $\mu\mu$sec cannot be distinguished with the mass spectrometer here employed.[19]

Until the theory of the electron impact induced transitions can suggest the most suitable form for the parameters, it seems pointless to attempt a semi-empirical treatment of the intensities of the ion fragments of $24<m/q<29$ of the mass spectra of the propanes or $36<m/q<43$ of the mass spectra of the butanes. It is apparent that the magnitude of the isotope effects on simple processes is such that, prior to quantitative determination of the isotopic isomers of a mixture from a mass spectrum, knowledge of the mass spectra of the individual isotopic isomers must be obtained experimentally. Thus the isotopic isomer analysis problem is on the same footing as the ordinary mass spectrometric isomer analysis problem. It is further apparent that the number of ions in the mass spectrum of a substance that can be employed for isotopic isomer analysis purposes is limited. A large number of ion states undergo enough rearrangement before dissociation that the position of a given tagged atom is lost. This latter fact increases the usefulness of Eq. (1), by removing a possible source of error.

In conclusion, the author takes pleasure in acknowledging his indebtedness to his colleagues in Shell Development Company, particularly Drs. O. Beeck, J. W. Otvos, and C. D. Wagner, for stimulating discussion of the material herein presented.

TABLE V. Relative intensities of C_3, C_2, and C_1 ion fragments in the mass spectra of $-C_0^{13}$, -1$-C^{13}$, and -2$-C^{13}$ butanes.

		n-butane-			*i*-butane-	
m/q	C_0^{13}	1$-C^{13}$	-2$-C^{13}$ [a]	C_0^{13}	1$-C^{13}$	-2$-C^{13}$
59		1.000	1.00		1.000	1.000
58	1.000			1.000[b]		
44		2.34	4.34		11.0	17.1
43	4.32	2.24	0.8	16.1	9.2	7.5
42	0.564	0.89	0.9	6.16	5.75	5.4
41	1.137	0.43	0.14	5.58	1.9	0.2
40	0.039	0.22	0.5	0.22	1.40	1.9
39	0.384	0.21	—	1.88	0.76	0.6
30		0.64	—		0.36	0.37
29	1.26	1.05	—	0.65	0.42	0.39
28	0.90	0.82	—	0.15	1.25	1.23
27	0.83	0.48	—	2.42	1.45	(0.6)
26	0.12	0.06	—	0.16	0.11	0.08
16		0.013	—	0.001	0.04	0.05
15	0.028	0.019	—	0.13	0.10	0.10
14				0.022	0.016	0.015

[a] The low concentration of this substance in the sample (9.2 percent) render all intensities but that of $m/q=44$, quite inaccurate.
[b] Sensitivity relative to $m/q=58$ of *n*-butane$-C_0^{13}$ (equal to unity) is 0.310.

[17] That these isotope effects here reported are *not* due to m/q dependent variations of the efficiency of collection of ions by the Westinghouse mass spectrometer has been experimentally demonstrated. A detailed report on studies of the efficiency of ion collection [i.e., discrimination—N. D. Coggeshall, J. Chem. Phys. **12**, 19 (1944)] in the Westinghouse mass spectrometer will be submitted for publication.

[18] R. E. Honig, Phys. Rev. **75**, 1319 (1949).

[19] See J. A. Hipple, Phys. Rev. **71**, 594 (1947) for the method of measuring the half-lives of metastable ions formed by electron impact.

The Infrared and Raman Spectra of Trimethylphosphine Oxide

L. W. DAASCH AND D. C. SMITH
Naval Research Laboratory, Washington, D. C.
(Received June 26, 1950)

The infrared absorption spectrum of solid trimethylphosphine oxide has been obtained over the range 450 to 5000 cm^{-1}. A vibrational assignment is proposed for nearly all the bands observed in the infrared spectrum as well as for the Raman frequencies observed in aqueous solution. It is shown that the fundamental frequencies of the skeletal vibrations are compatible with reasonable values of the force constants for phosphorus-oxygen and phosphorus-carbon bonds.

IN a study of the spectral properties of phosphorus compounds, available knowledge of the vibrational frequencies of even the simpler compounds proved too limited a basis for interpretation of the spectra of more complex molecules.[1] This was particularly true for organophosphorus compounds in the higher valence state, in which case no vibrational analysis appears to have been made. Trimethylphosphine oxide, the smallest and most symmetrical molecule of this type, was therefore selected for study.

EXPERIMENTAL

Trimethylphosphine oxide was prepared by the reaction of methyl magnesium chloride with $POCl_3$. The product was distilled and purified by sublimation in vacuum. It was a hygroscopic, white, crystalline solid with a sealed-tube melting point of 138–139.5°C.

TABLE I. Observed frequencies of trimethylphosphine oxide.*

Infrared (solid phase)	Raman (aqueous solution)
	256 m,d
	311 vvw
	369 vw
	671 s,sh
700 vw	
750 s	756 m,d
866 s	866 vvw
872 s	
950 s	937 vvw
1170 s	1120 vvw
1292 s	
1305 s	
1340 m	
1420 ms	1415 vw,d
1437 ms	
1482 vw	
1500 mw	
	1615 vvvw,sh
1672 m	1666? vvw
1952 vw	
2050 vw	
2090 vw	
2160 vw	
2255 vw	
2350 vw	
	2923 s
	2999 s
3410 s	

* Frequencies in cm^{-1}. v, very. w, weak. m, medium. sh, sharp. s, strong. d, diffuse.

[1] L. W. Daasch and D. C. Smith, Anal. Chem. (to be published).

The infrared spectrophotometer has been described.[2] A sample for infrared measurements was ground with petrolatum and placed between polished potassium bromide plates, whose edges were then sealed with soft wax to keep out moisture. All manipulations were completed in an atmosphere dried with calcium chloride. The remainder of the sample was dissolved in distilled water for the Raman work.* There was formed a nearly saturated solution having a slightly milky appearance when viewed along the length of the Raman tube (~15 cm).

The observed Raman and infrared frequencies together with notations for the intensity and sharpness of the bands are given in Table I. The infrared spectrum from 2 to 15 mu, obtained with a rock salt prism, is shown in Fig. 1. No bands were found between 15 and 22 mu, in which region a KBr prism was used.

DISCUSSION

Most of the trimethyl derivatives of Group V(A) elements have been shown by electron diffraction studies to have pyramidal structures of C_{3v} symmetry.[3] For similar compounds, such as PCl_3, conversion to the oxide ($OPCl_3$) results in a structure which maintains the C_{3v} symmetry.[4] It is therefore assumed that trimethylphosphine oxide has C_{3v} symmetry with the threefold axis lying on the phosphorus-oxygen bond.

The species and qualitative description of each fundamental for trimethylphosphine oxide are given in Table II. Vibrations of species A_1 and E are active in both Raman effect and infrared absorption, while A_2 is inactive in both. The fundamentals are divided for convenience of discussion into two types of vibrations, (a) those in which the methyl groups are considered as point masses and which are called skeletal vibrations, and (b) those in which the vibratory motion is largely confined to the methyl groups. The skeletal vibrations are designated ν_1 to ν_6, following the notation of Herzberg[4] and the methyl vibrations ν_7 to ν_{24}. Interaction

[2] Nielsen, Crawford, and Smith, J. Opt. Soc. Am. 37, 296 (1947).
* Raman spectrum obtained on a Lane Wells spectrograph by Drs. J. Rud Nielsen and R. L. Hudson at the University of Oklahoma.
[3] H. D. Springell, and L. O. Brockway, J. Am. Chem. Soc. 60, 996 (1938).
[4] G. Herzberg, *Infrared and Raman Spectra* (D. Van Nostrand Company, Inc., New York, 1945) pp. 322, 164, and 163.

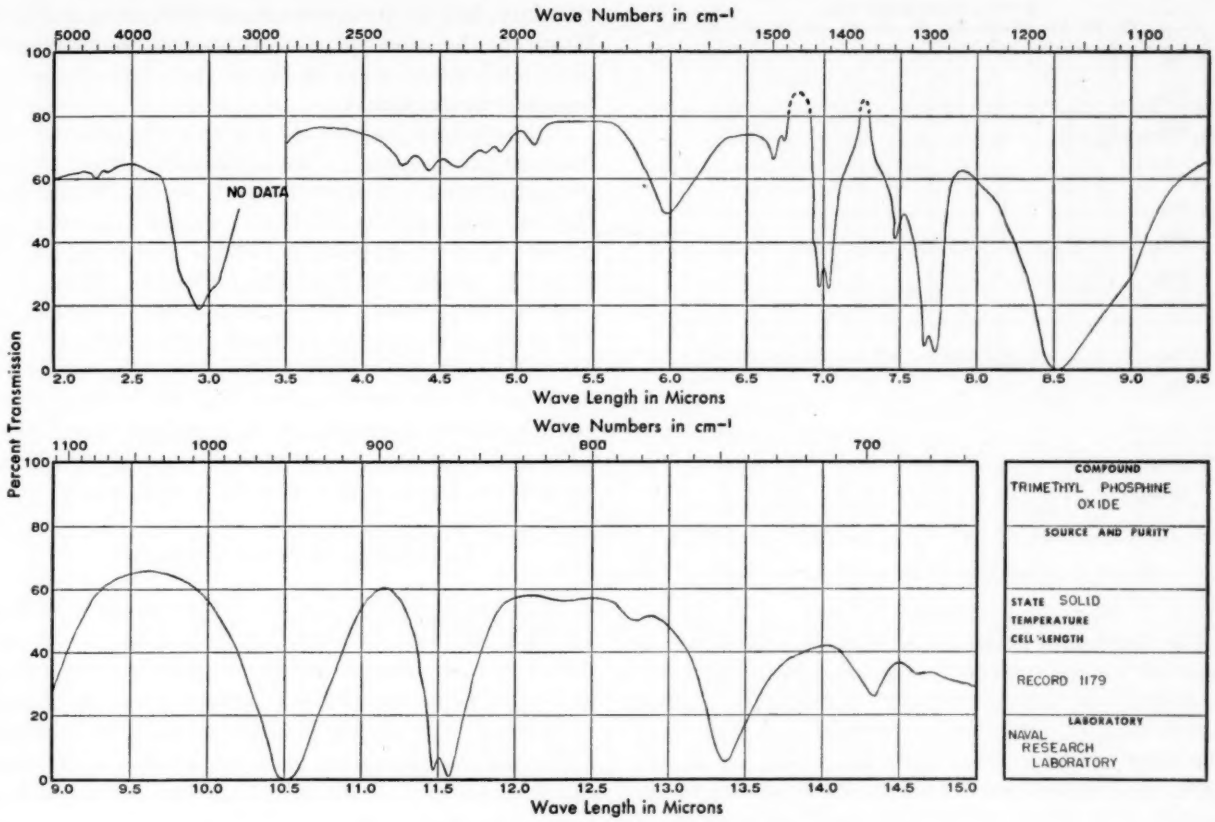

FIG. 1. Infrared spectrum of trimethylphosphine oxide.

between the skeletal and methyl vibrations certainly exists, and for this reason the descriptions given in Table II for the vibrations have only very rough meaning.

Assignment of Fundamentals

The skeletal fundamentals can be assigned by comparison with the assignment for trimethylphosphine[5] and other PX_3 and POX_3 molecules[4-6] (Fig. 2), by correlations between the intensity and sharpness of the observed bands in Raman and infrared spectra, and by the use of group frequencies.[1] Considering first the three totally symmetric skeletal fundamentals, ν_1 must be expected[1] to lie above 1100 cm^{-1} while ν_2 and ν_3 should have values near the corresponding fundamentals of $P(CH_3)_3$ at 653 and 263 cm^{-1}, respectively.[5] The Raman frequency at 256 cm^{-1} is the strongest line observed below 500 cm^{-1} and is therefore assigned to ν_3. The Raman band at 671 cm^{-1} is strong and sharp, indicating that it is polarized; it is accordingly assigned to ν_2. Because of its position and intensity the strong infrared band at 1170 cm^{-1} may confidently be assigned to the phosphorus-oxygen stretching frequency ν_1; in the Raman effect, this vibration appears as a weak band at 1120 cm^{-1}, the shift in position probably being due to the influence of the polar solvent.

TABLE II. Tentative assignment of the fundamental vibrations of trimethylphosphine oxide.

Designation	Description	Species	Frequency Raman	Frequency Infrared
	Skeletal			
ν_1	P—O stretch	A_1	1120	1170
ν_2	P—C sym. stretch	A_1	671	
ν_3	P—C sym. bend	A_1	256	
ν_4	P—C asym. stretch	E	756	750
ν_5	P—O bend	E	369	
ν_6	P—C asym. bend	E	311	
	Methyl vibrations			
ν_7	CH_3 sym. stretch in phase	A_1	2923	
ν_8	CH_3 sym. stretch out of phase	E	2923	
ν_9	CH_3 sym. bend in phase	A_1		1340
ν_{10}	CH_3 sym. bend out of phase	E		1292, 1305
ν_{11}	CH_3 asym. stretch in phase	A_1	2999	
ν_{12}	CH_3 asym. stretch in phase	A_2	inactive	
ν_{13}, ν_{14}	CH_3 asym. stretch out of phase	E, E	2999	
ν_{15}	CH_3 asym. bend in phase	A_1		(1340)?
ν_{16}	CH_3 asym. bend in phase	A_2	inactive	
ν_{17}, ν_{18}	CH_3 asym. bend out of phase	E, E		1420, 1437
ν_{19}	CH_3 rock in phase	A_1		872
ν_{20}	CH_3 wag in phase	A_2	inactive	
ν_{21}	CH_3 rock out of phase	E	937	950
ν_{22}	CH_3 wag out of phase	E	866	866
ν_{23}	CH_3 torsion in phase	A_2	inactive	
ν_{24}	CH_3 torsion out of phase	E	(~275)	

[5] Rosenbaum, Rubin, and Sandberg, J. Chem. Phys. **8**, 366 (1940).

[6] M. Delwaulle and F. Francois, Compt. rend. **220**, 817 (1945); **222**, 550 (1946); and **224**, 1422 (1947).

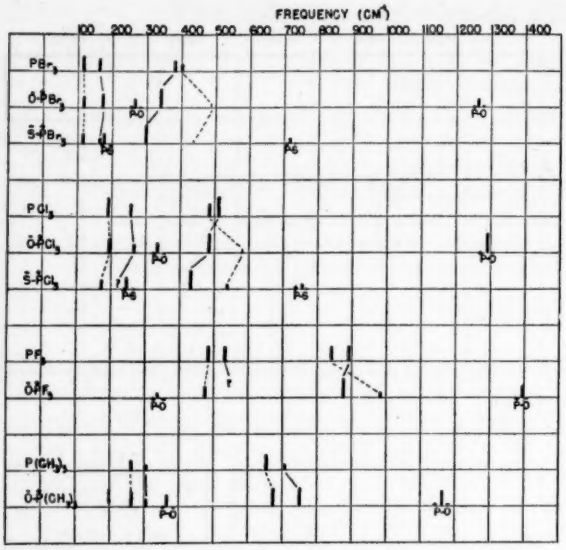

FIG. 2. Correlation of POX_3 and PX_3 molecules.

The degenerate skeletal vibrations ν_4 and ν_6 may be expected to appear near the corresponding frequencies for $P(CH_3)_3$ at 708 and 305 cm^{-1} respectively, while ν_5 should have an intermediate position but close to ν_6. The only available frequencies for ν_5 and ν_6 are the Raman lines at 369 and 311 cm^{-1}. The remaining fundamental, ν_4, is assigned to the strong infrared band at 750 cm^{-1}, which appears in the Raman effect as a diffuse band at 756 cm^{-1}. This assignment of skeletal fundamentals is fairly certain. Figure 2 shows that the frequencies correlate very satisfactorily with previous assignments for other OPX_3 and PX_3 molecules.

The methyl vibrations have been divided into three groups in Table II. The C—H stretching and bending vibrations ($\nu_7-\nu_{18}$) will occur near 3000 cm^{-1} and in the region from 1300 to 1450 cm^{-1}, respectively. The methyl rocking and wagging vibrations ($\nu_{19}-\nu_{22}$), where the group moves approximately as a unit, may be expected in the region from 700 to 1200 cm^{-1} by analogy with the position of corresponding vibrations in other molecules.[7] The remaining fundamentals (the methyl torsional vibrations ν_{23} and ν_{24}) usually occur at very low frequencies (275 cm^{-1} in ethane[7]). Specific assignments within each of these regions cannot be made with much certainty, but the tentative assignments given in Table II are for the most part satisfactory, although incomplete, and are as good or better than any of several possibilities considered.

TABLE III. Approximate calculation of fundamental skeletal frequencies and force constants.

	Assumed constants ($\times 10^5$ d/cm)				Calculated frequencies (cm^{-1})					
	f_1(P—O)	d_1(P—O)	f_2(P—C)	d_2(P—C)	ν_1	ν_2	ν_3	ν_4	ν_5	ν_6
A	8.0	0.1	3.0	0.3	1170	608	264	728	392	194
B	8.0	0.3	3.0	0.3	1175	605	312	781	346	312
C		(Observed frequencies)			1170	671	256	750	369	311

Although four inactive A_2 and two degenerate E vibrations are missing in the assignment, most of the strong infrared and Raman bands are accounted for. One infrared band at 3410 cm^{-1} requires separate explanation; it is similar to bonded hydroxyl and is probably caused by hydrate formation during the grinding procedure.† The fundamental vibrations of the oxide, however, are believed to be essentially unaffected (perhaps shifted slightly) by the water of hydration. There remain above 1482 cm^{-1} a number of weak bands which can readily be explained as combinations and overtones, but in view of the missing fundamentals the interpretation is of little significance.

Calculation of Force Constants

As a first approximation the force constants for the $P(CH_3)_3$ part of trimethylphosphine oxide can be assumed to be unchanged by the additional oxygen and can be obtained from the equations given by Kohlrausch[8] for XZ_3 molecules. The assumption is made reasonable by the aforementioned similarity between the frequencies for $P(CH_3)_3$ and the corresponding frequencies in $O=P(CH_3)_3$. Using only the two symmetrical skeletal frequencies 256 and 671 cm^{-1}—and values of 15 for the mass of CH_3, 35 for the approximate mass of the PO group, and 69° for the pyrimidal angle β[3]—the values 3.12 and 0.37×10^5 d/cm are obtained for the stretching and bending force constants of the P—C bonds. Neither of these force constants is very sensitive to changes in β or in the mass of the PO group, and when put back into the equations for the two asymmetrical fundamentals of an XZ_3 molecule the values of 357 and 755 cm^{-1} are obtained as compared to observed values of 369 and 750 cm^{-1}.

It was therefore assumed that the constants for stretching and bending of $P-CH_3$ bonds were close to 3.0 and 0.3×10^5 d/cm, respectively. These values, when used with the observed skeletal frequencies for $OP(CH_3)_3$ in the general equations for XYZ_3 molecules,[8] yield values of 8.2 and 0.13×10^5 d/cm for the stretching and bending force constants for the phosphoryl bond, P^+-O^-. The complete set of force constants so obtained is listed together with the frequencies calculated from it in line A of Table III. The agreement with the observed frequencies shown in line C is fair,

[7] H. M. Randall, R. G. Fowler, N. Fuson, and J. R. Dangl, *Infrared Determination of Organic Structures* (D. Van Nostrand Company, Inc., New York, 1949), pp. 46–66.

† Trimethylphosphine oxide is extremely hygroscopic. The water of hydration may also be responsible for some of the absorption around 1672 cm^{-1}, although this band has a satisfactory assignment as the combination $\nu_{17,18}+\nu_3$.

[8] K. W. F. Kohlrausch, *Der Smekal-Raman-Effekt*, Erganzungsband (Julius Springer, Berlin, Germany, 1938) (also Edwards Brothers, Ann Arbor, Michigan), pp. 70, 72.

except for ν_6. This discrepancy is largely removed by increasing the phosphoryl bending constant to 0.3×10^5 d/cm, as shown in line B. Although the observed frequencies are not reproduced with very great accuracy by this simple treatment, the calculations furnish approximate values for the force constants of the bonds.

ACKNOWLEDGMENT

The authors are indebted to Mr. R. B. Fox of this laboratory, who carried out the preparation of trimethylphosphine oxide, and to Drs. J. Rud Nielsen and R. L. Hudson, of the University of Oklahoma, who kindly supplied the Raman data.

THE JOURNAL OF CHEMICAL PHYSICS VOLUME 19, NUMBER 1 JANUARY, 1951

The Role of Surface Tension in Multilayer Gas Adsorption*

W. G. McMillan
Department of Chemistry, University of California at Los Angeles

AND

E. Teller
Los Alamos Scientific Laboratory, Los Alamos, New Mexico

(Received September 5, 1950)

The assumptions of the BET theory of multilayer gas adsorption are examined with regard to the possibility of taking account of the effect of surface tension. The surface energy of the adsorbed phase is calculated by the use of a Fourier analysis of the surface configuration. This energy is then used in the calculation of the corresponding factor in the partition function, leading ultimately to an isotherm equation which includes the surface tension effect. This isotherm is compared with experiment, with the result that the surface tension effect alone is found to overcorrect the BET theory. When compared with the result of recent theoretical treatments of the extension of the attractive forces into the adsorbed phase, our expression is shown to have the same dependence on layer thickness, but to be a relatively unimportant correction under usual conditions.

1. INTRODUCTION

THE BET[1,2] theory of multilayer gas adsorption has been found to explain qualitatively many of the features of the adsorption isotherms commonly met in the laboratory. Moreover, the work of Harkins and Jura[3,4] has confirmed,[5] by two independent methods, the essential validity of the surface areas obtainable by applying the BET theory to adsorption measurements in the neighborhood of one monolayer. It has been generally recognized, however, that even for cases of Type II isotherms,[6] involving adsorbents which are apparently free from such complications as "internal" surfaces (e.g., capillary structures), the BET isotherm, when fitted to the experimental points in the region of one monolayer, deviates seriously both above and below that region. This situation is illustrated in Fig. 1 in which the (dashed) theoretical BET isotherm is compared with the (solid) experimental isotherm in a typical case. It is seen that below the region of fit the BET isotherm predicts too low an adsorption, while at the higher pressures it deviates in the opposite direction. The discrepancy at low pressures is commonly ascribed to an inhomogeneity of the experimental adsorbent surface which the BET treatment ignored. It appears possible to take account of this surface inhomogeneity within the framework of that treatment by a simple extension[7,8] of the theory.

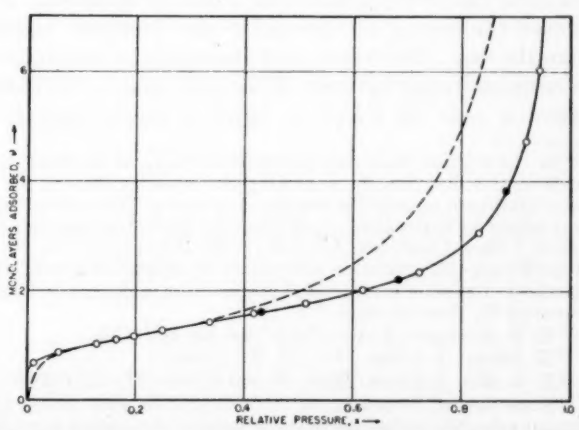

FIG. 1. Comparison of the BET isotherm (dashed curve) with the experimental isotherm (solid curve) in a typical case.

* Presented before the Division of Physical and Inorganic Chemistry at the 115th Meeting of the American Chemical Society, San Francisco, Spring, 1949.

[1] S. Brunauer, P. H. Emmett, and E. Teller, J. Am. Chem. Soc. **60**, 309 (1938).

[2] A comprehensive review of this theory is given by S. Brunauer, *The Adsorption of Gases and Vapors, Vol. I, Physical Adsorption* (Princeton University Press, Princeton, 1943), p. 151 *et seq.*

[3] W. D. Harkins and G. Jura, J. Am. Chem. Soc. **66**, 1362 (1944).

[4] W. D. Harkins and G. Jura, J. Am. Chem. Soc. **66**, 1366 (1944).

[5] See discussion by P. H. Emmett, J. Am. Chem. Soc. **68**, 1784 (1946).

[6] See reference 2, p. 150.

[7] W. G. McMillan, J. Chem. Phys. **15**, 390 (1947).

[8] W. C. Walker and A. C. Zettlemoyer, J. Phys. and Colloid Chem. **52**, 47 (1948); **52**, 58 (1948).

There exist several attempts to explain the disagreement between experiment and the BET theory at high relative pressures.[4,9–12] Actually the assumptions underlying the BET theory are crude and unrealistic. Apart from the question of surface homogeneity, the principal assumptions are: (a) the number of molecules (layers) adsorbed over a given site is independent of the numbers on adjacent sites; and (b) while the energy of adsorption E_1 in the first layer is unique, that in all higher layers is just the energy of liquefaction, E_L. Although neither of these two assumptions well represents the true state of affairs, they err in opposite directions; the partial compensation makes the BET result closer to the truth than are the assumptions on which it is based.

Assumption (a) permits large and erratic fluctuations of the thickness of the adsorbed phase even as we change from one site to a neighboring one. Such a situation is obviously uneconomical in total surface area, and will be opposed in any actual case by the surface tension. The effect of taking into account the surface tension with the retention of assumption (b) is to diminish these irregularities, i.e., to diminish the number of permissible configurations, and hence to *increase* the chemical potential in the adsorbed phase for any given amount adsorbed.[13] The change thus introduced is in the desired direction of decreasing the theoretical amount adsorbed from the BET value.

In this paper we calculate the surface tension correction, and show that it alone is too drastic: the resulting equation predicts an adsorption at high relative pressures which is considerably smaller than that observed experimentally. The reason for this result lies in the shortcomings of assumption (b), as has been anticipated by Halsey.[11] He used the qualitative argument that in the absence of cooperative effects no new layer is likely to be formed until the underlying layer is practically complete. He therefore proposed that the existence of multilayer adsorption is to be explained by the fact that forces emanating from the adsorbent influence the energy of adsorption also in layers higher than the first. This means that the energy of adsorption in such layers lies between E_1 and E_L, and in the most common case ($E_1 > E_L$) is therefore *larger* than E_L. This argues for a greater adsorption, which partially compensates the drastic decrease (from the BET value) found from the surface tension effect alone, bringing the predicted adsorption much closer to the experimental. It should be noted, however, that if assumption (b) is replaced in accordance with Halsey's suggestion but assumption (a) retained, the predicted adsorption will *exceed* that of the BET theory.

Among the forces effective over greater distances, the most usual ones are the $1/r^6$ van der Waals interactions. These have been considered by Hill,[12] who has shown that when the adsorbed phase is assumed to be a slab of *uniform* thickness, the resulting number of adsorbed layers is inversely proportional to the cube root of the logarithm of the relative pressure. Halsey had obtained empirically approximately this power for a few well-investigated cases. It is of interest to note that our treatment, which neglects the extension of the surface van der Waals forces beyond the first layer and treats the influence of surface tension in a consistent manner, gives rise to the same power law that Hill obtained. The proportionality constant is, however, considerably smaller in our result; furthermore, it contains the surface energy in the denominator, and thus tends to zero as that quantity becomes very large. Being already small relative to Hill's coefficient, the contribution of the surface tension term is not significantly altered by considering the surface energy to be infinite; evidently this yields an adsorbed phase of uniform thickness, and thus justifies that assumption of Hill. We conclude, therefore, that in the investigated cases the adsorption of many layers is governed by the slight variation in the energy of adsorption due to the influence of the van der Waals forces emanating from the adsorbent.

The fact that the two effects result in the same power law shows, however, that only a quantitative consideration can decide their relative importance. This quantitative comparison forms the subject of this paper.

2. SKETCH OF THE METHOD

The treatment to be given aims at elucidating the adsorption isotherm in the region of large adsorptions. A considerable simplification is introduced by the assumption of an adsorbed phase sufficiently thick that the first monolayer is always essentially completely filled, and that all adsorbed molecules except those in the outer surface have energetically identical situations. While the latter condition will later be removed, even the first condition alone restricts the applicability of the resulting equations to the high adsorption region.

Since we wish ultimately to calculate a partition function for the adsorbed phase with the inclusion of the surface energy, we must have a means of calculating that energy. Our model of the adsorbed phase will consist of (spherical) adsorbate molecules arranged on

[9] In the original BET paper (see reference 1) an attempt was made in this direction by employing the equation derived for a finite maximum permissible number n of layers. This was further generalized by S. Brunauer, L. S. Deming, W. E. Deming, and E. Teller, J. Am. Chem. Soc. **62**, 1723 (1940). When applied to Type II isotherms, this procedure is certainly of questionable validity, especially if small n is required, though it sometimes leads to an improved fit. (See reference 2, p. 159.)

[10] R. B. Anderson, J. Am. Chem. Soc. **68**, 686 (1946).

[11] G. Halsey, J. Chem. Phys. **16**, 931 (1948).

[12] T. L. Hill, J. Chem. Phys. **17**, 590 (1949); **17**, 668 (1949).

[13] Since the BET equation is so devised as to give an infinite amount adsorbed at the experimental saturation pressure, it might seem that the effect of the surface tension of the adsorbed phase has already been accounted for in this procedure. What has not been taken into account, however, is the *difference* in the surface tension effect for the semi-infinite liquid and for the adsorbed phase, a difference which we shall find dependent upon the average thickness of the layer.

the adsorbent surface with a simple cubic packing,† having lattice constant equal to the molecular diameter d. The molecules are thus arranged in piles of varying heights over the adsorption sites (which are taken to have a square lattice with spacing d). A particular geometrical state of the surface, in which the number of molecules in each pile is given, is termed a "conformation." In the partition function, each conformation is to be weighted by the Boltzmann factor of the corresponding surface energy. This surface energy is a complicated function of the pile heights, but emerges as a relatively simple function of the amplitudes of the Fourier components into which the surface may be analyzed (Section 3).

The conformation space is then constructed as a sub-space of the complete phase space, and the influence of the surface tension discussed qualitatively in these terms (Section 4). To make the treatment quantitative, the "conformation integral" is introduced, in analogy with the configuration integral,[14] as a factor in the canonical partition function. The integral is evaluated not only for the case of non-zero surface energy, but also for zero surface energy, where it is shown to yield the BET isotherm (Section 5).

The general surface tension term is then combined with Hill's result[12] to obtain a complete expression for the isotherm at high relative pressures (Section 6). Finally, order of magnitude estimates are made which permit comparison of this isotherm with experiment (Section 7).

3. FOURIER ANALYSIS OF THE SURFACE[15]

We shall assume the adsorbent surface to be a finite homogeneous plane, which we take to lie in the XY-plane. The (outer) surface of the adsorbed phase can then be described by a positive function, $z=z(x, y)$. The total area of this surface in excess of its projected area A on the XY-plane is

$$\Delta A=\int\int_A\{[(\partial z/\partial x)^2+(\partial z/\partial y)^2+1]^{\frac{1}{2}}-1\}dxdy$$

$$\cong(1/2)\int\int_A[(\partial z/\partial x)^2+(\partial z/\partial y)^2]dxdy, \quad (1)$$

the latter approximation being made on the assumption that the inclination of the surface is everywhere small:[16]

$$(\partial z/\partial x)^2+(\partial z/\partial y)^2\ll 1. \quad (2)$$

If we analyze $z(x, y)$ in terms of its Fourier components $F_{lm}(x, y)$,

$$z(x, y)=d\sum_{l,m}a_{lm}F_{lm}(x, y), \quad (3)$$

the excess surface area becomes

$$\Delta A=(d^2/2)\int\int_A\sum_{l,m}\sum_{l',m'}a_{lm}a_{l'm'}[(\partial F_{lm}/\partial x)(\partial F_{l'm'}/\partial x)$$
$$+(\partial F_{lm}/\partial y)(\partial F_{l'm'}/\partial y)]dxdy. \quad (4)$$

By virtue of the orthogonality of the individual components, this reduces to

$$\Delta A=(d^2/2)\sum_{l,m}a_{lm}^2\int\int_A[(\partial F_{lm}/\partial x)^2$$
$$+(\partial F_{lm}/\partial y)^2]dxdy. \quad (5)$$

Thus by comparison with Eq. (1) it is seen that the total excess surface area is obtainable simply as a sum of the excess surface contributions of the individual components. This surface area excess is maintained by thermal agitation against the restoring force of the surface energy.

The potential energy U of deformation of the surface is now given by the product, $U=\epsilon\Delta A$, of the surface energy‡ ϵ per unit area (of *actual* surface) and the total excess surface area. If for simplicity we adopt a square domain A bordered by the positive X- and Y- axes and containing a square array of N^2 adsorption sites each of area d^2, we may write a particular Fourier component as¶

$$F_{lm}(x, y)=N^{-1}[(2-\delta_{l0})(2-\delta_{om})]^{\frac{1}{2}}f_l(x)f_m(y), \quad (6)$$

where

$$f_l(x)=\begin{cases}\cos(2\pi lx/Nd) & 0\leq l\leq(N-1)/2\\ \sin(2\pi lx/Nd) & (N+1)/2\leq l\leq N-1.\end{cases} \quad (7)$$

Then,

$$U=(\epsilon d^2/2)\sum_{l,m}a_{lm}^2\int\int_A[(\partial F_{lm}/\partial x)^2+(\partial F_{lm}/\partial y)^2]dxdy$$
$$=(2\pi^2\epsilon d^2/N^2)\sum_{l,m}(l^2+m^2)a_{lm}^2. \quad (8)$$

If we explicitly denote the dependence of U upon the set of amplitudes $\{a\}$ by the symbol $U\{a\}$, and for brevity define a quantity β by

$$\beta^2=(2\pi^2/N^2)(\epsilon d^2/kT), \quad (9)$$

† This restriction is not critical, and is later relaxed (end of Section 5).

[14] J. E. Mayer and M. G. Mayer, *Statistical Mechanics* (John Wiley and Sons, Inc., New York, 1940), Chapter 10.

[15] L. Mandelstam, Ann. Physik 48, 609 (1913), has used a treatment similar to that given here in connection with the scattering of light by liquid surfaces.

[16] While this assumption is evidently not valid for those Fourier components of short wavelength, these will have equal amplitudes for both the adsorbed phase and the pure liquid. Since the thermodynamic properties are calculated relative to the pure liquid, the contribution of the short waves—and thus any error in their calculation—will cancel. For the same reason no question will arise concerning the differentiation of the series (3).

‡ We use the quantity ϵ as though it were a constant. A more detailed consideration of the dependence of ϵ upon the number of nearest neighbors, film thickness, etc. appears unwarranted in view of the other approximations in our treatment.

¶ All indices have range 0 to $(N-1)$ unless otherwise specified. For convenience, N is taken to be odd.

we may write

$$U\{a\}/kT=\beta^2\sum_{l,m}(l^2+m^2)a_{lm}^2. \quad (10)$$

This expression will find application in the evaluation of the partition function.

The complete Fourier sum according to Eqs. (3), (6), and (7) is

$$z(x,y)=(d/N)\sum_{l,m}a_{lm}[(2-\delta_{lo})(2-\delta_{om})]^{\frac{1}{2}}f_l(x)f_m(y). \quad (11)$$

The mean square thickness is then

$$\langle z^2\rangle=(1/A)\int\int_A[z(x,y)]^2dxdy$$
$$=(d/N)^2\sum_{l,m}a_{lm}^2; \quad (12)$$

that is, the mean square thickness in units of the molecular diameter is equal to the mean square amplitude.

For the BET case we may evaluate the mean square thickness directly. There the fraction of the surface covered by exactly n molecular layers[17] is

$$s_n/\sum_{i\geq 0}s_i=cs_0x^n/s_0(1+c\sum_{i\geq 0}x^i)$$
$$=cx^n(1-x)/[1+(c-1)x].$$

Therefore the mean square thickness measured in molecular units is

$$\langle n^2\rangle=\{c(1-x)/[1+(c-1)x]\}\sum_{n\geq 0}n^2x^n$$
$$=\{c(1-x)/[1+(c-1)x]\}(d/d\ \ln x)^2(1-x)^{-1}$$
$$=\nu(1+x)/(1-x), \quad (13)$$

in which the BET isotherm,

$$\nu=cx/[1+(c-1)x](1-x), \quad (14)$$

for the average number of layers ν has been used. Comparison with Eq. (12) shows that the BET amplitudes obey the relation

$$(1/N^2)\sum a_{lm}^2=\nu(1+x)/(1-x). \quad (15)$$

For the case of interest (i.e., several molecular layers adsorbed) $cx\gg 1$ at pressures near saturation ($x\to 1$), and Eq. (14) reduces to

$$\nu\cong(1-x)^{-1}. \quad (16)$$

Thus Eq. (15) becomes approximately

$$(1/N^2)\sum a_{lm}^2\cong 2\nu^2; \quad (17)$$

that is, for the BET case near $x=1$, the mean square Fourier amplitude is twice the square of the mean thickness.

4. THE CONFORMATION SPACE

A complete classical description in phase space of the adsorbed state would specify the values of the coordinate and momentum of each molecule in each degree of freedom. For our present purposes, however, it suffices to specify the adsorbed state no more definitely than to give the number of molecules over each of the adsorption sites, i.e., the height of each pile. Our model assumes that the various positions in which a molecule may be adsorbed are entirely equivalent except insofar as the heights of the piles are different; i.e., the states of one adsorbed molecule are equivalent to those of all other such molecules, independent of location in the adsorbed phase. However, the state of the aggregate depends in addition upon the number of molecules in each pile.

We shall now examine the contribution to the total volume in phase space, of that part dependent upon the partition of the molecules into the piles. This subspace, which we shall call the conformation space, has as its axes the numbers of molecules over each of the sites, i.e., the pile heights, so that a single point in this space completely specifies the number of molecules in each pile. The conformation space is therefore a hyperlattice. Now if we specify the number of molecules $\nu_{\lambda\mu}$ over the site having coordinates (λ,μ) in units of d on our adsorbent surface, then these $\nu_{\lambda\mu}$ are the N^2 coordinates of the conformation space. If ν is the average number of layers adsorbed,

$$\sum_{\lambda,\mu}\nu_{\lambda\mu}=N^2\nu, \quad (18)$$

and we see that all of the admissible conformations for a given amount adsorbed lie in a hyper-plane [the $(1,1,1,\cdots)$-plane] in the conformation space.

If all conformations were of equal energy the phase point would assume all positions in this plane with equal probability. The corresponding factor in the phase integral would then be the number of lattice points contained in the plane, or essentially the area of the plane in the all-positive region of conformation space. this corresponds to the BET case, in which the surface energy is neglected, and will be shown presently to lead to the BET equation in its limiting form, Eq. (16), at high relative pressures. When surface energy is included, however, not all conformations are of the same energy; the Boltzmann weighting factor makes those more probable which correspond to conformations of the adsorbed phase having relatively smooth surfaces. The phase point is thus to be found with greater probability in the central region of the hyperplane, where the $\nu_{\lambda\mu}$ are of fairly uniform magnitude.

[17] Here we use the BET notation (see reference 2) as far as convenient: s_n = the area of the surface covered by exactly n molecular layers; x, the relative pressure $=p/p^0$, where p is the equilibrium adsorption pressure and p^0 the saturation pressure; $c=\exp[(E_1-E_L)/RT]$, where E_1 and E_L are, respectively, the energy of adsorption into the first layer and the energy of liquefaction, per mole.

5. THE CONFORMATION INTEGRAL

In the canonical partition function $\mathbf{Q}$, that factor, $\mathbf{Q}_c$, arising from the various conformations, is what we shall call the conformation integral. We denote the potential energy of the conformation $\{\nu\}$ by $U\{\nu\}$ and define the conformation integral as

$$\mathbf{Q}_c = N\int\int\cdots\int_{\Sigma\nu_{\lambda\mu}=N^2\nu} \exp[-U\{\nu\}/kT]\prod_{\lambda,\mu}{}'d\nu_{\lambda\mu}, \quad (19)$$

where the prime on the product sign means that one of the $\nu_{\lambda\mu}$—say, ν_{00}, for convenience—is to be excluded (i.e., treated as a dependent variable). $\mathbf{Q}_c$ is a surface integral wherein the N^2-1 variables range over the surface of the hyperplane.

The potential energy U is a complicated function of the pile heights but from Eq. (10) is a relatively simple function of the amplitudes $\{a\}$. A change from the variables $\nu_{\lambda\mu}$ to the variables a_{lm} is therefore indicated. With the definitions (6) and (7), the transformation of Eq. (3) may be written in the discrete form

$$\nu_{\lambda\mu} = \sum_{l,m} F_{lm\lambda\mu} a_{lm}. \quad (20)$$

This transformation is orthogonal, as is easily shown by noting the form of its inverse,

$$a_{lm} = \sum_{\lambda,\mu} F_{lm\lambda\mu}\nu_{\lambda\mu}, \quad (21)$$

and thus has unit Jacobian. Some caution is necessary, however, since Eqs. (20) and (21) regard all N^2 variables as independent, whereas the integral (19) is taken over a *surface* having constant ν. From Eqs. (21) and (7), $a_{00}=N^{-1}\sum\nu_{\lambda\mu}=N\nu$, so that constancy of ν demands constancy of a_{00}. In each of the two sets of N^2 variables, $\{(N\nu), \nu_{01}, \nu_{02}, \cdots, \nu_{\lambda\mu}, \cdots\}$ and $\{a_{00}, a_{01}, a_{02}, \cdots, a_{lm}, \cdots\}$ we may thus regard the first member as a parameter; the residual N^2-1 independent members in either set may be used as the integration variables in Eq. (19). We therefore require the Jacobian J connecting these two residual sets. From the orthogonal property of (20), the Jacobian of the overall-transformation: $\{\nu_{00}, \nu_{01}, \cdots, \nu_{\lambda\mu}, \cdots\}\rightarrow\{(N\nu), \nu_{01}, \cdots, \nu_{\lambda\mu}, \cdots\}\rightarrow\{a_{00}, a_{01}, \cdots, a_{lm}, \cdots\}$ is unity; moreover, it is the product of the Jacobians for the two successive steps. From Eq. (18), the Jacobian of the first step is seen to be $\partial\nu_{00}/\partial(N\nu)=N$, while that of the second step is just the desired Jacobian J connecting the two sets of N^2-1 independent variables. J is thus seen to have the value N^{-1}, and we may write the integral (19) in the form

$$\mathbf{Q}_c = \int\int\cdots\int \exp[-\beta^2\sum_{l,m}(l^2+m^2)a_{lm}{}^2]\prod_{l,m}{}'da_{lm}, \quad (22)$$

wherein the integration extends over the permissible range of the a_{lm}.

At this point a geometric interpretation of the transformation (20) may be helpful. Because this transformation is orthogonal, the two sets of coordinate axes $\{\nu\}$ and $\{a\}$ in the conformation space are related to one another by a rotation. One may show that the direction of the coordinate a_{00} is that of the normal to the hyperplane (18), while its value, $N\nu$, is just the distance of the plane from the origin. The remaining N^2-1 coordinate axes a_{lm} are therefore "parallel" to the plane. For N a prime number (a trivial *physical* restriction) it may be shown that there exists an appropriate choice of phase which makes these N^2-1 amplitude axes rigorously equivalent, i.e., so that they transform into one another as the molecular piles are shuffled among the sites. In other words, these axes are symmetrically disposed with respect to the surface over which the integral (22) is to be taken; and the set of components in the ν-space defining any given amplitude axis is identical with the set for any other such axis except for suitable permutations of the components.

The problem of evaluating the integral (22) is complicated by the nature of the limits: the integration must extend over only such sets $\{a_{lm}\}$ which (1) are consistent with the average thickness ν, and (2) nowhere lead to negative values of the $\nu_{\lambda\mu}$. For the BET model, both of these conditions are satisfied. We may be sure that the amplitudes attained for a real system (with nonzero surface energy) will not be greater than for the BET case. On the other hand we can probably afford to permit amplitudes as large as those for the BET case since the integrand of (22) becomes smaller as the negative exponent increases. Accordingly we shall adopt as an *upper limit* the BET result, Eq. (17), and write (again denoting by a prime the omission of the parametric zero-zero term)

$$N^{-2}\sum_{l,m}{}' a_{lm}{}^2 = \nu^2. \quad (23)$$

We now approximate the exact but intractable limits of the integration (22) by treating the a_{lm} as mutually independent variables, all of which, owing to their complete equivalence, have the *same* range, $-\hat{a}\leq a_{lm}\leq\hat{a}$:

$$\mathbf{Q}_c = 2\prod_{l,m}\int_0^{\hat{a}} \exp[-\beta^2(l^2+m^2)a^2]da. \quad (24)$$

The maximum value, $\hat{a}$, is to be chosen, according to Eq. (23), such that the rms amplitude is equal to the average thickness of the layer:

$$\nu^2 = \langle a^2\rangle = (1/\hat{a})\int_0^{\hat{a}} a^2 da = \hat{a}^2/3;$$

thus,

$$\hat{a} = \nu\sqrt{3}. \quad (25)$$

Since the adsorption process, as commonly conducted, occurs at constant temperature and volume, our cri-

terion for equilibrium will be the equality of the partial molecular Helmholtz free energy (chemical potential) in the adsorbed and vapor phases. We choose for the standard state of the gaseous adsorbate the saturated vapor, and for the adsorbed phase the (semi-infinite) liquid state, so that the two phases are at equilibrium when each is in its standard state.

The chemical potential of the vapor at pressure p, relative to the saturated vapor at pressure p^0 is $kT \ln x$ $(x=p/p^0)$. For the adsorbed phase the Helmholtz free energy A relative to that in its standard state A^0 is given in terms of the corresponding canonical partition functions $\mathbf{Q}$ and $\mathbf{Q}^0$ as

$$\begin{aligned} A-A^0 &= -kT \ln(\mathbf{Q}/\mathbf{Q}^0) \\ &= -kT \ln(\mathbf{Q}_c/\mathbf{Q}_c^0), \end{aligned} \tag{26}$$

where the last equality arises from our assumption that $\mathbf{Q}_c$ is the only factor in $\mathbf{Q}$ which is different in the adsorbed phase from its value $\mathbf{Q}_c^0$ in the liquid state. The equilibrium condition is now obtained by differentiating (26) with respect to the total number $N^2\nu$ of molecules in the adsorbed phase, and equating the chemical potential so obtained to that for the vapor phase:

$$-kT \ln x = kT \frac{\partial}{\partial(N^2\nu)} \ln(\mathbf{Q}_c/\mathbf{Q}_c^0). \tag{27}$$

Using Eq. (24) for $\mathbf{Q}_c$, we obtain

$$\begin{aligned} -\ln x &= \frac{\partial}{\partial(N^2\nu)} \sum_{l,m} \ln \frac{\int_0^{\hat{a}} \exp[-\beta^2(l^2+m^2)a^2]da}{\int_0^{\infty} \exp[-\beta^2(l^2+m^2)a^2]da} \\ &= (1/N^2) \sum_{l,m} \frac{(\partial\hat{a}/\partial\nu)\exp[-\beta^2(l^2+m^2)\hat{a}^2]}{\int_0^{\hat{a}} \exp[-\beta^2(l^2+m^2)a^2]da}. \end{aligned} \tag{28}$$

The symmetry of the problem permits the replacement of the summation over l, m by an integration over the index $\eta=(l^2+m^2)^{\frac{1}{2}}$ between the limits $0 \leq \eta \leq \hat{\eta}$, where the maximum value $\hat{\eta}$ is determined by the condition

$$(\pi/2)\int_0^{\hat{\eta}} \eta d\eta = N^2. \tag{29}$$

Equation (28) thus becomes

$$-\ln x = (\pi/2N^2)(\partial\hat{a}/\partial\nu) \int_0^{\hat{\eta}} \frac{\exp[-\beta^2\eta^2\hat{a}^2]\eta d\eta}{\int_0^{\hat{a}} \exp[-\beta^2\eta^2 a^2]da}. \tag{30}$$

This may be shown immediately to reduce to the BET isotherm at high relative pressures by setting $\beta=0$: employing Eqs. (29) and (25), Eq. (30) yields

$$-\ln x = \partial \ln\hat{a}/\partial\nu = 1/\nu;$$

but for x near 1,

$$-\ln x = -\ln[1-(1-x)] \cong (1-x),$$

so that

$$\nu \cong (1-x)^{-1}, \tag{16}$$

which we recognize as Eq. (16). It should be noted, however, that this result is not a critical test of the method of evaluation except insofar as $\hat{a}$ is proportional to ν.

Returning to Eq. (30), and introducing the new variables $\omega=\beta^2\hat{a}^2\eta^2$, $\xi=a/\hat{a}$, we obtain

$$-\ln x = (\pi/4N^2\beta^2\hat{a}^3)(\partial\hat{a}/\partial\nu) \int_0^{\hat{\omega}} \frac{\epsilon^{-\omega}d\omega}{\int_0^1 \epsilon^{-\omega\xi^2}d\xi}. \tag{31}$$

The upper limit $\hat{\omega}$ has the value $\beta^2\hat{a}^2\hat{\eta}^2$ which, from Eqs. (9), (25), and (29), is seen to be

$$\hat{\omega} = 24\pi\nu^2(\epsilon d^2/kT). \tag{32}$$

For normal liquids the ratio $\epsilon d^2/kT$ may be shown to be about 3 (see Section 7). In the region of large adsorptions, to which our assumptions restrict the validity of these results, ν is considerably greater than unity. Thus, $\hat{\omega}$ is at least 100, and because of the negative-exponential form of the integrand we incur an entirely negligible error in replacing $\hat{\omega}$ by ∞. (This argument is of course invalid if $\beta=0$, so that we shall not expect the BET isotherm to result from the final expression merely by substituting $\beta=0$.) With $\hat{\omega}=\infty$, the integral in (31) has the value $1.327\cdots$, or roughly 4/3. We thus finally obtain

$$-\ln x = (kT/18\pi\epsilon d^2)\nu^{-3} \tag{33}$$

as the theoretical adsorption isotherm for the case in which the effect of surface tension has been included while retaining the other assumptions of the BET theory.

We may note in passing that although Eq. (33) is based specifically upon an adsorbed phase having simple cubic packing, this is not an essential feature of the method of derivation. If the packing is such as to give for the interlayer spacing a distance τ different from the molecular diameter d, the corresponding expression may be shown to be identical with Eq. (33) except for the replacement of d by τ. For cubic closest packing, $\tau=d(2/3)^{\frac{1}{2}}$, so that in this case the coefficient of ν^{-3} would be just (3/2) that given in Eq. (33). This difference is not important for our purposes, and we shall continue to employ the result for the simple cubic case.

6. THE ENERGY OF ADSORPTION IN HIGHER LAYERS

We now turn to a consideration of assumption (b) of Section 1, concerning the heat of adsorption into the

successive layers. Hill's detailed treatment[12] of the extension of the van der Waals' forces emanating from the adsorbent into the adsorbed phase (which is considered as a liquid-like slab of uniform thickness) leads in our notation to an equation [his Eq. (9), reference 12a] having—apart from the different proportionality factor—the same functional relation between x and ν as in Eq. (33):

$$-\ln x=\left[\frac{\pi}{6}\rho_1{}^4 d_{11}{}^6\sigma_1{}^3\frac{\varepsilon_{11}}{kT}\left(\frac{\rho_2 d_{12}{}^6\varepsilon_{12}}{\rho_1 d_{11}{}^6\varepsilon_{11}}-1\right)\right]\nu^{-3}, \quad (34)$$

where ρ is the molecular number density, d_{ij} the equilibrium distance between a pair of molecules of types i and j, ε_{ij} the (minimal) potential energy of such a pair at d_{ij}, and σ the effective molecular cross section. The subscript 1 refers to the adsorbate and 2 to the adsorbent.

Since we shall not need here more than a rough value of the coefficient of ν^{-3} in Eq. (34), we immediately approximate it as follows: Apart from packing factors of order unity, $d_{11}{}^6\approx\rho_1{}^{-2}\approx\sigma_1{}^3$; if in addition we set‖ $\rho_1\approx\rho_2$ and $d_{12}\approx d_{11}$, Eq. (34) reduces to

$$-\ln x=\frac{\pi}{6}\frac{\varepsilon_{11}}{kT}\left(\frac{\varepsilon_{12}}{\varepsilon_{11}}-1\right)\nu^{-3}. \quad (35)$$

The question of how the two expressions (33) and (35) are to be combined may be answered by returning to the evaluation of the complete partition function. In Section 5 we have dealt only with that part dependent upon the surface-deformation energy. Now, however, we wish to assume that the total energy of the adsorbed phase will depend not only upon the surface conformation, but also upon the distance (altitude) of each molecule above the adsorbent surface. For small amplitudes of the Fourier components, the particular surface conformation will not appreciably affect the energy of a nonsurface molecule at altitude z. In first approximation there will therefore be no mixing of these two effects, and the total energy will be expressible as a sum of the deformation potential energy, the altitude potential energy, and of course the kinetic energy. In Section 5, we assumed these two latter terms to be the same in the adsorbed phase as in the reference state (the semi-infinite liquid), and therefore to cancel out in the ratio of the partition functions. Now we assume only the kinetic energy term to cancel. The absence of mixing of the two remaining potential energy terms leads to one factor for each in the total partition function, giving two additive terms in the work function or the chemical potential. The evident conclusion therefore is that when both effects are considered the surface-tension term [right-hand side of (33)] is to be added to that of Hill [right-hand side of (35)]:

$$-\ln x=\left[\frac{\pi}{6}\frac{\varepsilon_{11}}{kT}\left(\frac{\varepsilon_{12}}{\varepsilon_{11}}-1\right)+\frac{1}{18\pi}\left(\frac{kT}{\epsilon d^2}\right)\right]\nu^{-3}. \quad (36)$$

7. COMPARISON WITH EXPERIMENT

According to Eq. (36), a plot of $\log\nu$ *vs.* $\log(-\ln x)$ should give a straight line of slope $-\frac{1}{3}$. As has already been shown by Halsey,[11] the data of Jura and Harkins[18] for the adsorption of N_2 and of water on TiO_2 (anatase) do indeed conform very nearly to the ν^{-3} power law of (36). The general isotherm of the type given by Eq. (36), namely

$$-\ln x=\kappa/\nu^3, \quad (37)$$

is plotted in Fig. 2 in the more familiar form of ν *vs.* x for various values of κ. It is seen that the experimental data just cited yield a value of $\kappa\approx 4$. It remains, therefore, only to examine the theoretical magnitude of this coefficient.

We first consider the van der Waals' term of Hill. We may note immediately a simple connection between ε_{11} and kT, ε_{11} being essentially the energy of one van der Waals' "bond" between two adsorbate molecules. With closest packing in the liquid, each molecule has about twelve nearest neighbors. The energy of vaporization per molecule is thus $(12/2)\varepsilon_{11}$, a quantity given by Trouton's rule as $\sim 12kT$. To the accuracy we require, therefore, $\varepsilon_{11}/kT\sim 2$. The ratio $\varepsilon_{12}/\varepsilon_{11}$ may be estimated as follows: when the first layer is filled, a first-layer molecule has about six neighboring molecules laterally, and perhaps three neighbors in the adsorbent surface below. To vaporize this molecule would then require something like $3\varepsilon_{11}+3\varepsilon_{12}$, a quantity symbolized[17] in the BET theory as E_1/N_0, where N_0 is Avogadro's number. This quantity is to be com-

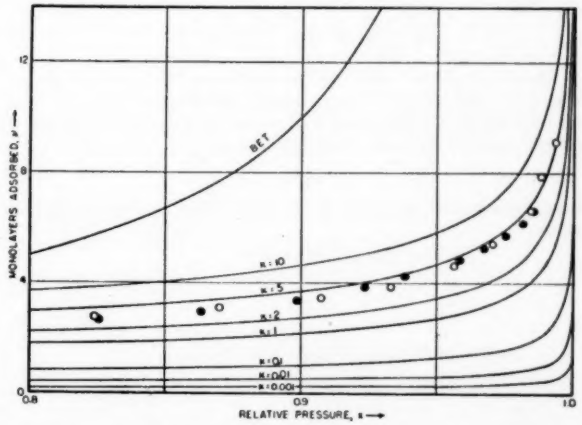

FIG. 2. Comparison of the BET isotherm and the isotherm of Eq. (37) with the experimental data of Jura and Harkins (see reference 18). ⊙—N_2 at 78°K, ●—Water at 298°K, on TiO_2 (anatase).

‖ We are here considering only the case where energy effects predominate. Differences in the densities and equilibrium distances may well overshadow these energy effects, but the approximation given will suffice for the crude estimate needed.

[18] G. Jura and W. D. Harkins, J. Am. Chem. Soc. **66**, 1356 (1944). The data shown in Fig. 2 were kindly made available by Dr. Jura.

pared with $E_L/N_0 \approx 6\varepsilon_{11}$, the energy of vaporization of a molecule from the semi-infinite liquid. Now the c-value[17] measures the difference between E_1 and E_L:

$$kT \ln c = (E_1 - E_L)/N_0 \approx 3(\varepsilon_{12} - \varepsilon_{11});$$

with $2kT \sim \epsilon_{11}$, we thus obtain

$$(\varepsilon_{12}/\varepsilon_{11}) - 1 \sim \ln c^{1/6}.$$

Using $c \sim 1000$ as a typical value, we finally obtain for the first term of the coefficient in Eq. (36),

$$\frac{\pi}{6}\left(\frac{\varepsilon_{11}}{kT}\right)\left(\frac{\varepsilon_{12}}{\varepsilon_{11}} - 1\right) \sim \frac{\pi}{3} \ln c^{1/6} \sim 1. \tag{38}$$

While this evaluation is certainly crude, it suffices to demonstrate that the term in question is of the experimentally observed order of magnitude.

We now consider the surface tension term. For a semi-infinite liquid, the surface energy ϵ per unit of *actual* surface is smaller than the (thermodynamic) surface energy e per unit of *apparent* surface by an amount kT/d^2. This difference arises from the thermal distortion of the surface: for a surface all of whose modes are classically excited, the excitation energy is kT per mode, the number of modes being simply the number $1/d^2$ of surface molecules per unit (undistorted) area. In most cases of interest, e and ϵ will not be very different, and we may use them interchangeably in order of magnitude calculations.

A simple consideration, like that given above based on the number of "bonds" which must be broken to vaporize a molecule from the surface of a liquid as compared with its interior, shows that the surface energy per molecule ϵd^2 is about one-third of the (molecular) energy of vaporization from the bulk liquid. This latter quantity, for normal liquids, is about $12kT$, so that $\epsilon d^2 \sim 4kT$, giving for the surface tension term[19] in Eq. (36):

$$kT/18\pi\epsilon d^2 \sim 1/72\pi \sim 0.005. \tag{39}$$

This value is three orders of magnitude smaller than the experimental value of κ, and does not make a significant contribution. In fact it may be noted that since it is already negligible, and since the surface energy ϵ appears in the denominator, we lose nothing by considering ϵ to be infinite. Then, however, no surface distortion is possible and the adsorbed phase becomes a slab of uniform thickness, as was indeed assumed in Hill's treatment. We conclude, therefore, that for cases in which the above approximations are substantially valid, multilayer adsorption is governed by the slight variation of the energy of adsorption due to the influence of the van der Waals' forces emanating from the surface.

It is now perhaps of interest to reexamine the above approximations to illuminate any possible exceptions to this conclusion. First, it seems unlikely that any liquid should have the ratio $kT/\epsilon d^2$ sufficiently larger than the above estimate to change the order of magnitude of the surface tension term. On the other hand, it is possible to imagine adsorbent-adsorbate pairs in which the quantity in Eq. (38) is much smaller than unity ($c \sim 1$), or even negative. This would presumably be the case for highly polarizable or dipolar molecules adsorbed on a substrate of low atomic number,[20] giving $\varepsilon_{11} > \varepsilon_{12}$. Under such circumstances the surface tension term might be significant provided one could go to sufficiently high relative pressures to give multilayer adsorption. Unfortunately, isotherms of the requisite character (Type III) have been little studied in this region, and we are aware of no data which might permit an experimental comparison in these unusual cases.

---

[19] Should it prove desirable to evaluate this term more precisely one may proceed by employing the Ramsey-Shields Equation relating at temperature T the surface tension γ, the surface entropy s and the critical temperature T_c:

$$\gamma = s(T_c - T), \tag{A}$$

where, for normal liquids, $s \approx 2.12/N_0^{\frac{1}{3}}d^2$. From the thermodynamic relation

$$\gamma = e - Ts \tag{B}$$

there follows

$$\begin{aligned}\epsilon &= \gamma + Ts - kT/d^2 \\ &= \gamma + \frac{T}{d^2}\left(\frac{2.12}{N_0^{\frac{1}{3}}} - k\right) \\ &= \gamma + 1.6T/d^2(\text{A}^2).\end{aligned} \tag{C}$$

In practice, since gas adsorption experiments are customarily carried out at temperatures near the boiling point T_b of the adsorbate, another approximate form is useful: for many substances $T_c \approx (5/3)T_b$, and we thus have approximately

$$\gamma = s[T_c - (3/5)T_c] = (2/5)sT_c = (2/5)e \approx (2/5)\epsilon,$$

or

$$\epsilon \approx (5/2)\gamma. \tag{D}$$

[20] See discussion of Type III isotherms in reference 2, pp. 163–166.

The Phase Diagram of the BaO-TiO_2 System*†

W. O. STATTON**
Laboratory for Insulation Research, Massachusetts Institute of Technology, Cambridge, Massachusetts
(Received June 19, 1950)

A method for accurately observing phase changes at high temperatures has been developed; it employs a microfurnace and uses samples of oxide mixtures weighing less than 1 mg. The samples were observed and their temperatures measured with an optical pyrometer specially adapted for this purpose and calibrated for the furnace radiation. An electrically heated resistance strip, in general of molybdenum, allows melting and crystallization of the oxide mixtures at any desired speed. The samples were placed directly on the strip and could be quenched by interruption of the current flow.

The binary system, BaO-TiO_2, was investigated. The existence of four compounds, $BaTi_4O_9$, $BaTi_2O_5$, $BaTiO_3$, and Ba_2TiO_4, was demonstrated by liquidus curves and x-ray diffraction. A phase change of $BaTiO_3$ below the solidus temperature was observed; all oxide mixtures with less than 80 mole percent TiO_2 showed this intermediate $BaTiO_3$ phase at about 1450°C.

Single crystals of $BaTi_4O_9$, $BaTi_2O_5$, and $BaTiO_3$ were grown from ternary melts of $BaCO_3$, TiO_2, and $BaCl_2$. The compound, $BaTi_4O_9$, showed extensive polymorphism. Attack by molten BaO mixtures on molybdenum and platinum produced the compounds, $BaMoO_4$, $Ba_3Pt_2O_7$, and $Ba_3Ti_2PtO_9$.

INTRODUCTION

BARIUM titanate, first noticed for its unusual dielectric properties by Wainer and Salomon in 1942–43,[1] and established as a new ferroelectric material in the Laboratory for Insulation Research in 1943–44,[2] has gained appreciable scientific and technical importance in the last few years. Its dielectric properties have been investigated systematically, especially on single crystals, and much has been learned about the mechanism of ferroelectricity.[3] However, a real understanding of the ceramic material presupposes a thorough knowledge of the phase diagram of its components. It was the

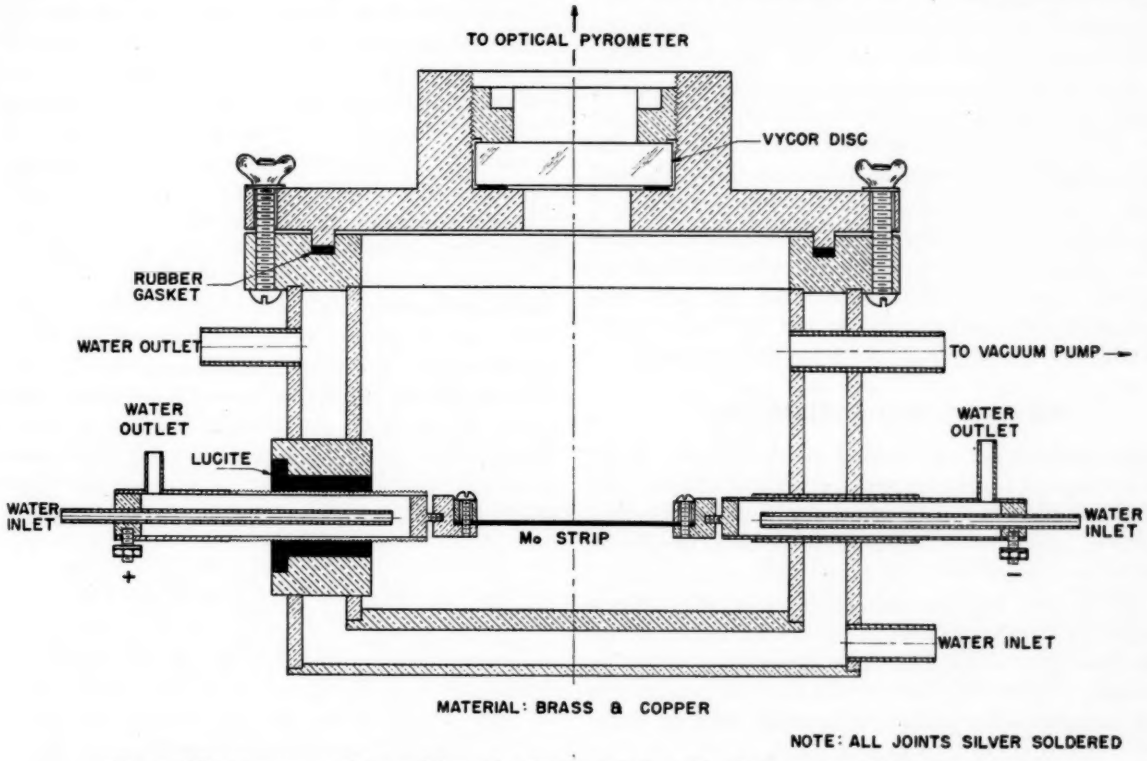

FIG. 1. Microfurnace used for melting point determinations. (The figure is three-fifths actual size.)

* Sponsored by the ONR, the Army Signal Corps, and the Air Force under ONR Contract N5ori-07801.
† From a thesis submitted in partial fulfillment of the requirements for the degree of Doctor of Philosophy in Inorganic Chemistry at the Massachusetts Institute of Technology.
** Present address: RCA Laboratories, Princeton, New Jersey.
[1] E. Wainer and A. N. Salomon, Titanium Alloy Manufacturing Company, Elec. Rept. 8 (1942), 9, and 10 (1943); E. Wainer, Trans. Electrochem. Soc. 89, Preprint 3 (1946).
[2] A. von Hippel and co-workers, NDRC Reports 14-300 (1944), 14-540 (1945); von Hippel, Breckenridge, Chesley, and Tisza, Ind. Eng. Chem. 38, 1097 (1946).
[3] A. von Hippel, Revs. Modern Phys. 22, 221 (1950).

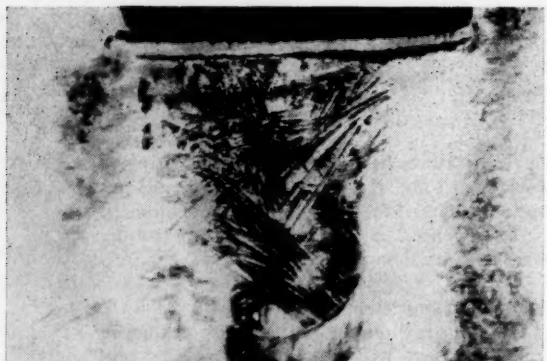

FIG. 2. Crystallization on molybdenum strip. (×25).

purpose of the present study to provide this knowledge for the system BaO-TiO_2.

There is no published record of previous research on the complete phase diagram of the binary system, BaO-TiO_2. The only closely related work is by Bunting and co-workers at the National Bureau of Standards[4,5] who prepared ceramic disks of varying mixtures in the ternary systems BaO-SrO-TiO_2 and BaO-MgO-TiO_2. The part of their data applicable to this research is confined to 9 mixtures of BaO and TiO_2 between the limits of 100 and 50 mole percent TiO_2. In this range the authors suggest the compounds $BaTiO_3$, $BaTi_4O_9$, and "others," basing their suggestions on measurements of the maturing temperatures and the dielectric constants of the ceramic mixtures and x-ray diffraction of the powdered products. Other authors[6–8] list the compounds, Ba_2TiO_4 and $Ba_2Ti_3O_8$, but no well-defined qualitative or quantitative study has been reported.

METHODS AND EQUIPMENT

More information was desired for the present study than is obtained from the usual methods of determining oxide phase diagrams (such as the study of fusion points of oxide mixtures or measurement of physical properties of ceramic preparations). The precise measurement of the solidus and liquidus temperatures or other phase transitions of oxides requires a direct visual observation of the heating process. Therefore, an adaptation of the technique of Burgess[9] was chosen for this research in which samples were placed on a small strip of metal electrically heated in a microfurnace and observed with a microscope-optical pyrometer.

A section of the microfurnace designed for the present research is shown in Fig. 1. A metal strip is held by removable copper clamps at the ends of water-cooled electrodes, one of which is insulated from the water-cooled furnace shell by a plug of Lucite. The removable lid is fitted with a seated gasket; either vacuum or pressure may be used in the furnace. A removable Vycor disk placed at the center of the lid allows visual observation of the heating process. The stabilized input voltage, controlled by a variac, feeds a transformer with a secondary rating of 5 volts, 50 amperes. The temperature can be changed in steps smaller than 5°C with this arrangement.

The optical pyrometer is a potentiometric, direct-reading type (Leeds and Northrup, #8622-C) covering the range from 775° to 2800°C. It was mounted in a heavy brass base on the lid of the furnace, thereby centering the line of sight on the middle of the heated metal strip. The focal length of the telescope was altered by extending one of the objective lenses 3 cm from its original position. This allows the focusing of the pyrometer on the metal strip at the close range of 10 cm and increased the magnification to about tenfold.

The metals that might be used as the resistance strip for the BaO-TiO_2 system are not numerous. Molybdenum was chosen since it has a high melting point‡ (2620°C), is ductile, is relatively inexpensive, and its emissivity is well known. Its major disadvantages are the formation of the volatile oxide MoO_3, and the attack by BaO to form a barium molybdate, as is shown later. The formation of the volatile oxide was avoided by using a moderate vacuum (30μ Hg).

The pyrometer scale was calibrated by comparison with a standardized instrument of identical design§ and agreed within the experimental error of 0.3 percent. The pyrometer reading refers to black body temperatures. A correction for the emissivity of molybdenum was made by using the data of Worthing.[10] The over-all correction factor was found by melting two materials of accurately known melting points in the microfurnace.

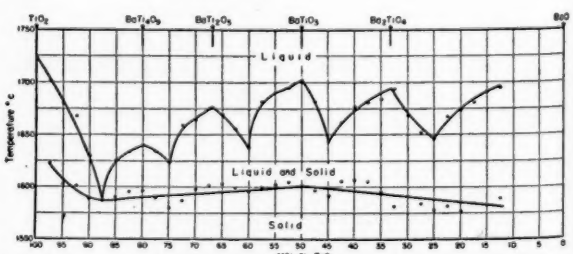

FIG. 3. Liquidus and solidus curves, BaO-TiO_2 system.

[4] Bunting, Shelton, and Creamer, J. Am. Ceram. Soc. **30**, 114 (1947).
[5] Shelton, Creamer, and Bunting, J. Am. Ceram. Soc. **31**, 205 (1948).
[6] H. P. Rooksby, Nature **159**, 609 (1947).
[7] J. W. Mellor, *Comprehensive Treatise on Inorganic Chemistry* (Longmans, Green and Company, London, 1927), Vol. VII, p. 54.
[8] J. N. Friend, ed., *Textbook of Inorganic Chemistry* (Griffen, London, 1921), Vol. V, p. 249.
[9] G. K. Burgess, U. S. Bur. Stds., Scientific Papers No. 198, 205, 242 (1920).

‡ The melting points of TiO_2 and BaO are 1825° and 1923°C, respectively.
§ Kindly furnished by the Heat Measurement Laboratory, Mechanical Engineering Department, M.I.T.
[10] A. G. Worthing, Phys. Rev. **28**, 190 (1926).

The averages of scale readings of 12 calibrating runs was 1768°C for platinum (mp 1774°C) after correcting for Mo emissivity, and was 1549°C for palladium (mp 1555°C). Thus it was deduced that the over-all temperature conversion should be the molybdenum emissivity correction plus a 6°C correction for absorption and reflection of light by the Vycor disk.

Calculated proportions of pure, reagent grade BaO and TiO_2 were accurately weighed to total 10 g. This mixture of oxides was then used as the master sample from which were taken individual samples after thorough mixing by mechanical rolling and manual stirring. Forty master samples were prepared in this manner to cover the range of compositions from pure TiO_2 to pure BaO, each master sample differing by 2.5 mole percent. The individual sample (<1 mg) was pressed on the molybdenum strip as compactly as possible. Strips 5×17 mm of pure molybdenum metal 8 mils thick were found to cover the field of view while not requiring an excessively large heating current. The temperature rise to final melting was obtained as quickly or as slowly as desired (from fractions of a second to an hour). The usual speed was 10 to 15 minutes for the heating from 1300 to 1750°C. Equilibrium was established very quickly for the small amount of sample present.

The melting-point transition was always definite and could be easily and accurately observed. By lowering the temperature of the strip a very few degrees, a recrystallization could be produced which started at the coldest parts of the strip. The alternating melting and freezing could be repeated many times unless the liquid was volatile and gradually boiled off. The shapes of the crystals which formed were characteristic of the composition and cooling rate; they were often needle-shaped (Fig. 2).

The sample was purposely placed at several locations on the strip so that the various areas could be compared. Thus, a progression of melting effects could be observed from the most central to the more lateral sample locations as the temperature of the strip increased. Some free molybdenum must be next to the flow area in order to obtain a temperature reading since the oxide emissivity differs from that of the metal.

To prepare samples for x-ray diffraction the edges of the molybdenum strips were bent into cup-like depressions to retain the molten mixtures. It is essential to use several milligrams of the oxide mixture since an appreciable volume decrease takes place on melting and enough product must remain for the analysis. The solidified melt, lifted under microscopic observation from the strip and pulverized in a small agate mortar, was rolled into a thin rod with a noncrystalline, quick-drying cement.

TABLE I. Oxide compositions at liquidus peaks.

Mole % TiO_2 near peak	Mole ratio BaO:TiO_2	Oxide formula	Chemical formula
80	1:4	$BaO \cdot 4TiO_2$	$BaTi_4O_9$
66.7	1:2	$BaO \cdot 2TiO_2$	$BaTi_2O_5$
50	1:1	$BaO \cdot TiO_2$	$BaTiO_3$
33.3	2:1	$2BaO \cdot TiO_2$	Ba_2TiO_4

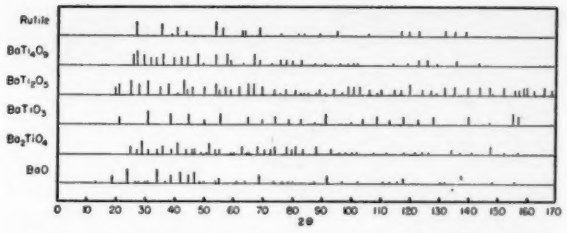

FIG. 4. X-ray patterns of components and compounds.

The x-ray source was a standard, sealed-off, water-cooled tube with copper target. A nickel filter absorbed all but the $K\alpha$ wavelengths of the copper spectrum. The tube was operated at 40 kv and 15 ma. The exposures in a standard Debye-Scherrer powder camera (57.3 mm diam) varied from one to six hours, depending on the nature and amount of the sample. Frequently high background radiation was obtained even on short exposures due to fluoroescence of the powder; a very thin ($\frac{1}{2}$ mil) nickel sheet placed over the film absorbed most of this radiation.

THE BINARY BaO-TiO_2 SYSTEM

1. Liquidus Curves

If an oxide mixture is heated to its solidus temperature, some liquid should form and a solid-liquid mixture should be present until the temperature is raised to the liquidus point where the entire sample will liquefy. This sequence was actually observed visually for all mixtures in the BaO-TiO_2 system. It was readily noted with experience that small amounts of the sample were still solid above the final solidus temperatures and appeared to be floating in the liquid as "islands." This was a true two-phase region in accordance with phase diagram principles.

The liquidus point for each mixture was obtained by observing the temperature at which the tiny crystalline islands finally liquefied, being verified by slight cooling of the strip and noting the temperature at which some solid first reappeared. The values of the liquidus temperature were obtained from several areas on each strip, and at least four independent runs with new molybdenum strips were made. Deviations from strip to strip were usually 5°C. The technique thus produced excellent precision for practically all of the samples (*ca.* 0.3 percent at 1650°C) and verified that the sample preparation was uniform and the method of observation satisfactory.

The curves obtained by connecting the liquidus and solidus temperatures of the varying oxide mixtures are shown in Fig. 3. The nature of the phase marked "solid" in Fig. 3 will be discussed in the next section.

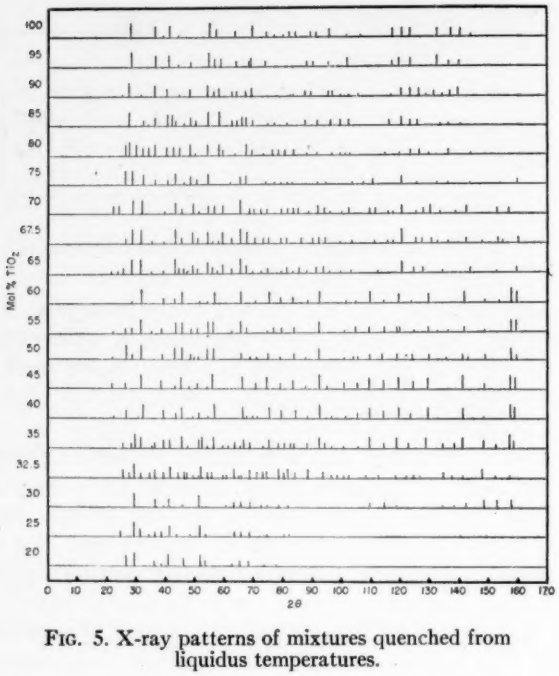

FIG. 5. X-ray patterns of mixtures quenched from liquidus temperatures.

Four distinct peaks occurred in the liquidus curves at compositions other than the pure oxides, TiO_2 and BaO. The peaks correspond to compositions which have the simple oxide mole ratios shown in Table I.

Further verification of the existence of these compounds was obtained by preparing samples for x-ray diffraction with 80, 67.5, 50, and 32.5 mole percent TiO_2. Since many details of the fine structure of x-ray patterns are lost in the reproduction process, Fig. 4 has been prepared to show clearly the positions of the lines and their approximate intensity,‖ and demonstrates that each compound has really a unique structure differentiating it from the other compounds and the pure oxides.

No evidence was found for the formation of a meso compound,[7,8] $Ba_2Ti_3O_8$. This compound would appear as a peak in the liquidus curve at 60 mole percent TiO_2 where actually a low eutectic point is observed in the curve (see Fig. 3). However, the compound, $BaTi_4O_9$, which had previously been suggested, is confirmed. The data of Bunting and his co-workers,[4,5] show a definite peak in the maturing temperature and a depression in the dielectric constant at 80 mole percent TiO_2 which corresponds to the compound, $BaTi_4O_9$. There is a shoulder at 65 mole percent TiO_2 in the curve of maturing temperatures which probably corresponds to the formation of the compound, $BaTi_2O_5$. The authors did not suggest this latter compound, nor did they extend their studies beyond the 50 mole percent TiO_2 mixture. The only compound previously found in BaO-rich mixtures was Ba_2TiO_4 as an oxide coating on certain electrodes. Rooksby[6] published the x-ray pattern for this compound, but the reproduction is too poor to enable a check with the pattern for Ba_2TiO_4 obtained in this research.

A true eutectic composition was found for the mixture of 87.5 mole percent TiO_2. As the temperature of 1585°C was reached in heating this mixture, the solid immediately flowed, and no crystalline matter remained. Compositions richer in TiO_2 than the true eutectic mixture show evidence of solid solution; the solidus line definitely curves upward from its point of meeting the liquidus curve at the eutectic point (see Fig. 3).

The x-ray pattern obtained for a composition different from any of the four compounds contains the lines of two compounds, with lines in the pattern being strongest for the most plentiful compound in the mixture. The continuous series of mixtures from TiO_2 to BaO in steps of 5 mole percent show the progressive appearance of the lines of the various compounds of the system (Fig. 5).

The liquidus and solidus curves extend down only to 12.5 mole percent TiO_2 and do not include mixtures richer in BaO, or BaO itself. It was found that these mixtures gave very low melting points on the molybdenum strips. In fact, the melting point for BaO was consistently found to be 1475°C in over a dozen determinations with samples of BaO from different sources. The melting point as determined by Schumacher[11] is given as an average of 1923°C. The answer to this anomaly was obtained by preparing an x-ray diffraction film for the product obtained by melting BaO on the molybdenum strips. The pattern of this film is in agreement with the published pattern[12] for the com-

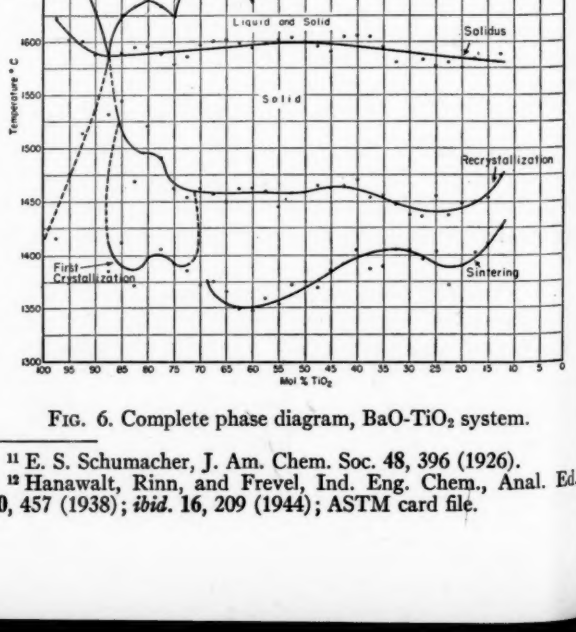

FIG. 6. Complete phase diagram, BaO-TiO_2 system.

‖ The estimated intensity of each line in the film is indicated by its height; the spacing corresponds to value of 2θ for each line, where θ is the angle of reflection of the x-rays from the corresponding planes of atoms in the crystal.

[11] E. S. Schumacher, J. Am. Chem. Soc. **48**, 396 (1926).

[12] Hanawalt, Rinn, and Frevel, Ind. Eng. Chem., Anal. Ed. **10**, 457 (1938); *ibid.* **16**, 209 (1944); ASTM card file.

pound $BaMoO_4$. Attack and etching of the molybdenum strip could be detected after the melting of compositions with less than 10 mole percent TiO_2.

Liebhofsky, Rochow, and Winslow[13] melted a barium molybdate in a platinum crucible and obtained a sharp break in the cooling curve at 1480°±5°C, in excellent agreement with the value of 1475°C found in the present research.

Schumacher obtained the melting point of BaO on tungsten in a manner somewhat analogous to the procedure of this research. He did not state unequivocally that no barium tungstate is formed in his procedure, but his evidence strongly indicated no attack. Attempts in the present research to melt BaO on tungsten resulted in values lower than Schumacher reported. However, he used a hydrogen atmosphere by which oxidation reactions can be avoided.

No probable stoichiometric compound of the oxides of barium and titanium at concentrations lower than 20 mole percent TiO_2 can be foreseen. Since the precise liquidus and solidus curves extend down to 12.5 mole percent TiO_2 before the irregularities appeared, it seems justifiable to assume that the entire range of compositions that can form compounds has been studied.

2. Transitions below the Solidus Curve

The previous description of the liquidus and solidus curves has ignored important aspects of the complete phase diagram. Visual observation of the melting process gave evidence of several important phase changes which occurred at temperatures below the solidus curve. The complete phase diagram is shown in Fig. 6. The values plotted are averages of several hundred individual determinations.

Compositions from 70 to 10 Mole Percent TiO_2

For all samples of mixtures with <70 mole percent TiO_2 three major phase changes were observed. At temperatures near 1375°C a reddening of the edges of the sample and a very slight liquid flow or condensation was observed. This was assumed to be a sintering reaction of the oxides corresponding to the firing temperatures that are used to produce dense ceramics in industrial processes. The mean deviation of the individual determinations for this sintering was about 15°C. It was not possible to obtain samples for x-ray studies from mixtures at this onset temperature since only the edges of the sample attain the sintering stage due to poor thermal contact.

The second phase transition for mixtures with less than 70 mole percent TiO_2 occurred at about 1460°C. In this case a general flow of the sample took place in which all of the oxide sample melted. However, crystals were formed out of this liquid flow even though the temperature was not changed. These crystals had a similar appearance for all mixtures, and the conclusion could be reached visually that they were identical in composition. Figure 7 indicates the appearance of the long needles formed at this transition.

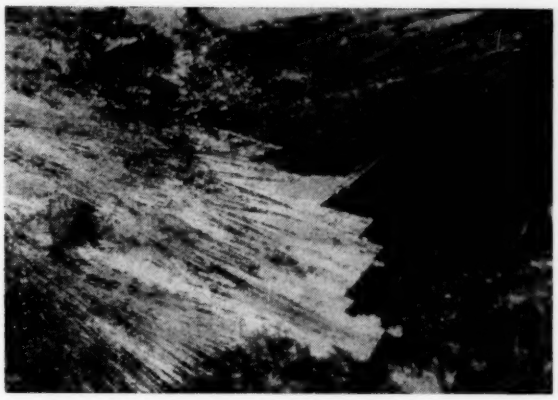

FIG. 7. Recrystallization at *ca.* 1460°C of oxide mixture containing 45 mole percent TiO_2. (×25).

The crystals formed rapidly whether the temperature was maintained constant or increased with various speeds. Figure 6 shows that the transition occurred at about the same temperature for almost the entire range of compositions below 70 mole percent TiO_2. The averages plotted on the diagram for this transition are the result of 6–10 separate determinations with a mean deviation of *ca.* 25°C.

The third phase transition for mixtures with less than 70 mole percent TiO_2 was described previously as the solidus transition. The needle-like intergrowths which had formed at the lower temperature of 1460°C did not change in any visible way until the temperature was increased to about 1600°C. At this higher temperature they suddenly partially melted and a general flow occurred, leaving a two-phase mixture of liquid and very tiny "islands" of solid. There was a distinct difference in size and appearance of the larger needle crystals and the very small island crystals (Fig. 8). The higher transitions were determined with much better precision due to more intimate mixing and contact with the metal strip after the initial melting.

If a single crystal or powdered cubic $BaTiO_3$ was used as the starting material, it behaved in its melting process identically to a 1/1 mixture of BaO and TiO_2. It sintered, flowed, recrystallized, and again melted at the same temperatures as this oxide mixture. These observations indicated that this behavior is a property of the compound, $BaTiO_3$. Furthermore, if single crystals of cubic $BaTiO_3$ were heated to about 1550°C (to avoid a vertical temperature gradient extremely thin crystals were selected) and the recrystallized long needles quenched, samples resulted which no longer contained any of the cubic $BaTiO_3$ x-ray pattern but an entirely different structure. This new pattern did not conform to any of the structures for the component oxides, the other barium titanate compounds or barium

[13] Liebhofsky, Rochow, and Winslow, J. Am. Chem. Soc. **61**, 969 (1939).

FIG. 8. Strip having regions of different temperature before quenching, and showing small, "island" crystals (right) and larger, needle crystals (middle and left). (×40).

molybdate, but consisted of the extra lines which had been found in all samples of oxide mixtures heated to this intermediate temperature (Fig. 9). The evidence exists, therefore, that near 1450°C an intermediate phase of $BaTiO_3$ is formed which reverts at 1600°C into the normal cubic structure. The existence of this new form of $BaTiO_3$ seems to account for the visual observation of the intermediate transitions and the presence of the new extra lines in the x-ray patterns.

Oxide melts for x-ray determinations always resulted in mixed phases of $BaTiO_3$ (see Fig. 9) since the presence of the vertical temperature gradient in the samples did not allow uniform phase transitions. Even melting single crystals of $BaTiO_3$ often resulted in mixed phases although the new intermediate structure was found to predominate.

One might suspect that oxygen loss has something to do with this complex situation. However, powdered crystals of cubic $BaTiO_3$ exhibited the identical sequence of phase transitions on strips of platinum either in vacuum or under one atmosphere of oxygen.

To investigate the reversibility of the reactions in the phase diagram, samples were cooled slowly (about 75°C/min) through the transition temperatures. Study of the x-ray patterns of such slowly cooled melts compared with patterns of corresponding compositions quenched from the liquidus temperature indicated that the reactions shown on the phase diagram (Fig. 6) are reversible, since lines of cubic $BaTiO_3$ and the intermediate phase both appear in all patterns of the slowly cooled melts and in the range 40 to 60 mole percent TiO_2 lines of the intermediate phase are stronger.

Compositions from 85 to 70 Mole Percent TiO_2

The samples with TiO_2 content from 72.5 to 85 mole percent (see Fig. 6) differed from those of the preceding region by exhibiting a formation of very small crystals at the first transition instead of a sintering process. This crystal formation took place generally after a brief, slight flow of the oxides. The crystals showed a tiny needle-like growth; unfortunately, not enough of this phase could be secured for x-ray determination.

In further heating of these small crystals, a transition was observed in which larger crystals were formed with identical appearance and x-ray pattern as for the intermediate form of $BaTiO_3$ described for the other region (see Fig. 9, 80 mole percent TiO_2 pattern). The temperature of this transition was higher for these mixtures, and the transition line in Fig. 6 sharply curves to higher temperatures with increasing TiO_2 content. A smooth curve was drawn through rather widely variant average values for the transition in this region.

If the 80 mole percent TiO_2 mixture is quenched from the liquidus temperature the x-ray structure previously discussed may not always result (Fig. 10, pattern *A*). Instead, pattern *B* may be obtained. Crystals can be grown from a ternary melt (see Fig. 12) which have the identical pattern, as shown in *C*. If these crystals are melted and quenched, pattern *D* results which is identical with pattern ***E***, once obtained by the author by quenching a composition of 85 mole percent TiO_2 from the liquidus temperature. Hence, there is a complicated kind of polymorphism in these titania-rich compounds which should be further investigated.

3. Melting Point of TiO_2

There has been much confusion in the literature regarding the true melting point of rutile. Chemical handbooks list the melting point as 1640°C which refers probably to the early determination of Ruff.[14] Other authors[15] report such varying values as 1560°, 1980°, and 1610°C. More recent determinations by von Wartenberg and co-workers[16] gave 1825° and 1850°C, a value checked by Bunting.[17] The melting point of TiO_2 obtained in this research did not agree with either the old or the more recent values, but was intermediate (1720°C). This value was precisely obtained for reagent grade powders of TiO_2 (anatase) from several

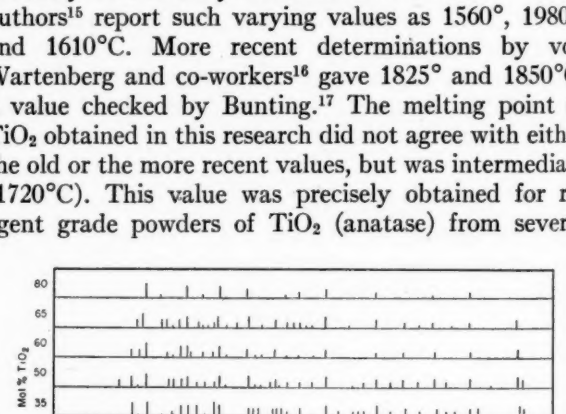

FIG. 9. X-ray patterns of mixtures heated to recrystallization temperatures.

[14] O. Ruff, Z. anorg. Chem. **82**, 373 (1913).
[15] See reference 7, Vol. VII, p. 38.
[16] H. von Wartenberg and W. Gurr, Z. anorg. Chem. **196**, 374 (1931); H. von Wartenberg and E. Prophet, Z. anorg. Chem. **208**, 369 (1932); von Wartenberg, Reusch, and Saran, Z. anorg. Chem. **230**, 257 (1937).
[17] E. N. Bunting, J. Research Nat. Bur. Standards **11**, 719 (1933).

manufacturers and also for pure single crystals of rutile. It is likely that the vacuum used in our system caused some reduction which lowered the melting point of the material. The phase diagram reported in this research may therefore give temperatures somewhat too low for samples in the region of high TiO_2 content. The values as reported are consistent and precise for our experimental conditions.

SINGLE CRYSTALS OF $BaTiO_3$, $BaTi_2O_5$, AND $BaTi_4O_9$

It was established early in the work on ferroelectric $BaTiO_3$ that single crystals could be grown by using $BaCl_2$ as a flux. This procedure was now used to grow single crystals of $BaTiO_3$, $BaTi_2O_5$, and $BaTi_4O_9$ and thus to confirm the existence of the latter two compounds. Tabular data of their interplanar spacings obtained from their x-ray diffraction patterns are reported elsewhere.[18]

1. Growth of $BaTiO_3$ Crystals

Barium titanate single crystals of hexagonal and cubic symmetry were first obtained by Blattner, Matthias, and Merz[19] from ternary melts on the basis of early work by Bourgeois,[20] a method later improved and simplified by Matthias.[21] Many repetitions and variations of this procedure indicated that the suggested proportion of $BaCO_3$:TiO_2 (25:5) did not consistently produce as perfect and large ferroelectric crystals as a 25:6 mixture. In several instances using the 25:5 ratio, black crystals were obtained which were cubic and not ferroelectric at room temperature; this never occurred in about 50 growths using the 25:6 ratio. Furthermore, the crystals tended to be more regular and large when the 25:6 ratio was used. This composition of optimum growth is a BaO:TiO_2 mole ratio of 1.31.

The formation of $BaTiO_3$ was observed over an extremely large range of compositions. The cubic form at room temperature was found in growths which had so little TiO_2 present that $Ba_3Pt_2O_7$ was formed simultaneously (see below). With increasing content of TiO_2 in the growth mixture, the tetragonal form was obtained instead of the cubic. The approximate mole ratio of BaO:TiO_2 in the mixture resulting in this change of structure was 1.5. Furthermore, the habit of the tetragonal growths showed a great dependence on the concentration of TiO_2. The growths ranged from perfect, dense plates to internal skeletal growths; extensive twinning and extreme parallel growth along the triad axis were also found.

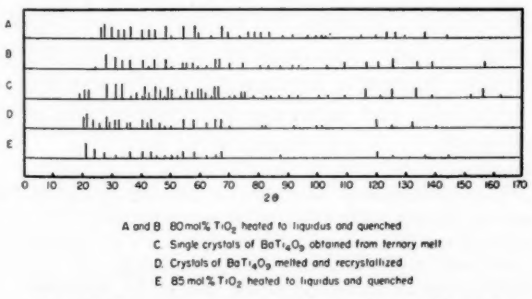
A
B
C
D
E
0 10 20 30 40 50 60 70 80 90 100 110 120 130 140 150 160 170
2θ
A and B 80 mol% TiO_2 heated to liquidus and quenched
C. Single crystals of $BaTi_4O_9$ obtained from ternary melt
D. Crystals of $BaTi_4O_9$ melted and recrystallized
E. 85 mol% TiO_2 heated to liquidus and quenched

FIG. 10. X-ray patterns showing polymorphism of mixtures rich in TiO_2.

FIG. 11. Monoclinic $BaTi_2O_5$. (×25).

Three growths with BaO:TiO_2 mole ratios of 1.96, 0.57, and 0.46 produced x-ray patterns of cubic $BaTiO_3$ which also contained as a minor constituent the strong lines of the new intermediate phase of $BaTiO_3$ described for the binary system.

Previously, the hexagonal form of $BaTiO_3$ has been produced from an alkali carbonate flux only.[19] It was surprising, therefore, to find that the growth containing a BaO:TiO_2 mole ratio of 0.39 produced white aggregates of an identical x-ray pattern.

2. Growth of Monoclinic $BaTi_2O_5$

Extremely long needles of this compound were formed from the ternary growth with 68.4 mole percent TiO_2. The crystals seen in Fig. 11 are typical of the extreme thinness of the needles.

The powder pattern of these crystals was identical to that of the oxide mixture of 67.5 mole percent TiO_2 which had been taken to the liquidus temperature in the microfurnace and quenched. Preliminary studies of the single crystals with a Buerger precession x-ray camera indicated that the crystals have monoclinic symmetry.

3. Growth of $BaTi_4O_9$

Growths rich in TiO_2, ranging from 71 to 84 mole percent, produced both single crystals and powders which were analyzed as $BaTi_4O_9$. Between 71 and 80 mole percent TiO_2 clear light amber crystals with irregular surfaces were produced (Fig. 12); above 80 mole percent TiO_2 small white crystalline aggregates resulted. Both types showed identical x-ray patterns

[18] W. O. Statton, Tech. Rep. XXXI, ONR Contract N5ori-07801, Lab. Ins. Res., M.I.T., April, 1950.
[19] Blattner, Matthias, and Merz, Helv. Phys. Acta **20**, 225 (1947).
[20] L. Bourgeois, Compt. rend. **103**, 141 (1886).
[21] B. Matthias, Phys. Rev. **73**, 808 (1948).

FIG. 12. Crystals of $BaTi_4O_9$. (×25).

which corresponded to one of the patterns obtained for the mixture with 80 mole percent TiO_2 in the binary study.

CRYSTALS FORMED IN TiO_2-POOR MELTS

1. Hexagonal $Ba_3Pt_2O_7$

This compound was formed by the chemical attack of molten BaO on the platinum crucible containing the reaction mixture if the BaO:TiO_2 mole ratio was <4. The $Ba_3Pt_2O_7$ hexagonal crystals are seen in Fig. 13 and the surface of the attacked platinum dish is pictured in Fig. 14 showing the depressions and etched pits caused by the growing crystals. Chemical analysis established the composition of these crystals. Calc for $Ba_3Pt_2O_7$: 45.1 percent Ba, 42.7 percent Pt; found: 46.4 percent Ba, 41.6 percent Pt. The existence of this compound was reported by Rousseau.[22]

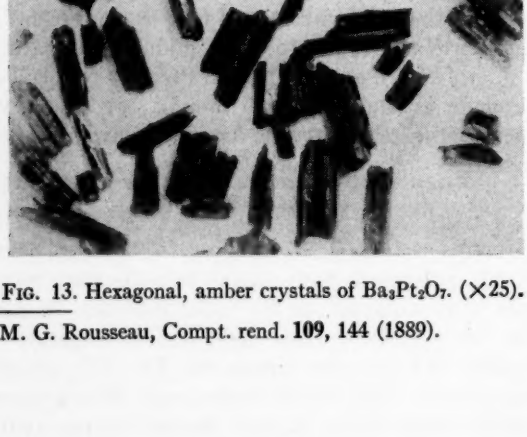

FIG. 13. Hexagonal, amber crystals of $Ba_3Pt_2O_7$. (×25).

[22] M. G. Rousseau, Compt. rend. **109**, 144 (1889).

The $Ba_3Pt_2O_7$ crystals showed dielectric constants up to 2700 at 130°C and 1 kc. These values, however, must be attributed to interfacial polarization because they rapidly decreased with increasing frequency.

2. Orthorhombic $Ba_3Ti_2PtO_9$

The mole ratio of BaO:TiO_2 in the melt leading to these orthorhombic needles ranged from 3.9 to 2.0 (that is, between the ratios producing tetragonal $BaTiO_3$ and hexagonal $Ba_3Pt_2O_7$). The determination of the composition of these crystals was made exceedingly difficult by the presence of white $BaTiO_3$ crystals¶ of similar size and chemical properties. Manual separation of the crystals under the microscope resulted in small samples which gave the approximate formula, $Ba_3Ti_2PtO_9$.

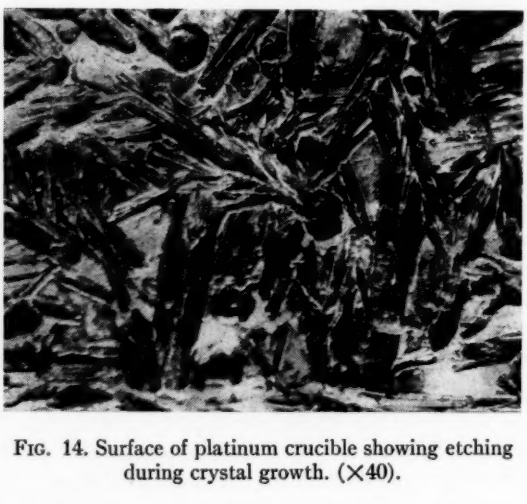

FIG. 14. Surface of platinum crucible showing etching during crystal growth. (×40).

There exists the possibility that these crystals are the same compound as the orthorhombic $Ba_4Ti_2PtO_{10}$ reported by Blattner *et al.*[23]

ACKNOWLEDGMENT

The author is grateful to Professor A. von Hippel for making available the facilities of the Laboratory for Insulation Research, for suggesting the problem, and for his advice and encouragement during the progress of the work.

¶ All compositions in hundreds of growths produced colored crystals of $BaTiO_3$ except that white needles of the cubic form resulted in these TiO_2-poor mixtures. This leads to the assumption that the color in the normal crystal growths might be mainly due to platinum as an impurity; in the case of the formation of the white $BaTiO_3$ the platinum impurity is removed by forming a barium platinate.

[23] Blattner, Gränicher, Känzig, and Merz, Helv. Phys. Acta **21**, 341 (1948).

Kinetics of the Rapid Gas Phase Reaction between NO, NO_2, and H_2O

LOWELL G. WAYNE* AND DON M. YOST
Gates and Crellin Laboratories of Chemistry, California Institute of Technology, Pasadena, California

(Received September 18, 1950)

Using the absorption of light by nitrogen dioxide as a measure of its concentration, the rate of the gas phase reaction $NO+NO_2+H_2O=2HNO_2$ was measured over a fivefold range of water vapor and nitrogen dioxide concentrations, with nitric oxide greatly in excess. Changes in light intensity were detected by means of an electron-multiplier photo-tube and recorded by photographing the screen of a cathode-ray oscilloscope. Half-times as short as 0.014 sec were observed. The reaction rate was found to depend more strongly upon the concentration of water vapor than upon that of nitrogen dioxide and to be kinetically consistent with a mechanism involving termolecular collisions.

The equilibrium constant of the reaction has been calculated and its order of magnitude experimentally confirmed, and a lower limit has been fixed for the rate of dissociation of nitrogen sesquioxide.

INTRODUCTION

FOLLOWING the successful application by Johnston and Yost[1] of the combination of multiplier photo-tube, cathode-ray oscilloscope, and camera to the study of the kinetics of the very rapid reaction between nitrogen dioxide and ozone, it appeared desirable to study by this technique other reactions whose rates are so great as to be unmeasurable by the common methods. The reaction between nitric oxide, nitrogen dioxide and water vapor is of interest because of its possible importance in connection with theories of rainfall. It was reported by Wulf,[2] who studied the equilibrium spectroscopically, to be practically instantaneous. The system was therefore selected for study.

Instances in the literature of the quantitative study of kinetics of homogeneous reactions involving water vapor as a primary reactant are rather rare, and most of these concern pyrolysis of hydrocarbons or other high temperature studies in which the effect of chain reactions is predominant. The reaction between water vapor and sulfur trioxide in the gas phase was studied[3] at room temperature by the Polanyi streaming method; in this case the product, sulfuric acid, appeared as a mist. The authors estimated that about one collision out of every hundred between molecules of the reacting species was effective. The system described here is comparable to the water-sulfur trioxide system in the respect that it, too, involves hydration of an acid anhydride (that of nitrous acid).

EXPERIMENTAL

In principle, and in many particulars, the procedure was the same as that employed by Johnston and Yost.[1] Essentially, the apparatus comprised four parts: a flow system in which gas streams containing the reacting substances could be metered and mixed, a device consisting of a reaction cell and quick-acting stopgate by means of which a non-equilibrium mixture could be trapped, an optical system producing a chopped beam of light which passed through a portion of the reaction cell, and a detecting and recording system comprising the multiplier photo-tube with its power source, the oscilloscope and the camera.

Figure 1 shows schematically the arrangement of the flow system. Nitric oxide, prepared as described below, entered the system at *A*, filled the two-liter bulb *B* (which served to cushion the effect of suddenly closing the system) and was divided into two streams. One of these passed through stopcock *C*, flowmeter *D* and water saturator *E*, the other through stopcock *F* and flowmeter *C* to *H*, where a much slower stream of oxygen was introduced. The stopcocks *J* and *K* permitted these sections of the flow system to be cut off from the mixing chamber *L* and from each other. Oxygen from a commercial oxygen cylinder was introduced at *M*; its pressure was adjusted by means of the bubbler *N* and its flow rate measured by flowmeter *P*. Stopcock *Q* served to shut off the oxygen stream. The oxygen served, as a result of its reaction with nitric oxide, to form the necessary small concentration of nitrogen dioxide.

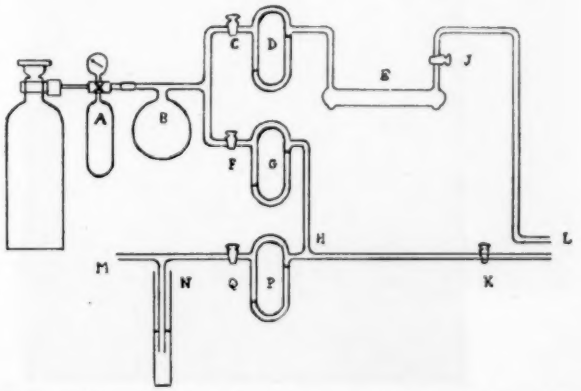

FIG. 1. Diagram of the flow system. *A*: Nitric oxide collecting system. *B*: Two-liter bulb. *D*, *G*, *P*: Capillary flow meters. *E*: Water saturator. *L*: To mixing chamber. *M*: Oxygen inlet. *N*: Bubbler.

* Present address, Mellon Institute of Industrial Research, Pittsburgh, Pennsylvania.

[1] H. S. Johnston and D. M. Yost, J. Chem. Phys. **17**, 386 (1949). See also L. G. Wayne and D. M. Yost, J. Chem. Phys. **5**, 767 (1950).

[2] E. H. Melvin and O. R. Wulf, J. Chem. Phys. **3**, 755 (1935).

[3] Goodeve, Eastman, and Dooley, Trans. Faraday Soc. **30**, 1127 (1934).

Dibutyl phthalate was used as the manometer fluid in capillary flowmeters, *D*, *G* and *P*. The capillaries were calibrated at several points throughout their ranges of utility by timing the displacement of a known volume of water.

Water saturator *E* consisted of a 120-cm length of 12-mm tubing filled with glass beads and sufficient water to occupy half the remaining volume. It was kept immersed in water at room temperature. A gravimetric water vapor determination showed it to be more than 99 percent efficient at the flow rates used.

Concentration of water vapor in the reaction mixture could be adjusted by diverting more or less of the total nitric oxide flow through stopcock *C*; the concentrations obtainable in this way ranged from about 0.5 to about 2.4 mole percent. The total nitric oxide flow rate was fixed by adjusting the valve on the supply cylinder.

The temperature of the flowing mixture was measured by means of a thermocouple of No. 50 *B* and *S* gauge constantan and 36-gauge copper placed axially in the stream issuing from the reaction cell. No attempt was made to control the temperature, which therefore varied slowly, usually between 23° and 25°C.

Tygon tubing was used for all connections. Since it was found that this tubing is slowly attacked by nitrogen dioxide, connections were arranged so as to expose a minimum of the tygon surface to the stream containing this component.

For experiments concerning possible time lag in the $NO_2+NO=N_2O_3$ equilibrium, the water saturator was removed from the system and nitrogen from a commercial "dry nitrogen" cylinder was introduced into the mixing chamber.

The mixing chamber and reaction cell were constructed on the same plan as those previously described[1] but were smaller. The cell was built of 1-mm Pyrex capillary tubing, its total volume being about 0.12 ml. The volume of the mixing chamber was found to be about 0.05 ml, and the total volume was, therefore, less than 0.2 ml. With a gas flow of 10 m/sec, the average age of the mixture in the light path was about 0.01 sec.

Apparatus and procedure for trapping a non-equilibrium system in the reaction chamber and for recording the progress of the reaction were essentially as described by Johnston and Yost.[1] Photographs of the oscilloscope screen (such as Figs. 2 and 3) provided a record of NO_2 concentration *vs.* time. Suitable amplification was secured by adjusting the oscilloscope controls so that the pattern appearing on the screen represented only the peaks of the square-wave modulated light intensity, the beam being off the screen during the dark period of each cycle. The position of the pattern envelope was sufficiently reproducible to be calibrated with respect to the control settings and the magnitude of the applied signal; such calibration was useful in permitting the approximate determination of the equilibrium constant from the photographic data.

Each photographic negative recorded the appearance of the trace through several sweeps of the beam across the screen (*ca.* 0.3–0.5 sec) as seen in Fig. 2, except in a few experiments made to demonstrate the absence of lag in the N_2O_3 dissociation equilibrium; in these a single-sweep device was used (Fig. 3). For measurement, the negative was projected in a microfilm reader onto a sheet of squared paper and the positions of successive peaks recorded.

Nitric oxide was generated by the method given by Johnston and Giauque[4] in which 50 percent sulfuric acid is dropped into a solution approximately 4 *N* in sodium nitrite and 1 *N* in potassium iodide. The gas evolved was passed through concentrated solutions of

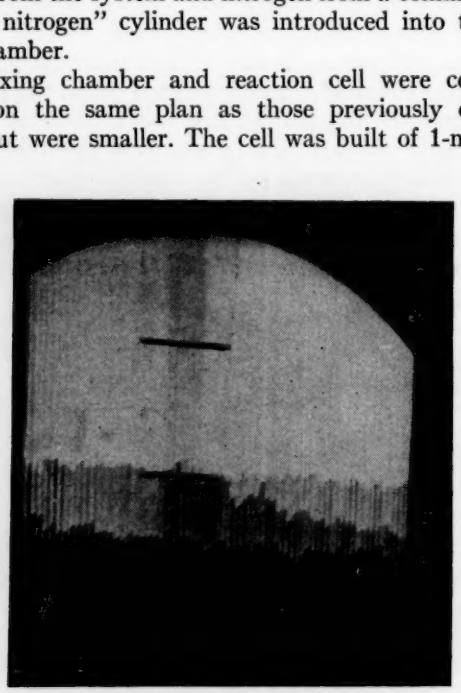

FIG. 2a. Run IV-59. N_2O_3 0.0078 atmos; H_2O 0.0151 atmos; half-time 0.083 sec.

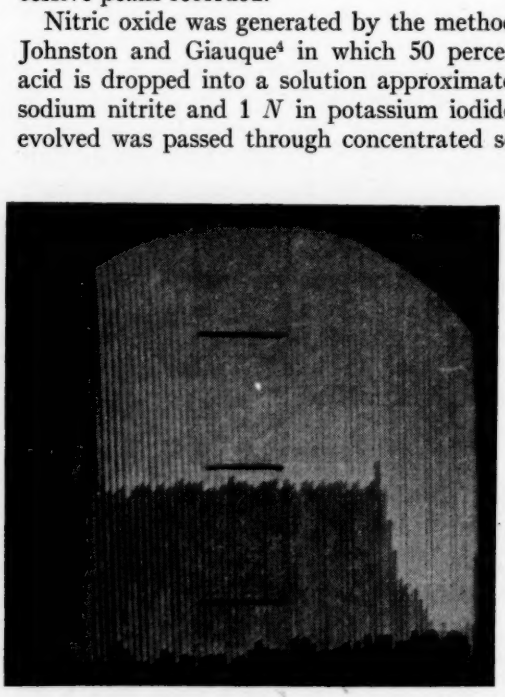

FIG. 2b. Run IV-52. N_2O_3 0.0148 atmos; H_2O 0.0230 atmos; half-time 0.014 sec.

[4] H. S. Johnston and W. F. Giauque, J. Am. Chem. Soc. **51**, 3194 (1929).

sodium hydroxide and potassium iodide and dried over phosphorous pentoxide, and finally condensed in a glass bulb at liquid-air temperature. It was then redistilled (the last five percent or so of each batch being discarded) and stored in a supply cylinder. Occasional testing showed not more than ½ percent of the stored gas unabsorbed by ferrous sulfate solution. No nitrogen dioxide could be detected.

THE EQUILIBRIUM CONSTANT

Because the reaction

$$NO(g)+NO_2(g)+H_2O(g)=2HNO_2(g) \qquad (1)$$

does not proceed to completion, a knowledge of its equilibrium constant is essential in interpreting its kinetics. Abel and Neusser[5] in reporting on the vapor pressure of HNO_2 above its aqueous solutions, have incidentally provided data from which the constant, K_2, for the equilibrium

$$N_2O_3(g)+H_2O(g)=2HNO_2(g) \qquad (2)$$

can be estimated to be of the order of magnitude of 2.4. On combining this with the value $K_3=2.1$ atmos found by Verhoek and Daniels[6] for the dissociation

$$N_2O_3(g)=NO(g)+NO_2(g) \qquad (3)$$

one readily calculates for K_1 the value 1.2 atmos.$^{-1}$ However, Abel and Neusser expressly pointed out that their experiments were not designed to permit an accurate determination of the quantities on which this estimate is based, and it is probably indicative of their lack of confidence in such a calculation that they made no attempt to correct their vapor pressure measurements for the effect of this equilibrium. (Their value of $P_{HNO_2}/(HNO_2)$, given as 0.0352 *l.* atmos/mole, is doubtless too high by 10 to 20 percent for this reason.) Thermodynamic data now available permit a more reliable calculation. The result still depends upon the vapor pressure data of Abel and Neusser and is therefore subject to the same 10 to 20 percent uncertainty, but the much more refined treatment of the thermodynamic properties of nitric acid given by Forsythe and Giauque[7] removes the order-of-magnitude uncertainty inherent in the above estimate. Consider the reactions

$$HNO_2(aq.)=HNO_2(g), \qquad (4)$$

$$\tfrac{1}{2}H_2+\tfrac{1}{2}N_2+O_2=HNO_2(aq.), \qquad (5)$$

$$\tfrac{1}{2}N_2+O_2=NO_2, \qquad (6)$$

$$\tfrac{1}{2}N_2+\tfrac{1}{2}O_2=NO, \qquad (7)$$

$$H_2+\tfrac{1}{2}O_2=H_2O(g). \qquad (8)$$

Combining these in the proportions $2(4)+2(5)-(6)-(7)-(8)$ yields the net reaction (1). Extrapolation of the results of Abel and Neusser to ionic strength zero gives $K_4=0.0305$, from which ΔF_4^0 is calculated to be 2080 cal/mole. Corresponding values for reactions (5) to (8) are, respectively, -13.020,[8] 12,275,[7] 20,650[7] and $-54,507$,[9] leading to the total -300 cal/mole and the value $K_1=1.65$ atmos^{-1}, in reasonable

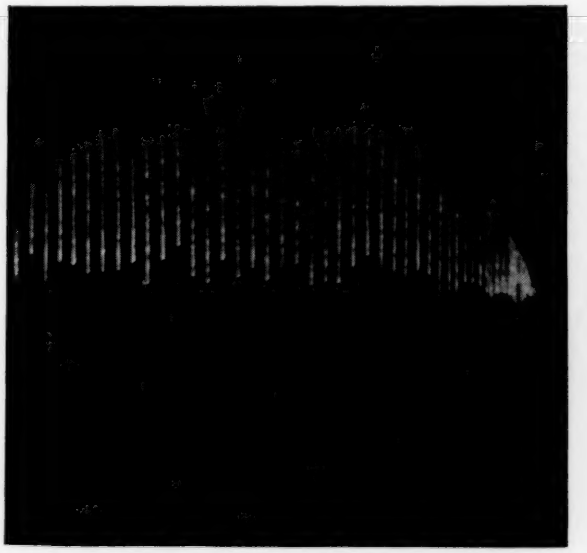

FIG. 3a. Blank for N_2O_3 dilution test.

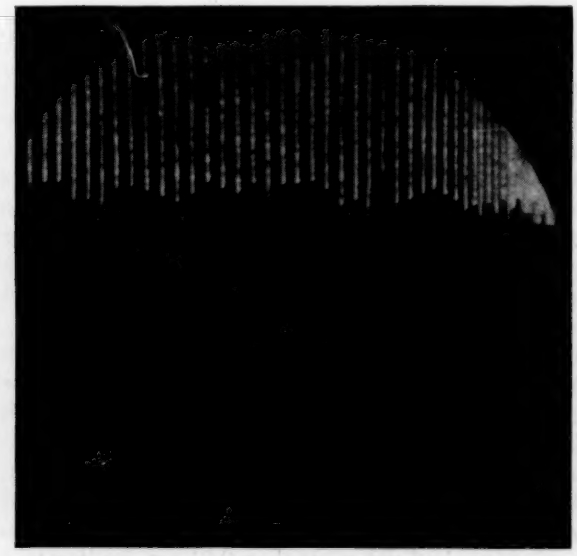

FIG. 3b. N_2O_3 dilution test, N_2/NO, 4.5.

[5] E. Abel and E. Neusser, Monatsh. Chem. **54**, 855 (1939).
[6] F. H. Verhoek and F. Daniels, J. Am. Chem. Soc. **53**, 1250 (1931).
[7] W. R. Forsythe and W. F. Giauque, J. Am. Chem. Soc. **64**, 48 (1942).
[8] W. M. Latimer, *Oxidation Potentials* (Prentice-Hall, Inc., New York, 1938).
[9] G. N. Lewis and Merle Randall, *Thermodynamics and the Free Energy of Chemical Substances* (McGraw-Hill Book Company, Inc., New York, 1923).

TABLE I. The equilibrium constant at 25° for reaction (1).

No.	$a\times10^2$ atmos	$b\times10^2$ atmos	$x_e\times10^2$ atmos	K_1 atmos^{-1}
29	1.80	1.89	1.54	3.1
31	1.80	1.89	1.54	3.1
33	1.80	1.49	1.12	1.67
35	1.80	1.49	1.14	1.68
38	1.85	0.96	0.82	1.28
39	1.90	0.95	0.78	1.08
45	1.43	0.98	0.78	1.44
46	1.46	0.98	0.78	1.44
49	1.49	1.47	0.82	0.92
51	1.49	2.3	1.26	1.68
52	1.48	2.3	1.26	1.68
			average:	1.74

agreement with that calculated from the data of Abel and Neusser. Multiplying by K_3 gives $K_2=3.5$.

An experimental confirmation of this predicted value was obtained by the interpretation of data from a number of the runs in which a relatively reliable estimate of equilibrium concentrations could be made. The results are shown in the last column of Table I. In Table I, a is the initial pressure of "available" N_2O_3, that is $P_{NO_2}+P_{N_2O_3}$; b is the initial water vapor pressure; x_e is the calculated equilibrium pressure of HNO_2.

Although individual values of K_1 differ from the logarithmic mean by factors of from *ca.* 0.5 to 2, the values which were considered most reliable for experimental reasons were those for runs 51 and 52, which fell very close to the mean; the agreement of this mean with the predicted value therefore provides satisfactory confirmatory evidence concerning the order of magnitude of K_1.

RATE OF DISSOCIATION OF NITROGEN SESQUIOXIDE

In order to explore the possibility that reaction (3) or its reverse proceeds slowly enough to cause complications in interpreting the kinetics of the main reaction, several tests were made in which $NO-NO_2$ mixtures were diluted with 2.1 to 4.5 volumes of nitrogen in the mixing chamber, then trapped in the reaction cell. For each test, a blank was provided by photographing a single-sweep trace on the oscilloscope while the diluted mixture was flowing through the cell.

Comparison of the blank with the test photograph showed no evidence of lag in attaining equilibrium. One such pair of photographs is shown in Fig. 3, from which it is seen that no significant increase in NO_2 concentration occurs during the 0.15 sec recorded by the camera.

From this observation it may reasonably be assumed that the lapse of at least two half-times for the dissociation required not more than 0.01 sec, leading to a lower limit of 150 sec^{-1} for the rate constant K_3 (assuming the dissociation is first order).

ORDER OF THE REACTION

In the system $NO-NO_2-H_2O$, equilibrium considerations exclude the possibility of the formation of oxygen or higher valent oxides and oxyacids of nitrogen, so that the only important product molecules are N_2O_3 and HNO_2. As shown in the previous section, there is no lag in the establishment of the N_2O_3 equilibrium, at least within the limits of observation with the apparatus. The only reactions to be considered are, therefore,

$$NO+NO_2+H_2O=2HNO_2 \quad (1)$$

and

$$N_2O_3+H_2O=2HNO_2. \quad (2)$$

The experiments were not designed to distinguish between these reactions. By maintaining the pressure of nitric oxide always at substantially one atmosphere, the advantage was gained that simultaneous occurrence of (1) and (2) would not complicate the rate expression, since the ratio $P_{NO_2}/P_{N_2O_3}$ was kept constant ($=2.1$).

The differential rate equation can thus be written

$$dx/kdt=Y[(a-x/2)(b-x/2)-x^2/K] \quad (9)$$

where x denotes P_{HNO_2} as a function of the time t, a is the initial value of $P_{NO_2}+P_{N_2O_3}$; b is the initial value of P_{H_2O}; k is the assumed rate constant of the forward reaction; K is a composite equilibrium constant for the over-all reaction, given by $K_1P_{NO}/(1+P_{NO}/K_3)$, which is about 1.1 for $P_{NO}=1$, (this is necessitated by the fact that NO_2 and N_2O_3 disappear at proportional rates,

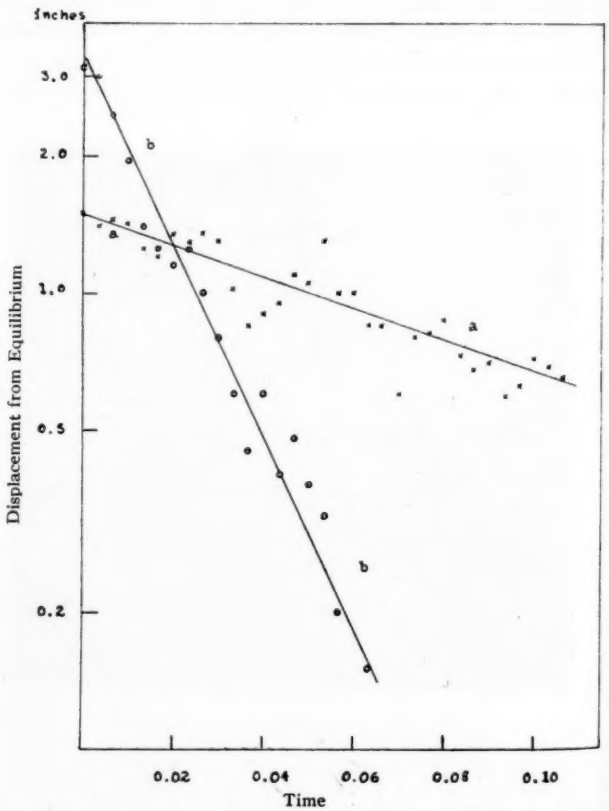

FIG. 4. Displacement from equilibrium *vs.* time in seconds (semi-log plot). Curve *a*, Run IV-59, corresponding to Fig. 2a. Curve *b*, Run IV-52, corresponding to Fig. 2b.

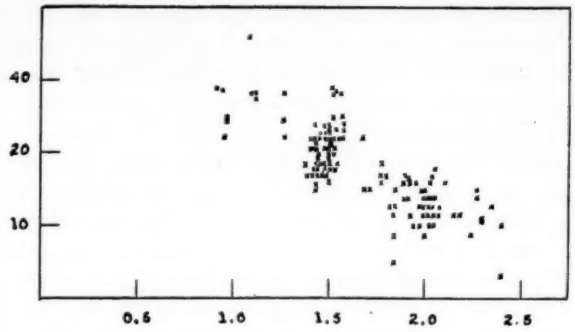

FIG. 5. $\tau F \times 10^4$ *vs.* $P_{H_2O_i} \times 10^2$.

but requires no assumption as to the mechanism of the reaction); and Y is a factor which may be variable, to represent any catalytic or inhibitory influence affecting the rate.

It is readily seen that if Y is constant (corresponding to the assumption that the reaction rate is proportional to the rate of bimolecular collisions between N_2O_3 and H_2O, or of ternary collisions involving NO, NO_2, and $H_2(O)$, and if K has the value 4, the polynomial in Eq. (9) reduces to the first degree in x. The solution of (9) is then of the form

$$x_e - x = x_e \exp(-mkl), \tag{10}$$

where x_e denotes the equilibrium pressure of HNO_2 and $m=(a+b)/2$. Under these conditions a plot of $\log(x_e-x)$ *vs.* t would produce a straight line whose slope would be proportional to m.

If Y is constant but K differs from 4, it can be shown that a plot of $\log(x_e-x)$ *vs.* t would produce not a straight line, but a curve having the asymptotic slope $-Fk/2$, where $F=[(a-b)^2+16ab/K]^{\frac{1}{2}}$. Furthermore the slope of the curve increases monotonically with time, and it is found that, for K not less than one, the initial value can never be less than $\frac{3}{4}$ of this limiting value. To test the second-order hypothesis, therefore, the data were plotted in terms of distance from equilibrium (in terms of the measurements made with the aid of the microfilm reader, as described above) *vs.* time, on semi-log paper, as shown in Fig. 4; the half-time τ (inversely proportional to the slope) was measured from the most plausible straight line through the

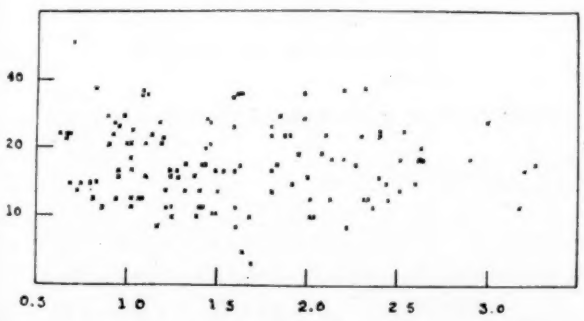

FIG. 6. $\tau F \times 10^4$ *vs.* $P_{[N_2O_3]} \times 10^2$.

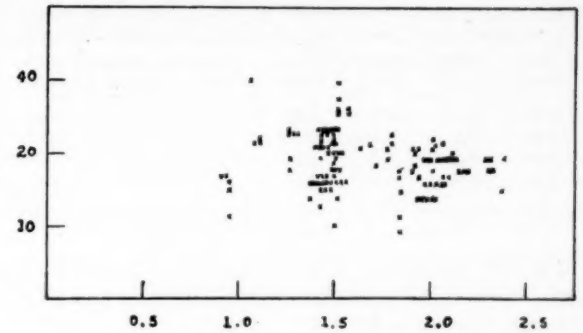

FIG. 7. $\tau F\left(b-\frac{x_\infty}{2}\right)\times 10^6$ *vs.* $P_{H_2O_i} \times 10^2$.

experimental points, and the constancy of the product τF was investigated.

When plotted against the initial pressure of water vapor (Fig. 5) the values of τF thus obtained revealed a distinct trend in the sense of inverse variation. A comparable plot of τF *vs.* the initial pressure a due to NO_2 and N_2O_3 (Fig. 6) displays no such trend; the individual values scatter widely throughout the range of initial pressures employed.

From this result it is clear that the dependence of the rate on pressure of water vapor must be of order higher than the first. The most satisfactory simple formulation proves to be that the rate is proportional to the square of the water vapor pressure; i.e., in Eq. (1), $Y=b-x/2$. As is shown in Appendix I, the constancy of the product $\tau F(b-x_e/2)$ affords a convenient test of the applicability of this hypothesis. When plotted against the initial pressures a and b (Figs. 7 and 8, respectively), the values of this product show no significant trend and noteworthily less scatter than the corresponding values of τF. The rate constants reported below are therefore based on the third-order formulation.

THE RATE CONSTANTS

Assuming the rate law

$$dx/dt = k(b-x/2)[(a-x/2)(b-x/2)-x^2/K] \tag{11}$$

the rate constant may be calculated from the relation

$$k = 2\ln 2/\tau F(b-x_e/2)$$

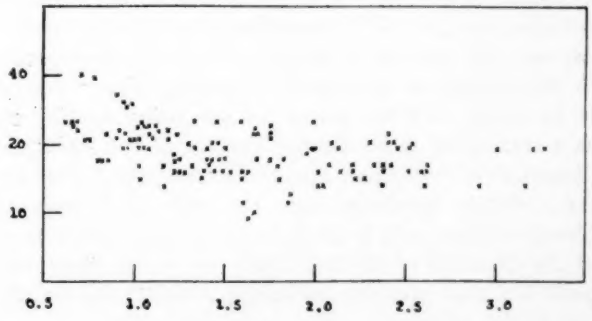

FIG. 8. $\tau F\left(b-\frac{x_\infty}{2}\right)\times 10^6$ *vs.* $P_{[N_2O_3]_i} \times 10^2$.

TABLE II.

$a\times10^2$ atmos	$b\times10^2$ atmos	$F\times10^2$ atmos	$A\times10^2$ atmos	$B\times10^2$ atmos	$C\times10^2$ atmos	a_e/s_i
0.5	2.5	4.7	0.65	2.9	5.0	1.06
1.5	2.3	7.1	0.25	4.1	4.6	0.95
1.5	1.5	5.7	1.02	3.3	3.0	0.87
2.5	1.0	6.2	1.03	3.7	2.0	0.62

where the denominator is the product represented in Figs. 7 and 8. The median value of this product from 123 experiments is 1.9×10^{-5}, leading to the result (at 23 to 25°C with $P_{NO}=1$ atmos) $k=7.3\times10^4$ atmos^{-2} sec^{-1} or $\log k=4.86$ with a probable error of 0.09, corresponding to a factor of 1.2.

Treating the forward reaction separately, one finds, if

$$-dP/dt=k'PP^2_{H_2O},$$
$$P=P_{NO_2}+P_{N_2O_3},$$
$$k'=\tfrac{1}{2}k=3.7\times10^4 \text{ atmos}^{-2} \text{ sec}^{-1}$$
$$=2.2\times10^7 l^2 \text{ mole}^{-2} \text{ sec}^{-1}.$$

If the assumption be made that N_2O_3 is the reacting species, so that

$$-dP/dt=k''P_{N_2O_3}P^2_{H_2O},$$
$$k''=3.1k/2=1.1\times10^5 \text{ atmos}^{-2} \text{ sec}^{-1}$$
$$=6.8\times10^7 l^2 \text{ mole}^{-2} \text{ sec}^{-1}.$$

Finally, for the reverse reaction if

$$-dP_{HNO_2}/dt=k'''P^2_{HNO_2}P_{H_2O},$$
$$k'''=k/K=6.6\times10^4 \text{ atmos}^{-2} \text{ sec}^{-1}$$
$$=4.0\times10^7 l^2 \text{ mole}^{-2} \text{ sec}^{-1}.$$

Appendix II contains a discussion of the approximations, assumptions, and uncertainties involved in arriving at these results.

DISCUSSION

Since the reaction proves to be very rapid in spite of the rather small concentrations of the reactants, it is of interest to determine whether the simple kinetic theory predicts a sufficiently high rate of triple collisions to account for the observations. For a typical mixture in which the pressures of water vapor and available N_2O_3 were both 0.015 atmos, the required collision rate at 25°C would be about 3×10^{18} per cc per sec. The number of binary collisions to be expected in this system is estimated, following Hinshelwood,[10] to be about 1.7×10^{14} per cc per sec, using 4×10^{-8} cm as a reasonable guess for the average of the molecular diameters of water and nitrogen sesquioxide molecules. As a simple approximation, the ratio of ternary to binary collision rate is taken to be the same as the ratio of the diameter of the third molecule to the mean free path for that species. Assuming 3×10^{-8} cm for the molecular diameter of H_2O, the number of ternary collisions per cc per sec is found to be about 8×10^{19}. Thus, assuming that N_2O_3 is the participating species, approximately one ternary collision in twenty-five results in reaction.

While this is a comfortable margin from the standpoint of collision frequency, it must be observed that the requirement of a certain spatial configuration for the reaction complex might easily reduce the probability of reaction for each otherwise suitable collision by an order of magnitude. If this picture is to apply it is necessary to conclude that the energy of activation must be practically nil. This, of course, is a common characteristic of third-order gas reactions and, in view of the probability that the heat of reaction (as well as the free energy change), is very small for this system, it is perhaps reasonable to expect it to be the case here also.

Since the rate of the reverse reaction is of the same order of magnitude as that of the forward reaction and since the amounts of products and of reactants in equilibrium mixtures are comparable, the considerations given above apply equally well to the reverse process. A curious consequence of the third-order law is that water vapor is apparently a catalyst in the formation of an acid anhydride (N_2O_3) from the acid vapor.

It should perhaps be remarked that although the third-order hypothesis is reasonably satisfactory in explaining both kinetics and mechanism of the reaction, yet because of the rather limited range of concentrations used in this study it cannot be regarded as well-established. The true explanation of the observed behavior may well be essentially more complex.

We wish to express here our great appreciation for the many helpful discussions with Dr. Oliver Wulf. We are thankful to Dr. Norman Davidson for general criticism. The work was supported in part by a grant from the Research Corporation, for which we are very grateful.

APPENDIX I

To investigate the properties of its solution, Eq. (11) may be conveniently rearranged to give

$$Rkdt=8dx/(a-x)(B+x)(C-x) \tag{12}$$

where $R=(4-K)/K$ and A, B, and C are the magnitudes of the roots of the polynomial in the denominator; specifically,

$$A=(F-a-b)/R=x_e, \tag{13}$$
$$B=(F+a+b)/R=x_e+2(a+b)/R, \tag{14}$$
$$C=2b. \tag{15}$$

Re-expressing (8) in terms of partial fractions, it becomes

$$\frac{1}{8}Rkdt=\frac{dx}{(A+B)(C-A)(A-x)}+\frac{dx}{(B+A)(B+C)(B+x)}-\frac{dx}{(C-A)(B+C)(C-x)}$$

or, remembering that $dx=d(B+x)=-d(A-x)=-d(C-x)$,

$$-\frac{1}{8}Rkdt=\frac{d\ln(1-x/A)}{(A+B)(C-A)}-\frac{d\ln(1+x/B)}{(B+A)(B+C)}-\frac{d\ln(1-x/C)}{(C-A)(B+C)}. \tag{16}$$

[10] C. N. Hinshelwood, *The Kinetics of Chemical Change* (Oxford University Press, London, 1940).

In view of (13), therefore,

$$\frac{d\ln(x_e-x)}{kdt}=\frac{1}{8}R(A+B)(C-A)+\frac{(C-A)d\ln(1+x/B)}{(B+C)kdt}+\frac{(A+B)d\ln(1-x/C)}{(B+C)kdt}. \quad (17)$$

As t increases without limit the last two terms of (17) approach zero, so that using (13), (14) and (15) the asymptotic slope is found to be

$$\frac{d\ln(x_e-x)}{kdt}=-\frac{F}{2}\left(b-\frac{x_e}{2}\right).$$

Since the half-time τ is inversely proportional to this slope, the product $\tau F(b-x_e/2)$ must be constant for a system conforming to the given rate law.

A straightforward extension of this analysis shows that the ratio of the final slope to the initial slope of the desired solution can be given by

$$s_e/s_i=1+\frac{CA(C-A)-AB(A+B)}{BC(B+C)}.$$

To illustrate the magnitude of this ratio, results of calculation for a few typical cases are shown in Table II.

APPENDIX II

For purposes of discussion, three principal approximations may be recognized: (i) the assumption of linear response of the detecting and recording system; (ii) neglect of complicating factors in interpreting the composition of the reacting mixture; (iii) uncertainty in the determination of the asymptotic half-time for each run. The first assumption was checked by calibration, as mentioned above; the errors due to nonlinearity of this sort in all probability would affect observed amplitude differences by less than five percent. A systematic error is indeed introduced in assuming that the quantity (x_e-x) is linearly dependent on the distance of the transmitted light in an exponential function of the concentration. This may be illustrated by a calculation which shows that in the most adverse case (amplitude change being the largest) the half-time calculated on this basis would be shorter than the true value by six percent. In most runs the error caused by this procedure would be certainly less than five percent.

Complicating factors in determining the composition of the reacting mixture are the presence of nitrogen tetroxide, the change of pressure of nitric oxide as a result of reaction, and the fact that the gas mixture at the exit end of the light path is older than that near the inlet. At 25°C, the dissociation constant of N_2O_4 is 0.14 atmos, from which it may be shown that $P_{N_2O_4}=7P^2_{NO_2}$, so that the pressure of N_2O_4 ranges up to about 10 percent of the total available N_2O_3, being in most cases nearer to five percent. If the tetroxide is a nonparticipating molecular species it should affect the half-time by providing a reservoir of N_2O_3 which would not be detected by absorption of light. This effect should be comparable in magnitude but opposite in sign to that of the systematic error discussed in the previous paragraph, providing some compensation in this respect. The change in P_{NO} due to its disappearance in the reaction is of the order of one percent and may legitimately be neglected. Non-uniformity of the gas mixture in the light path is not particularly disturbing because of the fortunate circumstance that the course of the reaction is approximately exponential, so that the half-time is roughly the same for all parts of the system and consequently is given by that of the integrated system. At any rate, the maximum age difference to be considered was about one hundredth of a second, so that no important effect would be expected except perhaps for those runs giving the very shortest half-time.

Uncertainty in the determination of the half-time is due to two principal causes, namely uncertainty in determining the proper slope on the semilog plot, due to scatter of the individual points, and uncertainty in the determination of the value x_e-x for the individual points due to drift of the pattern. As may be seen by examining Fig. 5, the points which are useful in the semi-log plot range over a period of only two or three half-times, so that the half-time estimated is likely to fall between the asymptotic value and the initial value. Since the slope changes most rapidly during the first half-time of the reaction, it is likely that the slope of the line chosen will differ from the asymptotic slope by considerably less than is indicated by the ratio s_e/s_i (Table II). The average error from this cause is probably of the order of 10 percent or less, except possibly in a few cases where the ratio a/b is unusually high.

The drift of the pattern on the oscilloscope screen following its sudden displacement presents a less easily handled problem. This effect is clearly evident on those photographs in which the half-time is very short; the observed displacement rises sharply to a maximum, then falls off more slowly. If it be assumed as a first approximation that this drift also follows an exponential law, its half-time may be estimated as about 0.10 to 0.15 sec. An attempt was made to estimate the magnitude of the uncertainty from this cause in the following way: on tracings derived from several runs of very short half-time, the sloping envelope of the latter portion was extrapolated linearly and the half-time was determined from a semi-log plot representing the data as distance from this line. This resulted in an increase of 20 to 25 percent for half-times estimated by the ordinary method as less than 0.02 sec. Since this process could not be applied in most cases, the trend of the discrepancy with increasing half-time could not be determined, but it seems likely that as the prominence of the maximum lessens, the disturbance of the measured half-time does also.

Intramolecular Isotopic Fractionation—the Example of Nitrous Oxide

J. M. McCrea*
Suffield Experimental Station, Ralston, Alberta, Canada
(Received September 11, 1950)

The spectroscopic results of Richardson and Wilson are used to calculate the partition function ratios for the isotopic species of nitrous oxide. A number of approximate calculations of types often necessary in other cases owing to limited data are given to show the errors introduced by these approximations.

INTRAMOLECULAR ISOTOPIC FRACTIONATION

THE equilibrium fractionation between the terminal and the central nitrogens in nitrous oxide may be calculated from more detailed spectroscopic information[1,2] than is available for molecules of greater complexity. In order to give some idea of the extent of error involved in calculations of fractionations or kinetic effects for molecules of more complicated geometry where the lack of detailed data forces the use of approximations, the calculation is carried out by various approximations as well as by full use of the data of Richardson and Wilson. Bigeleisen and Friedman, in addition to reporting the spectral data, carry out the calculation of the fractionation at a number of temperatures, and their values at 0°C and 25°C differ slightly from those obtained here because their observed frequency shifts differ slightly from those of Richardson and Wilson.

Urey, in a review on isotopic fractionation and methods of calculating it, mentioned the probability of intramolecular fractionation in a molecule such as N_2O with atoms of the same element in nonequivalent positions.[3] The principal difficulty in the calculation is obtaining the vibration frequencies for the isotopic species considered. For nitrous oxide, this is best done by using observed frequencies to evaluate constants in a molecular force field which includes a bond-to-bond interaction term such as given by the equations for the linear XYZ molecule

$$4\pi^2(\omega_1^2+\omega_3^2)=f_{xy}(1/M_x+1/M_y)+f_{yz}(1/M_y+1/M_z)-2f_{xz}/M_y$$

and

$$16\pi^4\omega_1^2\omega_3^2=(f_{xy}f_{yz}-2f_{xz}^2)(M_x+M_y+M_z)/M_xM_yM_z$$

used by Richardson and Wilson and by Bigeleisen and Friedman. If the frequencies of the $N^{14}N^{15}O^{16}$ and $N^{15}N^{15}O^{16}$ molecules are then evaluated, differences of only 0.02 cm^{-1} are encountered between these frequencies and the corresponding ones obtained by the same process from the slightly but distinctly different equations

$$4\pi^2(\omega_1^2+\omega_3^2)=F_{xy}(1/M_x+1/M_y)+F_{yz}(1/M_y+1/M_z)+F_{xz}(1/M_x+1/M_z)$$

$$16\pi^4\omega_1^2\omega_3^2=(F_{xy}F_{yz}+F_{xy}F_{xz}+F_{yz}F_{xz})(M_x+M_y+M_z)/M_xM_yM_z$$

due to Engler and Kohlrausch.[4] Evidently the fitting of the constants for the two cases compensates for the difference in the forms to a greater extent than the original data are numerically reliable.

Prior to the microwave determination of the moments of inertia of nitrous oxide,[5] two sets of distances were suggested, and the calculation has been performed with the now rejected over-all distance of 2.300A also.[6] Table I shows the zero-order frequencies and fundamentals for the isotopic species of nitrous oxide, except that the rotational constant g_{22} for the bending mode has been neglected in applying the anharmonic terms.[1,7]

Table II displays the partition function ratios calculated using the frequency data of Table I. The value obtained for the partition ratio $N^{15}N^{14}O^{16}/N^{14}N^{14}O^{16}$ is based on an isotope shift in ω_1 of 17.9 cm^{-1}, and, consequently, is larger than that reported by Bigeleisen and Friedman, who based their calculation on a shift of 16.3 cm^{-1}. The much smaller isotope shift in ω_1 on substitution of the central position all but eliminates the difference when the calculation is based on force constants derived from the $N^{14}N^{14}O^{16}$ and $N^{15}N^{14}O^{16}$ spec-

TABLE I. Zero-order and fundamental frequencies of nitrous oxide.

	$N^{14}N^{14}O^{16}$	$N^{15}N^{14}O^{16}$	$N^{14}N^{15}O^{16}$	$N^{15}N^{15}O^{16}$
ω_1 (cm^{-1})	1299.80	1281.90	1297.33	1279.18
ω_2	596.50	592.90	582.88	579.19
ω_3	2276.50	2252.90	2228.53	2204.55
ν_1	1284.97	1267.48	1282.70	1264.96
ν_2	585.81	582.36	572.70	569.15
ν_3	2223.47	2201.98	2177.51	2154.60
Zero-point energy	2367.73	2343.72	2330.51	2306.08

* Present address: The M. W. Kellogg Company, Jersey City 3, New Jersey.

[1] W. S. Richardson and E. B. Wilson, Jr., J. Chem. Phys. **18**, 694 (1950).

[2] J. Bigeleisen and L. Friedman, J. Chem. Phys. (to be published). The author is much indebted to them for supplying a manuscript of their paper in advance of publication.

[3] H. C. Urey, J. Chem. Soc. 562 (1947).

[4] Engler and Kohlrausch, Z. physik. Chem. **B34**, 214 (1936).

[5] Coles, Elyash, and Gorman, Phys. Rev. **72**, 973 (1947).

[6] G. Herzberg, *Infra-Red and Raman Spectra of Polyatomic Molecules* (D. Van Nostrand Company, Inc., New York, 1945), p. 173 and p. 398.

[7] D. M. Dennison, Revs. Modern Phys. **12**, 175 (1940).

tra, and the values recorded for the ratio $N^{14}N^{15}O^{16}/N^{14}N^{14}O^{16}$ are in substantial agreement.†

It is never necessary to neglect anharmonic corrections in calculations of this type provided the zero-order frequencies are known, and the error introduced by doing so in the case of nitrous oxide is about of the same order, but of the opposite sign, as that introduced by using observed frequencies instead of zero-order frequencies. An approximation of the latter type is very frequently necessary owing to a lack of detailed spectroscopic information. In the present case an error of about 5 percent is introduced into the all-important decimal part of the partition ratio by this approximation in the case where at least one molecular species is isotopically pure. When such partition ratios are combined to produce equilibrium constant, the magnitude of the error may be additive, while the decimal part of the partition ratio in general gets numerically smaller, so that high percentage errors or even inversion of sign in the decimal part of the equilibrium constant may result. For example, the percentage error in the equilibrium constant for the isomerization reaction of the last column of Table II due to this approximation is about 20 percent. A generalization as to the effect of anharmonic terms for molecules where they are unknown is certainly a great extrapolation, but it should be quite possible to say that errors of as much as 5 percent may be present in the decimal part of partition ratios with one isotopically pure species, and that these errors may add in forming the equilibrium constant algebraically. Since the main effect of the anharmonicity is in the exponent of the zero-point energy term, the percentage effect in the decimal part of the partition ratio is relatively independent of temperature.

If the vibration frequencies are calculated from Herzberg's valence force field,[8] a large difference is observed between the partition ratios obtained from them and those calculated from relations which include an interaction constant. This suggests that unless interaction terms are definitely known to be negligible, considerable reserve is necessary in accepting numerical values calculated from valence force fields. Pitzer has remarked on the sensitivity of these calculations to force constant selection,[9] and this sensitivity persists through to interaction terms. As Bigeleisen and Friedman point out in detail, nitrous oxide possesses a structure peculiarly suited to a large intramolecular fractionation, but the fact that considerable error may be introduced by neglect of the interaction term is worth noting also.

TABLE II. Partition ratios for nitrogen exchange in nitrous oxide.

	$\frac{N^{15}N^{14}O^{16}}{N^{14}N^{14}O^{16}}$	$\frac{N^{14}N^{15}O^{16}}{N^{14}N^{14}O^{16}}$	$\frac{N^{15}N^{15}O^{16}}{N^{14}N^{14}O^{16}}$	$\frac{N^{14}N^{15}O^{16}}{N^{15}N^{14}O^{16}}$ [a]
2.320A Molecule, exact at 25°C[b]	1.0851 (1.0814)	1.1239 (1.1246)	1.2308	1.0354 (1.0399)
Exact at 0°C[b]	1.0962 (1.0915)	1.1410 (1.1401)	1.2544	1.0409 (1.0445)
2.300A molecule, exact at 0°C	1.1041	1.1395	1.2617	1.0321
Approx. for 2.320A at 0°C				
Neglect anharmonicity	1.0984	1.1508	1.2673	1.0477
Use ν for ω	1.0941	1.1486	1.2497	1.0498
Valence forces	1.0819	1.1545	1.2518	1.0671

[a] This partition ratio is also the equilibrium constant for the reaction $N^{15}N^{14}O^{16} = N^{14}N^{15}O^{16}$.
[b] The figures in brackets are those obtained by Bigeleisen and Friedman, J. Chem. Phys. (to be published).

In the case carbon dioxide, the symmetry of the molecule eliminates the effect of the interaction constant in the calculation of the frequencies for CO_2^{18}, but it appears in the frequencies for $CO^{16}O^{18}$, and the equilibrium constant for the reaction

$$CO_2^{16}+CO_2^{18}=2CO^{16}O^{18}$$

becomes 3.982_8 at 0°C rather than the 3.999_0 reported earlier.[10] The corresponding reaction for nitrous oxide is

$$N^{14}N^{14}O+N^{15}N^{15}O=N^{15}N^{14}O+N^{14}N^{15}O$$

with an equilibrium constant of 0.990_8. Allowing for the factor of 4 due to symmetry numbers and two mass number shift on the introduction of O^{18} in carbon dioxide, the comparison is between 0.997_8 and 0.990_8, and, even though the interaction constant for carbon dioxide is nearly as large as that for nitrous oxide, its effect on the fractionation factor is greatly reduced owing to symmetry.

In conclusion, it should be stated that the purpose in reporting these calculations is merely to point out that intramolecular fractionation effects may be considerable and to use a molecule where considerable spectroscopic data is available to point out effects which introduce errors into the calculation of isotopic fractionation in cases where only limited spectroscopic information is at hand.

† It was noted that Bigeleisen and Friedman have used mass numbers rather than nuclear masses in evaluating the force constants and frequencies. This method gives ω_1 as 1297.5_8 while the use of nuclear masses gives 1297.5_2 cm^{-1} for $N^{14}N^{15}O^{16}$. The force constants exhibit more sensitivity in this regard than ω_1, and the set f_{xy}, 18.78_3; f_{yz}, 11.63_2; f_{xz}, 1.34_0 in units of 10^5 d/cm based on their assignments of frequencies but on nuclear masses rather than mass numbers is to be preferred.

[8] See reference 6, p. 174.
[9] K. S. Pitzer, J. Chem. Phys. **17**, 1341 (1949).
[10] H. C. Urey and Greiff, J. Am. Chem. Soc. **57**, 321 (1935).

An Atomic Distribution Function*

RICHARD H. KERR AND LOUIS H. LUND
Missouri School of Mines and Metallurgy, Rolla, Missouri

(Received September 22, 1950)

A simple form for the radial atomic distribution function for a monatomic liquid, involving the interatomic potential function of two atoms in the liquid, is developed. Assuming the potential function to be of the form $(\lambda/r^n)-(\mu/r^6)$ and arbitrary choices for μ, the theoretical distribution function is fitted to the left-hand side of the first peak of the experimental distribution curves of liquid argon and liquid mercury. Satisfactory values of n and potential well depths for these two liquids indicate the approximate validity of the derived radial atomic distribution function. Presented also is a comparison of the theoretical and experimental curves for liquid argon and liquid mercury.

INTRODUCTION

THE scattering of x-rays by monatomic liquids[1] has given information of their structure characterized by a radial atomic, or molecular, distribution function $\rho(r)$,[2] such that $4\pi r^2\rho(r)dr$ defines the average number of atomic, or molecular, centers to be found between r and $r+dr$ about any arbitrarily chosen atom in the liquid. Its ultimate utility lies, perhaps, in the fact that it provides a time-averaged representation of the atomic arrangements induced under the action of characteristic interatomic, or intermolecular, potentials in the liquid.

Theoretical attempts[3] to arrive at $\rho(r)$ for liquids have dealt as adequately as seemed feasible with the complicated statistical character of the possible configurations of the liquid. Lennard-Jones and Devonshire[4] have considered the liquid in the neighborhood of any one atom to be effectively a "smeared out" crystal lattice with the atoms free to vibrate under a simple restoring force about their mean positions. Wall,[5] in a further simplification, has retained the smearing of the crystal lattice, but has allowed the atoms to move about freely in a certain "free volume" about these lattice sites. Both methods allow a calculation of $\rho(r)$, of limited extent in r, which agrees reasonably well with experiment. More sophisticated approaches such as that by Mayer and Montroll[6] have dealt with the probability configuration integral for the system composed of all N atoms of the liquid. This method implies a knowledge of the potential energy of the liquid as a function of position of the N atoms with a subsequent $N-2$ fold integration to arrive at $\rho(r)$. A detailed knowledge of the potential energy as a function of position of the N atoms is not known and certain simplifying assumptions about the potential energy must be made. Such a method, while better representing a picture of the liquid averaged over all possible configurations of the liquid, still poses difficult and tedious mathematical techniques to effect the necessary integrations.

The use of the experimental atomic distribution functions calculated from x-ray scattering patterns has been indicated by Corner and Lennard-Jones[7] as a means of finding the forces between atoms in the liquid. At present, however, use of the method proposed by them is not possible, owing to the necessity of uniquely resolving the experimental curve into a sum of components, each of which is to represent a single peak of the theoretical curve.

A method has been proposed, however, and used by Hildebrand[8] in the case of liquid mercury to evaluate the parameters in the expression

$$E(r)=(\lambda/r^n)-(\mu/r^6) \qquad (1)$$

for the potential energy associated with a pair of atoms in the liquid. This method makes use of the experimental

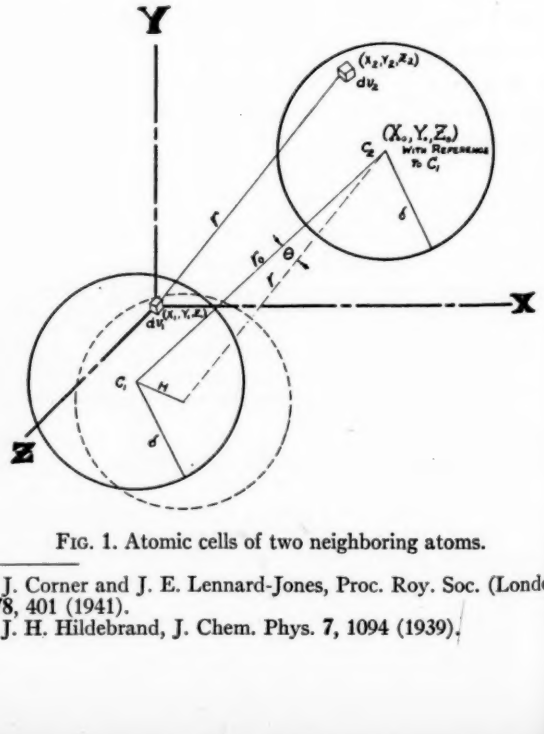

FIG. 1. Atomic cells of two neighboring atoms.

* Part of this work is from a thesis submitted by Richard H. Kerr to the Missouri School of Mines and Metallurgy toward the M. S. degree.

[1] N. S. Gingrich, Revs. Modern Phys. **15**, 90 (1943).

[2] F. Zernike and J. A. Prins, Z. Physik **41**, 187 (1927).

[3] Among others, J. G. Kirkwood and E. M. Boggs, J. Chem. Phys. **10**, 394 (1942); J. Corner and J. E. Lennard-Jones, Proc. Roy. Soc. (London) **A178**, 401 (1941); G. S. Rushbrooke, Proc. Roy. Soc. (Edinburgh) **60**, 182 (1940); J. H. Hildebrand, J. Chem. Phys. **1**, 1 (1939); C. N. Wall, Phys. Rev. **54**, 1062 (1938); G. S. Rushbrooke and C. A. Coulson, Phys. Rev. **56**, 1216 (1939).

[4] J. E. Lennard-Jones and A. F. Devonshire, Proc. Roy. Soc. (London) **163**, 53 (1937).

[5] C. N. Wall, reference 3.

[6] J. Mayer and E. W. Montroll, J. Chem. Phys. **9**, 2 (1941).

[7] J. Corner and J. E. Lennard-Jones, Proc. Roy. Soc. (London) **A178**, 401 (1941).

[8] J. H. Hildebrand, J. Chem. Phys. **7**, 1094 (1939).

atomic distribution functions, together with the heat of vaporization, and provides a simple and direct use of the liquid atomic distribution functions for the calculation of the parameters in Eq. (1). His results for liquid mercury as well as an application of his method here to the case of liquid argon, provide a semiquantitative check on the validity of the radial distribution function to be developed.

METHOD OF CALCULATION

Let us first imagine an atom, atom 1, (or molecule) of the liquid placed in a spherical cell of radius σ and a neighboring atom, atom 2, in a similar cell with the cell center of the latter at a mean distance r_0 from the center of the first. (See Fig. 1.)

The probability of atom 1 being in a volume element $dx_1dy_1dz_1$ at x_1, y_1, z_1, and atom 2 being simultaneously in $dx_2dy_2dz_2$ at x_2, y_2, z_2, is

$$Ae^{-E(r)/kT}dx_1dy_1dz_1dx_2dy_2dz_2, \tag{2}$$

where the origin of system x_2, y_2, z_2, is C_2 and of x_1, y_1, z_1, is C_1. $E(r)$ will be taken of the form indicated in Eq. (1), and A is a constant which may be determined by a proper normalization of the radial distribution function. We will suppose; for the moment, that each atom is trapped in its respective cell so that $E(r)$ is effectively infinite at the boundaries of the cells.

Replacing the coordinates x_2, y_2, z_2, in terms of a new set of coordinates X, Y, Z, relative to the center of atom 1 and defined by the relationships,

$$\begin{aligned} x_2&=x_1+X-X_0,\\ y_2&=y_1+Y-Y_0,\\ z_2&=z_1+Z-Z_0, \end{aligned}$$

where X_0, Y_0, Z_0, are the coordinates of the center of cell 2 relative to the center of cell 1, we have for expression (2),

$$Ae^{-E(r)/kT}dx_1dy_1dz_1dXdYdZ.$$

Now this last expression may be integrated, with fixed X, Y, Z, and hence constant r, over all x_1, y_1, z_1, consistent with each atom remaining in its cell to give the probability of the occurrence of relative coordinates X, Y, Z, between the two atoms. The triple integral involved is the volume common to two intersecting spheres of radius σ and having their centers H distance apart,[9] where

$$\begin{aligned} H&=(X-X_0)^2+(Y-Y_0)^2+(Z-Z_0)^2\\ &=r^2+r_0^2-2rr_0\cos\theta. \end{aligned}$$

When this probability of occurrence of relative coordinates X, Y, Z, is written in terms of relative spherical coordinates r, θ, ϕ, with the line of centers of the cells giving the direction of the polar axis, one may integrate with r constant over θ and ϕ between the limits $\theta=0$ to $\theta=\cos^{-1}(r^2+r_0^2-4\sigma^2)/2rr_0$ and $\phi=0$ to $\phi=2\pi$ to give the probability of finding the two atoms within a distance r to $r+dr$ of each other. Thus integrating and simplifying, we find for this latter probability

$$(16\pi^2A\sigma^5/15)r/r_0e^{-E(r)/kT}W(r)dr, \tag{3}$$

where[10]

$$W(r)=1-[5(r_0-r)^2/4\sigma^2]\times[1-(|r_0-r|/2\sigma)+(|r_0-r|^3/40\sigma^3)].$$

If N_0 is the average number of nearest neighbors surrounding a given atom in the liquid and $\rho(r)$ is the density of these atoms at a distance r from the given atom, then the probability of finding a neighboring atom a distance r from the given atom is $4\pi r^2\rho(r)dr/N_0$, which must be equal to expression (3). Hence,

$$4\pi r^2\rho(r)dr=(16\pi^2AN_0\sigma^5/15)r/r_0e^{-E(r)/kT}W(r)dr \tag{4}$$

expresses the number of nearest neighbors whose centers lie in a spherical shell of thickness dr and radius r.

Now in the above expression, let us remove the restriction of definite cell boundaries for the atoms in the following way. Let us take σ large enough to justify the approximation that $W(r)=1$. Since $E(r)$ falls to zero rapidly enough for $|r-r_0|$ for us to say that the atoms are much more likely to be found in the immediate vicinity of their cell centers than far removed from them, we might still, if we like, regard the two atoms as effectively imprisoned in their respective cells. The precise extent of the cell boundaries will, however, be of no immediate consequence. The factor $16\pi^2A\sigma^5N_0/15$, although large, we will, of course, suppose to be finite.

We are thus left with the equation,

$$4\pi r^2\rho(r)dr=(16\pi^2AN_0\sigma^5/15)r/r_0e^{-E(r)/kT}dr \tag{5}$$

for the number of nearest neighbor atoms to be found between r and $r+dr$.

In the following, Eq. (5) has been fitted directly to a portion of the experimental radial distribution functions for liquid argon[11] and mercury[12] for a semiquantitative determination of $E(r)$, of limited range, in the form of Eq. (1) for each liquid.

APPLICATION TO SOME SPECIFIC CASES

It seems reasonable to suppose that the contribution to the radial distribution function of coordination shells of higher order than the first should be small in the range $r\leq r_0$, hence Eq. (5) should be at least approximately valid along the left-hand side of the first peak of the experimental radial distribution curve. We will suppose, further, that the position of the first maximum of $4\pi r^2\rho(r)$ is the intermolecular distance at which $E(r)$ has its minimum value E_0. This value r_0 is readily

[9] Compare C. N. Wall, reference 3.

[10] C. N. Wall, reference 3. The function $W(r)$ which enters here as a geometrical factor is, apart from a constant factor, the Wall polynomial involving his "free-volume" radius.

[11] A. S. Eisenstein and N. S. Gingrich, Phys. Rev. **62**, 261 (1942).

[12] J. A. Campbell and J. H. Hildebrand, J. Chem. Phys. **7**, 330 (1943).

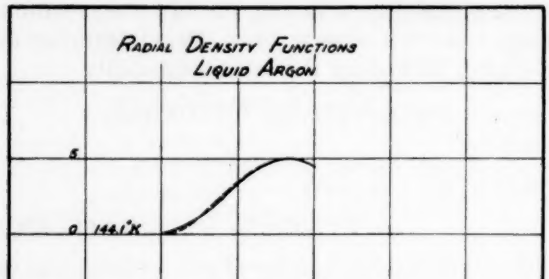

FIG. 2. Comparison of experimental and theoretical atomic distribution functions for liquid argon. Solid curve is experimental; dotted curve is theoretical.

obtainable from the graphs of the experimental radial distribution functions and for argon was sensibly constant over the temperature range. The value of r_0 for mercury showed a very slight increase with temperature; hence, an average value was used. Thus we find for liquid argon, $r_0=3.8$A, and for liquid mercury, $r_0=2.97$A.

Taking $E(r)$ as given by Eq. (1), i.e.,

$$E=(\lambda/r^n)-(\mu/r^6),$$

our assumptions require that $dE/dr=0$ when $r=r_0$, hence

$$\lambda=6\mu r_0^{n-6}/n. \tag{6}$$

Making the substitutions

$$y=4\pi r^2\rho(r)$$
$$y=y_0=(16\pi^2AN_0\sigma^5/15)e^{-E_0/kT}, \quad \text{when} \quad r=r_0,$$

we have for Eq. (5)

$$y=y_0r/r_0e^{(E_0-E)/kT}, \tag{7}$$

where y_0 is the value of the ordinate of the experimental curve for $r=r_0$.

Eliminating λ by substituting Eq. (6) in Eq. (7) and solving for μ we have

$$\mu=2.303nr_0^6kT\log(y_0r/yr_0)/ \\ n-6+6(r_0/r)^n-n(r_0/r)^6 \tag{8}$$
$$=(B/D)\log(y_0r/yr_0).$$

Now the experimental radial distribution functions for liquid mercury and argon are available for each liquid at several different temperatures. (See Figs. 2 and 3); hence, the following procedure has been adopted for each liquid.

At a particular temperature and for a fixed n, paired values of r and y from the left-hand side of the first peak of the experimental curve were substituted into Eq. (8) and the values of μ so obtained averaged over the several points. This calculation was done considering separately values of $n=7$, 8, 9, 10, 11, and 12. This process was repeated at each of the several temperatures available for each liquid and the results averaged, for a particular n, over the temperatures to give an over-all average μ. These results are shown in Tables I and II.[13]

It seems clear from these tables that one cannot pick a "best" n corresponding to, say, a criterion of a best agreement among the μ's for the various temperatures. A typical Van der Waals attractive force for atoms not possessing a permanent dipole moment such as argon atoms and whose potential is inversely proportional to the sixth power of the interatomic distance is independent of the temperature. In the case of monatomic mercury and in view of the several parameters involved

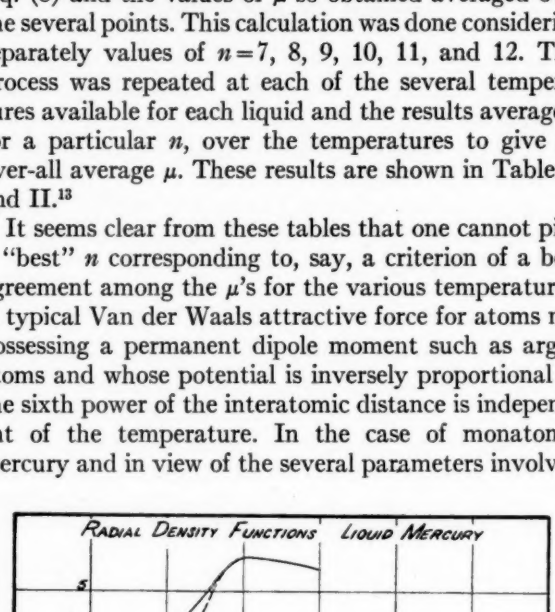

FIG. 3. Comparison of experimental and theoretical atomic distribution functions for liquid mercury. Solid curve is experimental; dotted curve is theoretical.

[13] The shape of the 126.7°K experimental argon curve appeared somewhat anomalous, considering the curves corresponding to temperatures above and below 126.7°K, and hence was not used.

in the fitting process, it seems very unlikely that a temperature-dependent part of the Van der Waals force, such as an orientation effect in the case of H_2O or HCl molecules, should or could be construed simply from such a table. One might note from the tables, however, that although the μ's do not decrease steadily with temperature for a particular n, there appears to be in most cases a tendency for a smaller μ to be associated with the higher temperatures. This situation would correspond to a more shallow well depth at the higher temperatures. To simplify matters, however, as indicated above, the μ's were averaged over the temperatures to give an over-all average μ.

Although one cannot arrive directly at a definitive value of μ from the tables, one can arrive at a semi-quantitative knowledge of the liquid intermolecular potential functions here by an independent choice of the μ which has been averaged over the temperature. It is also clear that if reasonable values of n and potential well depths were thus obtained, Eq. (7) for the radial distribution function could be presumed at least approximately correct. For mercury, the value $\mu=3.35\times10^{-10}$ as calculated and used by Hildebrand has been chosen.[14] It is, of course, clear that in the range of r which includes zero and the minimum of the interatomic potential, and which is the range with which we are concerned here, the value of μ chosen here cannot be expected to preclude other choices of this parameter. It is, however, felt that the value of μ used here is at least satisfactory for our purposes. Accordingly, for argon, a value of $\mu=1.02\times10^{-10}$ as calculated by Buckingham[15] has been chosen. This value is based on calculated crystal properties of argon and agrees closely with $\mu=1.11\times10^{-10}$, corresponding to an interaction for argon suggested by Herzfeld and Goeppert-Mayer[16] and would seem to be a reasonable choice in the liquid case considered here.

TABLE I. Values of μ (argon).

Temp. °K	$\mu\times10^{10}$ (ergs-A^6) $n=7$	$\mu\times10^{10}$ (ergs-A^6) $n=8$	$\mu\times10^{10}$ (ergs-A^6) $n=9$	$\mu\times10^{10}$ (ergs-A^6) $n=10$	$\mu\times10^{10}$ (ergs-A^6) $n=11$	$\mu\times10^{10}$ (ergs-A^6) $n=12$
84.35	5.93	2.57	1.88	1.38	1.07	0.86
91.80	3.78	1.71	1.15	0.82	0.63	0.50
144.10	5.60	3.41	1.72	1.23	0.95	0.75
μ_{Av}	5.10	2.85	1.58	1.15	0.88	0.71

TABLE II. Values of μ (mercury).

Temp. °C	$\mu\times10^{10}$ (ergs-A^6) $n=7$	$\mu\times10^{10}$ (ergs-A^6) $n=8$	$\mu\times10^{10}$ (ergs-A^6) $n=9$	$\mu\times10^{10}$ (ergs-A^6) $n=10$	$\mu\times10^{10}$ (ergs-A^6) $n=11$	$\mu\times10^{10}$ (ergs-A^6) $n=12$
−38	10.35	5.06	3.44	2.49	1.97	1.60
0	8.70	4.29	2.82	1.94	1.66	1.00
50	7.98	3.94	2.58	1.78	1.50	1.23
100	4.37	3.62	2.42	1.69	1.41	1.13
150	6.65	3.34	1.67	1.17	0.97	0.99
200	4.80	2.57	1.69	1.12	0.98	0.80
μ_{Av}	7.13	3.80	2.44	1.70	1.42	1.13

[14] J. H. Hildebrand, reference 8. This value of μ was calculated from the London dispersion formula, $\mu=-3\alpha^2\Delta E/4$, where ΔE is the ionization potential and α is the polarizability.

[15] R. A. Buckingham, Proc. Roy. Soc. A168, 264 (1938).

TABLE III. Comparison of the parameters in Eq. (1).

Research	n	$\mu\times10^{10}$ (ergs-A^6)	$\lambda\times10^{8}$ (ergs A^n)	$E_0\times10^{14}$ (ergs)	r_0(A)	Liquid
Hildebrand's method	10	1.15	1.39	1.61	3.76	argon
Fitting of Eq. (7)	10.4	1.02	2.09	1.43	3.80	
Hildebrand's method	9	3.52	5.49	21.0	2.86	mercury
Fitting of Eq. (7)	8.3	3.35	2.95	13.6	2.97	

Using the values of μ, then, as known, one can use the data from Tables I and II to find by graphical interpolation the corresponding values for n. One then easily calculates λ and the depth of the potential well for each liquid. These values are shown in Table III and the potential functions are shown in Figs. 4 and 5. Also shown, for comparison, in the same tables are Hildebrand's results for liquid mercury and the result of the application here of his method to liquid argon. It might be noted that when using Hildebrand's method one depends on the consistency of a certain identity to determine the choice of n, and in the application here to liquid argon the identity showed only slightly noticeably better fit for $n=10$ than for $n=9$ or $n=11$. A difficulty which arises when one handles this identity is that the numerator and denominator involve differences of very small quantities, so that they become very sensitive to the shape of the first peak of the radial distribution function.

One notes, however, the close agreement of the parameters obtained here with those obtained by application of Hildebrand's method to liquid argon. For mercury, although the n's are in relative agreement, the discrepancy in the depth of the potential wells is apparent.[17] The energy of dissociation of Hg_2 molecules, however, has been calculated by several observers[18] to be 10×10^{-14} to 11×10^{-14} erg, which is sufficiently close to the $E_0=13.6\times10^{-14}$ erg calculated here to give some support to this value. The potential well depth of 1.43×10^{-14} erg, in the case of liquid argon, is also in fair agreement with the depth of 1.80×10^{-14} corresponding to the interaction proposed by Buckingham to give the best correlation for gaseous and crystalline argon.[19]

It is interesting to note also that, although the choice

[16] K. H. Herzfeld and Goeppert-Mayer, Phys. Rev. 46, 993 (1938).

[17] It should be noted, however, that Hildebrand's calculations made use of the experimental distribution functions of Boyd and Wakeham, J. Chem. Phys. 7, 958 (1939). These experimental distribution functions appear to be somewhat in doubt, since the radiation used was not strictly monochromatic.

[18] Among others, Finkelnberg, Z. Physik 34, 551 (1933): Koernicke, Z. Physik 33, 219 (1925); Mrozowski, Z. Physik 140, 230 (1936).

[19] R. A. Buckingham, reference 15.

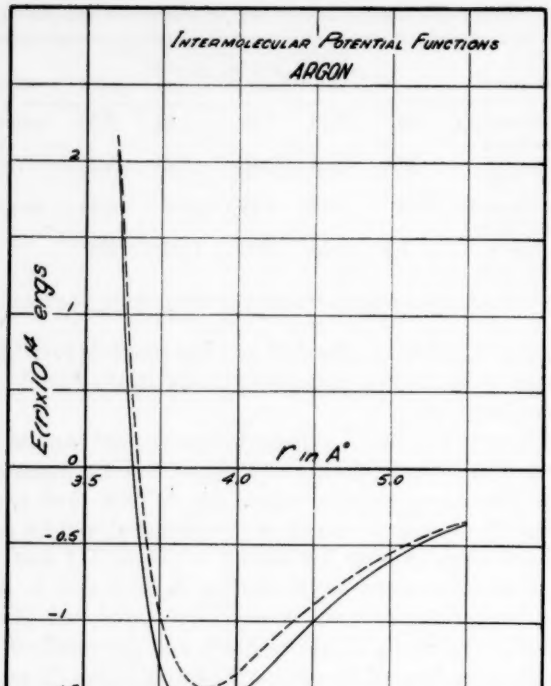

FIG. 4. Comparison of intermolecular potential functions for liquid argon. Solid curve, Hildebrand's method. Dotted curve from fitting of Eq. 7.

of μ is arbitrary to some extent, the choices of μ here lead, as they should, to an interaction between the argon atoms more closely resembling the interaction between hard spheres than does the mercury interaction.

Considering the fact that the portion of the experimental distribution curves used here ($r \leq r_0$) are influenced considerably by the large angle part of the experimental x-ray scattering curves and hence are not as reliable as one should desire, the results obtained here do not seem to be too bad. The results do, however, leave room for considerable improvement when refinements become available.

While it was perhaps clear from the outset that all of the parameters in the potential function (1) could scarcely be found uniquely from a simple fitting of the theoretical distribution curve to the experimental ones, the results obtained do seem to indicate the approximate validity of Eq. (7) in the range $r \leq r_0$, along with the fact that the initial shape of the distribution curve is influenced strongly by the values of the parameters in the form assumed for the interaction between two atoms in the liquid. It would also appear that if unambiguous values of μ for the liquid were known, Eq. (5) could be used in connection with the experimental distribution functions to give a reasonable evaluation of the parameters in Eq. (1), at least in a limited range.

Finally, Figs. 2 and 3 show the atomic distribution functions calculated from Eq. (7) using the potential functions found here in the fitting of this equation to the experimental data. Despite the cross-over of the theoretical and the experimental curves at 0°C and −38°C in the case of mercury, the general shape of the theoretical curves is in fair agreement with the experimental curves. This fit could be improved, however, by the use of a somewhat smaller value of μ, corresponding to a value of n in the neighborhood of 9, which would result in a lifting of the theoretical curves where they now fall under the experimental curves. The over-all fit of the theoretical curves for argon is good and for both liquids, with the exception of the 126.7°K experimental argon curve, whose shape appears somewhat anomalous,[20] the fit is seen to improve with increasing temperature. This increasing agreement between the theoretical and experimental curves for increasing temperature might be expected as a result of the smearing-out of the spherical cell boundaries in the development of the theoretical distribution function, thus corresponding to a somewhat more gas-like behavior of the liquid.

ACKNOWLEDGMENT

We wish to express our sincere thanks to Dr. J. H. Hildebrand of the University of California and to Dr. J. A. Campbell of Oberlin College, Oberlin, Ohio, for their having been so generous in supplying experimental data.

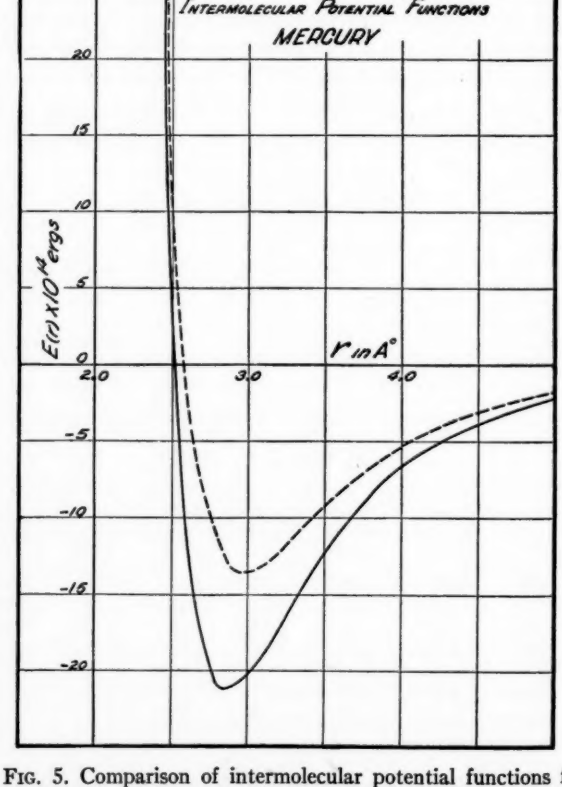

FIG. 5. Comparison of intermolecular potential functions for liquid mercury. Solid curve, Hildebrand's method. Dotted curve from fitting Eq. 7.

[20] See reference 13.

The Tensile Strength of Benzene*

J. J. DONOGHUE, R. E. VOLLRATH, AND E. GERJUOY
Department of Physics, University of Southern California
(Received June 26, 1950)

Measurements were made of the tensile strength of benzene, by the centrifuge method. The method is described, together with various features which have been incorporated into the procedure to insure uniformity of samples. There is evidence, which is not conclusive however, that the rupture strength increases as the amount of permanent gas dissolved in the liquid decreases. At any given permanent gas pressure in equilibrium with the liquid our results are highly variable. Although further confirmation is needed, it appears that the variability is a result of differing histories of our tubes and not of lack of uniformity of our benzene samples. Exposure of the glass surface to the atmosphere appears to decrease the tensile strength. Our highest observed rupture strength, 157 atmospheres, is believed to represent the adhesion strength of the benzene to the walls of a particular tube, and may be much less than the limiting tensile strength of benzene. No evidence for a temperature dependence of the tensile strength has been found, but this result is probably also not representative of the limiting tensile strength of benzene.

INTRODUCTION

THE tensile strengths of liquids have long been the subject of theoretical and experimental study. The past century has seen the development of a number of static or quasi-static methods for subjecting a liquid to a tensile stress. In recent years interest in the strengths of liquids has revived in connection with studies of cavitation erosion of bodies moving through liquids, and of cavitation produced during the projection of sonic energy into liquids. However refinements in the methods have not improved the reproducibility of the magnitude of the observed strengths. Critical surveys of the problem have been presented recently by Temperley and Chambers[1] and Blake,[2] among others, revealing extremely discordant results even among apparently identical tests on the same specimen of liquid. These authors, especially Blake, review the various theoretical attempts to predict tensile strengths which have been made in the past. There is a large gap between the lowest predicted strengths and the maximum observed values.[3]

The tensile strength of a liquid may be defined as the tension to which the liquid *must* be subjected in order to form an expanding cavity within the *volume* of the liquid. The reference to the volume of the liquid excludes the case of rupture of a liquid column resulting from separation of the liquid from the walls of the containing vessel when the liquid is placed under tension. Rupture under these circumstances clearly measures not the inherent strength of the liquid but rather the strength with which the liquid adheres to the walls. Although the above definition appears simple and straightforward, there remains the possibility that the tensile strength is a function of the liquid volume and shape, and that it cannot be defined independently of these.

This investigation was undertaken to determine a reliable value for the tensile strength of a single liquid, benzene, and to determine the factors affecting the tensile strength. The lack of reproducibility which has been noted shows that a reliable value is not easily achieved. It is reasonable to suppose that the variable and low strengths obtained in past measurements are the result of inadequate control of such variables as the purity of the liquid used, the quantity of the dissolved gas, and the degree of adhesion of the liquid to all solid surfaces in contact with the liquid, including suspended solids. A discontinuity formed by a gas-filled cavity or a non-wetting solid can limit to a relatively low value the tensile stress to which the liquid may be subjected without apparent rupture. If a cavity of spherical form within the liquid is in equilibrium with an external tension, T, the equilibrium radius, r, is given by the Kelvin relation $2\sigma/r = P_0 + T$ where σ is the interfacial or surface tension and P_0 is the gas pressure inside the cavity. For a surface tension of 75 dynes/centimeter, as for water, the equilibrium radius of a vapor bubble under a tension of 100 atmospheres, approximately 10^8 dynes/cm^2, is only 1.5×10^{-6} cm. Small insoluble gas bubbles also rapidly become unstable as the tension is increased.† It is evident that preparation of a bubble-free and "mote-free" liquid in a completely wetted container is necessary in any procedure which purports to determine the true tensile strength of a liquid.

* This work has been supported by the ONR under Contract N6ori-77, Task Order II at the University of Southern California. We have already briefly reported preliminary results: Technical Report No. 1 of this project, June 28, 1948, "Measurements on the Tensile Strengths of Liquids," distributed by the ONR; Phys. Rev. **73**, 538 (1948); Phys. Rev. **75**, 1456 (1949).

[1] H. N. V. Temperley and L. G. Chambers, Proc. Phys. Soc. **58**, 420 (1946).

[2] F. G. Blake, Jr., "The Tensile Strength of Liquids: A Review of the Literature," ONR, Contract N5ori-76, Project Order X, Technical Memorandum No. 9, June 11, 1949, Acoustics Research Laboratory, Harvard University.

[3] However our results and the results of Briggs have raised the observed strengths, while recent calculations of Benson and Gerjuoy, assuming the van der Waals or Berthelot equation of state remain valid at negative pressures, have resulted in lower predicted strengths. J. Briggs, Science **109**, 440 (1949) and **111**, 461 (1950). S. Benson and E. Gerjuoy, J. Chem. Phys. **17**, 914 (1949).

† See abstract by one of us, cited above. Phys. Rev. **73**, 538 (1948).

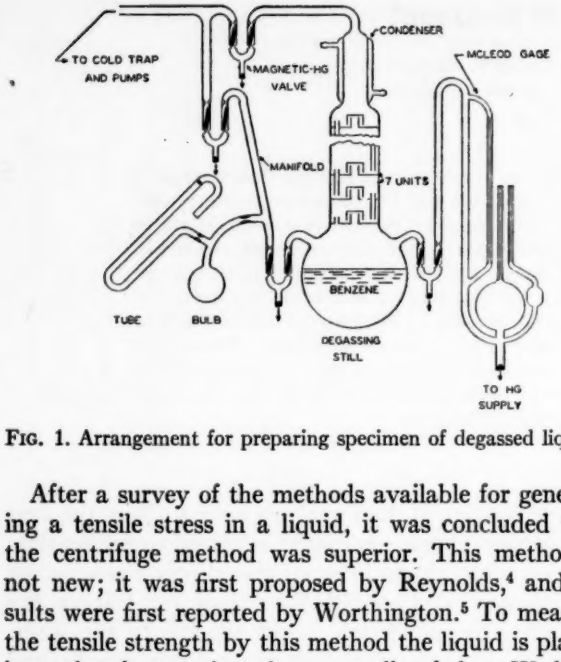

FIG. 1. Arrangement for preparing specimen of degassed liquid.

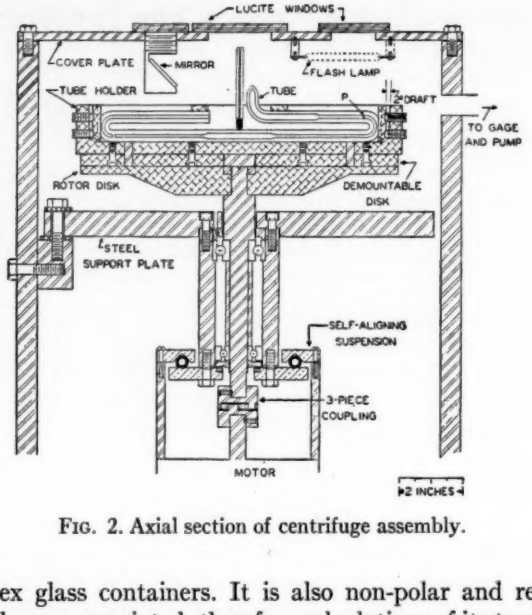

FIG. 2. Axial section of centrifuge assembly.

After a survey of the methods available for generating a tensile stress in a liquid, it was concluded that the centrifuge method was superior. This method is not new; it was first proposed by Reynolds,[4] and results were first reported by Worthington.[5] To measure the tensile strength by this method the liquid is placed in a tube of convenient shape, usually of glass. We have used a "*J*"-shape, closed at the straight end. The tube is mounted along a diameter of a horizontal disk which is rotated at increasing speed until a bubble appears in the tube at its center of rotation. The stress at rupture is determined by the effective length of the liquid column and the speed of rotation. Both of these quantities can be accurately measured, so that, in principle, the tensile strength of the liquid can be determined accurately.

Liquid specimens can be distilled into glass tubes from a system under a known gas pressure, so that the quantity of dissolved gas is readily controlled. The tubes are sealed off, thereby permitting repeated tests on the same specimen. Suspended solids are reduced to a minimum by slow condensation of the liquid into the specimen tube. The temperature dependence of the tensile strength can be conveniently studied. Finally, extensibility measurements are feasible. By extensibility is meant the magnitude of the negative compressibility or dilation of the liquid per unit tensile stress.

The choice of a liquid for these measurements was made on the basis of a number of considerations. Liquids of simple structure were favored, to simplify attempts to calculate strengths. Although water has been used in by far the greater number of cavitation and tensile strength studies, it was considered undesirable for this study, because of its high activity as a solvent. Also, its associated polar structure complicates many calculations of its tensile strength. Benzene was selected because it is easily purified, stable, and not an active solvent. More important, it does not attack the Pyrex glass containers. It is also non-polar and relatively non-associated; therefore calculations of its tensile strength should be comparatively simple. A further advantage in the choice of benzene over many organic compounds appeared subsequently, during handling of the liquid in the air-free system. No decomposition of the benzene was observable at the temperature required for sealing off the Pyrex tubes containing the specimens of benzene to be mounted on the centrifuge. This stability of benzene vapor at high temperatures has been previously noted.[6]

Our conclusions are described in detail below. They require additional confirmation which we are attempting to obtain. However, these experiments may not be completed for some time, and we have already long delayed reporting our findings. Thus, despite our present uncertainty concerning the cause of the variability in tensile strength which we have observed, we are in this paper presenting a description of our method and results, which we think are not without interest. Of particular interest are the very high maximum observed value (157 atmospheres) of rupture strength for benzene; the effects of dissolved gas which we have noted; the elimination of vibrations in the centrifuge, a point of previous criticism of this method; and the elimination of several other factors to which the variability might have been ascribed.

APPARATUS AND PROCEDURE

We will merely outline the method; further details are given elsewhere.[7] The procedure used to prepare and test a sample of benzene was briefly as follows: To prepare the benzene for test, it was first dried over

[4] O. Reynolds, Proc. Manchester Lit. Phil. Soc. **20**, 38 (1880).
[5] A. M. Worthington, Phil. Trans. Roy. Soc. A **183**, 355 (1893). Also, "On the Stretching of Liquids," British Association Report, 583 (1888).
[6] L. R. Herndon and E. Reid, J. Am. Chem. Soc. **50**, 3066 (1928).
[7] Donoghue, Vollrath, and Gerjuoy, Technical Report No. 2 of this project, "The Tensile Strengths of Liquids by the Centrifuge Method: The Tensile Strength of Benzene," to be distributed by the ONR.

sodium and then outgassed in the vacuum still of Fig. 1. Next, a small quantity was condensed into a sample bulb which had previously been sealed to the manifold, heated, and evacuated. After measurement of the air pressure over the benzene with the double-bulb McLeod gage, the bulb and the attached sample tubes were sealed off. The tube was then rinsed a number of times before the final filling to flush out any loose solids in the tube. The filled and sealed tube was then mounted in a tube holder of the type illustrated in Fig. 2. Tubes following number 10 were embedded in a casting resin for added support; later a short mercury thermometer was inserted at the center of the holder to indicate temperature changes during a test. The assembly was then checked for static balance, after which it was attached to a centrifuge, as illustrated in Fig. 2. The tube was then rotated at a slowly increasing speed until rupture occurred, as indicated by the sudden appearance of a bubble at the center of rotation or by the sudden disappearance of the end of the column. A sharp click or an increase in the intensity of vibration of the centrifuge frequently was heard at the moment of rupture. A flash lamp attached to the underside of the cover plate was used to illuminate the tube stroboscopically. The lamp was triggered by a calibrated Strobotac, whose flash rate was adjusted manually to equal the frequency of rotation. Thus the Strobotac also served to indicate the speed at the moment of rupture.

The benzene was of reagent quality, and was dried over phosphorus pentoxide before it was introduced into the still shown in Fig. 1. Sodium metal was first added to the still to assure dry benzene throughout the tests. By bringing the benzene into contact with both phosphorus pentoxide and sodium, the highly soluble gases, carbon dioxide and ammonia, were both removed.

The degassing still was of the bubble cap type described by Taylor,[8] and was highly efficient in eliminating dissolved gases.

The amount of air present over the benzene was measured with a double-bulb McLeod gage, also described by Taylor.[9] Pressures at the McLeod gage lower than 10^{-5} mm Hg could not be maintained with the still idle. This phenomenon has also been noted by Scott.[10] Care was necessary when measuring the lowest gas pressures, that the gas bubble in the capillary did not quickly dissolve (in the condensed benzene which always appeared above the mercury column) when under a pressure of several centimeters of mercury. This observation is of interest when the difficulties with the bubble in supposedly outgassed liquids in a Berthelot tube are recalled.[1,2]

The Pyrex sample tube and attached bulb for receiving benzene were sealed to the manifold as illustrated by Fig. 1. The surface of the tube received no cleaning other than that accomplished by annealing. No cleaning with acids was attempted for it was presumed that the surface changes known to accompany cleaning with aqueous solutions[11] were to be avoided as likely to decrease the uniformity of the forces of adhesion between the benzene and the glass surface. During evacuation of the manifold, the tube and bulb were heated to drive off adsorbed water vapor and air.

The magnetic mercury float valves were modifications of a design by Stock.[12] Upon opening the valve between still and manifold and cooling the bulb slightly below room temperature, sufficient benzene condenses in the bulb to fill the sample tube in a short time. After removal of the sample tube and bulb from the manifold, benzene was condensed into the tube and poured back into the bulb. This operation was repeated five times, to remove any loose solids present in the tube. The tube was filled to the point *P* indicated on Fig. 2; the effective liquid column length was approximately 10 centimeters.

Considerable effort was expended in developing the final tube and supporting framework or holder. It is necessary that the tubes be capable of withstanding the shock created by the deceleration of the ruptured column of liquid. Such sturdy tubes permit study of the reproducibility of the rupture strength and observations on the strength as a function of temperature. No lack of strength of the tubes was originally anticipated, since empty tubes installed on the centrifuge were subjected to the maximum speed of rotation without damage. However, frequent losses of samples due to fracture of the glass tubes when the liquid ruptured led to the trial of improved tubes and holders, culminating in the assembly of Fig. 2.

The centrifuge was designed to reach 18,000 rpm, at which speed tensions in excess of 150 atmospheres would be reached in benzene or water. A Dumore Type W-2 one-half horsepower universal motor powered the rotor; the speed was varied by means of a variable auto transformer. The suspension for the motor was similar to that described by Elsaesser[13] and recommended by Svedberg.[14] With such a support, the motor is free to align its shaft with that of the rotor. An aluminum alloy, 75 *ST*, was selected for the rotating disks, since it is superior in many ways to alloy steels. The ratio of Young's modulus to density is slightly superior for 75 *ST* to that of the steels it replaces, and it is not strained beyond the elastic limit at the maximum stress developed, about 50,000 lb/in.^{2}; also it is easily machined and requires no further heat treatment before use.

As Fig. 2 shows, the centrifuge assembly was sus-

[8] R. K. Taylor, Am. Chem. Soc. **52**, 3576 (1930).
[9] R. K. Taylor, J. Am. Chem. Soc. **50**, 2937 (1928).
[10] Scott, Shoemaker, Tanner, and Wendel, J. Chem. Phys. **16**, 495 (1948).
[11] H. S. Frank, J. Phys. Chem. **33**, 970 (1929).
[12] A. Stock, *Hydrides of Boron and Silicon* (Cornell University Press, Ithaca, New York, 1933), p. 176.
[13] R. Elsaesser, Siemens-Zeits. **5**, 580 (1925).
[14] The Svedberg and Kai O. Pedersen, *The Ultracentrifuge* (Oxford University Press, London, 1940).

TABLE I. Summary of rupture strength tests.

Tube	Gas pressure mm Hg	Total no. of tests	Strength, Atmospheres Test 2	Test 4	Highest	Test no.
0	*	5	+0.4	+0.8	0.9	3
1	10^{-4}	1	—	—	5.4	1
2	?	1	—	—	5.7	1
3†	5×10^{-5}	3	12.8	—	18.9	3
4	5×10^{-5}	7	13.6	19.9	26.5	7
5	10^{-5}	3	12.1	—	35.0	3
6	10^{-5}	7	6.1	8.0	18.6	7
7	10^{-5}	1	—	—	15.9	1
8	10^{-4}	1	—	—	26.8	1
9	10^{-4}	3	16.6	—	23.0	3
10	4×10^{-5}	6	6.3	14.5	27.2	5
11	4×10^{-5}	2	27.9	—	27.9	2
12	2×10^{-4}	6	44.5	54.9	81.5	6
13	5×10^{-5}	24	13.3	18.7	35.1	22
14	8×10^{-5}	39	23.6	17.8	60.0	6
15	8×10^{-5}	4	33.3	46.7	46.7	4
16	7×10^{-5}	1	—	—	138.	1
17	7×10^{-5}	1	—	—	157.	1
18	5×10^{-5}	6	36.6	44.8	45.2	5
19	2.6×10^{-2}	6	36.2	41.2	57.6	6
20	8.5	17	28.6	23.8	32.2	16
21	5.	14	14.9	14.7	18.0	14
22	3×10^{-2}	3	22.8	—	36.8	3
23	7.	2	22.0	—	22.0	2
24	7.	13	24.8	19.1	42.7	13
25	7.	4	17.0	19.4	20.3	3
26	7×10^{-2}	15	15.5	20.0	24.6	8–15
27	7×10^{-2}	12	16.5	24.4	43.1	7–12
28	1.5×10^{-4}	20	9.75	7.3	38.8	19
29	1.5×10^{-4}	7	11.5	10.8	27.2	7
30	1.9×10^{-4}	11	21.6	30.3	48.8	9, 10, 11
31	1.9×10^{-4}	8	21.2	24.4	36.2	7
32	0.6	8	12.3	13.8	26.6	6, 7, 8
34	10^{-2}	5	17.4	18.8	28.7	5

* An open tube, degassed by boiling at room temperature.
† Paired tubes were filled and sealed at the same time.

pended from a steel disk which was itself supported at three points within a steel cylinder. Beginning with tube 12, the cylinder was evacuated to reduce the air drag. Otherwise, with the tube holder in place the top speed of the centrifuge was limited to about 9000 rpm, equivalent to a nominal tension in the benzene of 40 atmospheres. Upon partially evacuating the centrifuge, vibrations that were formerly damped became excessive. These vibrations caused the first tube holder to fail structurally at 12,000 rpm. From a survey made of the resonant frequencies of the system, it was deduced that the support disk was the primary source of the trouble. When the thickness of the plate was increased to $\frac{3}{4}$ inch, the prominent resonances disappeared. Each of the following modifications of the system also contributed to the smooth operation of the centrifuge: (a) The support plate was mounted on rubber pads. (b) The coupling between rotor shaft and motor was changed from a hose-type to a three piece multiple point type. The latter construction permitted free relative axial motion of both shafts. (c) Finally, the original standard tolerance ball bearings of the rotor were replaced by close-tolerance class *C*-2 bearings with bronze retainers. The centrifuge now accelerates quietly at any ambient air pressure or rotational speed.

The conventional Strobotac lamp and discharge circuit were found to give a blurred image of the end of the liquid column when it moved at speeds above 6000 rpm, or about 6300 centimeters per second. A flash lamp and power supply that provided flashes of much shorter duration were constructed by Shapiro, Edwards, and Pound of Pasadena. The discharge circuit limited the duration of the flash to about two microseconds. The essential features of the circuit have been published elsewhere.[15] The discharge was triggered by a pulse from a General Radio Strobotac. The latter was checked frequently for correct calibration against the line frequency.

The tensile strength T in dynes/cm^2 is given by:

$$T=2\pi^2\rho l^2 n^2-P_0$$

where ρ is the density in g/cc, l and n are respectively the effective column length in cm. and speed in rev/sec. at the instant of rupture, and P_0 is the vapor pressure, which was negligible in all our experiments. This equation is fairly obvious; a derivation may be found in our expanded report.[7] A value for ρ of 0.875 g/cm^3 was used in all computations of T. This is the density of benzene at 23°C.

DISCUSSION OF RESULTS

The maximum observed rupture strength was 157 atmospheres. It was attained on the first and only test on tube 17. This is believed to be the highest reported strength for a liquid of this low surface tension (29

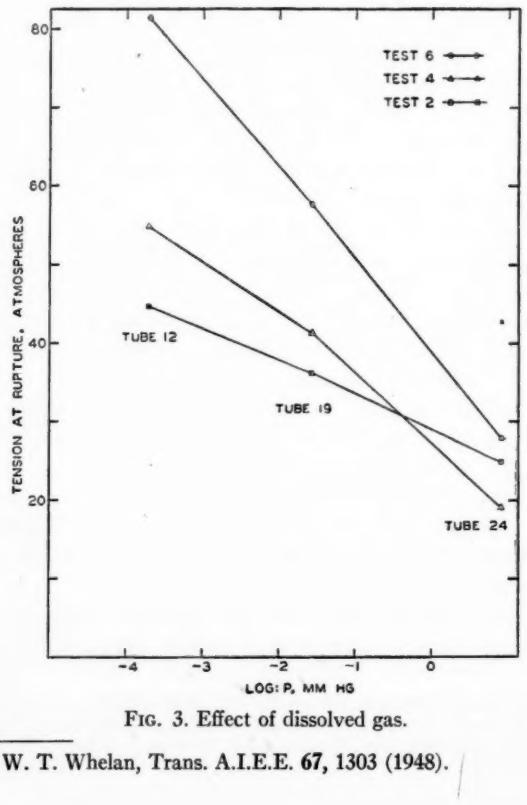

FIG. 3. Effect of dissolved gas.

[15] W. T. Whelan, Trans. A.I.E.E. **67**, 1303 (1948).

dyne/cm), and to be second in magnitude only to the recently reported results of Briggs,[3] who found a maximum rupture strength for water of over 250 atmospheres, using a similar method. Values of about 150 atmospheres for water have been reported by other observers. However, the reliability of these results have been questioned.[1,2] Moreover, these measurements estimated the tensile strengths from the known values at positive pressures of the coefficients of thermal expansion and volume compressibility; that these coefficients are unchanged at negative pressures of 150 atmospheres seems doubtful. The next to the largest strength observed by us was 138 atmospheres, for tube 16; also 81.5 atmospheres was observed on the sixth and last test on tube 12. These values were outstandingly high. The maximum strength observed for each specimen or tube tested is tabulated in Table I. The results for tests 2 and 4 are also given, to illustrate the trend toward higher strengths on successive tests on the same tube.

We have investigated a number of the factors affecting the tensile strength of benzene in Pyrex glass tubes. The variables studied include the condition of the glass surface; the quantity of dissolved gas, and the purity of the benzene. In addition, the effect of temperature changes and of prolonging the tension were also observed. The results of the observations on the role of these factors enumerated above will now be discussed.

The Effect of Dissolved Gas on the Rupture Strength

A comparison of the maximum observed rupture strength of benzene under a wide range of gas pressures is made in Fig. 3. These values were taken from our complete list of test results.[7] Results for tests 2, 4, and 6 illustrate the approach to the observed maximum strength. Each of tubes 12, 19, and 24 was the best (highest ultimate rupture strength) in its range of permanent gas pressures. For tube 24 the maximum strength, indicated by the *X* in the figure, was observed on test 13. The concentration of dissolved gas is given in terms of the pressure of the overlying gas. For convenience of presentation only, the pressure is plotted on a logarithmic scale.

A scatter diagram of the highest strength observed with each tube gives a similar but less marked dependence than that shown in Fig. 3. However we think the best tubes in each pressure range are probably the only ones of significance. It is our opinion moreover that the failure to reach equal or higher strengths on specimens prepared under similar conditions can be ascribed to inferior adhesion to the walls of the tubes. It is believed that mechanical vibrations in the centrifuge have not been severe enough to influence adversely our observed strengths; in any event they could only hasten the onset of rupture. Heavy solids are removed from the region of high tensile stress, so that even if they are non-wetting, or carry quantities of adsorbed gases, they do not affect the tensile strength as observed by this method. This conclusion would not hold for other methods, where the tensile stress is uniform throughout the specimen of liquid, or where the liquid is streaming through the region of high tensile stress.

Our results are evidence in favor of the hypothesis that the rupture strength is decreased by the addition of dissolved gas. How this effect is brought about is not clear, since as explained below, it appears that the gas in the body of the liquid is truly dissolved. Our results are not conclusive since the number of tests at any one pressure were relatively few, and the possibility remains that the higher observed rupture strengths were fortuitously associated with lower gas pressures. Nonetheless the trend indicated in Fig. 3 is interesting, especially when it is remembered that our highest observed strengths, of 157 and 138 atmospheres, were obtained with a permanent gas pressure less than 10^{-4} mm. (Table I).

Effect of Prolonged Tensile Stress on the Observed Strength

It was suggested that the time taken to reach rupture might have some bearing on the observed strength. Since gas bubbles and any other mobile nuclei of apparent density less than that of benzene would be swept to the center of rotation by the pressure gradient along the tube, such time measurements could be of significance in detecting the presence of such nuclei. In a number of tests the centrifuge was permitted to run from five to ten minutes at a speed slightly below the previously observed rupture strength. Prolonging the test in this way produced no significant variation of rupture strength. These negative results are a strong indication either that the specimens of liquid were quite free of mobile low density nuclei, gaseous or otherwise, or that rupture was not initiated on such nuclei in our tests.‡

The Temperature Coefficient of the Rupture Strength

If the van der Waals or Berthelot equations of state can be used to calculate tensile strengths, the temperature coefficient of the tensile strength of benzene should be at least one atmosphere per degree Centigrade, according to Benson and Gerjuoy.[8] Tests were made at various temperatures on a number of tubes, covering the full range of gas concentrations studied. No significant dependence of rupture strength on temperature was observed. However, this does not invalidate the use of the equation of state at negative pressures, for as

‡ Actually the differential equation for the motion of the bubbles shows that in the conditions of our experiment, bubbles less than about 10^{-5} cm in radius would move only a very short distance during the run (see reference 1). Thus we can assert only that the liquid was free of bubbles larger than 10^{-5} cm. We are indebted to the referee for calling our attention to this point.

explained below the observed strengths are believed to be limited by weak adhesion to the glass and not by the true strength of the liquid.

The Purity of the Prepared Samples of Benzene

The possibility of contamination of the benzene used to fill tubes following number 17 was investigated. The results were negative, as were the results of changes in the baking out procedure used to prepare the tubes. Details are given in our expanded report.[7]

The Condition of the Glass Surface

At the conclusion of the tests made to eliminate the possibility that the benzene had become contaminated following the preparation of tube 17, the preparation of the tubes that had exhibited the high liquid rupture strengths was re-examined. It was discovered that these tubes, numbers 12, 16, and 17, had a history slightly different from the others. Despite repeated efforts to duplicate these histories, we have so far been unable to prepare another tube yielding a comparable strength. The principal difference in the histories appears to be the use of freshly washed glass surfaces and minimum exposure to the atmosphere in the superior tubes.

When this investigation was undertaken, it was not realized or even considered that the adhesion strength of benzene and glass could be radically or rapidly affected by exposure to gases in the atmosphere. In this respect we seem to have underestimated nature's perversity. Considerable evidence exists that a radical change takes place on a glass surface exposed to attack by aqueous solutions or by water vapor.[11,16] The investigations conducted by Bangham[17] offer another clue to the conditions required at the glass-liquid interface for good adhesion. Bangham deduced from numerous observations that ability to adsorb and to wet are independent properties. Furthermore, he found an ordered structure in liquids adsorbed on surfaces not easily wetted. For example, the structure of the adsorbed film of water on some solids is similar to one of the high pressure forms of ice, and there exists a deep transition layer before the structure of liquid water is reached. It is possible that the adhesion forces across such a boundary layer are greatly reduced.

It is known that fine fissures are normally present in glass surfaces which have been exposed to the atmosphere.[18] In the present instance, the change of the glass surface on exposure to the atmosphere may have resulted in the formation of small areas of inferior wettability, covered by compounds formed by the reaction of the glass with water vapor and/or carbon dioxide. Such areas need only extend over extremely small areas to limit the rupture strength to the magnitude observed. For example, such an area, if circular, with a diameter of only 240A, would limit the rupture strength to 50 atmospheres. This figure is based on a simple model, explained in our expanded report. If the region bounding the area has adequate strength to resist removal by the applied tension, then reproducible strengths would be expected, as were observed, for example, for tubes 14 and 21. If successive applications of tension weaken the boundary and finally tear away some of the non-wettable area, the smaller area remaining does not promote rupture until a higher tension is reached. The latter behavior would explain the increase of the rupture strength observed on successive tests of many of the specimens.

The mechanism of rupture just proposed does not rule out the creation of nuclei by the release of gas by the surface layer of the glass.[19] The latter is filled with fissures after attack by water vapor.[18] However, if it is presumed rupture is initiated in this manner, it is difficult to explain the fact that many specimens, after initial increases on successive tests, attained a maximum value which was quite reproducible. The relatively obvious mechanism, that rupture is initiated at a cavity in the glass surface which is filled with gas and expands under an applied tension, is not favored by us. The required stability of such a cavity is not consistent with the expected behavior of a volume of gas in contact with an unsaturated liquid. The Kelvin relation shows the internal pressure in any small bubble is enormous. Such a bubble would be under excess pressure in any of the tubes of unsaturated liquid discussed here and must ultimately dissolve. Thus no gas bubble or gas pockets can remain in contact with an unsaturated liquid. The reproducibility of the maximum value on many of our tubes indicates that certainly no mobile nuclei were present, of the small sizes required to give breakdown at our observed strengths. Since the tubes were handled between successive tests, these nuclei, if present, would shift in position in the course of several tests and should have been found at least once in the immediate vicinity of the center. We are not prepared to explain the observations[19] that a period of extreme pressure increases the tensile strength. We will comment however that it is difficult to infer *quantitatively* from Harvey's data[19] the effect on the tensile strength of "pressurizing" the liquid.

It is our conclusion, based on examination of our data and on the evidence from the literature which we have discussed, that our observed variability is to be ascribed primarily to differing histories of our glass tubes. Although a trend toward higher strengths with decreasing amounts of dissolved gas has been noted, under the conditions of our experiment and at the per-

[16] Kenrick, Gilbert, and Wismer, J. Phys. Chem. **28**, 1297 (1924); J. H. Frazer, Phys. Rev. **33**, 97 (1929); G. H. Latham, J. Am. Chem. Soc. **50**, 2987 (1928); J. H. Frazer *et al.*, J. Phys. Chem. **31**, 897 (1927).

[17] D. H. Bangham, J. Chem. Phys. **14**, 352 (1946).

[18] T. C. Baker and F. W. Preston, J. App. Phys. **17**, 179 (1946), A. A. Griffith, Phil. Trans. Roy. Soc. **A221**, 163 (1921), N. W. Taylor, J. App. Phys. **18**, 943 (1947).

[19] E. N. Harvey *et al.*, J. Cell. Comp. Physiol. **24**, 1 (1944).

manent gas pressures at which we have worked, the observed rupture strength is thought to be a function mainly of the adhesion strength to the walls. Experiments which will definitely confirm or disprove these assertions are urgently required, but difficult to devise. The best procedure would be to subject the liquid to large stresses only at points far from the container walls. This immediately rules out a static stress, however. On the other hand, dynamic stresses (hydraulic and acoustic) generally result in quite low strengths, of the order of a few atmospheres.[1,2] It is of course possible that these low values have resulted from using impure liquids, but there is nothing in the literature[1,2] to suggest that the older static measurements of tensile strength used any purer liquids than have the more recent hydraulic and acoustic measurements.

THE JOURNAL OF CHEMICAL PHYSICS VOLUME 19, NUMBER 1 JANUARY, 1951

The Free Volume for Rigid Sphere Molecules

R. J. Buehler, R. H. Wentorf, Jr., J. O. Hirschfelder, and C. F. Curtiss
Department of Chemistry, University of Wisconsin, Madison, Wisconsin

(Received August 28, 1950)

The free volume is calculated for non-interacting rigid sphere molecules taking into account the exact geometry imposed by the face-centered cubic packing. The size and shape are quite different from that of the inscribed spheres which correspond to the Lennard-Jones and Devonshire approximation. At high densities the equation of state obtained from the exact treatment agrees well with the Eyring or Lennard-Jones and Devonshire equation. When the specific volume is greater than twice the cube of the collision diameters, the molecules are no longer confined to cages formed by neighboring molecules. At these low densities the free volume concept is ambiguous. The equation of state depends upon the shape and orientation of the cells with respect to the lattice positions of the molecules. A particular choice is considered which leads to an equation of state that at low densities is accurate through the second virial coefficient. There are other shapes and orientations of the cells which would lead to other equations of state having this same property.

I. INTRODUCTION

THE free volume or cell theory of the equation of state of dense gases and liquids has been used with limited success by Lennard-Jones and Devonshire,[1] Eyring,[2] and others. Its use involves two kinds of approximations: (1) approximations intrinsic to the free volume concept which have been discussed recently by Kirkwood[3] and (2) approximations in the calculation of the free volume itself. The free volume for non-interacting rigid spheres is defined as the volume of the cage in which the center of a particular molecule can move when all of the other molecules in the liquid or dense gas are held fixed in their mean lattice positions. For molecules with a more realistic energy of interaction, the free volume is given by the integral over a cell of the quantity $\exp(-E/kT)$ where E is the potential energy of the molecule within the cage. In the Lennard-Jones-Devonshire and other working cell theories the calculation of the integral is facilitated by "smearing" the energy, E, into a spherically symmetric function. The present paper is concerned with the errors introduced by this "smearing" or "spherification". The exact free volume and equation of state are calculated for rigid spheres and compared with the approximate free volume calculated on a Lennard-Jones-Devonshire basis. The complicated geometry of the "exact" free volumes is shown in Fig. 12. Note that their size and shape are quite different from that of the inscribed spheres which correspond to the Lennard-Jones-Devonshire method of averaging or smearing. The calculation of the exact free volume would be extremely difficult for molecules which have a more realistic energy of interaction. For a gas of rigid sphere molecules with volume per molecule v, the equation of state can be expressed directly in terms of the free volume, v_f:

$$pv/kT = v\frac{d(\log v_f)}{dv}. \tag{1}$$

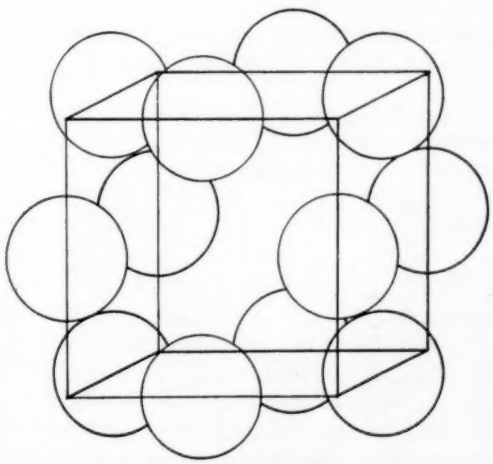

FIG. 1. The cage of twelve nearest neighbors.

[1] J. E. Lennard-Jones and A. F. Devonshire, Proc. Roy. Soc. 163A, 53 (1937).
[2] Kincaid, Eyring, and Stearn, Chem. Revs. 28, 301 (1941).
[3] J. G. Kirkwood, J. Chem. Phys. 18, 380 (1950).

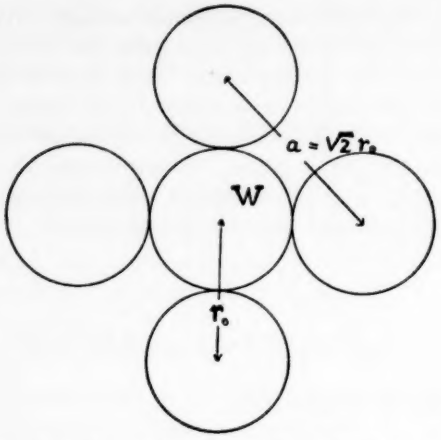

FIG. 2. The wanderer, W, escaping from the cage.

When the specific volume is greater than twice the cube of the molecular diameter, r_0, the molecules are no longer confined to cells by potential energy barriers. Under these conditions the free volume concept is not uniquely defined. A procedure is suggested which permits the free volume equation of state to be extended to low densities.

II. THE HIGH DENSITY MODEL

As in the Lennard-Jones-Devonshire theory, we take a face-centered cubic lattice as a model of a dense gas or liquid and consider all the molecules but one, which we call the "wanderer", to be fixed in their lattice positions. A cage is formed by the wanderer's twelve nearest neighbors which may be thought of as occupying the midpoints of the twelve edges of a cube, as shown in Fig. 1. If a denotes the distance between nearest neighbors in the lattice, then from the geometry of the lattice it follows that

$$a^3=\sqrt{2}v. \tag{2}$$

When $a=\sqrt{2}r_0$, or $v=2r_0^3$, the wanderer is just able to escape through the face of the cube, as shown in Fig. 2. Thus if the specific volume is less than $2r_0^3$ the free volume is ordinarily defined as the volume available to the center of the wanderer. The free volume is zero when $a=r_0$ (or $v=r_0^3/\sqrt{2}$), for then the neighboring molecules are in contact (Fig. 3). This is the highest density possible for rigid spheres, and the corresponding pressure is infinite.

In the range of specific volumes $r_0^3/\sqrt{2}\leq v\leq 2r_0^3$ the free volume is bounded by twelve intersecting spherical surfaces, for it is the volume within the cage which is farther than r_0 from all of the twelve lattice points. (The wanderer approaches up to a distance $(1/2)r_0$; its center up to a distance r_0. A sphere of radius r_0 will be called a "collision sphere.") An expression for this volume is:

$$v_f=\left\{\frac{20}{3}c^3-\frac{4}{3}c^2\sigma-4c^2(r^2-c^2)^{\frac{1}{2}}+2\sqrt{2}(c^3-6cr^2)\left(\sin^{-1}\frac{c}{\rho}+\sin^{-1}m\right)+8r^3\left(2\sin^{-1}u_1+\frac{\pi}{2}-\sin^{-1}w-\sin^{-1}t\right)\right\}. \tag{3}$$

Here:

$$c=a/\sqrt{2};$$
$$m=(c-2\sigma)/3\rho;$$
$$r=r_0;$$
$$t=(r^2+cr-c^2)/r\rho;$$
$$u_1=[(2r+c)(r+x_2)-(c+r)^2]/(r+x_2)\rho;$$
$$w=(r^2-cr-c^2)/r\rho;$$
$$x_2=\tfrac{1}{3}(2c-\sigma);$$
$$\sigma=(3r^2-2c^2)^{\frac{1}{2}};$$
$$\rho=(2r^2-c^2)^{\frac{1}{2}}.$$

Numerical values of the free volume and the compressibility, pv/kT, are given in Table I.

On the other hand, a strict application of the smearing technique would give an infinite potential at all points

TABLE I. Equation of state at high density.

	Free volume equations				
	Exact-free volume method		Eyring or Lennard-Jones Devonshire equation		H-S-E Modified virial equation
v/r_0^3	v_f/r_0^3 Eq. (3)	pv/kT	v_f/r_0^3 Eq. (6)*	pv/kT Eq. (5)	pv/kT Eq. (7)
0.7071	0.00000	∞	0.00000	∞	31.74
0.8104	0.00058	23	0.00042	22.50	21.31
0.8779	0.00254	14	0.00175	14.37	17.08
1.0240	0.01310	9.04	0.00947	8.61	11.49
1.1854	0.04066	6.48	0.02752	6.32	8.18
1.5573	0.1767	4.53	0.1143	4.32	4.80
2.0000	0.4912	3.77	0.2977	3.41	3.29

* Here we have chosen $\alpha=2^{1/6}[(4/3)\pi]$ making Eqs. (4) and (6) identical.

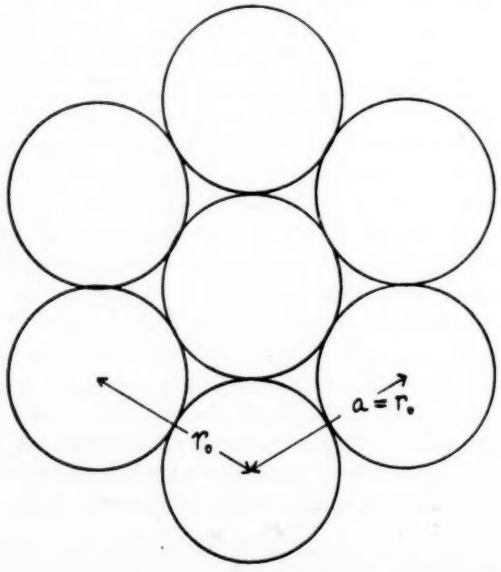

FIG. 3. The tightest possible packing, $a=r_0$, with infinite pressure.

farther than $a-r_0$ from the center of the cage as shown in Fig. 4, which is a cross section through the center of the cage in a plane containing six neighboring lattice points. Consequently one would obtain a free volume of

$$v_f=(4/3)\pi(a-r_0)^3 \tag{4}$$

and the equation of state from Eqs. (1) and (2) would have the simple form:

$$\frac{pv}{kT}=\frac{1}{1-a/r_0}. \tag{5}$$

In Table I it is seen that Eq. (5) furnishes a fairly good approximation to the results obtained from the exact formula.

Equation (5) is identical with the result of Eyring[4] and of Lennard-Jones and Devonshire[1] who assumed that the free volume could be given by

$$v_f=\alpha(v^{\frac{1}{3}}-v_0^{\frac{1}{3}})^3. \tag{6}$$

Here v_0 is the volume per molecule when the spheres are packed tightly together, and α is a constant which varies somewhat according to the kind of packing but does not enter the equation of state. Since v varies with a, and $v=v_0$ when $a=r_0$, it is clear that the free volumes given by Eqs. (4) and (6) are the same except for a constant factor, and hence lead to the same equation of state, Eq. (5).

Table I also gives values of pv/kT calculated from the Hirschfelder-Stevenson-Eyring[4] modified virial equation of state for rigid spheres:

$$\frac{pv}{kT}=1+\frac{b_0}{v}+\frac{5}{8}\frac{b_0^2}{v^2}+0.2869\frac{b_0^3}{v^3}+0.1928\frac{b_0^4}{v^4}. \tag{7}$$

Here b_0 is the second virial coefficient for rigid spheres.

$$b_0=\tfrac{2}{3}\pi r_0^3. \tag{8}$$

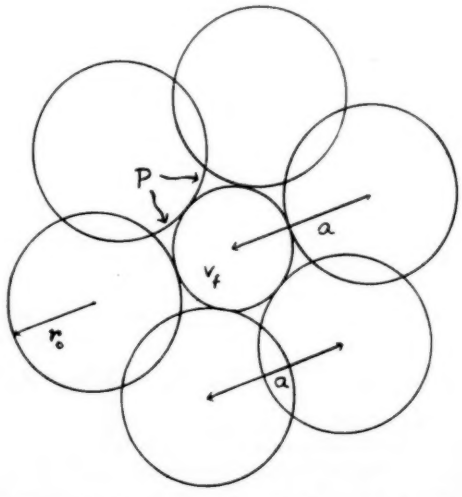

FIG. 4. Free volume, v_f, given by the "smearing" technique, neglecting pockets, P, lying outside a sphere of radius $a-r_0$.

[4] Hirschfelder, Stevenson, and Eyring, J. Chem. Phys. **5**, 896 (1937).

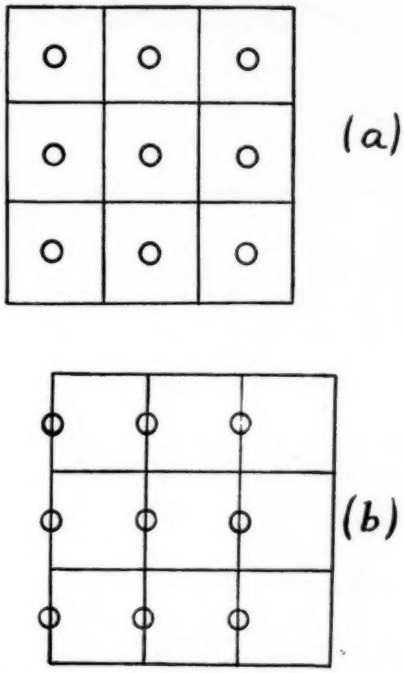

FIG. 5. Two methods of dividing a rectangular array of N molecules into N cells.

III. EXTENSION TO LOW DENSITY

The free volume concept of the liquid (or dense gas) state has been reviewed critically by Kirkwood.[3] In evaluating the classical phase integral he spans the volume containing the gas of N molecules by a lattice of N cells. It is then possible to derive the usual free volume theory as the first approximation to a rather general scheme. Here all the molecules are held in their mean lattice positions except one molecule which is allowed to wander. The volume within the cell in which the center of the wandering molecule can move is called the free volume. However, the choice of the shape and orientation of the cells with respect to the molecules is somewhat arbitrary. At high densities ($r_0^3/v>\frac{1}{2}$) this leads to an ambiguity in the value of the packing constant, α; but the equation of state is uniquely determined. However, at low densities ($r_0^3/v<\frac{1}{2}$) both the packing constant and the equation of state depend a great deal on the choice of the shape and orientation of the cells with respect to the molecules. The principal defect of the free volume concept is that it neglects the cooperative motion of neighboring molecules, and the possibility of two molecules occupying the same cell simultaneously is not considered.

As long as the density is sufficiently great the molecules are in reality confined to cages. Under these conditions it is natural to choose the equilibrium lattice points as the centers of the cells; each molecule is then symmetrically surrounded by a cell. As the density becomes lower, the wanderer continues to be the central molecule in a cage which is bounded either by the collision spheres of its nearest neighbors or else by mathe-

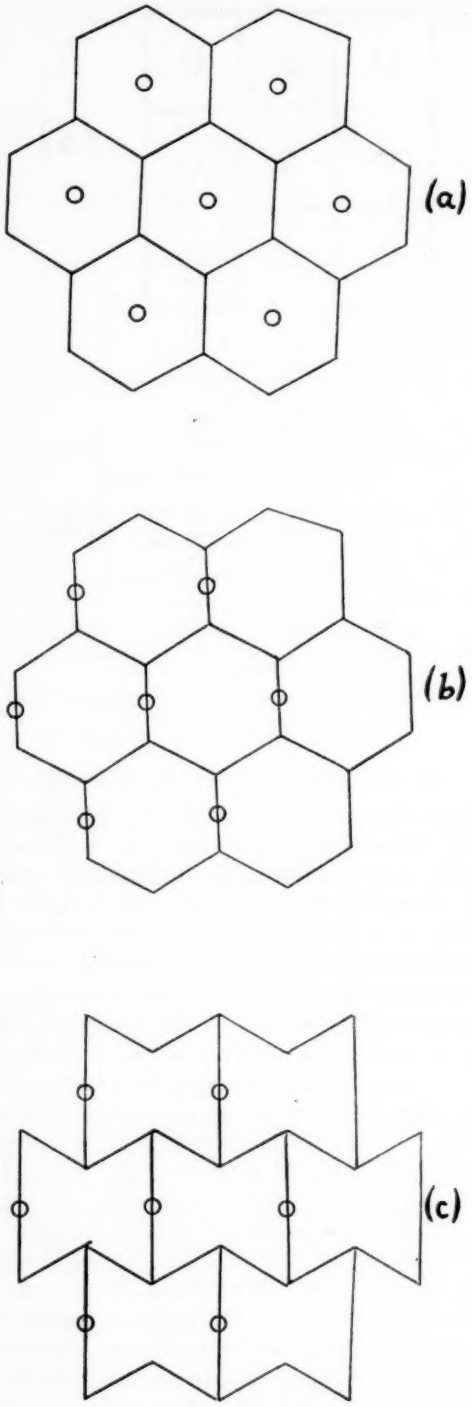

FIG. 6. Three methods of dividing a hexagonal array of N molecules into N cells.

matical partitions which bisect the distance between lattice points, whichever barrier appears first.

Thus the free volume is bounded by planes and spheres. When the density becomes smaller than $r_0^3/v=\sqrt{2}/8$, the free volume is bounded entirely by the bisecting planes. It is then exactly equal to the specific volume, v, and the equation of state becomes ideal, $pv=kT$. The Lennard-Jones-Devonshire and Eyring equations of state show this behavior when they are extrapolated to low densities. In another paper[5] the failure of the Lennard-Jones-Devonshire equation at low densities is demonstrated.

By choosing a different orientation and shape of the cells it is possible to obtain an equation of state which is correct through the second virial coefficient, instead of giving the ideal equation $pv=kT$, at comparatively low densities. This new cell division considers binary collisions between molecules properly and therefore seems preferable.

Figure 5 shows how a two-dimensional rectangular array may be divided into cells in two ways. With the cells centered on the molecules, binary encounters are excluded at low density. However, if the cells are chosen so that each molecule lies on the side of its cell, then binary encounters may occur. Similarly for a hexagonal two-dimensional array one could start with the cells centered on the molecules [Fig. 6(a)] and then rearrange the cells in one of two ways: (1) shift the whole cell structure to the right [Fig. 6(b)]; or (2) replace the vertical partitions with new ones passing through the molecules [Fig. 6(c)]. In the case of the three dimensional face-centered cubic array we have found the choice analogous to Fig. 6(c) to be simpler.* Both of these last two models give the correct value of the second virial coefficient for sufficiently low densities. However the cell patterns 6(b) and 6(c) lead to quite different equations of state. It therefore appears that even the requirement of giving the correct second virial coefficient does not uniquely specify the cell.

For purposes of calculation it will be convenient to consider a cell of the type of Fig. 5(b) [or Fig. 6(c)] as having a free volume which is the average of two free volumes obtained from Fig. 5(a) [or Fig. 6(a)]. This point of view is illustrated in Fig. 7. The "averaged" free volume, v_{fa}, is obtained from the "soft center" free

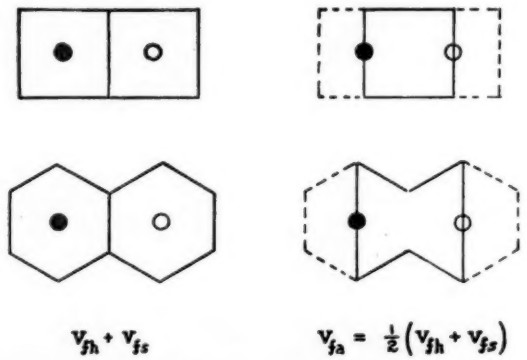

FIG. 7. Equivalence of the "averaged" free volume, v_{fa}, with models in which the lattice points lie on the edges of their cells. The solid circle is a fixed molecule; the hollow circle is the wanderer.

[5] Wentorf, Jr., Buehler, Hirschfelder, and Curtiss, J. Chem. Phys. **18**, 1484 (1950).

* This is essentially due to the fact that the partitions (except the vertical ones) are perpendicular bisectors of the lines joining adjacent molecules.

volume, v_{fs}, which the wanderer finds in a cell centered on its own lattice position and the "hard center" free volume, v_{fh}, which it finds in a cell centered on a fixed neighboring molecule.

$$v_{fa}=(1/2)(v_{fs}+v_{fh}). \tag{9}$$

In the three-dimensional case the shape of the "soft center" and "hard center" free volumes for different density regions are shown in Fig. 12. The equation of state has been calculated both from a "soft center" model which corresponds to the usual technique of centering the cells on lattice positions, and also from an "averaged" free volume in which the lattice positions lie on the sides of the cells. The two methods give identical results at high density; for low density the latter model gives the proper value of the second virial coefficient, while the former is ideal:

$$\left.\begin{aligned} &pv/kT \text{ ("soft center")}=1 \\ &pv/kT \text{ ("averaged")} \\ &\quad=\frac{1}{1-b_0/v}=1+\frac{b_0}{v}+\frac{b_0^2}{v^2}+\cdots \end{aligned}\right\} v>4\sqrt{2}r_0^3.$$

Note that the "averaged" free volume leads to the wrong third virial coefficient, b_0^2 instead of $(5/8)b_0^2$.

The partition function of a gas may be written in the form[3]

$$(N!)\sigma^N v_f^N j^N,$$

where j is the partition function of single molecule, v_f the free volume, and σ a factor varying from 1 to e. It is the factor σ which takes into account the "coopera-

TABLE II. Free volumes and derivatives.

	c/r_0	a/r_0	v/r_0^3	v_{fs}/r_0^3	v_{fh}/r_0^3	v_{fa}/r_0^3	$\frac{1}{r_0^2}\frac{dv_{fs}}{dc}$	$\frac{1}{r_0^2}\frac{dv_{fh}}{dc}$	$\frac{1}{r_0^2}\frac{dv_{fa}}{dc}$
Case 1	$(1/2)^+$	1.000	0.7071	0.0000	0.0000	0.0000	0.000	0.000	0.000
	0.74	1.047	0.8104	0.0006	0.0000	0.0003	0.053	0.000	0.027
	0.76	1.075	0.8779	0.0025	0.0000	0.0013	0.139	0.000	0.070
	0.78	1.103	0.9491	0.0064	0.0000	0.0032	0.269	0.000	0.135
	0.80	1.131	1.0240	0.0131	0.0000	0.0065	0.444	0.000	0.222
	0.82	1.160	1.1027	0.0247	0.0000	0.0124	0.668	0.000	0.334
	0.84	1.188	1.1854	0.0407	0.0000	0.0203	0.941	0.000	0.471
	0.86	1.216	1.2721	0.0627	0.0000	0.0314	1.269	0.000	0.634
	0.88	1.245	1.3629	0.0917	0.0000	0.0458	1.654	0.000	0.827
	0.90	1.273	1.4580	0.1299	0.0000	0.0650	2.099	0.000	1.049
	0.92	1.301	1.5573	0.1767	0.0000	0.0884	2.614	0.000	1.307
	0.94	1.329	1.6611	0.2349	0.0000	0.1175	3.202	0.000	1.601
	0.96	1.358	1.7695	0.3045	0.0000	0.1523	3.873	0.000	1.936
	0.98	1.386	1.8823	0.3941	0.0000	0.1970	4.651	0.000	2.326
Case 2	1.00	1.414	2.0000	0.4912	0.0000	0.2456	5.555	0.000	2.777
	1.02	1.442	2.1224	0.6132	0.0001	0.3066	6.613	0.011	3.312
	1.04	1.471	2.2497	0.7558	0.0005	0.3782	7.672	0.041	3.856
	1.06	1.499	2.3820	0.9198	0.0018	0.4608	8.729	0.094	4.412
	1.08	1.527	2.5194	1.1051	0.0044	0.5547	9.783	0.173	4.978
	1.10	1.556	2.6620	1.3112	0.0090	0.6601	10.829	0.279	5.554
	1.12	1.584	2.8099	1.5381	0.0159	0.7770	11.866	0.417	6.141
	1.14	1.612	2.9631	1.7856	0.0260	0.9058	12.887	0.591	6.739
Case 3	$(4/3)^+$	1.633	3.0792	1.9806	0.0357	1.0081	13.626	0.744	7.185
	1.16	1.640	3.1217	2.0533	0.0399	1.0466	13.884	0.807	7.346
	1.18	1.669	3.2861	2.3400	0.0586	1.1993	14.747	1.109	7.928
	1.20	1.697	3.4560	2.6417	0.0849	1.3633	15.388	1.534	8.461
	1.22	1.725	3.6317	2.9534	0.1213	1.5373	15.686	2.146	8.916
Case 4	$(3/2)^+$	1.732	3.6742	3.0278	0.1319	1.5798	15.664	2.336	9.000
	1.24	1.754	3.8132	3.2646	0.1730	1.7189	15.389	3.062	9.226
	1.26	1.782	4.0007	3.5688	0.2439	1.9063	15.022	4.029	9.528
	1.28	1.810	4.1943	3.8655	0.3343	2.0999	14.650	5.011	9.830
	1.30	1.838	4.3940	4.1547	0.4445	2.2996	14.272	6.008	10.140
	1.32	1.867	4.5999	4.4364	0.5747	2.5055	13.888	7.021	10.454
	1.34	1.895	4.8121	4.7102	0.7254	2.7178	13.498	8.049	10.774
	1.36	1.923	5.0309	4.9762	0.8968	2.9365	13.097	9.093	11.095
	1.38	1.952	5.2561	5.2343	1.0893	3.1618	12.701	10.152	11.426
	1.40	1.980	5.4880	5.4842	1.3030	3.3936	11.760	11.760	11.760
Case 5	2^+	2.000	5.6569	5.6569	1.4681	3.5625	12.000	12.000	12.000
	1.42	2.008	5.7266	5.7266	1.5378	3.6322	12.098	12.098	12.098
	1.44	2.036	5.9719	5.9719	1.7832	3.8776	12.442	12.442	12.442
	1.46	2.064	6.2243	6.2243	2.0355	4.1299	12.790	12.790	12.790
	1.48	2.093	6.4835	6.4835	2.2948	4.3892	13.142	13.142	13.142

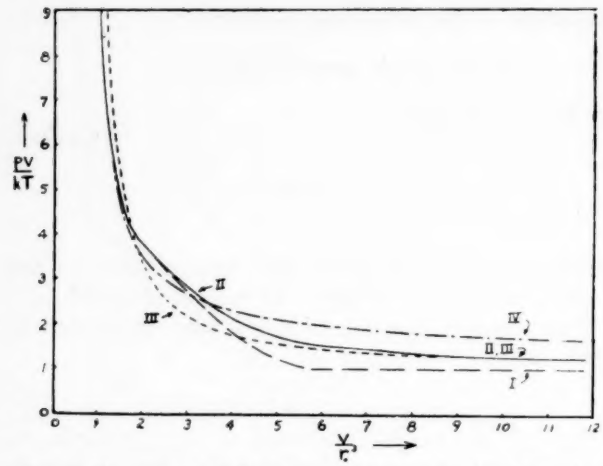

FIG. 8. The compressibility factor, pv/kT, as obtained from four equations of state for rigid spheres. I. The "soft center" method. II. The "averaged" free volume method. III. The H-S-E modified virial equation, Eq. (7). IV. The Eyring equation, Eq. (5).

tive" motion and contributes the "communal" entropy. The approximate free volume discussed above is an approximation to v_f. No attempt is made to approximate σ. Of course, as long as σ is constant it does not affect the equation of state but somewhere (undoubtedly gradually) between the extreme high density and the extreme low density, it must affect the result.

Numerical values of the "hard center," "soft center," and "averaged" free volumes are given in Table II. Values of the derivatives with respect to $c=a/\sqrt{2}$ which enter into the equation of state are also given. The compressibility, pv/kT, for rigid spheres calculated on four different bases is given in Fig. 8. The four curves are: I. The result of the "soft center" model in which the cell is centered on the mean position of the wanderer. II. The result of the "averaged" free volume in which the mean position of the wandering molecule is on the side of the cell. III. The Hirschfelder-Stevenson-Eyring equation, Eq. (7). IV. The Eyring equation, Eq. (5). It should be noted that the Eyring equation has been extended to low densities where it was not intended to apply. The first three of these four curves are also given in Table III.

Some difficulty is encountered if one attempts to employ the "smearing" (i.e., averaging over angles) technique of Lennard-Jones and Devonshire in connection with the "averaged" free volume. If one is to average over angles, the cell must necessarily be a sphere, and consequently the cells cannot be made to "pack". If the cells are chosen to be spheres of volume v, which will overlap slightly, then the resulting equation of state for rigid spheres obtained from the "averaged" free volume is discontinuous (Fig. 9, curve A). A corresponding calculation was made replacing the rigid sphere potential by the Lennard-Jones potential:

$$E(r)=4\epsilon[(r_0/r)^{12}-(r_0/r)^6]. \tag{10}$$

Formulas were used which differed from those of the Lennard-Jones and Devonshire theory by the inclusion of the "hard center" model. The resulting isotherm (curve B) resembles the rigid sphere result quite closely. Both are satisfactory in high and low density limits, but have an unrealistic hump for intermediate densities. In the case of rigid spheres this hump is eliminated by calculating the free volume exactly without averaging over angles (curve C); the same would presumably be true for the Lennard-Jones potential.

IV. GEOMETRY OF THE THREE DIMENSIONAL MODEL

The free volume equation of state for rigid spheres depends on the way in which the cells are chosen. The choice which has been made here, for a face-centered lattice, has the advantages of (1) mathematical simplicity which arises from choosing partitions which are perpendicular bisectors of lines joining neighboring molecules and (2) yielding an equation of state with the proper value of the second virial coefficient at low density.

The face-centered lattice may be divided into cells in the following way. Let one lattice point be fixed at the origin of a Cartesian coordinate system, and put the twelve neighboring lattice points at $(0, \pm c, \pm c)$, $(\pm c, 0, \pm c)$, and $(\pm c, \pm c, 0)$. Then the distance between nearest neighbors is

$$a=\sqrt{2}c. \tag{11}$$

About each lattice point put twelve planes which are the perpendicular bisectors of the lines joining nearest neighboring lattice points. About the origin, for instance, we have the planes $\pm y\pm z=c$, $\pm z\pm x=c$, and $\pm x\pm y=c$. These twelve planes form a dodecahedron as shown in Fig. 10. The defining property of this figure is that it contains all the points lying nearer to its center than to any other lattice points. From this point

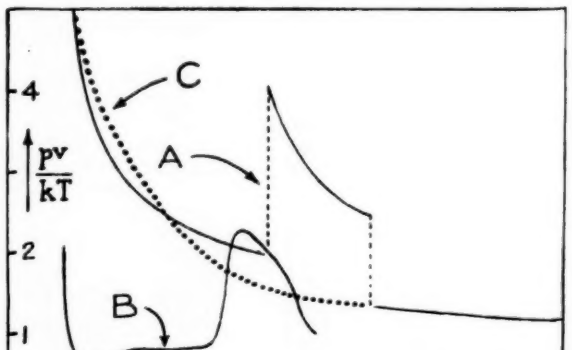

FIG. 9. The effect of averaging over angles. Curve A is the result of using the "smearing" technique (i.e., averaging over angles) together with the "averaged" free volume for the case of rigid spheres. Curve B is the corresponding result for molecules obeying the Lennard-Jones potential, Eq. (10), at a reduced temperature of $\epsilon/kT=0.75$. Curve C is the result for rigid spheres obtained in Section IV, in which angular dependence is included.

of view it is clear that these figures will "pack" together to fill the space, and also that each has volume v.

The "soft center" free volume is defined to be the volume within the dodecahedron which is farther than r_0 from any of the twelve neighboring lattice points. This "soft center" free volume is identical with that considered in Section II for densities sufficiently high so that it is bounded completely by the collision spheres. For lower densities the center of the wanderer is confined either by the collision spheres or by the bisecting planes, whichever barrier appears first.

The "hard center" free volume is the volume inside the dodecahedron which lies outside a collision sphere centered at the origin. In this model it is unnecessary to consider the twelve neighboring collision spheres. This is a consequence of choosing bisecting planes as the cell walls. Any point inside the dodecahedron lies nearer to the origin than to any of the twelve neighboring lattice positions, and hence the regions excluded by the neighboring collision spheres are already excluded by the central collision sphere.

TABLE III. The compressibility, pv/kT.

	v/v_0	"Soft center" method	"Averaging" method	H-S-E modified virial equation, Eq. (7)
Case 1	0.7071	∞	∞	31.738
	0.8104	23	23	21.314
	0.8779	14	14	17.084
	0.9491	11.0	11.0	13.904
	1.0240	9.04	9.04	11.488
	1.1027	7.38	7.38	9.629
	1.1854	6.48	6.48	8.179
	1.2721	5.797	5.797	7.037
	1.3629	5.291	5.291	6.129
	1.4580	4.845	4.845	5.397
	1.5573	4.535	4.535	4.804
	1.6611	4.271	4.271	4.317
	1.7695	4.070	4.070	3.913
	1.8823	3.856	3.856	3.577
Case 2	2.0000	3.768	3.768	3.294
	2.1224	3.667	3.672	3.054
	2.2497	3.519	3.535	2.849
	2.3820	3.353	3.383	2.673
	2.5194	3.187	3.230	2.520
	2.6620	3.028	3.085	2.387
	2.8099	2.880	2.951	2.271
	2.9631	2.742	2.827	2.168
Case 3	3.0792	2.648	2.743	2.101
	3.1217	2.615	2.714	2.078
	3.2861	2.479	2.600	1.997
	3.4560	2.330	2.482	1.925
	3.6317	2.160	2.359	1.861
Case 4	3.6742	2.112	2.326	1.847
	3.8132	1.948	2.218	1.803
	4.0007	1.768	2.099	1.750
	4.1943	1.617	1.997	1.703
	4.3940	1.489	1.911	1.660
	4.5999	1.377	1.836	1.620
	4.8121	1.280	1.771	1.584
	5.0309	1.193	1.713	1.551
	5.2561	1.116	1.662	1.521
	5.4880	1.001	1.617	1.493
Case 5	5.6569	1.000	1.588	1.474
	5.7266	1.000	1.577	1.467
	5.9719	1.000	1.540	1.443
	6.2243	1.000	1.507	1.421
	6.4835	1.000	1.477	1.400

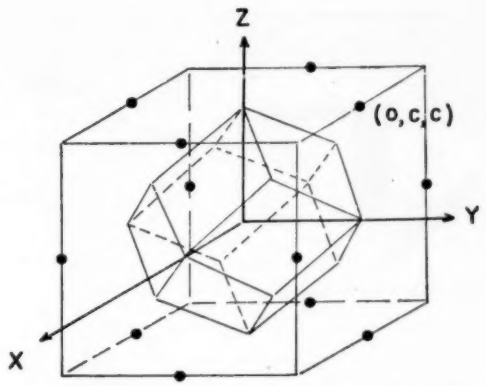

FIG. 10. The dodecahedron formed by planes bisecting the distances from the neighboring molecules to the origin.

The "averaged" free volume may be thought of as being determined by a cell which is formed by combining halves of the dodecahedra about neighboring molecules as in the case of the two dimensional analog shown in Fig. 7. The whole lattice may be partitioned into identical cells of this type (Fig. 11) which have the lattice points located in their faces.

As can be seen from Fig. 12, which shows the appearance of the free volumes at several densities, it is necessary to consider several density ranges owing to the fact that the bisecting planes and collision spheres intersect in various ways. Although the "soft center"

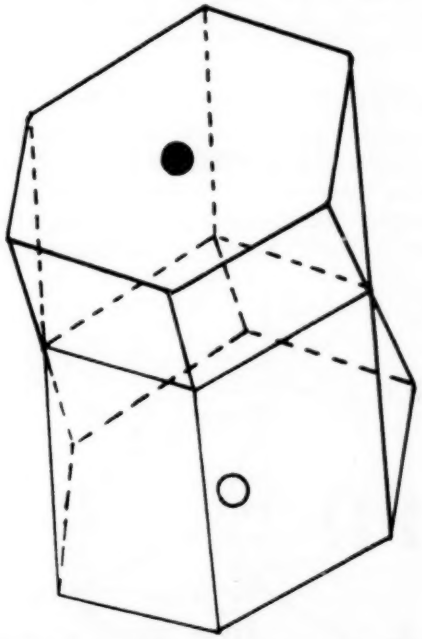

FIG. 11. The cell corresponding to the "averaged" free volume, obtained by combining halves of adjacent dodecahedra. White sphere is the wanderer; black sphere is a neighboring molecule. These spheres are centered in the hexagonal faces.

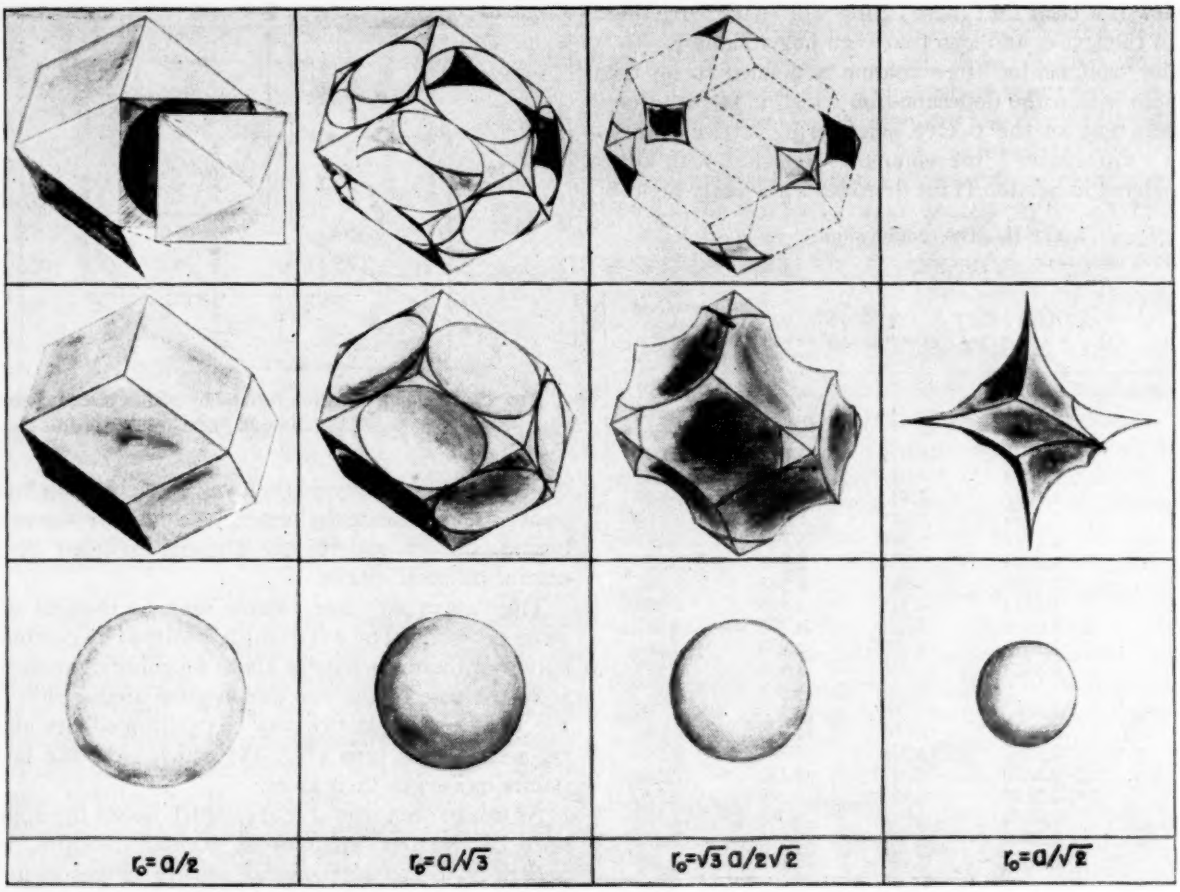

FIG. 12. Pictorial representation of free volumes. The figures in the top row represent the shapes of the free volumes for the "hard center" model for different densities. The figures in the second row illustrate the sort of free volumes which one obtains from the "soft center" model. In the bottom row are shown the corresponding "smeared" free volumes. The density increases from left to right. The four densities selected are those values which partition the entire density range into the five cases described in detail in Section IV.

and "hard center" free volumes are quite different in appearance, it is helpful to note that the collision sphere about a neighboring molecule in the former model and the collision sphere about the origin in the latter necessarily intersect the bisecting plane at the same points. Five distinct density ranges are determined as follows:

Case 1: (High density—this is the case considered in Section II. $1 \leq a/r_0 \leq \sqrt{2}$; $1/\sqrt{2} \leq v/r_0^3 \leq 2$). The "soft center" free volume is bounded wholly by the collision spheres. The "hard center" free volume is zero since the entire dodecahedron lies within a distance of r_0 from its center.

Case 2: ($\sqrt{2} \leq a/r_0 \leq 2\sqrt{2}/3$; $2 \leq v/r_0^3 \leq 16/3\sqrt{3}$). Six

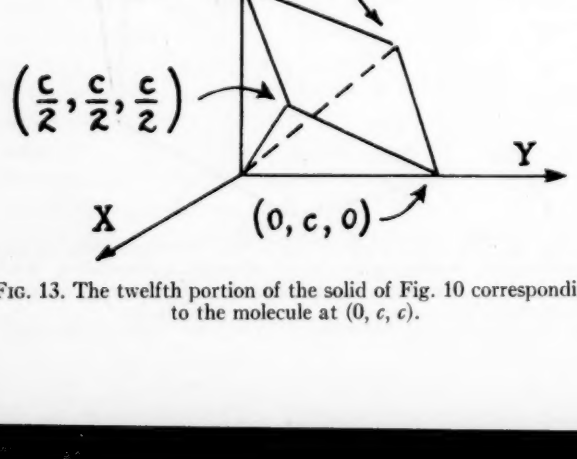

FIG. 13. The twelfth portion of the solid of Fig. 10 corresponding to the molecule at $(0, c, c)$.

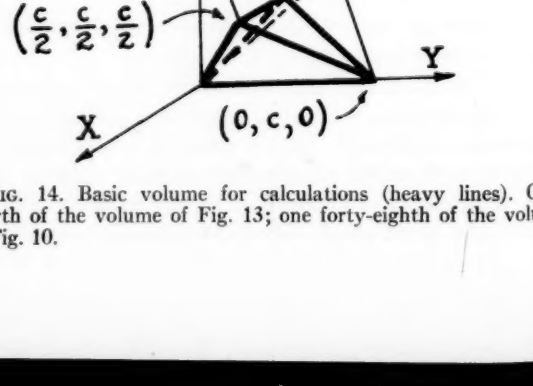

FIG. 14. Basic volume for calculations (heavy lines). One-fourth of the volume of Fig. 13; one forty-eighth of the volume of Fig. 10.

corners of the dodecahedron lie outside the collision spheres. The "hard center" free volume consists of six isolated regions.

Case 3: $(2\sqrt{2}/\sqrt{3}\leq a/r_0\leq\sqrt{3};\ 16/3\sqrt{3}\leq v/r_0^3\leq 3\sqrt{3}/\sqrt{2})$. All 14 corners of the dodecahedron lie outside the collision spheres. The "hard center" free volume consists of 14 isolated regions.

Case 4: $(\sqrt{3}\leq a/r_0\leq 2;\ 3\sqrt{3}/\sqrt{2}\leq v/r_0^3\leq 4\sqrt{2})$. The collision spheres intersect the faces of the dodecahedron but not its edges.

Case 5: $(2\leq a/r_0;\ 4\sqrt{2}\leq v/r_0^3)$. The collision spheres do not intersect the dodecahedron.

The details of the calculations are given in the appendix. The various integrals may be directly usable in other geometrically similar problems, for example, in other quite different theories of liquids.

The authors wish to express their appreciation to Prof. C. A. Boyd, who prepared Fig. 12. The computing was done by Ruth Schoemaker, Marjorie Leikvold, Mary Nordling, Phyllis Rood, and Ruth Schmidt.

This work was made possible by the financial assistance of the Navy Bureau of Ordnance, under contract number NOrd 9938.

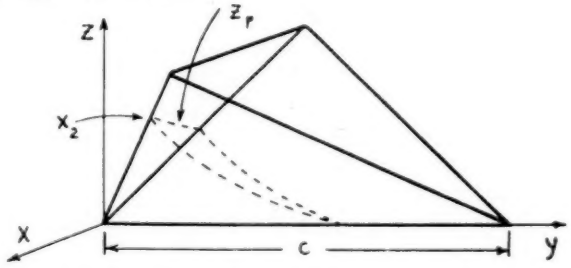

FIG. 15. Case 1. The "soft center" free volume lies under the broken curve. The "hard center" free volume is zero.

APPENDIX

Since each model has a twelve-fold symmetry, it is sufficient to consider only a one-twelfth portion of it. If we focus our attention on the molecule at $(0, c, c)$ and take the twelfth portion of the total figure corresponding to this molecule, as shown in Fig. 13, then the other eleven neighbors are sufficiently distant so that their collision spheres need not be considered. The problem is further simplified by slicing the new figure into four equivalent pieces and taking just one of these, as shown in Fig. 14. This last volume is bounded by the planes $x=z$, $y=z$, $x=0$, and $y+z=c$. The "soft center" free volume is given by 48 times the volume which (1) is bounded by these four planes and (2) lies outside the sphere $x^2+(y-c)^2+(z-c)^2=r_0^2$. The "hard center" free volume is 48 times the volume which (1) is bounded by the four planes and (2) lies outside the sphere $x^2+y^2+z^2=r_0^2$.

Figures 15, 16, and 17 show the intersections of the planes and collision spheres for cases 1, 2, and 3. The broken arcs are intersections of a sphere about the point $(0, c, c)$ and define the "soft center" free volume, while the solid arcs are intersections of a sphere about the origin and define the "hard center" free volume. Expressions for the free volumes were obtained from the following integrals for cases 1, 2, and 3 (superscripts are used to denote cases):†

† In the expression for $v_{fs}^{(3)}$, k is the volume of a cap of the sphere about $(0, c, c)$ which is cut off by the plane $y+z=c$. The integral represents the portion of this cap which is cut off by the plane $x=z$.

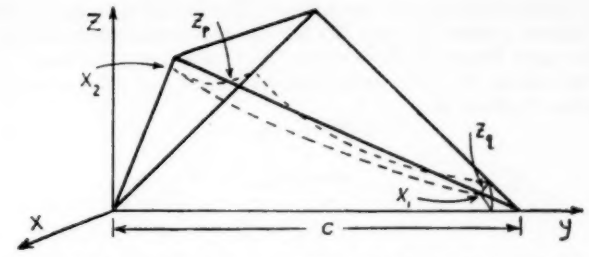

FIG. 16. Case 2. The "soft center" free volume lies under the broken curve. The "hard center" free volume is the small pocket at the extreme right.

$$v_{fs}^{(1)}=48\int_0^{x_2}\int_x^{z_p}\int_z^{y_s} dydzdx$$

$$v_{fs}^{(2)}=48\Big\{\int_0^{x_1}\int_x^{z_q}\int_z^{c-z} dydzdx+\int_0^{x_1}\int_{z_q}^{z_p}\int_z^{y_s} dydzdx+\int_{x_1}^{x_2}\int_x^{z_p}\int_z^{y_s} dydzdx\Big\}$$

$$v_{fh}^{(2)}=48\int_0^{x_1}\int_x^{z_q}\int_{y_r}^{c-z} dydzdx$$

$$v_{fs}^{(3)}=v-12k+48\int_{z_1}^{z_2}\int_{y_1}^{c-z}\int_z^{x_s} dxdydz$$

$$v_{fh}^{(3)}=48\Big\{\int_0^{x_1}\int_x^{z_q}\int_{y_r}^{c-z} dydzdx+\int_{y_2}^{c/2}\int_{z_3}^{y}\int_{x_3}^{z} dxdzdy+\int_{c/2}^{y_3}\int_{z_3}^{c-y}\int_{x_3}^{z} dxdzdy\Big\}.$$

Here:

$$y_s=c-[r^2-(z-c)^2-x^2]^{\frac{1}{2}}$$
$$z_p=c-[(r^2-x^2)/2]^{\frac{1}{2}}$$
$$x_2=\tfrac{1}{3}(2b-\sigma)$$
$$z_q=\tfrac{1}{2}[b-(2r^2-c^2-2x^2)^{\frac{1}{2}}]$$
$$x_1=\tfrac{1}{3}(c-\sigma)$$
$$y_r=(r^2-x^2-z^2)^{\frac{1}{2}}$$
$$x_3=(r^2-y^2-z^2)^{\frac{1}{2}}$$
$$z_3=[(r^2-y^2)/2]^{\frac{1}{2}}$$
$$y_2=r/\sqrt{3}$$
$$y_3=\tfrac{1}{3}(2c-\sigma)$$
$$x_s=[r^2-(y-c)^2-(z-c)^2]^{\frac{1}{2}}$$
$$y_1=c-[r^2-z^2-(z-c)^2]^{\frac{1}{2}}$$
$$z_1=\tfrac{1}{3}(c-\sigma)$$
$$z_2=\tfrac{1}{3}(c+\sigma)$$
$$k=\frac{\pi}{3}h^2(3r-h)$$
$$h=r-c/\sqrt{2}$$
$$r=r_0.$$

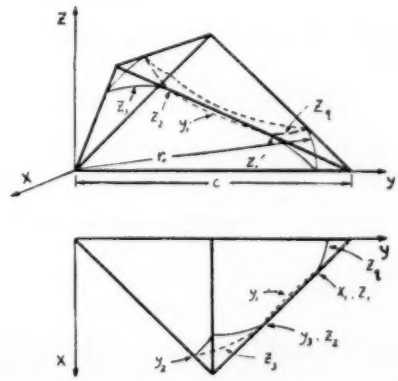

FIG. 17. Case 3. The "soft center" free volume lies under the broken curve in the upper figure. The "hard center" free volume consists of the two small pockets bounded by the solid curves. The lower figure shows the projection of the intersections on the xy plane.

Cases 4 and 5 may be solved by inspection. For case 4 the collision spheres intersect the faces of the dodecahedron but not its edges. Hence the "soft center" free volume is given simply by the volume of the dodecahedron diminished by twelve spherical caps of volume k.

$$v_{fs}^{(4)}=v-12k$$

$$k=\frac{\pi}{3}h^2(3r_0-h)$$

$$h=r_0-c/\sqrt{2}$$

The "hard center" free volume for case 4 may be obtained by starting with the dodecahedron of volume v, and attaching temporarily twelve spherical caps to its faces. Now by subtracting a sphere of radius r_0 both the caps and the excluded volume within the dodecahedron are removed, and the "hard center" free volume remains.

$$v_{fh}^{(4)}=v+12k-(4/3)\pi r_0^3.$$

For case 5 the collision spheres and bisecting planes fail to intersect. Hence the "soft center" free volume is the whole of the dodecahedron.

$$v_{fs}^{(5)}=v.$$

The "hard center" free volume is the volume of the dodecahedron minus the volume of a sphere of radius r_0.

$$v_{fh}^{(5)}=v-(4/3)\pi r_0^3.$$

The "averaged" free volume, $v_{fa}=(1/2)(v_{fs}+v_{fh})$, is the same in cases 4 and 5 because of the accidental canceling of the volume of the caps.

$$v_{fa}^{(4,5)}=v-\tfrac{2}{3}\pi r_0^3=v-b_0.$$

The resulting equation of state is

$$\left(\frac{pv}{kT}\right)^{(4,5)}=\frac{1}{1-b_0/v}.$$

For the first three cases, the result cannot be expressed so simply. The integrals given above lead to the following expressions for the free volumes. Expressions for the derivatives with respect to c are also given. The compressibility, pv/kT, given in Table III was calculated from

$$\frac{pv}{kT}=\frac{c}{3v_f}\frac{dv_f}{dc}$$

which follows from Eqs. (1), (2), and (11).

$$v_{fs}^{(1)}=\left[\frac{20}{3}c^3-4c^2\tau-2\sqrt{2}(6cr^2-c^3)\left(\sin^{-1}\frac{c}{\rho}+\sin^{-1}m\right)-\frac{4}{3}c^2\sigma+8r^3\left(2\sin^{-1}u_1+\frac{\pi}{2}-\sin^{-1}w-\sin^{-1}l\right)\right]$$

$$v_{fs}^{(2)}=\left[4c^3+\frac{4}{3}c^2\sigma+2\sqrt{2}(6cr^2-c^3)\left(2\sin^{-1}s-\sin^{-1}m-\frac{\pi}{2}\right)+8r^3\left(2\sin^{-1}l+2\sin^{-1}u_1+\sin^{-1}u_3-\sin^{-1}u_4-\frac{3\pi}{2}\right)\right]$$

$$v_{fh}^{(2)}=\left[\frac{4}{3}c^3-\frac{4}{3}c^2\sigma+2\sqrt{2}(c^3-6cr^2)\sin^{-1}s+8r^3\left(\sin^{-1}\alpha_1+\sin^{-1}\alpha_2-2\sin^{-1}l+\frac{\pi}{2}\right)\right]$$

$$v_{fs}^{(3)}=\left[2c^3-4\pi h^2(3r-h)+\frac{16}{3}c^2\sigma+4\sqrt{2}(c^3-6cr^2)\left(\frac{\pi}{2}-\sin^{-1}m-\sin^{-1}s\right)+64r^3\left(\frac{\pi}{4}-\sin^{-1}u_1\right)\right]$$

$$v_{fh}^{(3)}=\left[2c^3-\frac{8}{3}c^2\sigma+2\sqrt{2}(c^3-6cr^2)(\sin^{-1}m+\sin^{-1}s)+8r^3\left(2\sin^{-1}u_1+\sin^{-1}\alpha_1+\sin^{-1}\alpha_2-2\sin^{-1}l+\frac{\pi}{3}\right)\right]$$

$$\frac{dv_{fs}^{(1)}}{dc}=\left\{20c^2-\frac{8}{3}\left(c\sigma-\frac{c^3}{\sigma}\right)-4\left(2c\tau-\frac{c^3}{\tau}\right)-6\sqrt{2}\rho^2\left(\sin^{-1}\frac{c}{\rho}+\sin^{-1}m\right)-2\sqrt{2}(6cr^2-c^3)\left(\frac{\sqrt{2}r^2}{\tau\rho^2}+\frac{d}{dc}\sin^{-1}m\right)+16r^3\frac{d}{dc}\sin^{-1}u_1+8r^3(1-w^2)^{-\frac{1}{2}}\left(\frac{r+2c}{r\rho}-\frac{wc}{\rho^2}\right)-8r^3(1-l^2)^{-\frac{1}{2}}\left(\frac{r-2c}{r\rho}+\frac{lc}{\rho^2}\right)\right\}$$

$$\frac{dv_{fs}^{(2)}}{dc}=\left\{12c^2+\frac{8}{3}\left(c\sigma-\frac{c^3}{\sigma}\right)+6\sqrt{2}\rho^2\left(2\sin^{-1}s-\sin^{-1}m-\frac{\pi}{2}\right)+2\sqrt{2}(6cr^2-c^3)\left(2\frac{d}{dc}\sin^{-1}s-\frac{d}{dc}\sin^{-1}m\right)+8r^3\left(2\frac{d}{dc}\sin^{-1}u_1+\frac{d}{dc}\sin^{-1}u_3-\frac{d}{dc}\sin^{-1}u_4+2\frac{d}{dc}\sin^{-1}l\right)\right\}$$

$$\frac{dv_{fh}^{(2)}}{dc}=\left\{4c^2-\frac{8}{3}\left(c\sigma-\frac{c^3}{\sigma}\right)-6\sqrt{2}\rho^2\sin^{-1}s+2\sqrt{2}(c^3-6cr^2)\frac{d}{dc}\sin^{-1}s+8r^3\left(\frac{d}{dc}\sin^{-1}\alpha_1+\frac{d}{dc}\sin^{-1}\alpha_2-2\frac{d}{dc}\sin^{-1}l\right)\right\}$$

$$\frac{dv_{fs}^{(3)}}{dc}=\left\{6c^2+\frac{32}{3}\left(c\sigma-\frac{c^3}{\sigma}\right)+12\sqrt{2}\rho^2\left(\sin^{-1}m+\sin^{-1}s+\frac{\pi}{2}\right)+4\sqrt{2}(6cr^2-c^3)\left(\frac{d}{dc}\sin^{-1}m+\frac{d}{dc}\sin^{-1}s\right)-64r^3\frac{d}{dc}\sin^{-1}u_1\right\}$$

$$\frac{dv_{fh}^{(3)}}{dc}=\left\{6c^2-\frac{16}{3}\left(c\sigma-\frac{c^3}{\sigma}\right)-6\sqrt{2}\rho^2(\sin^{-1}m+\sin^{-1}s)+2\sqrt{2}(c^3-6cr^2)\frac{d}{dc}\sin^{-1}m+8r^3\left(\frac{d}{dc}\sin^{-1}\alpha_1+\frac{d}{dc}\sin^{-1}\alpha_2+2\frac{d}{dc}\sin^{-1}u_1-2\frac{d}{dc}\sin^{-1}l\right)\right\}.$$

Here:

$$c=a/\sqrt{2}$$
$$h=r-c/\sqrt{2}$$
$$l=r(2\sigma+c)/3\rho(r^2-z_1^2)^{\frac{1}{2}}$$
$$m=(c-2\sigma)/3\rho$$
$$r=r_0$$
$$s=\sqrt{2}(c-\sigma)/3\rho$$
$$t=(r^2+cr-c^2)/r\rho$$
$$u_1=[(2r+c)(r+x_2)-(c+r)^2]/(r+x_2)\rho$$
$$u_3=[(2r-c)(r-z_1)-(c-r)^2]/(r-z_1)\rho$$
$$u_4=[(2r+c)(r+z_1)-(c+r)^2]/(r+z_1)\rho$$
$$w=(r^2-cr-c^2)/r\rho$$
$$x_2=\tfrac{1}{3}(2c-\sigma)$$
$$z_1=\tfrac{1}{3}(c-\sigma)$$
$$\alpha_1=(r+2z_1)/\sqrt{2}(r+z_1)$$
$$\alpha_2=(r-2z_1)/\sqrt{2}(r-z_1)$$
$$\sigma=(3r^2-2c^2)^{\frac{1}{2}}$$
$$\rho=(2r^2-c^2)^{\frac{1}{2}}$$
$$\tau=(r^2-c^2)^{\frac{1}{2}}$$

$$\frac{d}{dc}\sin^{-1}l=\frac{1}{(1-l^2)^{\frac{1}{2}}}\left[\frac{1-4c/\sigma}{3\rho(r^2-z_1^2)^{\frac{1}{2}}}+\frac{lc}{\rho^2}+\frac{lz_1}{r^2-z_1^2}\frac{dz_1}{dc}\right]$$

$$\frac{d}{dc}\sin^{-1}m=(\sigma\rho+4c\rho+3mc\sigma)/[3\rho^2\sigma(1-m^2)^{\frac{1}{2}}]$$

$$\frac{d}{dc}\sin^{-1}s=(\sqrt{2}\sigma\rho+2\sqrt{2}c\rho+3sc\sigma)/[3\rho^2\sigma(1-s^2)^{\frac{1}{2}}]$$

$$\frac{d}{dc}\sin^{-1}u_1=\frac{1}{\rho(1-u_1^2)^{\frac{1}{2}}}\left[1+\frac{cu_1}{\rho}-\frac{1}{r+x_2}\left(-(2r+c-u_1\rho)\frac{dx_2}{dc}+2(c+r)\right)\right]$$

$$\frac{d}{dc}\sin^{-1}u_3=\frac{1}{\rho(1-u_3^2)^{\frac{1}{2}}}\left[-1+\frac{cu_3}{\rho}-\frac{1}{r-z_1}\left((2r-c-u_3\rho)\frac{dz_1}{dc}+2(c-r)\right)\right]$$

$$\frac{d}{dc}\sin^{-1}u_4=\frac{1}{\rho(1-u_4^2)^{\frac{1}{2}}}\left[1+\frac{cu_4}{\rho}+\frac{1}{r+z_1}\left((2r+c-u_4\rho)\frac{dz_1}{dc}-2(c+r)\right)\right]$$

$$\frac{d}{dc}\sin^{-1}\alpha_1=\frac{1}{(1-\alpha_1^2)^{\frac{1}{2}}}\frac{\sqrt{2}-\alpha_1}{r+z_1}\frac{dz_1}{dc}$$

$$\frac{d}{dc}\sin^{-1}\alpha_2=\frac{-1}{(1-\alpha_2^2)^{\frac{1}{2}}}\frac{\sqrt{2}-\alpha_2}{r-z_1}\frac{dz_1}{dc}$$

$$dx_2/dc=\tfrac{2}{3}(1+c/\sigma)$$

$$dz_1/dc=\tfrac{1}{3}(1+2c/\sigma).$$

THE JOURNAL OF CHEMICAL PHYSICS VOLUME 19, NUMBER 1 JANUARY, 1951

The Absorption Spectrum of Sulfur Hexafluoride in the Vacuum Ultraviolet Region*

TA-KONG LIU,† GEORGE MOE, AND A. B. F. DUNCAN
Department of Chemistry, University of Rochester, Rochester, New York

(Received November 23, 1949)

The spectrum of sulfur hexafluoride has been investigated down to wavelengths about 600A. The maximum of the first electronic transition is found at about 1050A. Three other transitions occur between this wavelength and 802A, where strong continuous absorption begins, and nothing further can be resolved at shorter wavelengths. Qualitative suggestions are offered about the dissociation of SF_6 and the value of its ionization potential.

THE sulfur hexafluoride molecule is known to have the form of a regular octahedron from the results of electron diffraction measurements and from studies of the Raman and infrared spectra.[1] No electronic spectra of this molecule, or of any other molecule with octahedral symmetry, have been reported previously. We have found a few electronic transitions, occurring in the vacuum ultraviolet region, which will be discussed here.

EXPERIMENTAL

The first experiments[2] were made with a Cario and Schmitt-Ott spectrograph. Continuous absorption was found, which extended from 1563A to shorter wavelengths at a pressure of 20 cm in a 40-cm absorbing path.‡ The first samples of SF_6 were slightly contaminated with SO_2 and the absorption bands of this molecule appeared on some of the first plates. In later investigations, more carefully purified samples were available. A vacuum grating spectrograph[3] with a 2-meter radius of curvature grating was used. The grating was used at near normal incidence.

The sample of SF_6 was obtained from the General Chemical Company. The vapor was passed through copper turnings heated at 400–500°C to remove possible lower fluorides. Sulfur dioxide and hydrogen fluoride were other possible impurities present. They were removed by thorough scrubbing with 10 percent aqueous potassium hydroxide solution. The water introduced was absorbed by fused potassium hydroxide, and the SF_6 was condensed by liquid air. This complete process was repeated three times. Final drying was accomplished by passing the gas through tubes packed with fused potassium hydroxide and then through fresh phosphorus pentoxide. The purified sample was fractionated by sublimation in vacuum, and the middle fraction only was kept for use.

A large number of plates in the region 1520–620A were taken at pressures ranging from a few microns to several hundred microns. Eastman III-0 U. V. Sensitized Spectroscopic Plates and Ilford QIII plates were used. The light source was the usual Lyman continuum, with helium as the carrier gas. Sharp source lines, due to 0 IV and 0 V, were used as wavelength standards.

RESULTS AND DISCUSSION

Four rather broad absorption bands were found at wavelengths less than 1100A. The separations between

TABLE I. Absorption spectrum of SF_6.

Band centers Wavelength (A)	Band centers Wave no.	Widths (cm^{-1})	Approximate experimental f-numbers
1053.9	94886	9000	0.007
936.1	106826	1660	0.0019
872.0	114679	5300	0.0042
830.2	120453	4400	0.008

* This work was supported in part under Contract N6onr-241, Task I, with the ONR, United States Navy.

† Present address: Academia Sinica, Shanghai, China.

[1] G. Herzberg, *Infrared and Raman Spectra of Polyatomic Molecules* (D. Van Nostrand Company, Inc., New York, 1945), p. 336.

[2] The authors are indebted to Mr. Norman Blake, who made these exploratory experiments.

‡ At 621 mm, in a 1-meter path, the absorption extends to 2170A.

[3] Ta-kong Liu and A. B. F. Duncan, J. Chem. Physics **17**, 241 (1949).

centers are very large, so that the bands must arise from different electronic transitions. No vibrational structure can be resolved. The positions of centers, widths and intensity estimates are shown in Table I.

The *f*-numbers in the fourth column of Table I were estimated in the following way. The absorption coefficients at the maxima of the bands were obtained from the pressures, path length, density differences and the slopes of the density-log exposure curves. The integrated absorption coefficients were obtained with the assumption that the absorption coefficient-frequency curves had the shape of isosceles triangles.

A strong continuous absorption begins fairly sharply at 802A (15.5 ev) and extends to the short wavelength limit of our observations (600A). This continuous absorption can be seen at pressures lower than the pressures at which the bands appear. This continuum is ascribed to dissociation of the molecule. It is significant that the beginning of the continuum corresponds to the appearance potential of the SF_5^+ ion observed by Dibeler and Mohler[4] at 15.9±0.2 ev. These investigators found that no SF_6^+ ions appeared in the electron bombardment of SF_6, which suggests that the ionization potential lies higher than the dissociation energy of SF_6 into SF_5^+ and F^-.

A crude estimate of the ionization potential may be obtained from thermochemical data, assuming that the interpretation of the beginning of the continuum is correct. We have the following thermochemical equations:

$$SF_6(g)=SF_5^+(g)+F^-(g)-15.5 \text{ ev}$$
$$F(g)+e=F^-(g)+EA_F \text{ ev}$$

from which

$$SF_6(g)=SF_5^+(g)+F+e-(15.5+EA_F) \text{ ev} \quad (1)$$

where EA_F is the electron affinity of F. From data[5] on the heat of formation of SF_6 and the heat of sublimation of S we calculate for the dissociation of $SF_6(g)$ into its elements

$$SF_6(g)=S(g)+6F(g)-(14.27+3D_{F_2}) \quad (2)$$

where D_{F_2} is the heat of dissociation $F_2(g)=2F(g)$. All of the above thermal quantities, where temperature dependent, are estimated at 291°K. It is assumed, very approximately, that the energy of breaking one S−F bond is one-sixth of the value of (2),

$$SF_6(g)=SF_5(g)+F-(14.27+3D_{F_2})/6 \text{ ev} \quad (3)$$

If it is assumed that the energy of the process

$$SF_6^+(g)=SF_5^+(g)+F(g) \quad (4)$$

has the same value as in (3), we obtain the ionization energy

$$SF_6(g)=SF_6^+(g)+e-(13.12+(EA_F-D_{F_2}/2)) \text{ ev}. \quad (5)$$

The quantity $(EA_F-D_{F_2}/2)$ may be obtained from a Born-Haber cycle which involves theoretically computed crystal energies and other thermochemical data. In fact the most reliable value for EA_F was obtained in this way,[6] using experimental values of D_{F_2}. However, the experimental value of the latter has been the subject of much controversy recently,[7] and a reliable value cannot be assumed at present, with consequent uncertainty in EA_F. But we need only the difference of these values. Using the data of reference 6, corrected to 291°K where necessary, we computed $(EA_F-D_{F_2}/2)$ from the data on LiF, NaF, KF, RbF, and CsF with the results, respectively, 2.87, 2.93, 2.89, 2.90, and 2.82. With an unweighted average value of $(EA_F-D_{F_2}/2)=2.88$ ev, Eq. (5) gives an estimated ionization potential of 16.0 ev for SF_6. In spite of the uncertainties in the thermochemical data and in the approximations in (3) and (4), it appears that the ionization potential is a little higher than the dissociation energy of SF_6 into SF_5^+ and F^-.

We investigated the possibility that some of the observed transitions might belong to a Rydberg series which converged to an ionization potential at about 16 ev. It was not possible to find any two band centers which fitted convincingly into a series.

It is expected from selection rules for electronic transitions with octahedral symmetry that allowed transitions will occur to excited states with F_{1u} symmetry. While the lowest excited state with this symmetry is expected to be an antibonding molecular state, the possibility may be considered also that the electron can be excited to a Rydberg (united atom) state of about the same energy and symmetry. The excited electron in this case may be considered qualitatively to be in a $4p$ orbital, similar to $4p$ of sulfur.

We have estimated by the method of Slater[8] the approximate energy of a $4p$ term of *S* based on an ion configuration sp^2d^2, and find a value of about 3 ev. Assuming that the S atom has this configuration in SF_6^+ at the estimated ionization potential 16 ev, the transition to the Rydberg state should occur at about 13 ev or 955A. These qualitative considerations will not permit a definite assignment, but the relative narrowness and lower transition probability suggest that the *second* (936A) band may possibly arise from a transition to this Rydberg state.

[4] V. H. Dibeler and F. L. Mohler, J. Research Natl. Bur. Standards **40**, 25 (1948).

[5] F. R. Bichowsky and F. D. Rossini, *Thermochemistry of Chemical Substances* (Reinhold Publishing Corporation, New York, 1936).

[6] J. E. Mayer and L. Helmholz, Z. Physik **75**, 19 (1932).

[7] H. Schmitz and H. J. Schumacher, Z. Naturforschung **2a**, 359 (1947); E. Wicke, Z. Elektrochem. **53**, 212 (1949); A. D. Caunt and R. F. Barrow, Nature **164**, 753 (1949); N. W. Nathans, J. Chem. Physics **18**, 1122 (1950).

[8] J. C. Slater, Phys. Rev. **36**, 57 (1930).

The Recombination of Methyl Radicals

D. M. MILLER* AND E. W. R. STEACIE
Division of Chemistry, National Research Council, Ottawa, Canada

(Received September 19, 1950)

An investigation has been made of the rate at room temperature of recombination of methyl radicals by photolysing mercury dimethyl in the presence of nitric oxide and comparing the rates of the reactions

$$CH_3+CH_3\rightarrow C_2H_6 \quad (1)$$

and

$$CH_3+NO\rightarrow CH_3NO. \quad (2)$$

It is concluded that $k_1^{\frac{1}{2}}/k_2$ is approximately equal to 3×10^{-5}. If Forsyth's value for k_2 is accepted, this leads to a collision yield for methyl radical recombination of 4.4×10^{-5}.

INTRODUCTION

IN nearly all systems involving methyl radicals ethane is produced as a result of the recombination

$$2CH_3\rightarrow C_2H_6.$$

A knowledge of the rate constant k_E for this reaction would provide a means whereby the radical concentration could be found from a measurement of the rate of formation of ethane since

$$R_{C_2H_6}=k_E[CH_3]^2.$$

However, there appears to be little information concerning the rate of this reaction.

Evans and Szwarc[1] on theoretical grounds favor a collision efficiency in the neighborhood of unity while other estimates are as low as 10^{-6}.[2]

To make a more direct measurement of the collision efficiency it is necessary to have a method by which the radical concentration can be determined. The low concentration of the radicals eliminates the possibility of measurement by any physical means so a chemical method must be sought. The main requirement is a reaction of methyl radicals, the collision yield of which is known, so that the rate of recombination can be found by comparison with this reaction. Probably the most satisfactory reaction for this purpose is that of methyl radicals with nitric oxide. This reaction has been studied by Forsyth[3] using a Paneth mirror technique. A small amount of nitric oxide was introduced into the gas stream just below the furnace and the change in the rate of mirror removal by the radicals noted. From his results, Forsyth calculated that one in 73,000 collisions between methyl radicals and nitric oxide results in reaction at room temperature. This reaction was employed by Marcus and Steacie[4] who obtained the collision efficiency for the recombination in the following way:

Mercury dimethyl was decomposed photo-chemically to provide a source of methyl radicals, the photolysis being carried out in the presence of nitric oxide so that the methyl radicals were removed by the reactions

$$CH_3+CH_3\rightarrow C_2H_6 \quad (1)$$

and

$$CH_3+NO\rightarrow \text{Products}. \quad (2)$$

The rate with which nitric oxide was consumed is

$$-R_{NO}=k_N[NO][CH_3]$$

and the rate with which ethane was formed is

$$R_{C_2H_6}=k_E[CH_3]^2.$$

From these expressions,

$$\frac{k_E^{\frac{1}{2}}}{k_N}=\frac{R_{C_2H_6}^{\frac{1}{2}}[NO]}{-R_{NO}}.$$

Since k_N is known from Forsyth's work, k_E can be calculated provided that $R_{C_2H_6}$, $-R_{NO}$ and $[NO]$ are known. From k_E the collision yield C_E of reaction (1) can then be calculated.

Marcus and Steacie obtained a value of 5×10^{-3} as an upper limit for C_E. However, their work was only exploratory and no attempt was made to replenish the nitric oxide as it was consumed. In the present work, a refinement of this method, nitric oxide was introduced into the reaction mixture at a continuous rate allowing steady-state conditions to be approximately attained. An improved analytical system was used and the gases were circulated to ensure better mixing and sampling.

A number of workers have investigated the photolysis of mercury dimethyl.[2] Gomer and Noyes[5] worked over a wide range of temperature, pressure, and light intensity, and proposed the following mechanism

$$Hg(CH_3)_2\rightarrow HgCH_3+CH_3\rightarrow Hg+2CH_3 \quad (3)$$

$$CH_3+CH_3\rightarrow C_2H_6 \quad (1)$$

$$CH_3+Hg(CH_3)_2\rightarrow A \quad (4)$$

$$CH_3+A\rightarrow C_2H_6+Hg+2CH_3 \quad (5)$$

* National Research Council of Canada Postdoctorate Fellow.

[1] M. G. Evans and M. Szwarc, Trans. Faraday Soc. **45**, 940 (1949).

[2] For a review of the earlier work, see E. W. R. Steacie, *Atomic and Free Radical Reactions* (Reinhold Publishing Corporation, New York, 1946).

[3] J. S. A. Forsyth, Trans. Faraday Soc. **37**, 312 (1941).

[4] R. A. Marcus and E. W. R. Steacie, Z. Naturforsch. **4a**, 332 (1949).

[5] R. Gomer and W. A. Noyes, J. Am. Chem. Soc. **71**, 3390 (1949).

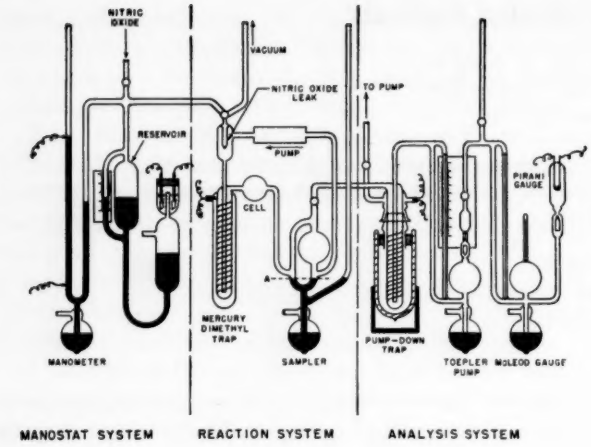

FIG. 1.

or $\rightarrow C_2H_6+HgCH_3+CH_3$

or $\rightarrow C_2H_6+Hg(CH_3)_2$

$$CH_3+Hg(CH_3)_2\rightarrow CH_4+CH_2HgCH_3 \qquad (6)$$

$$CH_3+CH_2HgCH_3\rightarrow C_2H_6HgCH_3 \qquad (7)$$

where A is an intermediate complex. From plots of $R_{C_2H_6}/R_{CH_4}$ *versus* R_{CH_4} they obtain an activation energy of 9–10 kcal for reaction (6) and an activation energy for ethane production by reaction (5) of about the same order as (1). However, they found that the pre-exponential factor for (5) was so low that chain reactions were negligible.

At room temperature then, the important steps in the photolysis of mercury dimethyl appear to be

$$(CH_3)_2Hg\rightarrow HgCH_3+CH_3$$
$$HgCH_3\rightarrow Hg+CH_3$$
$$CH_3+CH_3\rightarrow C_2H_6.$$

The recombination to produce ethane would be the fate of at least 95% of the methyl radicals in the absence of nitric oxide, while in the presence of nitric oxide methyl radicals would also disappear by the reaction

$$CH_3+NO\rightarrow CH_2=NOH$$

the formaldoxime thus formed being stable at the low temperature.[6,7]

EXPERIMENTAL

The apparatus is shown diagrammatically in Fig. 1. The nitric oxide was contained in a manostat similar to that employed by Taylor,[8] and was introduced into the reaction system at a continuous rate through a fine leak. The amount of nitric oxide consumed during a run was determined by measuring the volume displaced by mercury in the manostat reservoir.

The mercury dimethyl was contained in a trap similar to the Ward still[9] and its vapor pressure maintained at 4.5 mm during a run.

A cylindrical quartz cell of 5 cm length and 5 cm diameter was used. The gas was circulated through the reaction system with the mercury in the sampler at A. The system could be evacuated by lowering the mercury or a sample taken by raising the mercury above the inlet and outlet tubes and opening the stopcock at the top of the sampler. Since mercury dimethyl attacks ordinary hydrocarbon stopcock grease a silicone—10 percent silica type grease[10] was used on this stopcock.

For experiments with a total pressure of 0.45 cm an ordinary single stage diffusion pump was used to circulate the gas. For high pressures a Puddington pump[11] was employed.

Separation of the gases in the sample was effected by means of the pump-down trap. A temperature of $-219°$ was obtained by pumping on liquid nitrogen contained in a Dewar flask surrounding the trap. Higher temperatures were obtained by replacing the Dewar flask with an ordinary jacket and operating as a Ward still.

The ultraviolet radiation was provided by a Hanovia S-500 medium pressure mercury lamp. The light was not filtered nor was any collimation attempted, although for some experiments the light intensity was reduced by introducing a wire screen between the lamp and the cell.

Materials

The mercury dimethyl was synthesized by Dr. L. C. Leitch. It was stored over Drierite in a bulb separated from the rest of the system by a mercury cutoff.

Nitric oxide was prepared by the reduction of the nitrite ion according to the equation

$$2NO_2^-+4H^++2I^-\rightarrow 2NO+I_2+2H_2O.$$

It was purified by passage through two towers, the first containing beads moistened with concentrated sulfuric acid and the second containing beads moistened by 50% KOH solution. It was then passed through a trap cooled by a dry-ice acetone paste and twice distilled from the temperature of liquid oxygen to that of liquid nitrogen.

Tank nitrogen was freed of its oxygen by passage over hot copper turnings.

The acetone was obtained from the Baker Chemical Company and met the ACS standard of purity.

Procedure

An excess of mercury dimethyl was condensed in the mercury dimethyl trap at $-125°$ and the noncon-

[6] H. W. Thompson and M. Meissner, Nature **139**, 1018 (1937).
[7] H. A. Taylor and H. Bender, J. Chem. Phys. **9**, 761 (1941).
[8] H. S. Taylor and C. O. Strother, J. Am. Chem. Soc. **56**, 586 (1934).
[9] E. C. Ward, Ind. Eng. Chem., Anal. Ed. **10**, 169 (1938).
[10] J. R. Farnand and I. E. Puddington, Can. J. Research, **F.27**, 318 (1949).
[11] I. E. Puddington, Ind. Eng. Chem., Anal. Ed. **17**, 592 (1945).

densibles pumped off. With the mercury in the sampler at A the temperature of the trap was raised to −19° and held there throughout the run. Nitrogen was also introduced in some experiments.

The manostat was adjusted to give the correct flow rate of nitric oxide into the system. Several preliminary runs were usually necessary to determine this flow rate.

The gases were circulated for several minutes before the run was started to allow them to mix. The stopcock between the leak and the manostat was opened and time allowed for the nitric oxide concentration to reach approximately its steady-state value, and the run started by removing the lamp shutter. When the required time had elapsed a sample was taken and passed over into the analysis system.

With the pump-down trap at −219° the noncondensible fraction, consisting mainly of N_2, CH_4, and H_2 was separated. The temperature was then raised to −135° and a fraction containing the ethane and nitric oxide was removed. The amount of this fraction was measured in the gas burette and a portion of it transferred to the McLeod-Pirani system for analysis.

Analysis of the Nitric Oxide-Ethane Fraction

The Pirani gauge was calibrated against the McLeod gauge over a considerable range of pressures for pure nitric oxide, pure ethane, and known mixtures. It was found that the composition of the mixture could be determined at any pressure by linear interpolation between the values for pure ethane and pure nitric oxide. The method was checked against mass spectrometer analyses. The error from this source produced in the ratio $k_E^{\frac{1}{2}}/k_N$ was less than 5 percent provided that the percent of ethane in the C_2H_6-NO fraction lay between 15 and 65.

RESULTS

The first results were obtained using mercury dimethyl as a radical source. No inert gas was present and the total pressure was 4.5 mm. These results are listed in Table I.

If the mechanism assumed for this system is correct, the ratio $k_E^{\frac{1}{2}}/k_N$ should be a constant for any concentration of either methyl radicals or nitric oxide. The data in Table I have been listed in order of increasing nitric oxide concentration to show the effect of this increase on the ratio. As the concentration is increased from 3.4×10^{-9} to 7.6×10^{-9} M cc^{-1} no regular change in the ratio can be detected. Beyond this range, however, the ratio rises considerably. This may be due to the nitric oxide concentration not reacing a steady state, or to errors in the assumed mechanism such as

1. Ethane formation may also take place through a nonradical mechanism of the type

$$(CH_3)_2Hg \rightarrow C_2H_6 + Hg.$$

Although the amount of ethane formed by this means is insignificant in the absence of nitric oxide, it assumes a greater importance as ethane production by a free radical mechanism is reduced.

2. The recombination may occur partly or entirely on the walls giving an order between one and two for the ethane formation. If this were true, an increase in pressure would reduce the rate of diffusion of the radicals to the wall and thus reduce the ratio.

Several experiments were performed in which the over-all pressure was increased by the addition of nitrogen. The results for total pressures of 5 and 10 cm are given in Table II. The average values of the ratio obtained for the three different pressures (excluding experiments 33, 37, and 81) are

Pressure	$k_E^{\frac{1}{2}}/k_N$
0.45 cm	2.9×10^{-5} M$^{\frac{1}{2}}$ cc$^{-\frac{1}{2}}$ sec$^{\frac{1}{2}}$
5.0	2.9×10^{-5}
10.0	3.3×10^{-5}

Thus there appears to be no change in the order of recombination between pressures of 0.45 and 10.0 cm.

The rate of light absorption for each experiment has been calculated as the rate of ethane formation plus half the rate of nitric oxide disappearance. This is based on the assumption that the quantum yield for the production of ethane is unity. The light absorption is given in the last column of Tables I and II, headed I_a. Fivefold variation in I_a can be seen to produce no significant change in the ratio.

TABLE I.—Values of $k_E^{\frac{1}{2}}/k_N$ with mercury dimethyl as a radical source—pressure 4.5 mm.

Experiment number	$-R_{NO}$ M cc^{-1} sec^{-1}	$R_{C_2H_6}$ M cc^{-1} sec^{-1}	NO M cc^{-1}	$k_E^{\frac{1}{2}}/k_N$ M$^{\frac{1}{2}}$ cc$^{-\frac{1}{2}}$ sec$^{\frac{1}{2}}$	I_a quanta cc^{-1} sec^{-1}
43	3.72×10^{-10}	6.75×10^{-12}	1.85×10^{-9}	1.3×10^{-5}	1.2×10^{14}
28	3.87	14.0	3.42	3.3	1.3
57	8.25	55.2	3.56	3.2	2.6
30	3.87	13.9	4.04	3.9	1.3
46	3.72	5.5	4.24	2.7	1.2
58	8.25	20.4	4.65	2.5	2.6
44	3.72	2.7	5.24	2.3	1.2
32	3.87	4.4	5.75	3.1	1.2
31	3.87	4.1	6.40	3.4	1.2
59	8.25	10.5	7.55	3.0	2.6
37	3.87	4.2	10.66	5.7	1.2
33	3.87	2.6	24.6	10.3	1.2

TABLE II. Values of $k_E^{\frac{1}{2}}/k_N$ found with mercury dimethyl as a radical source and added nitrogen.

Experiment number	$-R_{NO}$ M cc^{-1} sec^{-1}	$R_{C_2H_6}$ M cc^{-1} sec^{-1}	NO M cc^{-1}	$k_E^{\frac{1}{2}}/k_N$ M$^{\frac{1}{2}}$ cc$^{-\frac{1}{2}}$ sec$^{\frac{1}{2}}$	I_a quanta cc^{-1} sec^{-1}
		Mercury dimethyl pressure—0.45 cm Temperature—300°A Total pressure—5.0 cm			
75	12.0×10^{-10}	75.6×10^{-12}	3.6×10^{-9}	2.6×10^{-5}	4.1×10^{14}
73	14.4	81.0	4.4	2.8	4.9
74	12.0	28.5	5.6	2.5	3.8
76	12.0	38.8	5.7	2.9	3.9
77	11.8	19.4	7.2	2.7	3.7
78	12.3	20.3	10.7	3.9	3.9
		Total pressure—10.0 cm			
87	14.9×10^{-10}	71.3×10^{-12}	6.4×10^{-9}	3.6×10^{-5}	5.0×10^{14}
86	13.0	110	6.5	5.3	4.6
90	14.0	45.0	6.6	3.1	4.5
82	17.5	52.5	6.7	2.6	5.6
85	15.0	36.8	7.5	3.0	4.8
88	14.9	71.3	6.4	3.6	5.0
83	18.1	41.0	8.0	2.8	5.8
84	16.8	37.4	8.6	3.1	5.3
92	14.8	14.2	9.0	2.3	4.7
80	17.1	66.0	9.7	4.2	5.6
91	15.2	21.0	10.1	3.1	4.7
81	18.4	87.5	15.2	7.0	6.1

The total absorption of light in the cell was measured by means of a Beckman spectrophotometer and found to be 20 percent in the 2537A region.

The high values of the ratio in experiments 33, 37, and 81 probably result from a delay in reaching a steady nitric oxide concentration. Excluding these experiments, the average for $k_E^{\frac{1}{2}}/k_N$ is 3.1×10^{-5} M$^{\frac{1}{2}}$ cc$^{-\frac{1}{2}}$ sec$^{\frac{1}{2}}$. From Forsyth's value of 1.4×10^{-5} for the collision efficiency of the nitric oxide-methyl radical reaction and the collision number 2.2×10^{14} cc M^{-1} sec^{-1} calculated from kinetic theory,

$$k_N = 1.4\times10^{-5}\times2.2\times10^{14} = 3.1\times10^{9} \text{ cc M}^{-1}\text{ sec}^{-1}$$

and

$$k_E = (3.1\times10^{9}\times3.1\times10^{-3})^2 = 9.2\times10^{9} \text{ cc M}^{-1}\text{ sec}^{-1}.$$

The collision number for the methyl radical recombination, that is, the number of collisions between radicals, is 2.1×10^{14} cc M^{-1} sec^{-1} and the collision yield

$$C_E = \frac{9.2\times10^{9}}{2.1\times10^{14}} = 4.4\times10^{-5}.$$

As a further check on the method, three experiments were made in which acetone was substituted for mercury dimethyl as a radical source. No inert gas was added and a pressure of 10 cm of acetone was used. The noncondensible fraction, consisting mainly of CO, was difficult to separate entirely from the ethane-nitric oxide fraction, especially in the presence of such large amounts of acetone. It was, therefore, necessary to revert to the mass spectrometer for analysis of the ethane-nitric oxide fraction. The results obtained from these experiments are given in Table III along with two experiments in which no nitric oxide was present. An analysis for methane was made in experiments 96 and 98, and in both cases less than 5 percent of the noncondensible fraction was found to be methane.

A review of the available information on the photolysis of acetone has been made by Noyes and Dorfman.[12] They conclude that the mechanism for the acetone photolysis at room temperature and intensities such that methane production is low, is

$$\begin{aligned} CH_3COCH_3 + h\nu &\rightarrow CH_3 + COCH_3 \\ CH_3 + COCH_3 &\rightarrow CH_3COCH_3 \\ COCH_3 &\rightarrow CO + CH_3 \\ 2COCH_3 &\rightarrow (COCH_3)_2 \\ 2CH_3 &\rightarrow C_2H_6. \end{aligned}$$

The introduction of nitric oxide results in two additional reactions

$$\begin{aligned} CH_3CO + NO &\rightarrow \text{products} \\ CH_3 + NO &\rightarrow \text{products}. \end{aligned}$$

Despite the fact that this system is complicated by the presence of the stable acetyl radical, the results obtained are the same to within 20 percent (see Table III) as those obtained using mercury dimethyl.

DISCUSSION

The technique involved in the present investigation possesses the great advantage of relative simplicity of interpretation. It is, however, difficult to carry out accurately, and is probably not very suitable for further refinement. We feel, therefore that the results are re-

[12] W. A. Noyes and L. M. Dorfman, J. Chem. Phys. **16**, 788 (1948).

TABLE III. The photolysis of acetone as a source of radicals.

Experiment number	R_{CO} M cc^{-1} sec^{-1}	$R_{C_2H_6}$ M cc^{-1} sec^{-1}	$-R_{NO}$ M cc^{-1} sec^{-1}	NO M cc^{-1}	$k_E^{\frac{1}{2}}/k_N$ M$^{\frac{1}{2}}$ cc$^{-\frac{1}{2}}$ sec$^{\frac{1}{2}}$
93	3.8×10^{-10}	5.4×10^{-10}	...	...	...
96	4.1	5.1	...	...	...
98	2.76	0.58	15.7×10^{-10}	8.7×10^{-9}	4.2×10^{-5}
99	3.18	0.71	13.2	3.8	2.4
100	2.74	0.94	14.9	6.6	4.3

liable as to order of magnitude, but that the final result may be in error by a factor of 4 or 5. This, however, is not serious, since the main interest is the order of magnitude of the collision efficiency, and since past estimates have been so widely at variance. The value of the ratio $k_E^{\frac{1}{2}}/k_N$ should be considered to be an upper limit since it is possible that ethane may arise by sources other than recombination. However, the relatively close agreement between the results with acetone and those with mercury dimethyl suggests that this is not serious.

In order to obtain the collision efficiency of the recombination of methyl radicals from the ratio $k_E^{\frac{1}{2}}/k_N$, it is necessary to employ Forsyth's value for the collision yield of the reaction of CH_3 with NO. Since the experimental ratio involves $k_E^{\frac{1}{2}}$, any error in C_N, will be squared in C_E. The greatest uncertainty in C_E probably arises from this source, and it is our intention to do further work on the reaction of methyl radicals with nitric oxide. In the meantime, it seems unlikely that Forsyth's estimate is greatly in error, and we believe that our estimate of 4.4×10^{-5} for C_E is reliable to within one power of ten.

Since this work was completed two brief reports of other work on the rate of recombination of methyl radicals have appeared.

Lucas and Rice[13] have reported experiments on the acetaldehyde photolysis using intermittent light, and also varying distances from the illuminated region to the wall. Their results lead to the conclusion that the chain breaking step in the acetaldehyde photolysis has a collision efficiency of unity. However, the acetaldehyde photolysis is complex; its interpretation is difficult, and it is by no means established that the step concerned is the recombination of methyls. The results may, therefore, have no direct bearing on the present work, but it is significant that a recombination reaction appears to occur at every collision.

Gomer[14] investigated the photolysis of mercury dimethyl by a sector method, and concluded that the rate constant for the recombination of methyls is 7×10^{13} cc M^{-1} sec^{-1} at 175°C. This corresponds to a collision efficiency of the order of unity. The technique of the sector method is relatively simple, but the interpretation of the results is a matter of some difficulty and is very dependent on questions of mechanism. We feel that the work is reliable, and we are unable to offer an explanation of the discrepancy between his work and our own. It is possible that the difference could be explained by a large error (*ca* a factor of 100) in Forsyth's value for CH_3+NO, but we feel that this is unlikely. It is hoped that future work may settle the cause of the discrepancy.

The possibility of wall effects being of importance in our work requires some consideration. The fact that the reaction is of the second order does not preclude a wall reaction. However, the absence of any effect of foreign gas pressure makes wall effects unlikely. In any case, if wall effects are of importance, the collision efficiency calculated for the gas reaction will merely become an upper limit. Wall effects cannot offer an explanation of the discrepancy between our results and those of Gomer, since if the collision efficiency for the gas reaction were unity the wall reaction could not possibly be of importance.

If we accept the value of 4.4×10^{-5} for the collision efficiency of the recombination of methyls, there remains the question whether there is an activation energy for the reaction. The extreme possibilities are $E=0$ and a steric factor of 4.4×10^{-5}, and $E=6.0$ kcal and a steric factor of unity. It seems unlikely that the activation energy is appreciable, but a value of 1–2 kcal for E is by no means excluded.

It has recently been found[15] for a series of reactions of the type

$$CH_3+RH\rightarrow CH_4+R$$

that the steric factors are of the order of $5\times10^{-4}\ P_E^{\frac{1}{2}}$, where P_E is the steric factor for the methyl radical recombination. If this is *ca* 4×10^{-5}, then the steric factors of the aforementioned series of reactions are about 3×10^{-6}.

[13] V. E. Lucas and O. K. Rice, J. Chem. Phys. **18**, 993 (1950).
[14] R. Gomer, J. Chem. Phys. **18**, 998 (1950).
[15] A. F. Trotman-Dickenson and E. W. R. Steacie, J. Am. Chem. Soc. **72**, 2310 (1950); J. Chem. Phys. (to be published).

The Relative Rates of Reaction of Hydrogen and Tritium Hydride with Chlorine*

W. M. JONES
Los Alamos Scientific Laboratory of the University of California, Los Alamos, New Mexico

(Received August 14, 1950)

The ratio of the specific rate constant for H_2 to that for HT in the photo-chemical reaction with chlorine has been determined at four temperatures and is represented by $R=(1.35\pm0.03)\exp\{(552\pm7)/RT\}$ to within about 0.3 percent. The ratio is found to be the same when the reaction is initiated by the tritium β-particles. The data are considered from the viewpoint of the theory of absolute reaction rates.

INTRODUCTION

THE relative rates of reaction of species differing only in isotopic constitution are of considerable practical interest, particularly in connection with isotope enrichment, and of theoretical interest as well, in the testing of theories of reaction kinetics. The relatively large differences in kinetic behavior exhibited by the isotopes of hydrogen should make relative rate studies involving tritium a worthwhile supplement to corresponding data obtained with deuterium.

Rollefson[1] has measured the relative rates of photochemical reaction of hydrogen and deuterium with chlorine at 0°C and 32°C by comparing the rate of each isotope with that of carbon monoxide. Farkas and Farkas[2] studied the photo-chemical reaction of chlorine with a mixture of hydrogen and deuterium in which the latter was present principally as deuterium hydride. In the present work the relative rates of reaction of hydrogen and tritium hydride were determined.

The chain mechanism of Nernst is generally accepted for the reaction between hydrogen and chlorine, in which the principal steps of interest here are (1) and (1′):†

$$\mathrm{H_2+Cl}\xrightarrow{k_1}\mathrm{HCl+H} \qquad (1)$$

$$\mathrm{H+Cl_2}\rightarrow\mathrm{HCl+Cl}. \qquad (1')$$

Step (1) is the rate determining step, involving an activation energy of about 6000 cal, while (1′) is much faster.

In the HT reaction step (1) has two counterparts:

$$\mathrm{HT+Cl}\xrightarrow{k_{2a}}\mathrm{H+TCl} \qquad (2a)$$

$$\mathrm{HT+Cl}\xrightarrow{k_{2b}}\mathrm{T+HCl}. \qquad (2b)$$

In the present work the relative rates of (1) and the sum of (2a) and (2b) were compared; that is, $R=k_1/k_2$ was determined, in which $k_2=k_{2a}+k_{2b}$.

For the case of measurement of the relative rates in the same reaction vessel we may write from Eq. (1) and Eqs. (2a) and (2b):

$$\frac{-d(\mathrm{H_2})}{dt}=k_1(\mathrm{Cl})(\mathrm{H_2}) \quad \text{and} \quad \frac{-d(\mathrm{HT})}{dt}=k_2(\mathrm{Cl})(\mathrm{HT})$$

whence

$$R=k_1/k_2=\log[(\mathrm{H_2})_i/(\mathrm{H_2})_f]/\log[(\mathrm{HT})_i/(\mathrm{HT})_f] \qquad (3)$$

in which i and f refer to the initial conditions and to the final conditions after the reaction has been carried to the desired degree of completion. It is thus seen that the relative rates are independent of the chain carrier concentrations and thus of the small and variable amounts of impurities which, by introducing chain breaking steps, make reproducibility very difficult in absolute rate measurements. Such impurities are normally present in such small amounts as to react with but a negligible fraction of the hydrogen.

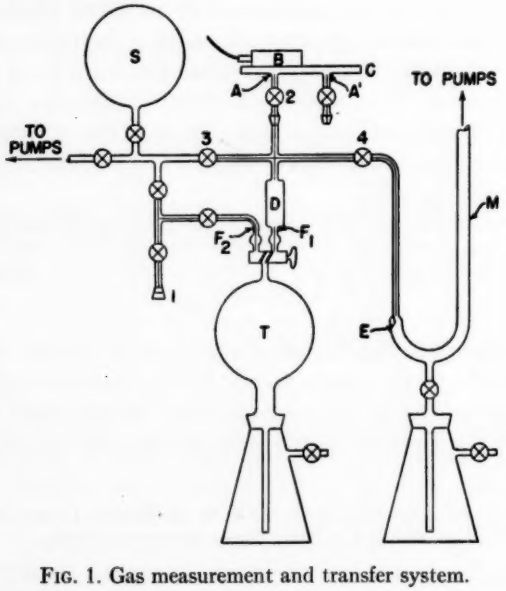

FIG. 1. Gas measurement and transfer system.

EXPERIMENTAL

The experimental method may be understood from the discussion below with reference to Fig. 1.

* This paper is based on work performed under University of California Contract with the AEC.

[1] G. K. Rollefson, J. Chem. Phys. **2**, 144 (1934).

[2] L. Farkas and A. Farkas, Naturwiss. **22**, 218 (1934).

† For a general discussion and survey of this reaction reference may be made to W. A. Noyes and P. A. Leighton, *The Photochemistry of Gases* (Reinhold Publishing Corporation, New York, 1941).

A mixture of hydrogen and tritium, sufficiently dilute in the latter so as to insure its presence almost entirely as HT, is allowed to react with chlorine, either under the influence of light or in the dark under the influence of the tritium β-radiation. The hydrogen is determined by pressure measurements, and the tritium is determined by the counting of the x-rays emitted from a small cell, provided with a thin metal window and containing some of the hydrogen-tritium hydride gas. The pressure and counting data, determined before and after reaction, are used, along with certain corrections mentioned later, to compute R from (3). Details are discussed below.

Initially, mercury filled the Toepler pump T of one-liter volume and extended up to the fiducial mark F_1 on a section of capillary tubing. Counting cell A', identical to the fixed cell A and used to monitor the behavior of the counting equipment over the time of experiment, was provided with a standard taper and was initially attached at joint 1. The system was brought to a high vacuum with a mercury diffusion pump, and a mixture of H_2-HT was admitted from bulb S so as to fill cells A and A' and volume D of about 100-cc capacity to the desired pressure. The mercury in the manometer M was brought up to a definite position E, defined by a teat of cobalt glass. Uniform temperature over the region containing gas was attained with a large fan. Temperatures were read at D and A with two mercury thermometers, graduated in 0.02°C intervals and calibrated against a standard platinum resistance thermometer. The pressure was read on the manometer M, constructed of 1-in. i.d. Trubore tubing, with a cathetometer, estimates of the meniscus positions being made to 0.001 cm. The valves to A and A' and the stopcock 3 were then closed, A' was transferred to its position on the counting block C, and the counting of A and A' with counter B was commenced. The cylindrical Pyrex reaction vessel was then attached at joint 1. The reactor was 55 mm o.d., had a volume of 200 cc, and was provided with a stopcock, separated from the main volume by a section of 1-mm capillary tubing so as to permit immersion in a bath. The reactor already contained the appropriate amount of chlorine, frozen down with liquid nitrogen. The gas bounded by 2, 3, F_1, and E was then transferred with T to the reactor. On the final transfer the mercury was raised to fiducial mark F_2. Knowledge of the volume between F_2 and the reactor stopcock allowed a correction for the gas not transferred to the reactor. The reactor was then transferred to the constant temperature medium. If the reaction was to be induced by light, time was allowed for temperature equilibrium to be attained before the reactor was exposed to the A-H6 mercury vapor lamp which was located at a suitable distance. The time for reaching temperature equilibrium was shortened by appropriate preliminary adjustment of the water bath when it was used as the constant temperature medium. Light passed through the surrounding bath and entered the reactor from the side. In some of the experiments the reactor was backed by a curved reflector of sheet aluminum in order to provide more uniform illumination. This had no apparent effect. The time of reaction varied from twenty minutes to several hours for the photo-chemical experiments. Times were longer for some of the β-particle-induced reactions. For a given value of R there is an optimum extent of reaction for which R is subject to minimum fractional error (see Appendix). For the present experiments it was desirable to carry the reaction to about 90 percent completion. Unfortunately the sensitivity of the reaction frequently did not allow this situation to be realized. After the reaction had progressed to what was estimated to be the proper extent, the reactor was removed from the bath, the chlorine and hydrogen chloride were frozen out with liquid nitrogen, and the unreacted hydrogen was transferred back into the volume bounded by 2, 3, F_1, and E. Meanwhile, the counting of the gas in A had been completed, the contents of A removed, and valve 2 closed. The pressure and temperature of the unreacted gas were determined, valve 2 was opened and inert H_2 was added until the gas had very nearly the same density as had prevailed in the measurement of the gas before reaction. This was done to eliminate the correction for different amounts of self-absorption in the counting of the gas before and after reaction. The gas was thoroughly mixed by alternate lowering and raising of the Toepler pump according to a schedule demonstrated to provide adequate mixing. When the system was at uniform temperature, with valve 2 open and with the mercury-gas interfaces at F_1 and at E, the pressure was measured. This measurement was made to verify that cancellation of the self-absorption corrections was assured and, in one case, to allow for such a correction. Valve 2 was then closed and the counting of A and A' was commenced. A correction, in addition to those already mentioned, must be made to the counting data of A to allow for the fact that after reaction A contains a different fraction of the total active gas than was the case before reaction. This correction is due to the different volumes involved, amounts to an average correction of 2.3 percent in R, and can be made with negligible uncertainty. It was also necessary to correct the pressure measurements for the HT and T_2 present, Corrections for the He^3 which grew from tritium decay subsequent to the preparation of the H_2-HT mixture were not needed. Correction was made to the counting data for the T_2 present, recognizing the twofold greater specific activity of T_2. For this calculation an approximate absolute value of the tritium content was needed, as well as the equilibrium constant for the equilibrium $H_2+T_2=2HT$. The gas composition will be mentioned later, and the equilibrium constant has the value 2.57.[3] It was estimated that the correction for the T_2 consumed in the reaction was negligible. It may be mentioned that the differing reaction rates cause

[3] W. M. Jones, J. Chem. Phys. 16, 1077 (1948).

the instantaneous distribution of H_2, T_2, and HT to differ from the equilibrium values. Errors could result if there were processes by which equilibration could be reached during the experiment. This does not seem very likely, however. In this connection Bonhoeffer and Harteck[4] have found that the ratio of orthohydrogen to parahydrogen is not altered toward the equilibrium value when gas enriched in parahydrogen is allowed to react partially with chlorine. Small corrections were made to both the pressure and counting data for the contents of the reactor stopcock, which did not undergo reaction. It was also assumed that half of the gas in the capillary section between the reactor stopcock and the main reactor volume behaved like the contents of the main reactor volume, while the remaining gas in the capillary did not react at all. This latter uncertainty amounts to about 0.07 percent in the final results and is much less than the over-all precision.

The pillbox-shaped sample cells A and A' were of brass and had $\frac{1}{8}$-in. bellows valves and standard taper joints. The cell volume was about 8 cc. The diameter of the cells was $1\frac{1}{2}$-in. and the cell end consisted of a network of $\frac{1}{8}$-in. holes so as to give about 50 percent transmission. A window of 0.0005-in. dural was waxed onto this grille with Apiezon W. The cells fitted snugly in holes in the bottom of a trough milled in the counting block C. The cells rested on a shoulder so that the cell windows were $\frac{1}{64}$-in. below the level of the trough, into which the counter B fitted closely. The counter B had a side window of 0.0005-in. dural, and its extreme positions in the trough, determined by stops, placed the counter and cell windows opposite each other. This arrangement provided for exact reproduction of geometry. The need for adjusting the gas density by addition of inert H_2 has been mentioned. Fortunately exact adjustment was not necessary, since the counting rate drops by only about 0.08 percent per mm. Hg pressure of inert H_2 added to an active mixture at 15 cm Hg pressure. The weak tritium β-particles cannot penetrate the dural windows, and the counting rate is due to the x-rays which are generated, mostly in the cell window, by the β-particles. The observed counting rate is only a small fraction of the disintegration rate in the sample cell, but counting rates of 200–400 counts per second are observed for cells with pressures of about 15 cm Hg of gas in which the tritium is present at 1–2 atomic percent. The counter was of the methane flow type and was operated in the proportional region. A scaling circuit was used in conjunction with the pulse amplifier. The counter was made by drilling out the center of a rectangular block and is a modification of that used by Prestwood and Wahl.[5] Small corrections for dead time losses and for background were made. The performance of the counting arrangement was quite satisfactory and was much superior to that of ordinary Geiger counters. In general the accuracy of the counting appeared to be governed by statistical uncertainties and usually corresponded to a probable error of about 0.2 percent. The same counter was used throughout the experiments described.

It was thought at the outset that the behavior of the counting apparatus should be monitored by the cell A', identical in construction to A and filled at the same time with active gas in order to present a similar spectrum to the counter. In practice corrections due to changes in the counting equipment over the time of an experiment were not warranted.

The experiments were performed at four different temperatures. At the lowest temperature the reactor was set in an unsilvered dewar vessel containing freely evaporating liquid ammonia. The temperature was measured during the reaction with a copper-constantan thermocouple fastened to the reactor and calibrated against the vapor pressure of ammonia.[6] The change in R occasioned by temperature variation due to different atmospheric pressures was negligible, and the temperature given in Table I is an average for the three experiments at this temperature. For the experiments at 0°C the same Dewar was used with an ice-water slush. Water was occasionally removed and ice added to maintain the temperature. In the experiments at 33.25°C and 70.75°C a water bath constant to 0.01°C was used. Temperatures were measured with a calibrated copper-constantan thermocouple. In the first series of experiments, the photo-chemical runs at 33.25°C, it was necessary to correct the values of R for the fact that the reacting gas was warmer than the bath due principally to the heat of reaction (Draper effect). The correction was about 1.5 percent in the worst case. The correction was made on the basis of a separate and similar experiment in which the pressure rise on illumination was observed on a manometer communicating with the reacting gas and protected from corrosion with pure H_2. This experiment allowed an evaluation of the heat transfer coefficient from the reacting mixture to the bath. The auxiliary experiment, since it measures the average temperature rise of the gas on illumination, may not properly estimate the correction insofar as the reaction does not occur uniformly throughout the reactor and insofar as the gas can maintain a temperature gradient. However, the agreement of the corrected values with the much slower β-particle induced runs at the same temperature probably indicates that the error in the correction is not serious. In all other runs the correction was small enough so that it did not have to be made. The warming up of the gas due to recombination of chlorine atoms (Budde effect) was found by the same method to be approximately that found by Kistiakowsky,[7] not more than about 0.1°C, and constitutes a negligible part of the correction.

[4] K. F. Bonhoeffer and P. Harteck, Z. physik. Chem. **4B**, 113 (1929).

[5] R. J. Prestwood and A. C. Wahl, J. Am. Chem. Soc. **71**, 3137 (1949).

[6] R. Overstreet and W. F. Giauque, J. Am. Chem. Soc. **59**, 254 (1937).

[7] G. B. Kistiakowsky, J. Am. Chem. Soc. **51**, 1395 (1929).

Tank chlorine of the Ohio Chemical and Manufacturing Company was used. The first batch of gas was dried by passage over a one-meter column of P_2O_5, followed by bulb to bulb distillation in which a middle fraction was retained. The gas was then stored in a one-liter bulb provided with a freezing-out leg. Apiezon *N* (and later Apiezon *L*) stopcock grease was used. Subsequently the drying step was eliminated and the material was stored as a solid in a small bulb surrounded by liquid nitrogen until it was to be used. A considerable amount of time was lost, especially at first, because of the unpredictable behavior of the reactants. Except for the experiments at 33.25°C, in which a possible dependence of *R* on excess chlorine was looked for, it was not considered necessary to measure the chlorine pressure accurately. The pressure was read with a mercury manometer in which the limb exposed to chlorine was protected to some extent by a layer of oil. Pressures could be estimated to 1 to 2 mm mercury. In the experiments where a more accurate pressure was thought desirable the rough pressure was used in conjunction with an air buffer and another manometer. Care was taken to have the chlorine at higher pressure than the air on opening the stopcock between the two gases. By closing the reactor stopcock soon after pressure equalization and by using capillary tubing and a ballast volume, air was kept from the reactor, and the mercury was not appreciably corroded except after considerable use.

In preparing the mixture of hydrogen and tritium hydride it was desirable to have the tritium content in the range one to two percent since this concentration represented a reasonable compromise between counting rate and T_2 content. Appropriate pressures of enriched gas (about 40 percent T) and pure hydrogen, measured with a cathetometer, were added to the one-liter bulb *S*. The enriched gas was freed from He^3, the tritium decay product, by taking the tritium up in uranium and removing the remaining gas. The enriched and inert gases were purified by the decomposition of uranium hydride. The uranium was finely divided and had previously been outgassed at temperatures well above those required for the decomposition of the hydride. In the case of the enriched gas care was taken to evolve the gas completely from the uranium in order to avoid discrimination effects. The interior of the storage bulb had been coated with a thin mirror of palladium obtained by vacuum evaporation of ringlets of palladium wire from a tungsten filament. The total weight of palladium was 15 milligrams. The mirror was oxidized to an amber color in the annealing furnace. The bulb was then evacuated, about 2 cm Hg pressure of hydrogen added, and a flame was then brushed over the bulb, instantly restoring the metal. A surface of this sort should rapidly promote equilibrium among the diatomic molecules.[8,9] As an added precaution the gas was allowed to stand for a week before use. No effects attributable to lack of attainment of equilibrium were observed over a time in which the tritium β-radiation should have established the equilibrium in the absence of a catalyst. The tritium content of the gas was obtained from the dilution data and the content of the enriched gas, which was originally based on gas density measurements. The calculated atomic percentages of tritium in the two preparations were found in this way

TABLE I.

T, °K	P_{Cl_2}, cm Hg at 25°C	P_{H_2+HT}, cm Hg at 25°C	Atomic fraction of T in initial gas	Time of reaction, hours	Fraction of H_2 consumed (approximate)		$R_{corrected}$
234.68	30.3	8.2	0.0148	8.7	0.75		4.40
	29.7	8.9	0.0148	9.8	0.90		4.43
	30.3	8.6	0.0148	10.0	0.89		4.43
						Av.	4.43±0.01
273.16	30.7	8.8	0.0148	6.9	0.84		3.73
	30.0	8.4	0.0148	4.8	0.79		3.67
	30.0	9.0	0.0148	8.0	0.97		3.72
	31.0	8.0	0.0194	116.	0.90		3.76*
	31.0	6.9	0.0194	14.1	0.84		3.71*
						Av.	3.72±0.02
306.41	15.56	7.1	0.0148	0.33	0.86		3.33
	30.10	9.0	0.0148	0.28	0.57		3.32
	30.93	9.5	0.0148	0.50	0.56		3.32
	29.09	9.3	0.0148	0.33	0.76		3.34
	31.2	7.3	0.0194	16.3	0.93		3.35*
	31.0	7.4	0.0194	16.3	0.94		3.35*
						Av.	3.33±0.01
343.91	26.5	5.4	0.0148	4.5	0.76		3.03*
	28.5	8.3	0.0148	8.0	0.85		3.05*
						Av.	3.04±0.01

[8] H. W. Melville and E. K. Rideal, Proc. Roy. Soc. **153A**, 89 (1935).
[9] Beeck, Smith, and Wheeler, Proc. Roy. Soc. **A177**, 62 (1940).

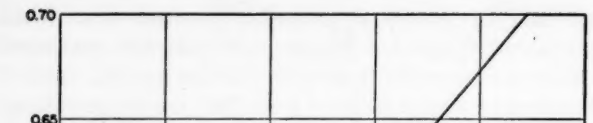

FIG. 2. Plot of experimental data.

to be 1.48 and 1.92 percent. As a check the composition of the second preparation relative to the first was determined by counting and was found to be 1.96 percent. The second sample was also analyzed on a mass spectrometer and found to contain 1.94 percent tritium. The error in R due to uncertainty in the tritium content should be less than 0.1 percent.

RESULTS AND DISCUSSION

The data are given in Table I. Columns two and three give the chlorine and total hydrogen pressures in the reactor at 25°C. Since the hydrogen pressure needs to be known accurately only in the measuring volume D, and since the ratio of this volume to the reactor volume is not known accurately, the pressures in column three are only approximate. Column seven gives the final values of R, including the several corrections mentioned. The uncertainty is the mean deviation.

It was thought that the value of R might depend slightly on the ratio of chlorine to the hydrogen chloride produced since these two species compete for atomic hydrogen in reaction (1′) and in the reverse of reaction (1). By altering concentrations and the extent of reaction in the experiments at 33.25°C the ratio of average chlorine to average hydrogen chloride concentrations was varied from 2.0 to 5.4. There was no apparent trend in R, and the effect is assumed absent at the other temperatures as well. For the conditions prevailing in these experiments, this result is in accord with the discussion of Potts and Rollefson,[10] who have studied the inhibitory effect of hydrogen chloride on the photo-chemical reaction between hydrogen and chlorine. The effect may well exist at low concentrations of chlorine. Indeed, the occurrence of the reverse of reaction (1) under such conditions has been suggested in connection with the relative rate experiments of Farkas and Farkas,[2] in which the consumption of hydrogen relative to that of deuterium was observed to fall as the reaction proceeded.

The starred values of R were obtained from experiments performed in the absence of light and initiated by the tritium β-particles. As can be seen there is no difference between these values of R and those obtained from the photochemical reactions.[11]

The values of $\log_{10}R$ are plotted against $1/T$ in Fig. 2, giving a linear relationship within experimental error. R is represented by $R=(1.35\pm0.03)\exp\{(552\pm7)/RT\}$. Thus the ratio of frequency factors is equal to the collision theory value of 1.38 within the experimental uncertainty, and the hydrogen reaction has the lower activation energy by 552 calories. The constants and their uncertainties, expressed as probable errors, were obtained by the method of least squares. The average deviation between the observed and computed values of R is about 0.3 percent.

We wish now to examine the data with a view to a possible difference in the activation energies of reactions (2a) and (2b), assuming that the Arrhenius equation may be applied. It is also assumed that (2a) and (2b) have equally effective collision numbers, and that the sum of these collision numbers is related to that for (1) by the collision theory.‡ If (2a) and (2b) have different activation energies, Q_{2a} and Q_{2b}, then a plot of $\log R$ against $1/T$ will not be a straight line, but would in the present case be concave down. If the experiments were performed at sufficiently low temperatures the slower reaction would be excluded, the apparent activation energy would approach the smaller of $Q_{2a}-Q_1$ and $Q_{2b}-Q_1$, while the apparent ratio of frequency factors would approach twice the value to be expected if Q_{2a} and Q_{2b} were equal. If the measurements were made at sufficiently high temperatures, the observed activation energy would approach $[(Q_{2a}-Q_1)+(Q_{2b}-Q_1)]/2$, and the frequency factor ratio would approach that expected for equal values of Q_{2a} and Q_{2b}. It may be seen from Fig. 2 that there is no evident tendency toward concavity. In addition the ratio of frequency factors obtained is not greater than the collision theory value. The data were treated from the viewpoint of the effect which a difference in Q_{2a} and Q_{2b} would have on the frequency factor ratio obtained. If it is granted that the experimental results exclude a frequency factor ratio greater than 1.39 (i.e., 0.01 unit greater than the collision theory value), then (2*a*) and (2*b*) cannot differ

[10] J. C. Potts and G. K. Rollefson, J. Am. Chem. Soc. **57**, 1027 (1935).

[11] S. C. Lind, *The Chemical Effects of Alpha Particles and Electrons* (The Chemical Catalogue Company, Inc., New York, 1928).

‡ From the thermodynamic point of view of absolute rate theory the effect of the symmetry number two for hydrogen which occurs in the rotational partition function is to increase the concentration of the critical complex for hydrogen, so giving a larger reaction rate. From a kinetic point of view the effect is due, in the present linear model, to the two equivalent ends of the hydrogen at which chlorine may react. In the case of HT the symmetry number is one, but this is counteracted by the existence of two reactions, (2a) and (2b), each of which contributes to the removal of HT.

in activation energies by more than about 100 calories. If Q_{2a} and Q_{2b} are indeed different by about this amount, the observed difference in activation energies would then be quite closely the average difference indicated above. It is evident that this procedure is not a very sensitive one for determining a difference in Q_{2a} and Q_{2b}, and that this difference could be much larger if the actual situation were not that assumed. The "tunneling" phenomenon of absolute reaction rate theory, by giving opposite curvature to the relationship between $\log R$ and $1/T$, might, for example, influence the frequency factor ratio in such a manner as to conceal a difference in Q_{2a} and Q_{2b}. A direct search for a possible difference in (2a) and (2b) would be very desirable. Professor Rollefson has suggested that this might be possible if the experiment were carried out in the presence of sufficient oxygen and the splitting of the radioactivity between hydrogen chloride and water determined. The experimental difficulties of preventing exchange in such an experiment might be rather considerable, however.

In considering the question of reaction rates from the viewpoint of the theory of absolute reaction rates there may, at least in principle, be a distribution of intermediate complexes through which the reaction is regarded as passing, and the total rate will then be obtained by integration. In practice such a procedure would present a considerable amount of work, which would probably not be justified in view of the approximate methods employed in the construction of potential energy surfaces. In addition the variety of effective intermediate configurations will be greatly restricted by the exponential dependence of the rate constants on the energy of activation. It is therefore ordinarily assumed that the reaction proceeds through a single intermediate state.[12]

The semi-empirical method of the theory of absolute reaction rates has been applied to hydrogen-halogen reactions by Wheeler, Topley, and Eyring[13] (WTE). The critical complex was assumed for simplicity to have a linear HHCl structure. For the reaction between tritium hydride and atomic chlorine two complexes, HTCl and THCl, are then to be expected, and these might differ considerably in properties. Indeed, if the force constants and molecular dimensions obtained by WTE[13] are assumed, we obtain the ratios of rate constants for reactions (1), (2a), and (2b), which are given in Table III. The ratios were calculated utilizing Eq. (28) of WTE and take account of the "tunneling" effect. The molecular constants needed are given in Table II. The moment of inertia of the linear complex is I, the stretching frequency is ν_+, the imaginary frequency corresponding to motion along the direction of decomposition is ν_-, and the bending frequency is ν_ϕ. Frequencies were computed from the force constants given by WTE. The small differences of the values for HHCl from those of WTE are negligible.

Comparison of Tables I and III shows that the calculated ratios of rate constants are substantially smaller than those observed. Table III shows that there is a very large difference in the theoretical rates of (2a) and (2b). In addition reaction (1) has, on this theory, a higher activation energy than reaction (2a), causing the theoretical temperature coefficient of k_1/k_2 to differ even in sign from the experimental results (the temperature dependence of the frequency factor ratio is not large for the frequencies of Table II in the temperature range considered.) In computing the values of Table III it was found that the ratios of frequency factors were substantially larger than 1.35, the experimental value.

It was previously noted by WTE themselves that their calculations did not satisfactorily predict the relative reaction rates of hydrogen and deuterium with chlorine. The relative rates were found experimentally to be 13.4 and 9.75 at 0°C and 32°C, whereas the theoretical ratios are 5.4 and 4.7. The value of 3.3 at 32°C given by WTE appears to involve some error. Thus the theoretical values are low, although the activation energy is of the correct sign. The experiments of Farkas and Farkas[2] are open to some question, because of the presence of some D_2 and because the ratio of rate constants dropped as the reaction proceeded. If, however, we take the relative rates at the start of the reaction as a measure of the relative rates of H_2 and HD, this has the value 3.8 at 30°C, and the computed value of 2.2 is again low. Steiner and Rideal[14] studied the reaction rates between deuterium and hydrogen chloride and between hydrogen and deuterium chloride at 900°K, in which the slow steps were inverse to the steps which have so far been considered. At the higher temperatures the fractional difference in the relative rates is smaller. It was also necessary to correct for the simultaneous occurrence of a bimolecular reaction. Nevertheless Steiner and Rideal found that the dis-

TABLE II. Properties of complexes.

System	I, Molecular weight and Angstrom units	ν_ϕ cm^{-1}	ν_+ cm^{-1}	ν_- cm^{-1}
H−H−Cl	8.62	491	2489	716 i
H−T−Cl	11.33	334	1488	711 i
T−H−Cl	21.43	460	2485	426 i

TABLE III. Theoretical relative rates.

T, °K	k_1/k_{2a}	k_1/k_{2b}	k_1/k_2
234.68	0.99	35.3	0.96
273.16	1.19	26.2	1.14
343.91	1.47	16.2	1.29

[12] J. L. Magee, J. Chem. Phys. 8, 677 (1940).
[13] A. Wheeler, B. Topley, and H. Eyring, J. Chem. Phys. 4, 178 (1936).
[14] H. Steiner and E. K. Rideal, Proc. Roy. Soc. **173A**, 503 (1939).

crepancy between experiment and the WTE theory was of the same sort as has been mentioned.

It is not easy to decide, granting the fundamental correctness of the absolute rate theory, whether the discrepancies which have been mentioned are due to the incorrectness of the model chosen or simply to the approximate nature of the calculations. It was suggested by WTE themselves that the disagreement of theory with the experimental absolute rate of reaction of hydrogen with chlorine and with the relative rates of hydrogen and deuterium could be attributed to too large frequencies computed for the intermediate state. The calculations lead to conclusions which seem to be even at qualitative variance with the most direct interpretation of the HT data, however, and the suggestion of Magee,[12] that the complex may be triangular, seems particularly inviting.

Magee investigated the effects of directed valence on reactions of this type, using the simple Heitler-London theory, and concluded that a triangular complex would be more stable than a linear complex, although the breakdown of the method at small separations made it difficult to draw conclusions regarding quantitative details. Magee also pointed out that the change from a linear to a triangular complex might bring the theory into better agreement with experiment. When a vibrational degree of freedom is replaced by one of rotation, the frequency factor is increased, while the zero point energy of the complex is decreased. Both of these effects increase the theoretical rate toward agreement with the experimental values for the absolute reaction rates of hydrogen with chlorine and bromine atoms (see reference 12, page 685).

The triangular complex, applied to the reactions of H_2, HT, and D_2 with chlorine, should also improve the computations on relative rates, both in regard to frequency factors and in regard to activation energies. The calculations on the linear model show that the ratios of the frequency factors, which are not very temperature dependent in the neighborhood of room temperature, are larger than the experimental values, while the computed differences in activation energies are too small. The latter circumstance is due to the too large zero point energies of the complexes. Replacing a vibrational degree of freedom by one of rotation, in passing from the linear to the triangular model, will increase the frequency factors for the H_2, HT, and D_2 reactions, but the effect will be greater for the heavy molecules (unless the frequency replaced is very low, in which case the mass dependence disappears), and the ratio of frequency factors will be lowered in the direction of the experimental values. The comments in this connection of Glasstone, Laidler, and Eyring at the top of page 226 of their book[15] do not appear to be correct. The removal of a vibrational frequency will increase the difference in activation energies and, in particular, acts to eliminate the anomalous temperature dependence of Table III. The effect on the activation energy, since this quantity occurs in an exponential, would be expected to override the decreased ratio of frequency factors so that the triangular model should increase, relatively, the rate of the light hydrogen isotope. A triangular model would also decrease the large difference in the rates of (2a) and (2b) given in Table III.

It must be admitted that the arguments reviewed above rest on a rather insecure foundation. A further theoretical study of the triangular complexes might be worthwhile.

Finally we wish to recall that in the relative rate calculations mentioned it has been assumed that the transmission coefficients are the same for the isotopic reactions. The considerations of Hirschfelder and Wigner[16] and of Hulbert and Hirschfelder[17] show that this may not be so. Unfortunately such calculations depend on a detailed knowledge of the potential energy surface in the neighborhood of the activated state which is not at present available.

I thank Professor G. K. Rollefson and Dr. T. W. Newton for their interest and suggestions.

APPENDIX

(*A*) Given two counting rates A_1 and A_2. It is desired to divide a total counting time T between the determination of A_1 and A_2 in such a way that A_1/A_2 is known with maximum fractional accuracy.

Let the times devoted to the determination of A_1 and A_2 be t_1 and $t_2=T-t_1$. Then the mean square fractional errors in A_1 and A_2 are $(A_1t_1)^{-1}$ and $A_2^{-1}(T-t_1)^{-1}$, and $(A_1t_1)^{-1}+A_2^{-1}(T-t_1)^{-1}$, the mean square fractional error in A_1/A_2, is at a minimum when

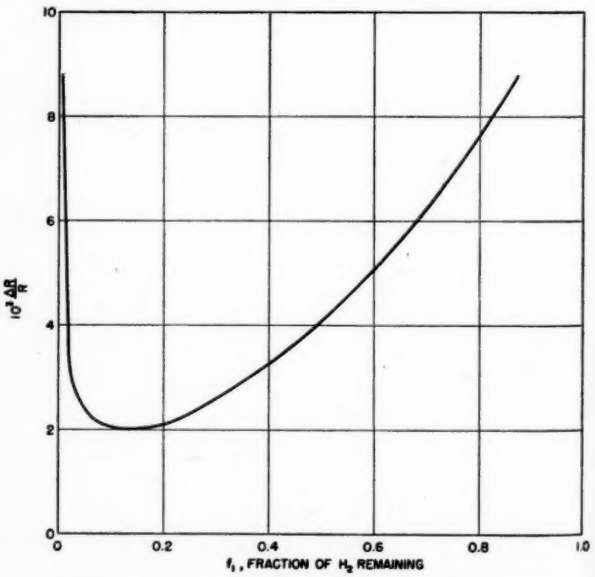

FIG. 3. Fractional error in R as function of extent to which reaction is carried.

[15] Glasstone, Laidler, and Eyring, *The Theory of Rate Processes* (McGraw-Hill Book Company, New York, 1941).

[16] J. O. Hirschfelder and E. Wigner, J. Chem. Phys. **7**, 616 (1939).

[17] H. M. Hulbert and J. O. Hirschfelder, J. Chem. Phys. **11**, 276 (1943).

$t_1/T-t_1=(A_2/A_1)^{\frac{1}{2}}$, i.e., the times spent are inversely proportional to the square roots of the counting rates.

(B) In Eq. (3) suppose that each pressure measurement is considered to be subject to a constant error, a, and that the fraction of the initial hydrogen remaining at the end of reaction is f_1. If $\alpha=\ln[(H_2)_i/(H_2)_f]$, then it follows from standard error theory that

$$\left(\frac{\Delta\alpha}{\alpha}\right)^2=\left(\frac{a}{P_1}\right)^2\cdot\left(1+\frac{1}{f_1^2}\right)\Big/\ln^2 f_1, \tag{1B}$$

in which $(\Delta\alpha/\alpha)^2$ is the mean square error in α and P_1 is the initial pressure. Incidentally, the fractional error in (1B) above is at a minimum for $f=0.32$.

In Eq. (3), suppose that the initial corrected counting rate due to HT is A_1 and that at the end of the experiment the activity has dropped to $A_2=f_2A_1$, where f_1 and f_2 are related by $R=\ln f_1/\ln f_2$. Then it may be shown that the mean square error in $\beta=\ln f_2$ is given by

$$\left(\frac{\Delta\beta}{\beta}\right)^2=\left(\frac{1}{A_1t_1}+\frac{1}{f_2A_1}\cdot\frac{1}{T-t_1}\right)\Big/\ln^2 f_2. \tag{2B}$$

If the time t_1 is chosen according to (A) for minimum fractional error in β, Eq. (2B) becomes

$$\left(\frac{\Delta\beta}{\beta}\right)^2=\frac{[1+f_2^{\frac{1}{2}}]^2}{f_2A_1T\ln^2 f_2}, \tag{3B}$$

which is at a minimum for $f_2=0.08$.

The mean square error in R is given by

$$(\Delta R/R)^2=(\Delta\alpha/\alpha)^2+(\Delta\beta/\beta)^2. \tag{4B}$$

If the root mean square error in R is calculated from (4B) as a function of f_1 for the circumstances of the present experiments, there is a minimum in the neighborhood of $f_1=0.9$. Figure 3 shows this error as a function of f_1 for $P_1=15$ cm Hg, $a=0.005$ cm Hg, $A_1=200$ counts/sec, $T=4$ hours, and $R=3$. The steep rise near complete reaction is due principally to error in the measurement of the final pressure. Calculations of this sort serve as a useful guide even though the precision of the experimental data is affected by factors in addition to those considered here. Similar considerations have been applied to the kinetics of exchange reactions involving radioactive isotopes.[18]

[18] N. Davidson and J. H. Sullivan, J. Am. Chem. Soc. **71**, 739 (1949).

THE JOURNAL OF CHEMICAL PHYSICS VOLUME 19, NUMBER 1 JANUARY, 1951

The Rate Constant of Ethane Formation from Methyl Radicals

ROBERT GOMER* AND G. B. KISTIAKOWSKY
Gibbs Chemical Laboratory, Harvard University, Cambridge, Massachusetts

(Received August 25, 1950)

The rotating sector technique has been applied to a determination of the rate constant of methyl radical recombination in the photo-decompositions of acetone and mercury dimethyl, using the small but accurately measurable rate of methane formation as a measure of methyl steady-state concentration. The resulting value of the recombination rate constant is 4.5×10^{13} (moles/cc)$^{-1}$ sec^{-1}, with an activation energy of $E=0\pm700$ cal regardless of radical source. The determination of this constant permits the evaluation of the rate constants for several other reactions of methyl radicals. It is found that hydrogen abstractions have steric factors of the order of 10^{-4}.

THE absolute rates of elementary reactions in the gas phase are known with certainty for only a very limited number of such processes, although quotients and ratios of rate constants may often be found with some accuracy. The recombination of methyl radicals

$$CH_3+CH_3\rightarrow C_2H_6;\quad R_{C_2H_6}=k_1.(CH_3)^2 \tag{1}$$

is important in this respect, since a knowledge of k_1 permits the evaluation of many other reactions involving methyl radicals.[1,2] Reaction (1) is also of considerable intrinsic interest, since it represents an association of radicals neither as simple as single atoms, nor so complex as to provide enough parameters to fit any theory.

Previous quantitative work on this reaction seems confined to that of Allen and Bawn[3] and recently Marcus and Steacie.[4] A discussion of earlier, largely qualitative work is given by Steacie.[5] Allen and Bawn used Polanyi flame technique and were able to estimate only an upper limit for the collision efficiency of Eq. (1), which they believed to be $\frac{1}{10}$ or less under their conditions. Marcus and Steacie compared the rate of the reaction,

$$CH_3+NO\rightarrow CH_3NO;\quad -R_{CH_3}=k_2.(CH_3).(NO) \tag{2}$$

with that of Eq. (1) and found $k_2/k_1^{\frac{1}{2}}=2.8\times10^3$ (moles/cc)$^{-\frac{1}{2}}$ sec$^{-\frac{1}{2}}$. Using Forsyth's[6] value for the steric factor of Eq. (2), $s_2=1.4\times10^{-5}$, they concluded that reaction (1) had a steric factor $s_1=5\times10^{-3}$. Forsyth's value of s_2 is based on mirror removal experiments in a flow system, under conditions such that radicals (produced by pyrolysis of dimethyl ether) seemed to disappear by a first-order wall reaction. It is doubtful whether his results indicate anything other than a surface recombination, or possibly a poisoning of mirrors by NO. Any

* AEC Postdoctoral Fellow, 1949–50.

[1] A. F. Trotman-Dickenson and E. W. R. Steacie, J. Am. Chem. Soc. **72**, 2310 (1950).

[2] L. M. Dorfman and R. Gomer, Chem. Rev. **46**, 499 (1950). This paper contains references to pertinent work on acetone and mercury dimethyl photo-chemistry.

[3] A. O. Allen and C. E. H. Bawn, Trans. Faraday Soc. **34**, 463 (1937).

[4] R. A. Marcus and E. W. R. Steacie, Z. Naturforsch. **4a**, 332 (1949).

[5] E. W. R. Steacie, *Atomic and Free Radical Reactions* (Reinhold Publishing Corporation, New York, 1946).

[6] J. S. A. Forsyth, Trans. Faraday Soc. **37**, 312 (1941).

error in k_2 appears to the second power in k_1 by the method of Marcus and Steacie. A preliminary description of the present work has appeared in this journal.[7]

PRINCIPLE OF THE METHOD

The uncertainties of the experiments just discussed made it desirable to have an absolute method, free from assumptions about the rates of other reactions, that could be applied in a stationary, isothermal system. An adaptation of the light intermittency method comes closest to meeting these requirements.

The theory of the rotating sector has been worked out by Dickinson[8] and by Briers, Chapman, and Walters[9] for the general case:

$$A+h\nu\rightarrow nX\cdot; \qquad \mathrm{R}_{X\cdot}=nI_a \qquad \text{(a)}$$
$$X\cdot+X\cdot\rightarrow X_2; \qquad -\mathrm{R}_{X\cdot}=2\mathrm{R}_{X_2}=2k_b.(X\cdot)^2. \qquad \text{(b)}$$

If the ratio of dark to light space in the sector is called p, and the ratio of radical steady-state concentrations under intermittent and steady illumination y,

$$y=X\cdot/\bar{X}\cdot, \qquad \text{(I)}$$

(all barred quantities referring to steady illumination), it can be shown that y will change smoothly from $1/(p+1)$ to $1/(p+1)^{\frac{1}{2}}$ as the speed of light interruption is increased from zero to infinity. If y can be determined experimentally, plots of y *vs* $\log\Delta t$ can be compared with the corresponding theoretical curves of y *vs* $\log\Delta\tau$, and the mean life time θ of the radical $X\cdot$ can be found. Δt is defined as the time of one light flash and $\Delta\tau$ as the time of one flash in units of mean lifetime:

$$\Delta\tau=\Delta t/\theta. \qquad \text{(II)}$$

θ is the mean life of a radical under conditions of steady illumination. The recombination rate constant is then given by

$$k_b=1/(4\theta^2.\bar{\mathrm{R}}_{X_2}). \qquad \text{(III)}$$

Usually y is found by comparing the rates of a chain propagation step under interrupted and steady illumination, since the rate of such a reaction is proportional to the radical steady state concentration, without affecting it or the kinetics outlined above. It should be possible, however, in the absence of a chain step to use a "pilot reaction,"

$$X\cdot+Y\mathrm{H}\rightarrow X\mathrm{H}+\text{other product(s)};$$
$$\mathrm{R}_{X\mathrm{H}}=k_c.(X\cdot).(Y\mathrm{H}), \qquad \text{(c)}$$

as a measure of $X\cdot$, provided the number of radicals disappearing by reaction (c) is small compared to that disappearing by (b), so that $X\cdot$ is still nearly proportional to $I_a^{\frac{1}{2}}$.

[7] R. Gomer, J. Chem. Phys. **18**, 998 (1950).

[8] W. A. Noyes, Jr. and P. A. Leighton, *The Photochemistry of Gases* (Reinhold Publishing Corporation, New York, 1941), pp. 202–209.

[9] Briers, Chapman, and Walters, J. Chem. Soc. **1926**, 562 (1926).

It was decided to use acetone and mercury dimethyl as sources of methyl radicals because the mechanism of ethane and methane formation in these systems seems sufficiently established. It has been shown by several workers[1,2] that at least above 100°, where the CO quantum yield is unity and acetyl radicals may be neglected, the following reactions account for ethane and methane formation in the photolysis of acetone:

$$\mathrm{CH_3}+\mathrm{CH_3}\rightarrow\mathrm{C_2H_6}; \quad \mathrm{R}_{\mathrm{C_2H_6}}=k_1.(\mathrm{CH_3})^2 \qquad (1)$$
$$\mathrm{CH_3}+(\mathrm{CH_3})_2\mathrm{CO}\rightarrow\mathrm{CH_4}+\mathrm{CH_2COCH_3}; \quad \mathrm{R}_{\mathrm{CH_4}}=k_3.(\mathrm{CH_3}).(\mathrm{CH_3COCH_3}). \qquad (3)$$

Methane is formed by an analogous process in mercury dimethyl photolysis:

$$\mathrm{CH_3}+(\mathrm{CH_3})_2\mathrm{Hg}\rightarrow\mathrm{CH_4}+\mathrm{CH_2HgCH_3}; \quad \mathrm{R}_{\mathrm{CH_4}}=k_4(\mathrm{CH_3}).(\mathrm{CH_3HgCH_3}), \qquad (4)$$

but in addition to reaction (1) ethane seems to be formed by

$$\mathrm{CH_3}+(\mathrm{CH_3})_2\mathrm{Hg}\rightarrow\mathrm{C_2H_6}+\mathrm{CH_3}+\mathrm{Hg}; \quad \mathrm{R}(5)_{\mathrm{C_2H_6}}=k_5(\mathrm{CH_3})(\mathrm{CH_3HgCH_3}). \qquad (5)$$

Reaction (5) is possibly more complex than written,[2] but is unimportant, since no methyl radicals are used up. The amount of ethane formed by reaction (5) can be calculated.[2] The fate of acetonyl and $\mathrm{CH_2HgCH_3}$ radicals is not definitely established, but is probably recombination with methyl radicals. This has no bearing on the present work. The evidence for reactions (1), (3), and (4) is discussed at some length at the end of this paper.

The sector technique just outlined can therefore be applied, if sufficiently high light intensities are used to insure that $\mathrm{R}_{\mathrm{C_2H_6}}/\mathrm{R}_{\mathrm{CH_4}}$ is large. In the present experiments this ratio was kept at 10 or higher. The quantity y is then equal to $\mathrm{R}_{\mathrm{CH_4}}/\bar{\mathrm{R}}_{\mathrm{CH_4}}$, $\bar{\mathrm{R}}_{X_2}$ is given by $\bar{\mathrm{R}}_{\mathrm{C_2H_6}}$ in the case of acetone and by $\bar{\mathrm{R}}_{\mathrm{C_2H_6}}-(k_5/k_4)\bar{\mathrm{R}}_{\mathrm{CH_4}}$ in the case of mercury dimethyl.[2]

EXPERIMENTAL

Merck Reagent Grade Acetone was fractionated in a good column, dried over fresh $\mathrm{CaSO_4}$, and bulb-to-bulb distilled in vacuum. Mercury dimethyl was prepared by the method of Gilman and Brown,[10] fractionated repeatedly over fresh $\mathrm{Ag_2O}$, the 92.0° (uncorrected) fraction being retained. The sample was further bulb-to-bulb distilled in vacuum at −20°. Both reagents were thoroughly degassed at −78° before use. Purities were checked by vapor pressure measurements from −130 to +20°.

An all-glass, mercury cutoff apparatus was used, capable of holding a vacuum of 10^{-6} mm of Hg. The analytical part of the system was similar to one previously described.[2] In the case of acetone all the noncondensable products of each run, instead of aliquot

[10] H. Gilman and R. E. Brown, J. Am. Chem. Soc. **52**, 3314 (1930).

portions, were put over hot CuO, so that the total amount of methane was determined directly as the non-condensable residue after combustion of CO. Ethane was separated in each case by repeated fractionation at −160 to −140°. Products were measured with a double range McLeod gauge, capable of measuring pressures from 10^{-6} to 1 mm of Hg.

The reaction system consisted of the cell to be described, connected via a graded seal to a freeze-out trap and a Pearson manometer with a magnification factor of 38.7. A cutoff with ground-in floats connected an auxiliary storage bulb to the cell system. Connection to the rest of the apparatus was made through a cutoff having arms constructed of 32-mm tubing, so that the volume of an arm constituted an appreciable fraction of the reaction system's volume. With this arrangement it was possible to set the Pearson gauge for the desired pressure, admit approximately the proper amount of reactant, and obtain the exact pressure by raising or lowering the mercury in the wide arm cutoff. Pressures could be set to 0.05 mm of Hg. Freezing out of condensable portions of the reaction mixtures after a run was greatly speeded up by repeated raising and lowering of mercury in the wide arm cutoff, thereby agitating the gas mixture.

Corresponding runs with and without light interruption were made as closely consecutive as possible. Times of illumination were so adjusted that approximately equal amounts of methane were formed in corresponding runs. In the case of mercury dimethyl the reaction was periodically stopped and the gas in the cell system remixed by freezing and evaporating, so that initial rates were maintained. This was also done in some low pressure acetone runs. In some static runs intensity variation was achieved by inserting Lektromesh screen between light source and cell.

A cylindrical quartz cell with optically flat windows, 9 cm long and 2.5 cm in diameter, of measured volume 40 cc, was mounted in an aluminum cylinder of 2.5-cm wall thickness, extending 4 cm beyond the cell windows. This cylinder was heated electrically and housed the 12-cc reservoir of a mercury regulator. The latter activated an electronic relay of the type described by Linnell,[11] controlling a small part of the total heating current. Temperature could be controlled to ±0.3° over the entire range used, as determined with Anschütz precision thermometers, mounted in the aluminum block.

Unfiltered light from a Hanovia S-100 medium pressure Hg arc was collimated with a quartz lens so thas the resulting beam filled the whole cell as uniformly at possible. When hot, the luminous portion of the arc may be seen as a narrow band, about 2 mm wide and 2.5 cm long in the center of the arc tube. This property was utilized by mounting the rotating sector less than 1 cm in front of the arc, interposing a slit of 4-mm width. With this arrangement the arc image on the sector disk was a strip about 4 mm wide and parallel to the sector's slot edges, so that times of partial illumination were negligible for the slot widths used. The squareness of resulting light pulses was seen oscilloscopically. Sector disks were 30 cm in diameter and driven by means of belts and pulleys. Speeds, determined stroboscopically or by direct timing, were constant to better than one percent. Experiments on mercury dimethyl were carried out with a sector of $p=1$, having 8 alternating slots of 5-cm mean width. Acetone experiments employed a sector of $p=3$, having two 10-cm wide openings.

Provision was made for running the arc on direct or alternating current. Input voltage was stabilized with a Sola constant voltage transformer. Although the S-100 arc is designed for ac operation, it may be run on dc by starting with a Tesla coil. It suffices to touch the arc housing with the coil (e.g., a leak tester). A current limiting rheostat in series with the arc is essential, since its resistance is very low when cold. The current should be held initially to 1.3 amperes. After 2 to 3 minutes the arc warms up and its resistance increases sharply, so that the rheostat must be adjusted to prevent the arc from going out. If this should happen, it is necessary to wait till the arc is quite cold before another attempt may be made. Stable operation is achieved after 10 to 15 minutes, and the arc may now be run at 0.75 to 1.5 amperes. High currents shorten the arc life very appreciably. It is wise to reverse the arc current after each run, so that both electrodes are given equal wear. A 200-ohm rheostat in parallel with the main resistance facilitates fine adjustment.

A RCA 935 photo-tube and 180-volt battery supply were used with a 0.5-megohm load and vacuum tube voltmeter to monitor the light output. On ac operation the arc was stable to within one percent over periods of hours. Manual adjustment sufficed to insure nearly the same stability on dc operation.

RESULTS AND DISCUSSION

Results on acetone at 125° and 175° are shown in Tables I and II. Results on mercury dimethyl at 175° and 220° are shown in Tables III and IV. Figures 1 to 4 show the resulting fit to the theoretical curves when θ has been given the indicated assignments. Allowance for intensity variation has been made by adding $\frac{1}{2}\log(\bar{R}x_2/\bar{R}x_2')$ to $\log\Delta t$. $\bar{R}x_2$ is the actual (bimolecular) rate of ethane formation and $\bar{R}x_2'$ the rate to which the points have been normalized.

At the relatively low light intensities (and hence relatively long lifetimes) of these experiments, rectangular light pulses of 120 cycles/second are of sufficiently high frequency to result in $y\cong 1/(p+1)^{\frac{1}{2}}$. In other words, this frequency is already equivalent to steady illumination. This made it permissible to run the arc on ac; the resulting 120-cycle semisinusoidal light wave corresponds to a square wave of even higher frequency. This

[11] R. H. Linnell and H. M. Haendler, Rev. Sci. Instr. 5, 364 (1949).

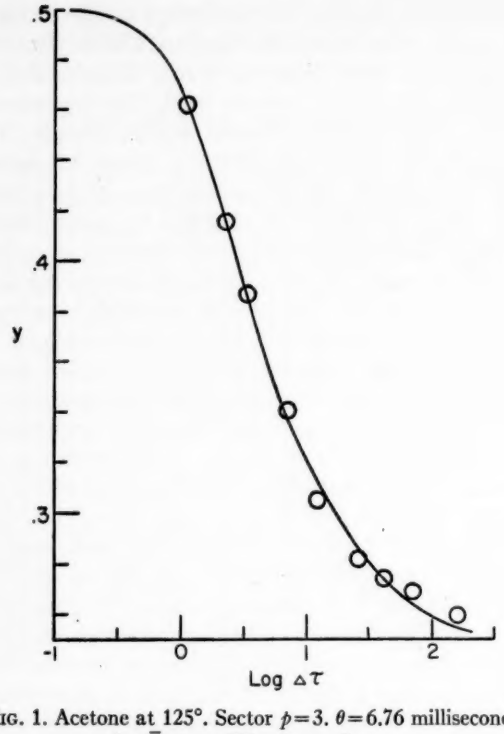

FIG. 1. Acetone at 125°. Sector $p=3$. $\theta=6.76$ milliseconds for $\bar{R}_{C_2H_6}=630$ microns/hour.

point was experimentally verified, as shown in Figs. 2 and 3.

At pressures of 21 mm (at 175°) of mercury dimethyl, this substance is so strongly absorbing that it is not permissible to use the cell volume as the effective reaction volume. The correction was made by finding the apparent value of k_1/k_4^2 from a plot of $\bar{R}_{C_2H_6}/\bar{R}_{CH_4}$ *vs* $\bar{R}_{CH_4}$, using the runs of Table III. The value found was then compared with that obtained in a previous investigation,[2] where either low pressures or a very short cell had been used. The correction factor turned out to be 0.54, so that the effective reaction volume for 21 mm of mercury dimethyl at 175° was 21.6 cc. The value of k_1/k_4^2 found at 220° agrees with that previously found, as should be the case, since a pressure of only 10 mm of mercury dimethyl was used in the present experiments. Hence, no volume correction had to be made at 220°. It may be mentioned in passing that the intercepts of the $\bar{R}_{C_2H_6}/\bar{R}_{CH_4}$ *vs* $\bar{R}_{CH_4}$ plots (equal to k_5/k_4) are the same as those found previously,[2] which is also to be expected, since these have the dimension of pure numbers, and must therefore be independent of reaction volume.

Similar plots for acetone at 125 and 175° lead to values of k_1/k_3^2 of 8.01 and 0.553 (moles/cc)·sec, respectively. From these values $E_3-\frac{1}{2}E_1=9.5$ kcal, which is in good agreement with the value of 9.7 kcal reported

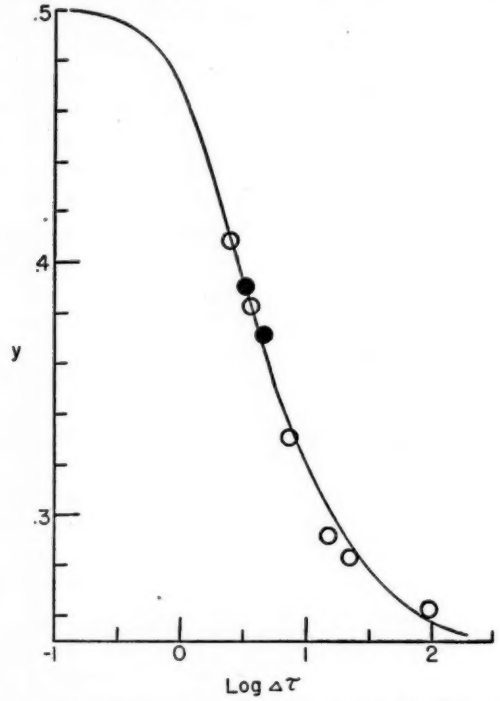

FIG. 2. Acetone at 175°. Sector $p=3$. $\theta=11.5$ milliseconds for $\bar{R}_{C_2H_6}=235$ microns/hour. Solid points, dc runs; other points, ac runs.

TABLE I. Acetone at 125°. Acetone pressure = 50 mm (at 125°). Sector $p=3$ (2 slots). Rates of product formation ($R_{product}$) in microns/hour. Rates$\times 1.93\times 10^{-13}$ = rates in moles/cc/second. Barred quantities ($\bar{R}$) refer to steady illumination, $y=R_{CH_4}/\bar{R}_{CH_4}$.

Run	$\bar{R}_{CH_4}$	$\bar{R}_{C_2H_6}$	$\bar{R}_{CO}$	R_{CH_4}	$R_{C_2H_6}$	R_{CO}	y	Sector rpm
36	38.1	628	673	17.6	150	178	0.462	1040
37	39.0	631	677	15.1	157	172	0.387	324
38	39.3	636	678	16.3	159	177	0.415	498
39	38.7	632	672	10.4	159	171	0.269	16.1
40	39.0	642	682	10.7	161	174	0.274	27.4
41	40.8	651	697	11.5	166	175	0.282	43.2
42	39.0	640	688	11.9	159	174	0.305	90.0
43	38.4	632	675	13.1	157	175	0.341	155
48	39.3	632	685	10.2	159	171	0.260	6.95
31	53.2	1075	1115					
32	20.1	566	590		acetone pressure = 25 mm			
33	26.8	279	316					
34	17.1	114	139					
35	40.4	610	657					

TABLE II. Acetone at 175°. Acetone pressures as indicated (at 175°). Symbols and conditions as in Table I.

Run	$\bar{R}_{CH_4}$	$\bar{R}_{C_2H_6}$	$\bar{R}_{CO}$	R_{CH_4}	$R_{C_2H_6}$	R_{CO}	y	Sector rpm
50[a]	24.3	225	255	6.90	56.6	65.6	0.284	29.7
51[a]	25.0	218	257	7.29	57.2	65.3	0.292	43.0
53[a]	26.0	239	266	9.95	58.5	68.3	0.383	188
52[a]	24.8	230	256	8.20	56.8	65.9	0.331	90.0
54[a]	25.4	236	261	10.4	57.0	67.7	0.409	272
55[a,b]	34.1	419	453	13.3	108	123	0.390	272
56[a,b]	33.6	432	469	12.5	108	122	0.372	187
44[c]	13.7	150	170					
45[d]	39.1	304	344					
46[a]	25.4	235	262					
47[a]	12.9	53.5	68.8					

[a] Pressure = 15 mm.
[b] Dc run.
[c] Pressure = 10 mm.
[d] Pressure = 20 mm.

TABLE III. Mercury dimethyl at 175°. Pressure of mercury dimethyl = 21 mm (at 175°). Sector $p=1$ (8 slots). Symbols as in Table I. Rates $\times 3.58\times10^{-13}$ = rates in moles/cc/second.

Run	$\bar{R}_{CH_4}$	$\bar{R}_{C_2H_6}$	R_{CH_4}	$R_{C_2H_6}$	y	Sector rpm
1	10.8	271	7.62	149	0.706	1775
2	8.79	165	5.92	80.9	0.673	1775
3	8.46	160	5.90	82.1	0.697	330
4	8.80	167	5.84	85.3	0.664	228
5	8.70	164	4.75	83.3	0.546	10.2
6	8.29	162	5.46	81.8	0.659	70.8
7	7.80	142	5.40	69.5	0.692	3060
8[a]	14.5	384	8.86	187	0.665	330
9[a]	12.8	352	8.33	178	0.650	197
10[a]	13.0	335	7.41	176	0.570	18.6
11[a]	11.8	289	6.62	137	0.561	44.5
15	8.64	190	5.61	94.6	0.649	51.9
16	9.39	211	5.87	107	0.625	43.0
12[a]	15.4	440				
13	16.5	493				
14	9.84	216				
1a	10.7	288				
1b	6.87	108				

[a] Dc run.

by Dickenson and Steacie.[1,12] This agreement and the fact that acetone is much less strongly absorbing than mercury dimethyl indicate that the cell volume may safely be used as the effective one.

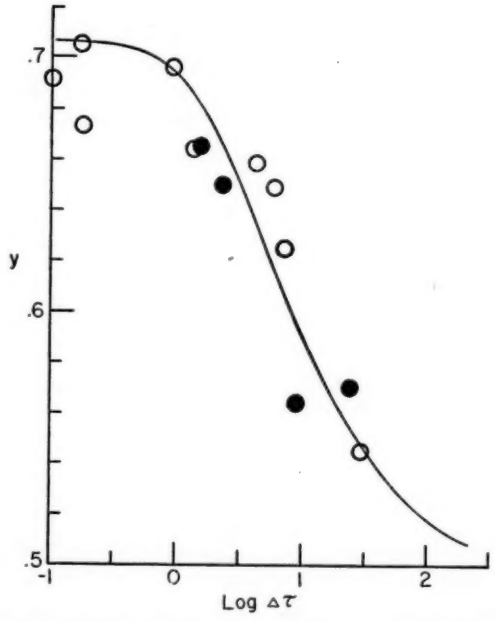

FIG. 3. Mercury dimethyl at 175°. Sector $p=1$. $\theta=12.6$ milliseconds at $\bar{R}(1)C_2H_6=100$ microns/hour. Solid points, dc runs; other points, ac runs.

[12] Dorfman and Noyes (see reference 2) obtained $E_3-\frac{1}{2}E_1=6.5$ kcal from their values of k_1/k_3^2 at 25 and 122°. However, their value of k_1/k_3^2 at 122° is in fair agreement with that of Dickenson and Steacie[1] and the present work. A private communication from Professor Noyes' laboratory by Dr. A. J. C. Nicholson informs us that the discrepancy may be due in part to the fact that Noyes and Dorfman used light beams of smaller diameter than their cell, so that a change in effective volume with temperature may have occurred at the pressures used. Dr. Nicholson states that the matter is being pursued further in Professor Noyes' laboratory.

TABLE IV. Mercury dimethyl at 220°. Mercury dimethyl pressure = 10.0 mm (at 220°). Sector $p=1$ (8 slots). Symbols as in Table I. Rates $\times 1.93\times10^{-13}$ = rates in moles/cc/second.

Run	$\bar{R}_{CH_4}$	$\bar{R}_{C_2H_6}$	R_{CH_4}	$R_{C_2H_6}$	y	Sector rpm
17	12.5	150	7.97	74.8	0.636	43.1
22	13.5	166	7.57	84.4	0.561	10.2
23	14.0	169	8.06	83.6	0.576	29.6
24	12.5	148	7.82	74.4	0.626	52.0
25	12.7	150	7.90	74.2	0.622	90.0
26	12.1	148	8.29	72.4	0.685	157
27	12.3	148	8.49	74.8	0.690	268
28	11.8	147	6.30	72.1	0.534	6.90
29	12.5	162	8.63	81.0	0.690	1040
30	12.4	164	8.44	81.7	0.681	1040
18	6.47	43.9				
19	30.6	687				
19a	31.4	711				
20	15.0	193				
21	15.0	201				

k_1 may now be calculated from Eq. (III). The values of k_5/k_4 used to find $\bar{R}x_2$ for mercury dimethyl runs are 7.8 and 3.2 at 175 and 220°, respectively. The resulting values of k_1 are shown in Table V. The relative accuracy of these values is believed to be 10 percent for the acetone and 50 percent for the mercury dimethyl experiments. It is seen that the values of k_1 are independent of radical source or of sector p value within these limits. E_1 may therefore be assigned the value $E_1=0\pm0.7$ kcal.

It has been shown independently by several workers[1,2] that k_1/k_3^2 and k_1/k_4^2 are not dependent on pressure in the range 5 to 100 mm Hg. This can be interpreted only as meaning that reaction (1) is free from third-body restrictions in this range. It is therefore permissible to compare the values of k_1 at different temperatures, even though they were obtained at different pressures.

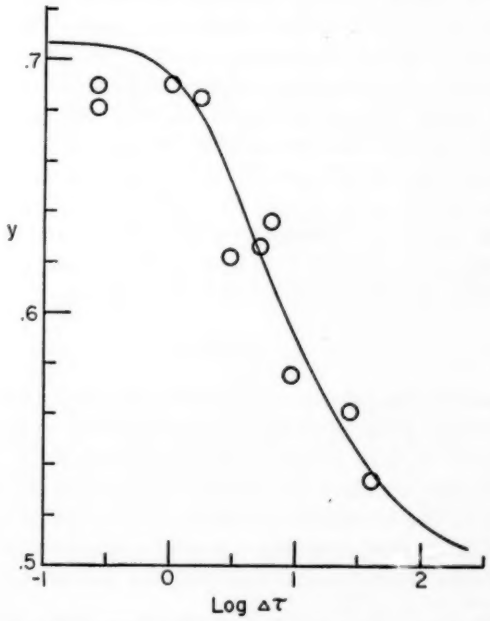

FIG. 4. Mercury dimethyl at 220°. Sector $p=1$. $\theta=13.5$ milliseconds at $\bar{R}(1)C_2H_6=107$ microns/hour.

TABLE V. Rate constant of ethane formation.

Radical source	Temperature °C	$k_1\times10^{-13}$ (moles/cc)$^{-1}$ $\times$sec^{-1}	$k_1 . T^{-\frac{1}{2}}\times10^{-12}$ (moles/cc)$^{-1}$ sec^{-1} . (°K)$^{-\frac{1}{2}}$
Acetone	125	4.5	2.3
Acetone	175	4.2	2.0
Mercury dimethyl	175	4.6	2.2
Mercury dimethyl	220	6.7	3.0

A comparison of the collision theory with the observed rate constant shows that $s\sigma^2=4.47\times10^{-16}$ cm^2, where s is the steric factor and σ the collision diameter. Thus, the association of methyl radicals is seen to occur on nearly every classical collision between them. This is of interest because, as noted before, the high efficiency of the recombination reaction persists down to 5-mm pressure. At this pressure the newly formed energy-rich ethane molecules suffer approximately 10^8 collisions per second, so that their lifetime must be at least 10^{-7} second before they fall apart into methyl radicals. The combination of the high efficiency of the recombination reaction with the long life of the energy-rich product is really quite surprising because the former is indicative of loose requirements, in regard to orientation and phase of motion, for association, whereas the latter suggests stringent requirements for dissociation.

The absence of third-body requirements for the association reaction means, of course, that the dissociation of ethane into methyl radicals is of first order (i.e., has the "high pressure" unimolecular rate constant) down to 5-mm pressure. Using the value of the association rate constant here found and the calculated[13] equilibrium constant between ethane and methyl radicals, one finds that the frequency factor A in the unimolecular rate constant of the dissociation reaction, $Ae^{-E/RT}$, is 2×10^{15} sec^{-1}. E is the dissociation energy (about 78 kcal) because the association reaction has zero activation energy. It is, perhaps, of some interest that Partington's recent value[14] for the first-order decomposition rate of ethane in the presence of NO at 530° leads to a frequency factor of about 10^{15} if E is set equal to 78 kcal.

The above data permit an application of the Rice-Kassel theory of unimolecular reactions to the energy-rich ethane molecules. One form of this theory gives for the mean life of such molecules the expression:

$$\tau_e=1/A\cdot C, \qquad \text{(IV)}$$

where C is the inherent probability of a sufficient fraction of the internal energy of the molecule being concentrated in the proper oscillator. Since, for a given equilibrium constant, the frequency factor A is proportional to the recombination rate constant, large values of the latter tend to reduce the mean lives of energy-rich molecules. The classical value of the probability C is given by the expression:

$$C=[(\epsilon-\epsilon_0)/\epsilon]^{\alpha-1}, \qquad \text{(V)}$$

where ϵ is the total internal energy of the molecule and ϵ_0 is the amount needed for the reaction in a certain oscillator; α denotes the number of participating oscillators, i.e., those among which the energy is fluctuating. If one takes $\epsilon_0=78$ kcal and guesses ϵ as 85 kcal, perhaps a trifle high, α must be given the value eight to make $C=10^{-9}$ consistent with a lifetime of 10^{-7} sec for the abovementioned value of A. This is not physically impossible because the total number of internal vibrations in ethane is 17, not counting internal rotation, but is certainly rather high in comparison with numbers which have been calculated for other unimolecularly decomposing molecules by the same theory.

Because of this theoretical difficulty, it seems desirable to explore the possibility that the interpretation of the present experiments is fundamentally wrong, in the sense that the measurements may be furnishing information on some other reaction than the recombination of methyl free radicals. One possibility is to suppose that ethane formation proceeds by the mechanism:

$$\begin{aligned}&CH_3+CH_3CO\rightarrow C_2H_6+CO;\\ &R_{C_2H_6}=k_6(CH_3)(CH_3CO),\end{aligned} \qquad (6)$$

and by the equivalent reaction with CH_3Hg in the case of dimethyl mercury. Experimental evidence against this mechanism is very abundant. Thus, the study by Anderson and Rollefson[15] of the changes in the quantum yield of CO with temperature in the photolysis of acetone, biacetyl, and acetyl bromide clearly shows that the acetyl radical breaks up thermally at temperatures above 110.° If reaction (6) were important at higher temperatures, the yield of ethane should be equal to that of carbon monoxide, which is contrary to the findings of Dorfman and Noyes,[2] Herr and Noyes,[16] Dickenson and Steacie,[1] Anderson and Rollefson,[15] and the present work. In some of the Dorfman and Noyes experiments at 122° the light intensities were so low that the ratio of yields of carbon monoxide and ethane was equal to ten; but in those experiments, as well as in the present work, the sum of methane and ethane yields equalled that of carbon monoxide, in accordance with the accepted mechanism and contrary to reaction (6).

If in addition to reaction (6) carbon monoxide is also formed by the reaction,

$$CH_3CO\rightarrow CH_3+CO; \quad R(7)_{CO}=k_7(CH_3CO), \qquad (7)$$

CO can exceed ethane; but in this case the increase with temperature in the yield of acetone decomposition must be due to the competition of Eq. (6) or Eqs. (6) and (7)

[13] Glasstone, Laidler, and Eyring, *The Theory of Rate Processes* (McGraw-Hill Book Company, Inc., New York, 1941), p. 263.
[14] R. G. Partington, Disc. Faraday Soc. **2**, 114 (1947).
[15] H. W. Anderson and G. K. Rollefson, J. Am. Chem. Soc. **63**, 816 (1941).
[16] D. S. Herr and W. A. Noyes, Jr., J. Am. Chem. Soc. **62**, 2052 (1940).

TABLE VI. Rate constants of some methyl radical reactions. Values of steric factors (s) have been found by assigning arbitrary collision diameters (σ), taken from reference 2.

Reaction	k (moles/cc)$^{-1}$ sec^{-1}	$s\sigma^2$ cm^2	s
$CH_3+CH_3\rightarrow C_2H_6$	$2.1\times10^{12}\cdot T^{\frac{1}{2}}$	4.5×10^{-16}	1.0
$CH_3+(CH_3)_2CO\rightarrow CH_4+\cdots$	$1.8\times10^{10}\cdot T^{\frac{1}{2}}e^{-9500/RT}$	2.3×10^{-18}	1.7×10^{-3}
$CH_3+(CH_3)_2Hg\rightarrow CH_4+\cdots$	$4.1\times10^{9}\cdot T^{\frac{1}{2}}e^{-9000/RT}$	5.6×10^{-19}	2.9×10^{-4}
$CH_3+(CH_2)_2O\rightarrow CH_4+\cdots$	$1.4\times10^{9}\cdot T^{\frac{1}{2}}e^{-9000/RT}$	1.7×10^{-19}	1.7×10^{-4}
$CH_3+C_4H_{10}\rightarrow CH_4+\cdots$	$3.6\times10^{9}\cdot T^{\frac{1}{2}}e^{-8200/RT}$	3.6×10^{-19}	4.9×10^{-4}

with the following reaction:

$$CH_3+CH_3CO\rightarrow(CH_3)_2CO;\qquad R_{Ac}=k_8(CH_3)(CH_3CO). \tag{8}$$

The ratio of the rates of reactions (6) and (8) must be intensity-independent, and the rise with temperature of ethane yield must be due to a greater activation energy of reaction (6); but the present experiments show that the reaction yielding ethane has no activation energy and are completely inconsistent with a value $E_6-E_8\cong 8$ kcal, which follows from the above scheme. Finally, Dickenson and Steacie,[1] studying acetone decomposition in the presence of hydrogen donors (YH), found the following expression, derived on the basis of reactions (1), (3), and (c), to represent their results:

$$R_{CH_4}/R_{C_2H_6}^{\frac{1}{2}}=(k_3/k_1)^{\frac{1}{2}}.Ac+(k_c/k_1)^{\frac{1}{2}}.YH. \tag{VI}$$

In absence of hydrogen donors this expression reduces to one which has been obtained by Dorfman and Noyes:[2]

$$R_{C_2H_6}/R_{CH_4}^2=(k_1/k_3^2).Ac^2. \tag{VII}$$

Reactions (6) and (7) lead, however, to the expression,

$$R_{CH_4}/R_{C_2H_6}^{\frac{1}{2}}=(2k_7/k_6)^{\frac{1}{2}}(k_3.Ac+k_c.YH)_7, \tag{VIII}$$

which is inconsistent with experimental data.

The experimental observations on the mercury dimethyl system are entirely analogous,[2] and if a reaction like (6) were responsible for ethane formation, the identity of the corresponding rate constants in acetone and in dimethyl mercury would be surprising.

Hill[17] has recently made an Eyring-type calculation of the rate of reaction (1) and found $s_1=1.4\kappa$, κ being the transmission coefficient. This result is wholly consistent with the findings of the present work.

The determination of the value of k_1 makes possible the calculation of rate constants for several reactions of the type (c), for which the ratio $k_c/k_1^{\frac{1}{2}}$ is known. Table VI lists the results of such calculations, the data for acetone being taken from the present work and those for other reactions from reference 2. This table shows that the steric factors for reactions of type (c) are all of the order of 10^{-4}, which is in good agreement with Hill's calculation[17] for reaction 3.

The importance of "hot" methyl radicals in mercury dimethyl photolysis has recently been suggested,[18] although the experimental evidence is not strong. It may be noted that the effect on reaction (1) cannot be appreciable. At the highest intensities used, the methyl radical steady state concentration was about 10^{-12} moles/cc, the total gas concentration 10^{-7} moles/cc. It follows that every methyl radical underwent on the average 10^5 collisions before hitting another methyl radical. The possible effect of "hot" radicals on reactions of type (c) must also be small, since only about one in 10^4 collisions meeting the energy requirements is effective. These points are verified by the fact that the value of k_1 does not depend on the radical source (present work) and that $k_c/k_1^{\frac{1}{2}}$ for butane does not depend on whether mercury dimethyl[2] or acetone[19] is used as source of methyl radicals. Further, if quenching of any "hot" radicals were incomplete, deviations from Eq. (VII) should be observed with variation in intensity.

In conclusion it is interesting to point out that there have recently appeared values for the rate constant of the chain terminating step in acetaldehyde photolysis,[20,21] which are in agreement with the present value of k_1. While Dodd[20] considers the termination reaction to be more probably a reaction of methyl and formyl radicals and Rice[21] seems to favor Marcus and Steacie's[4] value for s_1, it seems reasonable from the agreement that the termination reaction in acetaldehyde photolysis is the recombination of methyl radicals.

ACKNOWLEDGMENT

One of us (R.G.) wishes to thank the AEC for financial assistance.

[17] T. L. Hill, J. Chem. Phys. **17**, 1125 (1949).

[18] M. K. Phibbs and B. de B. Darwent, Trans. Faraday Soc. **45**, 541 (1949).

[19] Private communication from Dr. A. F. Trotman-Dickenson. Dr. Dickenson also finds excellent agreement between the two radical sources for other hydrogen abstraction reactions (unpublished results from Dr. Steacie's laboratory).

[20] R. E. Dodd, J. Chem. Phys. **18**, 234 (1950).

[21] V. E. Lucas and O. K. Rice, J. Chem. Phys. **18**, 993 (1950).

Hexacovalent Bond Orbitals. IV

GEORGE H. DUFFEY
Chemistry Department, South Dakota State College, Brookings, South Dakota

(Received October 2, 1950)

Six equivalent bond orbitals of D_3 symmetry are set up. Application of the orthogonality and normalization conditions leads to solutions when the composition is $s^n p^{1+2m} d^{5-n-2m}$. The coefficients in the angular wave functions are expressed in terms of four parameters. The trigonal prism orbitals and the trigonal antiprism orbitals previously discussed can be obtained on assigning values to some of the parameters.

IN the preceding parts of this series[1] the author has used the method of directed valence bonds in discussing trigonal prism and trigonal antiprism bond orbitals. Recently Fumi and Castellan[2] have stated that the trigonal trapezohedral arrangement of six equivalent bonds (symmetry D_3) can arise in *spd* hybridization. An introduction to orbitals of this more general type is now presented.

The first *spd* hybrid orbital of D_3 symmetry may assume the form

$$\psi_1 = as + bp_z + cp_x + dp_y + ed_z + fd_{xy} + gd_{x+y} + hd_{x+z} + id_{y+z}. \quad (1)$$

Under the operations of the group one obtains from ψ_1 the following bond orbitals:

$$\begin{aligned}\psi_2 = {} & as + bp_z + (c\cos120^\circ - d\sin120^\circ)p_x \\ & + (c\sin120^\circ + d\cos120^\circ)p_y \\ & + ed_z + (f\cos120^\circ + g\sin120^\circ)d_{xy} \\ & + (-f\sin120^\circ + g\cos120^\circ)d_{x+y} \\ & + (h\cos120^\circ - i\sin120^\circ)d_{x+z} \\ & + (h\sin120^\circ + i\cos120^\circ)d_{y+z}, \quad (2)\end{aligned}$$

$$\begin{aligned}\psi_3 = {} & as + bp_z + (c\cos120^\circ + d\sin120^\circ)p_x \\ & + (-c\sin120^\circ + d\cos120^\circ)p_y \\ & + ed_z + (f\cos120^\circ - g\sin120^\circ)d_{xy} \\ & + (f\sin120^\circ + g\cos120^\circ)d_{x+y} \\ & + (h\cos120^\circ + i\sin120^\circ)d_{x+z} \\ & + (-h\sin120^\circ + i\cos120^\circ)d_{y+z}, \quad (3)\end{aligned}$$

TABLE I. Angular coordinates of the maxima in the bond orbitals.

Bond orbital number	θ	φ
1	θ_1	φ_1
2	θ_1	$120^\circ + \varphi_1$
3	θ_1	$240^\circ + \varphi_1$
4	$180^\circ - \theta_1$	$-\varphi_1$
5	$180^\circ - \theta_1$	$120^\circ - \varphi_1$
6	$180^\circ - \theta_1$	$240^\circ - \varphi_1$

$$\begin{aligned}\psi_4 = {} & as - bp_z + cp_x - dp_y + ed_z \\ & + fd_{xy} - gd_{x+y} - hd_{x+z} + id_{y+z}, \quad (4)\end{aligned}$$

$$\begin{aligned}\psi_5 = {} & as - bp_z + (c\cos120^\circ + d\sin120^\circ)p_x \\ & + (c\sin120^\circ - d\cos120^\circ)p_y \\ & + ed_z + (f\cos120^\circ - g\sin120^\circ)d_{xy} \\ & + (-f\sin120^\circ - g\cos120^\circ)d_{x+y} \\ & + (-h\cos120^\circ - i\sin120^\circ)d_{x+z} \\ & + (-h\sin120^\circ + i\cos120^\circ)d_{y+z}, \quad (5)\end{aligned}$$

$$\begin{aligned}\psi_6 = {} & as - bp_z + (c\cos120^\circ - d\sin120^\circ)p_x \\ & + (-c\sin120^\circ - d\cos120^\circ)p_y \\ & + ed_z + (f\cos120^\circ + g\sin120^\circ)d_{xy} \\ & + (f\sin120^\circ - g\cos120^\circ)d_{x+y} \\ & + (-h\cos120^\circ + i\sin120^\circ)d_{x+z} \\ & + (h\sin120^\circ + i\cos120^\circ)d_{y+z}. \quad (6)\end{aligned}$$

The *s*, *p*, and *d* functions are defined in the same way as in paper I[1] of this series. The *z* axis coincides with the threefold axis (C_3) and the *x* axis coincides with a twofold axis (C_2'). To clarify the orientation of the axes one may refer to Table I.

Without loss of generality three functions orthogonal to $\psi_1, \cdots, \psi_6$ can be set up as follows:

$$\psi_7 = -\sqrt{3}jp_x + \sqrt{3}kd_{xy} + \sqrt{3}ld_{y+z}, \quad (7)$$

$$\psi_8 = \sqrt{3}jp_y + \sqrt{3}kd_{x+y} + \sqrt{3}ld_{x+z}, \quad (8)$$

$$\psi_9 = (6)^{\frac{1}{2}}es - (6)^{\frac{1}{2}}ad_z. \quad (9)$$

Application of the orthogonality and normalization conditions gives the following equations:

$$b^2 = \tfrac{1}{6}, \quad (10)$$

$$a^2 + e^2 = \tfrac{1}{6}, \quad (11)$$

$$c^2 + f^2 + i^2 = \tfrac{1}{3}, \quad (12)$$

$$d^2 + g^2 + h^2 = \tfrac{1}{3}, \quad (13)$$

$$cd - fg - ih = 0, \quad (14)$$

$$j^2 + k^2 + l^2 = \tfrac{1}{3}, \quad (15)$$

$$cj - fk - il = 0, \quad (16)$$

$$dj + gk + hl = 0. \quad (17)$$

[1] G. H. Duffey, J. Chem. Phys. **17**, 1328 (1949); **18**, 128 (1950); **18**, 510 (1950).

[2] F. G. Fumi and G. W. Castellan, J. Chem. Phys. **18**, 762 (1950). Note that the hybridizations sp^2d^3 and p^2d^4 *can* lead to arrangements having six equivalent bonds since orbitals of trigonal trapezohedral symmetry (and trigonal prism symmetry) can be formed with hybridizations $s^n p^{1+2m} d^{5-n-2m}$ where n and m may vary independently from 0 to 1.

One can set

$$b=1/(6)^{\frac{1}{2}}, \tag{18}$$

$$a=[1/(6)^{\frac{1}{2}}]\cos\alpha, \tag{19}$$

$$e=[1/(6)^{\frac{1}{2}}]\sin\alpha. \tag{20}$$

Consider the two coordinate systems in the usual discussion of Eulerian angles.[3] In the X, Y, Z coordinate system draw three perpendicular vectors from the origin to the points: $(1/\sqrt{3}, 0, 0)$, $(0, 1/\sqrt{3}, 0)$, and $(0, 0, 1/\sqrt{3})$. If we assume these points become $(-i, -f, c)$, (h, g, d), and (l, k, j) in the x, y, z coordinate system, the equations expressing the length squared and the perpendicularity of the vectors are identical with Eqs. (12) to (17). The transformation equations yield the following expressions, where the independent parameters ϑ, ψ, φ have been replaced by $90°-\beta$, γ, δ, respectively:

$$c=(1/\sqrt{3})\cos\beta\cos\delta, \tag{21}$$

$$f=(1/\sqrt{3})(\sin\delta\cos\gamma+\sin\beta\sin\gamma\cos\delta), \tag{22}$$

$$i=(1/\sqrt{3})(\sin\delta\sin\gamma-\sin\beta\cos\gamma\cos\delta), \tag{23}$$

$$d=(1/\sqrt{3})\cos\beta\sin\delta, \tag{24}$$

$$g=(1/\sqrt{3})(\cos\delta\cos\gamma-\sin\beta\sin\gamma\sin\delta), \tag{25}$$

$$h=(1/\sqrt{3})(\cos\delta\sin\gamma+\sin\beta\cos\gamma\sin\delta), \tag{26}$$

$$j=(1/\sqrt{3})\sin\beta, \tag{27}$$

$$k=(1/\sqrt{3})\cos\beta\sin\gamma, \tag{28}$$

$$l=-(1/\sqrt{3})\cos\beta\cos\gamma. \tag{29}$$

Thus one obtains solutions to the orthogonality and normalization equations when the over-all composition of the bond orbitals is $s^n p^{1+2m} d^{5-n-2m}$ where

$$n=\cos^2\alpha, \tag{30}$$

$$m=\cos^2\beta. \tag{31}$$

Setting $\cos\gamma=0$ and $\cos\delta=1$ yields the general trigonal prism orbitals of symmetry D_{3h}. Setting $\cos\beta=1$ and $\cos\delta=\sqrt{3}/2$ yields the general trigonal antiprism orbitals of symmetry D_{3d}. The choice of axes differs somewhat from the choice in paper III.[1]

One would expect that orbitals of symmetry D_3 would be employed in strained structures of type AB_3 where B is a chelating group (as an example consider $Cr(C_2O_4)^{-3}$). The fact that AB_3 can be resolved into optical isomers does not prove that A here employs octahedral orbitals.*

[3] E. T. Whittaker, *Analytical Dynamics* (Dover Publications, New York, 1944), p. 9.

* Preliminary calculations indicate that the best trigonal trapezohedral orbitals of composition sp^3d^2 have strengths decreasing from 2.924 to 2.737 as φ_1 (see Table I) goes from 30° to 0°.

THE JOURNAL OF CHEMICAL PHYSICS VOLUME 19, NUMBER 1 JANUARY, 1951

The Entropies of Melting of Metals

R. A. ORIANI
Research Laboratory, General Electric Company, Schenectady, New York

(Received September 18, 1950)

The melting process can be conceived as consisting of first an expansion, and then a disordering of the crystalline structure. The entropy contribution from the first effect is calculated by analogy with the process occurring in a volume expansion within an individual phase; the entropy contribution from the melting disorder is then obtained by difference from the measured entropy of fusion. Tentative conclusions of heuristic value are drawn from the relative magnitudes of the various quantities. A simple model for the melting process is adopted, making possible a correlation between the amount of disordering during melting and the structural contribution to the entropy of melting.

INTRODUCTION

THE melting of a crystal is accompanied by an abrupt change in internal energy, molar volume, and entropy. If the crystal is that of a molecular compound, such as benzene, contributions to the increase of internal energy and entropy arise from (a) change in the character of the vibrations among the unit molecules; (b) change in the internal vibrations within each molecule by virtue of the change in the average force field felt by each molecule; (c) acquisition of rotational degrees of freedom; (d) disordering of the structure. Crystals made up of atoms possess an entropy of melting to which only (a) and (d) contribute, since the atoms do not have internal degrees of freedom, and hence are simpler to treat. Such substances are the metals, simple ionic crystals, and the crystals of the rare gases. Another interesting case where there is no change in the internal coordinates during melting is that of the organic and inorganic crystals whose molecules possess free rotation in three dimensions in the crystalline state, e.g., methane, SF_6. In this discussion, we shall limit our attention to the metals.

At the melting point there is a discontinuous change in properties accompanying the discontinuous change in volume, whereas within any one phase there is a gradual change in properties accompanying a gradual change in volume. However, the vibrational and configurational contributions are proportioned differently

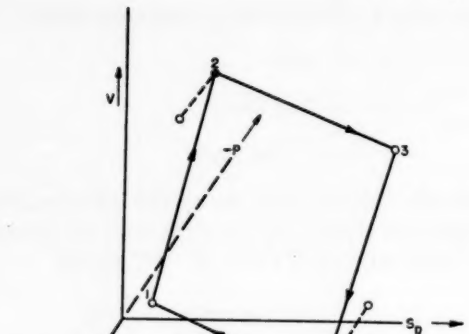

FIG. 1. Expansion-order cycle.

during a one-phase volume change as compared to a volume change during melting, as can be seen by a consideration of the properties of glasses and the nature of cooperative processes. In the first place, the heat capacity of a crystal and that of its corresponding glassy modification are very similar, as are the molar volumes;[1] since a glass is presumably characterized by its possession of a frozen-in configuration of the corresponding liquid state, and the crystal by a definite structure having long-range order, it appears that the structural contribution to the heat capacity in both these solids is small if not negligible. Secondly, the heat capacity of a liquid metal is larger, though only by a small amount than that of its crystal at the same temperature,[2] showing that the rates of change of the vibrations with temperature, or with volume, are very similar despite the greater incoherence in the liquid.

Therefore, we have the situation that in a crystal and in a liquid, a volume expansion is accompanied by an increase in entropy chiefly due to the change in the vibrational degrees of freedom of the assembly, while the configuration remains essentially unchanged. On the other hand, at the crystal-liquid transition there is in addition an entropy change associated with the change in the structure, since the liquid lacks the long-range regularity of the crystal. If one could compute the change in entropy associated with the volume change together with the change in vibrational character, then one could obtain the entropy change associated with the disordering during melting by subtracting the first from the experimental entropy of fusion. This assumes, of course, that at the melting point there exists no change in the type of bonding, i.e., in the distribution of valence electrons, since this would produce a change of entropy that is not presaged by the phenomena within either phase. Such a transformation would probably be indicated by an anomalous change in the electrical resistivity at the melting point.

Such a dissociation of the entropy of melting into two terms, though in a sense artificial, may be of help in understanding the process as well as the marked spread in the experimental entropies of fusion among the metals. Furthermore, from the calculated entropy of melting disorder one may obtain a measure of how disordered a liquid is with respect to its crystal in terms of an adopted model. Finally, such an analysis may help our understanding of the crystal-melt interface, as well as of grain interfaces.

METHOD OF COMPUTATION

As a consequence of the foregoing arguments, the contribution to the entropy of melting of the volume change together with the change in vibrational character may be approximated by

$$(\partial S/\partial V)_T = -\alpha/\beta, \tag{1}[3]$$

and therefore

$$\Delta S_V = -(\alpha/\beta)\Delta V_f, \tag{2}$$

where S is entropy, V is molar volume, α is the cubic coefficient of thermal expansion, and β is the isothermal compressibility, all evaluated for either the crystalline or the liquid phase. Equation (2) is the integrated form of (1), where ΔV_f is the experimental molar volume increase during melting, and ΔS_V is that part of the entropy of fusion associated with volume and vibrational changes only. The entropy of melting disorder, ΔS_D, is then

$$\Delta S_D = \Delta S_f - \Delta S_V, \tag{3}$$

in which ΔS_f is the experimental entropy of fusion.

This dissociation of the entropy of melting into two terms can be visualized by the aid of Fig. 1, in which the following cycle is pictured: (T_0 = melting temperature, P_0 = 1 atmos pressure).

1. Normal crystal, (T_0, P_0)
   Application of negative pressure; heat input
   $\Delta S_D(1\to2)=0$
   $\Delta S_V(1\to2)>0.$
2. Expanded crystal (T_0, $-P$)
   Negative pressure released; heat input
   $\Delta V\ (2\to3)=0$
   $\Delta S_V(2\to3)=0$
   $\Delta S_D(2\to3)>0.$
3. Normal liquid (T_0, P_0)
   Positive pressure applied; heat withdrawn
   $\Delta V\ (3\to4)<0$
   $\Delta S_V(3\to4)<0$
   $\Delta S_D(3\to4)=0.$

[1] W. Kauzmann, Chem. Revs. 43, 219 (1948).
[2] G. Frenkel, *Kinetic Theory of Liquids* (Oxford University Press, London, 1946), Chapter 3.
[3] E. A. Guggenheim, *Thermodynamics* (Interscience Publishers, Inc., New York, 1949).

4. Compressed liquid $(T_0, +P)$
Pressure released;
heat withdrawn.
$\Delta V\ (4\rightarrow 1)=0$
$\Delta S_V(4\rightarrow 1)=0$
$\Delta S_D(4\rightarrow 1)<0.$

1. Normal crystal (T_0, P_0)

Thus, within the framework of the assumptions of this method, both liquid state and crystalline state data can be used to compute ΔS_V by Eq. (2),* though it would appear that the latter is to be preferred since the data for the liquid state probably contain a somewhat larger contribution from changes in local order with change of volume.

Another way of computing $(\partial S/\partial V)_T$ is from an equation of state for either phase. For example, we may use the Einstein model of a crystal as applicable to the metals near the melting temperatures, particularly for the alkali metals, and write[4]

$$S=3Nk\left\{-\ln[1-\exp(-h\nu/kT)]+\frac{h\nu/kT}{\exp(h\nu/kT)-1}\right\}, \quad (4)$$

in which all the oscillator frequencies ν_i are taken as the same. In Eq. (4), N is the Avogadro number, k is the Boltzmann constant, h the Planck constant, and ν the oscillator frequency. Then

$$\frac{dS}{dV}=\frac{dS}{d\nu}\frac{d\nu}{dV}=-\gamma\frac{\nu}{V}\frac{dS}{d\nu}, \quad (5)$$

where $\gamma\equiv -V/\nu(\partial\nu/\partial V)=$ the Gruneisen constant which expresses the variation of lattice frequency with volume. It can be experimentally obtained by using the Debye theory of specific heats together with an empirical equation of state for the crystal, or by measurements of thermal expansion and compressibility.

Differentiating (4) with respect to ν and substituting in (5) we have

$$\frac{dS}{dV}=\frac{3Nk\gamma}{V}(h\nu/kT)^2\frac{\exp(h\nu/kT)}{[\exp(h\nu/kT)-1]^2}\cdot$$

$$=\frac{\gamma C_V}{V}=\frac{\gamma C_P}{V}-\frac{T\alpha^2\gamma}{\beta}$$

since

$$C_V=C_P-\frac{VT\alpha^2}{\beta}\cdot$$

Hence

$$dS/dV\approx\gamma C_p/V \quad (6)$$

which is accurate enough in view of the spread in the experimental values of γ. Integrating (6), we have

$$\Delta S_V=(\gamma C_p/V)\Delta V_f \quad (7)$$

in which C_p and V are to be evaluated for the crystal at some convenient temperature near the melting point.

The data that are available for such calculations are disappointingly meager and of low precision. One would like to have thermal expansion coefficients and compressibilities as functions of temperature, but one is fortunate to obtain values at room temperature and pressure. The most important and most poorly known

TABLE I. Data used in calculations.

Metal	T_0 °K	Solid state V_{293}° cm³/g mole	δV[a]	$10^3\alpha$[b] deg⁻¹	$10^{10}\beta$[c] cm²/g	V_{T_0} cm³/g mole	γ[d]	±%	$V_{(T_0-100)}$ cm³/g mole	$C_p{}_{(T_0-100)}$ cal/deg g mole	Liquid state $10^3\alpha$[e] deg⁻¹	$10^6\beta$[f] atmos⁻¹
Ag	1234	10.28	0.038	0.081	9.87	11.1	2.37	1.7	11.0	7.30		
Al	931.7	10.00	0.06	0.099	13.43	10.6	2.11	3.0	10.5	7.48		
Au	1336	10.22	0.051	0.058	5.77	10.8	2.82	7.8	10.8	7.39		
Cu	1357	7.13	0.042	0.070	7.19	7.66	2.05	4.4	7.61	7.28		
Pb	600.5	18.28	0.035	0.12	23.72	18.9	2.73	—	18.7	6.78		
Li	453	13.09	(0.016)	0.18	86.92	13.5	1.36	14.0	13.2	7.03		
Na	371	23.71	0.025	0.22	156.2	24.1	1.41	11.4	23.6	6.46	0.280	21.0
K	336	45.47	0.026	0.25	356.5	46.0	1.44	7.0	44.8	6.55	0.290	40.3
Cs	302	71.07	0.026	0.29	700	71.3	1.39	7.2	69.2	5.64		
Fe	1803	7.10	(0.02)	0.033[d]	5.826	7.46	1.90	15.7	7.44	10.0		
Cd	594	12.94	0.047	0.126	18.3	13.4						
Mg	923	13.96	0.041	0.075	9.84	14.6						
Hg	234.2	14.19[g]	0.037	0.171	—	14.19					0.182	4.1
Ge	1231.6	13.3	(0.009)	0.023	14.11	13.6						
Ga	303	11.8	(−0.032)	0.054	20	11.8						
Sn	505	16.3	0.028	0.095	6.72	16.6					0.1	3.1

[a] See reference 5, also Smithells, *Metals Reference Book* (New York, 1949), p. 418.
[b] See reference 5.
[c] J. Waser and L. Pauling, J. Chem. Phys. 18, 747 (1950).
[d] See reference 4.
[e] International Critical Tables.
[f] O. J. Kleppa, J. Chem. Phys. 17, 668 (1949).
[g] This figure for solid mercury is the molar volume at the melting point, *Handbook of Chemistry and Physics* (Chemical Rubber Publishing Company, 1949).

* Kubaschewski (see reference 5) has unaccountably represented this quantity by $C_p/(T_0\alpha)$, which by his calculations gives values between 70 and 400 cal/mole deg, a quantity far larger than the total entropy of fusion.

[4] J. C. Slater, *Introduction to Chemical Physics* (McGraw-Hill, Book Company, Inc., New York, 1939), Chapter 13.

TABLE II. Calculated results.

Metal	Structure[a]	g	ΔS_f[b] cal/mole deg	ΔV_f cm³/mole	$\Delta S_V'$[c] cal/mole deg	$\Delta S_V''$[d]	$\Delta S_V'''$[e]	$\Delta S_V'/\Delta S_f$	$\Delta S_D'$[f]	σ
Ag	$A1$	1	2.19	0.42	0.81	0.66		0.37	1.38	0.11
Al	$A1$	1	2.74	0.64	1.05	0.96		0.38	1.69	0.15
Au	$A1$	1	2.27	0.55	1.30	1.07		0.57	0.97	0.068
Vu	$A1$	1	2.29	0.32	0.73	0.63		0.32	1.56	0.13
Pb	$A1$	1	2.04	0.66	0.79	0.66		0.38	1.25	0.096
Li	$A2$		1.53	(0.22)	0.10	0.16		0.07	1.4	0.10
Na	$A2$		1.70	0.60	0.199	0.23	0.195	0.12	1.50	0.11
K	$A2$		1.70	1.20	0.196	0.25	0.208	0.11	1.50	0.11
Cs	$A2$		1.65	1.85	0.180	0.21		0.11	1.47	0.11
Fe	$A2$		1.97	(0.15)	0.2	0.38		0.1	1.8	0.1
Cd	$A3$	1	2.46	0.63	1.02			0.41	1.44	0.10
Mg	$A3$	1	2.34	0.60	1.07			0.46	1.27	0.086
Hg	$A10$		2.38	0.518[g]			0.558	0.23[h]		
Ge	$A4$		4.9	(0.1)	0.05			0	4.9	
Ga	$A11$		4.42	−(0.38)	−0.24			−.05	4.66	
Sn	$A5$		3.41	0.47	1.54		0.4	0.45	1.87	

[a] Strukturbericht symbols.
[b] ΔS_f, experimental entropy of fusion, from tabulation by D. Turnbull, J. App. Phys. 21, 1022 (1950).
[c] Volume and vibrational contribution to the entropy of fusion calculated by Eq. (2) from solid state data.
[d] Same, calculated by Eq. (7).
[e] Same, calculated from Eq. (2) from liquid state data.
[f] Disordering contribution to the entropy of fusion, by Eq. (3), using solid state data for ΔS_V.
[g] *Handbook of Chemistry and Physics* (1949).
[h] For Hg this ratio is $\Delta S_V'''/\Delta S_f$.

set of data is that for the volume expansion at melting; use is made of the data collected by Kubaschewski,[5] who gives the fraction of the molar volume of the crystal by which the metal expands on melting. The ΔV_f was computed by $(\delta V)V_{To}$, and V_{To}, the molar volume at the melting point, To, was calculated by application of thermal expansion data to the molar volume at room temperature, which in turn was calculated from the atomic weight and the density at room temperature.

For the Einstein-solid calculations, the temperature at which Cp and V were computed was chosen at 100 degrees lower than the melting point, chiefly so that the empirical heat capacity equations given by Kelley[6] would better apply. The values of Gruneisen's constant are taken from Slater;[4] we use the mean values wherever more than one value exists, and we indicate the percent spread of the values about the given mean. Table I presents the experimental and calculated values only

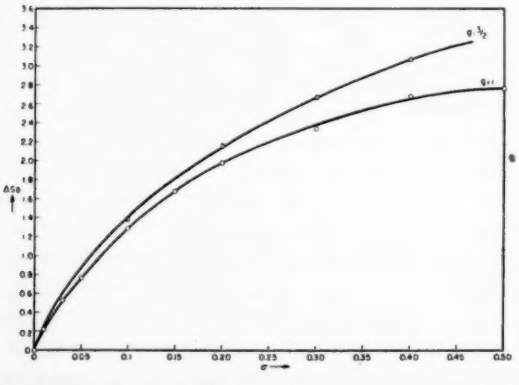

FIG. 2. Entropy of melting disorder *vs* disorder parameter.

[5] O. Kubaschewski, Trans. Faraday Soc. 45, 931 (1949).
[6] K. K. Kelley, Bull. No. 371, Bur. of Mines (1934).

for the metals for which sufficient data exist to enable at least one of the three types of computations to be carried out.

RESULTS

The poorness of the data, as well as the approximations made necessary in the calculations by the scarcity of data, make the intercomparison of the results listed in Table II, risky and tentative. Nevertheless, some interesting observations of heuristic value may be made.

The fact that the ΔS_V as calculated by the methods outlined is in all cases smaller than the measured entropy of fusion is encouraging, since if ΔS_V had turned out larger than ΔS_f it would have been clear indication that the methods are wrong. Further, the agreement for any one metal among the $\Delta S_{V's}$ computed by the various methods is a sign that at least the hypotheses underlying this work form a self-consistent set. The agreement is particularly striking for the alkali metals, for which the Einstein model of a crystal is expected to be especially applicable. Unfortunately, compressibility data for solid mercury could not be discovered, so that an intercomparison cannot be made for this metal for which the ΔV_f is particularly well known. The case of tin must be pointed out as the most egregious example of disagreement, but the coefficient of thermal expansion in the liquid state is known very unprecisely.

Although no great importance should be attributed to the numerical values of ΔS_V tabulated, it is interesting and possibly significant to find that the $\Delta S_V'/\Delta S_f$ values are clustered at around 0.1 for the bcc lattices, whereas the ratio has the value of about 0.4 for the fcc and hexagonal close-packed metals. In other words, the entropy of disordering is proportionately greater in the melting of a bcc lattice as compared with that of the fcc

and hcp lattices, and this can be correlated with the greater free volume and complexity of the bcc lattice. The nearly zero values of $\Delta S_V'/\Delta S_f$ for germanium and gallium, and for tin as well if one uses the $\Delta S_V'''=0.4$ cal/mole deg, might be correlatable with the great complexity of the crystal lattices, leading one to expect large contributions from the entropy of disordering. However, it should be mentioned that the values of ΔV_f are but poorly known; furthermore, these three are the only metals which display an increase in electrical conductivity upon melting,[5] so that there might be a change in the type of bonding during melting. Consequently, one must be cautious in interpreting these numbers as indicating a large change in order, though it is not at all certain that the anomalous change in electrical conductivity signifies a change in bonding.

DEGREE OF DISORDERING DURING MELTING

In order to relate the calculated values of $\Delta S_D'$ to a change in the degree of order during the melting process, it is necessary to set up a model suitable for statistical calculations. For this purpose, the lattice dissociation picture of Lennard-Jones and Devonshire[7] has been adopted in a somewhat modified form to take account of other than the closest-packed lattice. The melting process may then be represented by the scheme: N atoms on N lattice positions $\xrightarrow{T_0}$ $(N\sigma)$ atoms on (gN) interstitial positions $+N(1-\sigma)$ atoms on N lattice points. g is the ratio of interstitial sites to lattice points.
Hence,

$$\Delta S_D=k\ln(W_1W_2),$$

where W_1 = number of ways of arranging $(N\sigma)$ atoms on (gN) interstitial positions

$$=\frac{(gN)!}{[gN-N\sigma]!(N\sigma)!} \tag{8}$$

and W_2 = number of ways of arranging $N(1-\sigma)$ atoms on N lattice points

$$=\frac{N!}{[N-N(1-\sigma)]![N(1-\sigma)]!}. \tag{9}$$

Using Stirling's relation for the factorials, this reduces to

$$\Delta S_D=R[g\ln g-2\sigma\ln\sigma-(1-\sigma)\ln(1-\sigma)-(g-\sigma)\ln(g-\sigma)]. \tag{10}$$

It is easy to show that if $\sigma=0$, i.e., if all atoms stay on the lattice points, Eq. (10) gives $\Delta S_D=0$. Also, it is clear that for $g=1$, as is the case for $A-1$ and $A-3$ structures, the entropy of disordering should reach a maximum when one-half of the atoms have exchanged lattice for interstitial points, and this is the behavior of the equation. In Table II are given the values of "g" for the $A1$, $A2$, and $A3$ lattices, as well as values of σ calculated using Eq. (10) with the tabulated values of ΔS_D; Fig. 2 shows the variation of ΔS_D with σ for various values of the ratio g.

It is to be expected that the closest-packed structures would have the smallest value of g, and that g should increase as the complexity or looseness of the structure increases. It is more interesting to inquire why a given σ should produce a larger ΔS_D the larger the g ratio is. This can be looked at in two ways. Firstly, it is clear that there is greater disorder when an atom that has left a lattice point has a choice of two equivalent disordered positions (i.e., $g=2$) than when it has only one possibility per lattice point. Secondly, the more complex a structure is, the more can it be disordered by a small change in its elements. The values of σ tabulated in Table II are not to be taken too literally, but it appears significant that in all the cases calculated, the fraction of dislocated atoms comes out to be about 0.1, despite the large change in g between the bcc on the one hand and the fcc and hcp lattices on the other. This points up the small amount of disorder that occurs in the crystal-liquid transition.

It is interesting too that crude as this picture of melting disorder is, it displays the rudiments of the transition from long-range order to simply short-range order that is presumed to be characteristic of melting. By long-range order is meant that the positions of atoms far removed from any one given atom can be predicted from the positions of the atoms in the first one or two coordination shells. The values of σ obtained by the present concepts mean that in an assembly of atoms taken from the liquid roughly one in every ten atoms in any one line of atoms will be disordered; since this holds for any atom line, there will be a crystallite region of roughly 1000 ordered atoms at the melting point. Thus, the position of an atom about 5 atoms removed from a given central atom will not be predictable from the local order. The net result is something similar to the Mott-Gurney[8] theory of liquid structure, as consisting of minute ordered domains separated by interfaces of misfit.

[7] J. E. Lennard-Jones and A. F. Devonshire, Proc. Roy. Soc. (London) **A169**, 317 (1939).

[8] N. F. Mott and R. W. Gurney, Trans. Faraday Soc. **35**, 364 (1939).

Analysis of the 774 cm^{-1} (ν_6) Absorption Band of F_2CO

ALVIN H. NIELSEN*
K-25 Research Laboratories, Carbide and Carbon Chemicals Division, Union Carbide and Carbon Corporation,† Oak Ridge, Tennessee
(Received September 11, 1950)

The absorption band at 774 cm^{-1} in F_2CO, which has the appearance of a parallel-type band for a symmetric top, has been resolved into its rotational fine structure with a grating. An analysis of the band has been performed and reveals the band center to be 774.40 cm^{-1} and the average B'' for the two close moments of inertia to be 0.3925 cm^{-1}. The moments of inertia in the upper and lower states are very nearly identical and the coefficient of the $(v_6+\frac{1}{2})^2$ term in the energy is estimated to be 1.4 cm^{-1}.

I. INTRODUCTION

In a recent letter to the editor[1] the infrared and Raman spectra of F_2CO were reported from this laboratory. The infrared bands were all observed with prism optics and the six most intense bands were selected as the fundamental modes. All but one of the bands appeared to have three branches, and with the exception of the band at 774 cm^{-1}, the central branches were quite broad. The envelope of the band at 774 cm^{-1}, however, resembled the envelope of a parallel-type band in that its Q branch was very intense and sharp. It was anticipated that this band might yield to resolution by means of a prism-grating spectrograph. The present paper is a report on this measurement and an analysis of the data obtained.

II. EXPERIMENTAL DETAILS

The automatically recording prism-grating spectrograph[2] of the Department of Physics of the University of Tennessee was used in this experiment. The dispersing elements were a thirty-degree rocksalt prism for monochromatizing the beam, and an 1800 line-per-inch replica grating made by R. W. Wood. Calibration of the grating was effected with the mercury 1.0139976μ[3] line recorded in several orders. The detection system used in this experiment was a Golay pneumatic detector and amplifier, made by the Eppley Laboratories, with a Leeds and Northrup type G speedomax to record the output signal. Fiducial marks were impressed on the chart at intervals of 1 minute of arc by a solenoid pen. Grating angles for the respective spectral lines were obtained by interpolation between these marks.

The F_2CO was contained at a pressure of 5 cm of mercury in a fluorothene absorption cell 10 cm long closed with rocksalt windows.

An attempt was made to record the band at the temperature of dry ice in order to ascertain whether or not certain ones of the absorption maxima observed could be attributed to upper stage transitions. This attempt failed because in the 95 to 100 percent relative humidity at this time of year the cell windows acquired a layer of condensed water which rendered them opaque before the run could be completed.

III. EXPERIMENTAL RESULTS

Figure 1 shows a tracing of an actual record of the rotational structure of the band at 774 cm^{-1}. Frequencies of the lines and their rotational assignments are given in Table I. As is customary, the number in parenthesis is the J value of the lower state. The band is well resolved into rotational lines which are quite evenly spaced at about 0.7 cm^{-1}. To bring out as many lines as possible, sufficient gas was used so the Q branch is 100 percent absorbed. The lines $R(0)$, $R(1)$ and $P(1)$, $P(2)$ and $P(3)$ are very weak and are obscured by the Q branch. Lines $P(4)$ and $P(7)$ are much more intense than would be expected, and it is suggested that they are overlaid by Q' and Q'', the Q branches of the upper stage transitions 2←1 and 3←2. As has been remarked, the attempt to test this suggestion failed in the present investigation. In general, the rotation lines observed were quite sharp as would be expected in a symmetrical top model, and it is on this assumption that the following analysis is made.

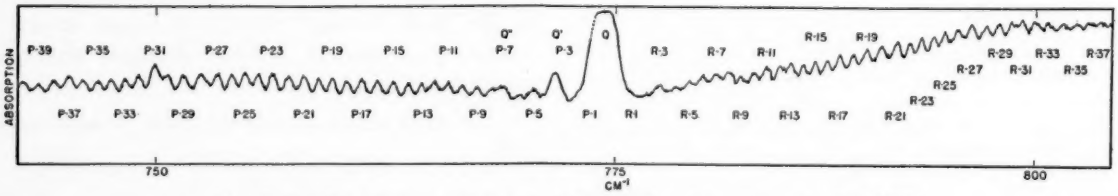

FIG. 1. Tracing of an actual record of the rotational structure of ν_6 in F_2CO.

* The University of Tennessee, Knoxville, Tennessee.
† This document is based on work performed for the AEC by Carbide and Carbon Chemicals Division, Union Carbide and Carbon Corporation, Oak Ridge, Tennessee.
[1] P. J. H. Woltz and E. A. Jones, J. Chem. Phys. **17**, 502 (1949).
[2] A. H. Nielsen, J. Tenn. Acad. Sci. **XXII**, No. 4, 241 (1947).
[3] M. H. M. Hunt and J. S. Campbell, Phys. Rev. **50**, 397 (1936).

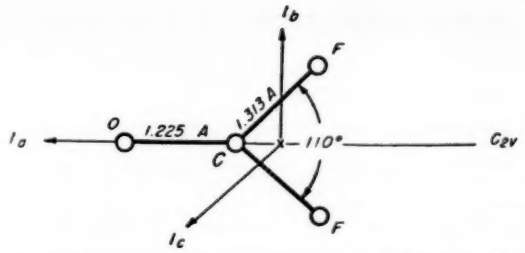

FIG. 2. Geometry and dimensions of the F_2CO molecule.

IV. ANALYSIS

The molecule F_2CO is a planar model with C_{2v} symmetry as shown in Fig. 2. Using reasonable values of the internuclear distances (O=C)=1.225A for H_2CO; (C−F)=1.313A and the F–C–F angle as 110°,[4] the moments of inertia $I_a \leq I_b \leq I_c$ may be computed to be 72.96×10^{-40} g cm², 73.59×10^{-40} g cm² and 146.55×10^{-40} g cm² respectively. It is, thus, evident that with these assumptions the model is very closely an oblate symmetrical top with a $\delta=(I_a/I_b)^2=0.982$. As may be seen from the tables of King, Hainer, and Cross,[5] the K splitting to be expected with levels for a model with such a small asymmetry coefficient would hardly be expected to be observable in the infrared. An oscillation which causes the dipole moment to change along the largest moment of inertia, I_c, of such a model is a parallel-type band. For F_2CO the in- and out-of-the-plane mode ν_6, is such a mode of oscillation. It is, therefore, the only parallel-type band of the six fundamental vibrations and it is natural to assign this frequency as ν_6. The grating record shown in Fig. 1 bears out the close approximation to the symmetrical top.

In Fig. 3 is shown a graph of the relation $R(J-1)$

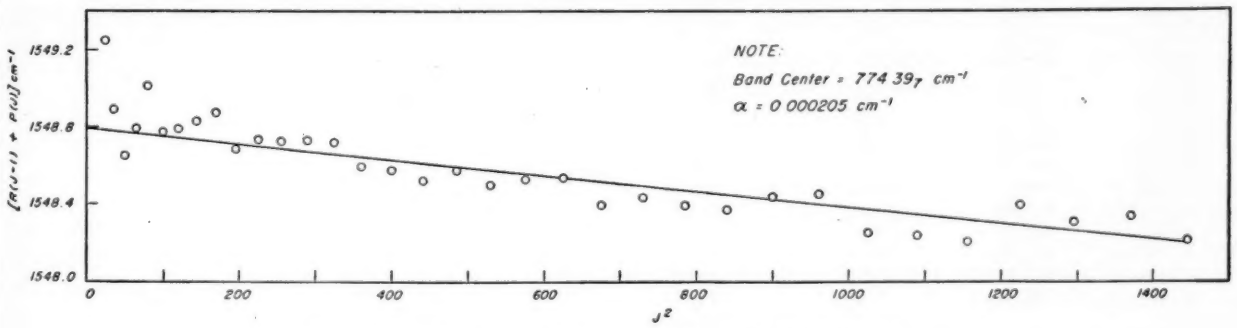

FIG. 3. Graph of $R(J-1)+P(J)$ *vs.* J^2 giving the band center and α.

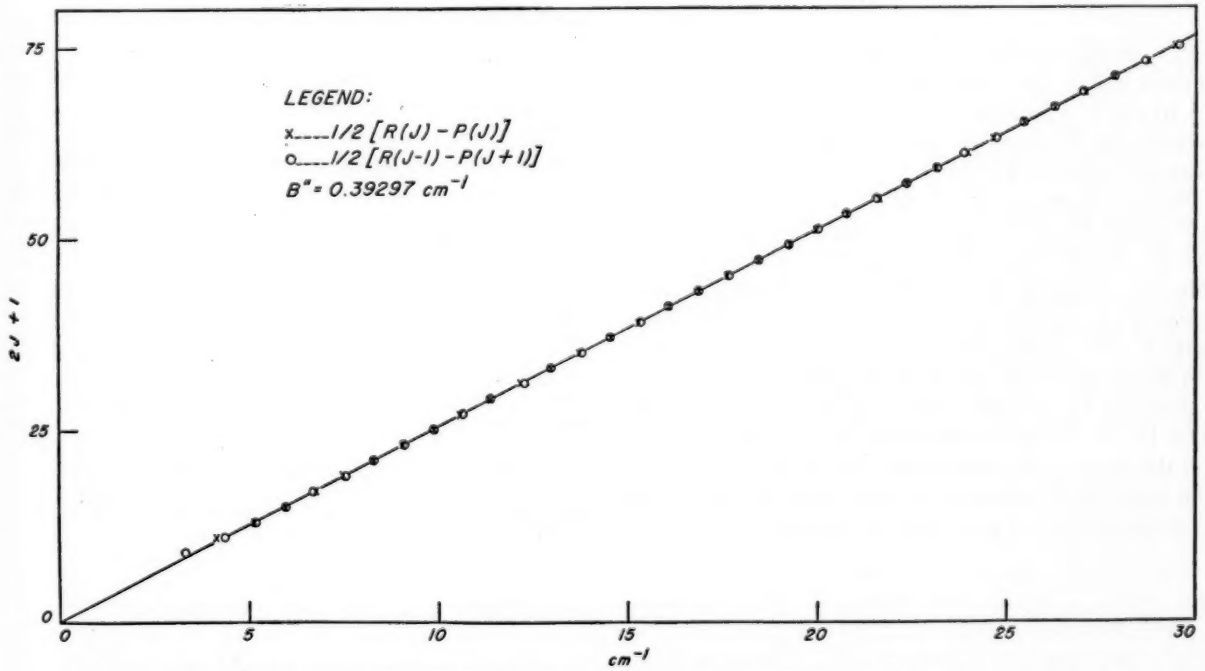

FIG. 4. Graph of the relations $\Delta_2F''=\frac{1}{2}[R(J-1)-P(J+1)]$ and $\Delta_2F'=\frac{1}{2}[R(J)-P(J)]$ *vs.* $2J+1$ giving B'' and B'.

[4] I. L. Karle and J. Karle, J. Chem. Phys. **18**, 963 (1950).
[5] King, Hainer, and Cross, J. Chem. Phys. **7**, 880 (1943).

TABLE I. The rotation-vibration frequencies of ν_6 in F_2CO.

R-branch		*P*-branch	
Identification	Frequency (cm^{-1})	Identification	Frequency (cm^{-1})
R(3)	777.45		
R(4)	778.40	*P*(4), *Q'*	771.58
R(5)	779.12	*P*(5)	770.85
R(6)	779.89	*P*(6)	769.68
R(7)	780.71	*P*(7), *Q''*	768.76
R(8)	781.58	*P*(8)	768.08
R(9)	782.27	*P*(9)	767.33
R(10)	783.08	*P*(10)	766.50
R(11)	783.85	*P*(11)	765.71
R(12)	784.64	*P*(12)	764.88
R(13)	785.29	*P*(13)	764.13
R(14)	786.15	*P*(14)	763.39
R(15)	786.90	*P*(15)	762.58
R(16)	787.64	*P*(16)	761.73
R(17)	788.41	*P*(17)	760.99
R(18)	789.21	*P*(18)	760.21
R(19)	789.97	*P*(19)	759.38
R(20)	790.73	*P*(20)	758.61
R(21)	791.55	*P*(21)	757.79
R(22)	792.29	*P*(22)	757.03
R(23)	793.10	*P*(23)	756.21
R(24)	793.92	*P*(24)	755.43
R(25)	794.58	*P*(25)	754.62
R(26)	795.40	*P*(26)	753.82
R(27)	796.16	*P*(27)	753.03
R(28)	796.94	*P*(28)	752.24
R(29)	797.73	*P*(29)	751.43
R(30)	798.51	*P*(30)	750.60
R(31)	799.19	*P*(31)	749.94
R(32)	799.97	*P*(32)	749.05
R(33)	800.80	*P*(33)	748.27
R(34)	801.59	*P*(34)	747.40
R(35)	802.46	*P*(35)	746.71
R(36)	803.25	*P*(36)	745.85
R(37)	803.94	*P*(37)	745.09
		P(38)	744.28
		P(39)	743.42
		P(40)	742.69

$+P(J)$ plotted *versus* J^2. The intercept of the resulting straight line is the band center which is found to be 774.40 cm^{-1}. The slope of this line, α, the difference between the *B*-values in the lower and upper states, is observed to be 0.000205 cm^{-1}.

Figure 4 shows the $\Delta_2F''=\frac{1}{2}[R(J-1)-P(J+1)]$ and $\Delta_2F'=\frac{1}{2}[R(J)-P(J)]$ plotted *versus* $(2J+1)$ to give B'' and B', respectively. It may readily be seen that the difference between B'' and B' is not obtainable from this graph as the two sets of points are virtually coincident. B'', from this graph, has the value 0.3929 cm^{-1}.

A somewhat more sensitive method for obtaining B'' is shown in Fig. 5 where $\Delta_2F''/(2J+1)$ is plotted *versus* $(2J+1)^2$. In this graph the intercept is $2[B''-(3/2)D]$ and the slope is the centrifugal expansion coefficient *D*. The centrifugal stretching is obviously negligible, and $B''=0.3925$ cm^{-1}. For a nearly symmetric top B'' gives

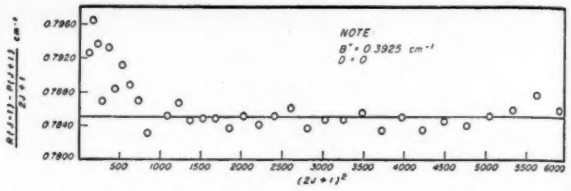

FIG. 5. Graph of $\Delta_2F''/(2J+1)$ *vs.* $(2J+1)^2$ giving B'' and *D*.

the average value of the two nearly equal moments of inertia. The average moment of inertia from B'' is found to be 71.30×10^{-40} g cm^2 as compared with the average value of I_a and I_b, 73.27×10^{-40} g cm^2 from the model in Fig. 2.

As was pointed out earlier the lines labeled Q' and Q'' in Fig. 1 are more intense than is reasonable if they were attributable to $P(4)$ and $P(7)$ alone. They have, therefore, been ascribed to the upper stage transitions 2←1 and 3←2. It is clear from the positions of Q, Q', and Q'' that the levels $v_6=0$, $v_6=1$, and $v_6=2$ are nearly equally spaced. If it is assumed that the anharmonic terms $x_{ij}(v_i+g_i/2)(v_j+g_j/2)$ are all negligible except $x_{66}(v_6+\frac{1}{2})^2$, the coefficient x_{66} can be calculated and is found to be 1.4 cm^{-1}.

V. CONCLUSION

The moments of inertia using the model assumed in Fig. 2 give the least axis of inertia I_a along the C_2 axis, and the average of I_a and I_b about 2.7 percent larger than the observed average.[6] F_2CO appears, therefore, accidentally to be very closely an oblate symmetric top. The vibration-rotation interaction term, the centrifugal stretching term, and the coefficient of the $(v_6+\frac{1}{2})^2$ term in the energy for ν_6 are very small. Attempts to resolve the rotational fine structure of any of the other bands of F_2CO were not successful.

The writer wishes to thank Miss Patricia J. H. Woltz and Mr. George Burke for cell and sample preparation and handling, and Drs. E. A. Jones and D. F. Smith with whom the work was discussed.

[6] While this paper was being prepared for publication, Dr. D. F. Smith of this laboratory observed a great many lines in the microwave spectrum of F_2CO. Using the value of B'' suggested by the present analysis, he has been able to observe and identify eleven lines of the series $J=0$, $K=3\leftarrow4$ in the region 29,000 to 32,000 mc/sec. From the analysis of these lines, he has obtained a preliminary average value of B'' of 0.3965 cm^{-1} as compared with the infrared value of 0.3925 cm^{-1}. The moments of inertia I_a, I_b, and I_c are found to be 69.98×10^{-40} g cm^2, 71.70×10^{-40} g cm^2 and 141.68×10^{-40} g cm^2. It is thus seen that the least axis of inertia does lie along the C_2 axis though its value is somewhat less than that determined from Fig. 2. A complete report of the microwave work will appear in an early Journal.

THE JOURNAL OF CHEMICAL PHYSICS VOLUME 19, NUMBER 1 JANUARY, 1951

Isoconjugate Spectra and Variconjugate Sequences*

JOHN R. PLATT
Department of Physics, University of Chicago, Chicago, Illinois
(Received August 3, 1950)

Two molecules are *isoconjugate* or, more strictly, *iso-π-electronic* if they have the same number and geometrical arrangement of π-electrons bound about equally tightly in a planar conjugated system. Their π-electron spectra then show close resemblances. Example: aniline-styrene.

A *variconjugate sequence* is a series of such molecules in which the binding of some of the π-electrons and the appearance of the spectra slowly changes. Example: fluorobenzene (iso-π-electronic with benzene), phenol, aniline (iso-π-electronic with styrene). Here the heteroatoms are formally saturated and no transitions of nonbonding electrons (*n*-bands) are observed. Second example: phenyl cyanide (almost iso-π-electronic with benzene), benzaldehyde, phenyl azomethane (iso-π-electronic with styrene). Here the heteroatoms are formally conjugated and *n*-bands appear at long wavelengths in addition to the π-spectra. The location of the π-bands partly determines that of the *n*-bands.

The π-spectrum of every organic molecule with a closed-shell ground state lies on a variconjugate sequence between the π-spectra of two conjugated hydrocarbons. Several such sequences involving 90-odd compounds are displayed, showing the different binding of π- and *n*-electrons by different heteroatoms, and the interaction of *n*-bands of neighboring heteroatoms.

An examination is made of the general problem of assigning observed electronic transitions in organic-molecule spectra to particular theoretically predicted transitions. It is shown how variconjugate sequences could be useful in making such assignments.

THIS paper attempts to summarize and justify some general laws governing spectra of organic molecules. It has three major parts which are almost independent. First, the exposition of these general laws. Second, their application to particular cases as shown in the figures. Third, a discussion of needed work on the problem of correlating predicted and observed transitions.

I. SOME GENERAL LAWS OF THE SPECTRA OF ORGANIC MOLECULES

Types of Resemblances between Organic Spectra

Atoms with the same number and kind of outer electrons have similar spectra. This is shown in isoelectronic sequences; and in homologous sequences such as the alkalis, where the total number of electrons is not constant.

Organic molecules with the same number and kind of outer electrons have similar electronic spectra. It is generally accepted that for visible and near ultraviolet absorption, two groups of outer electrons determine the spectra.[1–5] These are the nonbonding electrons, or *n*-electrons, on heteroatoms; and the π-electrons of conjugated systems. We may find resemblances between spectra in which one or the other of these groups is constant: that is, *isohetero* spectra; or *iso-π-electronic* spectra. The great intensity of the π-electronic transitions and the fact that their location partly determines the location of the *n*-bands makes the iso-π-electronic class of more importance to us.

Conditions for Resemblance

Two organic molecules are iso-π-electronic if they have the same number of π-electrons, with approximately the same geometrical arrangement and bound about equally tightly, in a planar conjugated system. These are necessary and sufficient conditions for a close correspondence to exist between their π-spectra.

It is not necessary for the molecules to be *isoconjugate*, i.e., to have the same number of atoms and *π-orbitals* in the conjugated system. This is shown by the spectral pairs in Fig. 4, aniline-styrene, and thionaphthene-naphthalene, which are iso-π-electronic but not isoconjugate. But naturally an isoconjugate pair can have an especially close spectral resemblance, when the binding is about equal. This is shown by the pair, benzaldehyde-styrene, of Fig. 14, and by the aza-aromatics of Fig. 15. (Detailed discussion of the figures will be found in Section II.)

The more restrictive condition that the molecules are *isosteric* is even less necessary. This implies that they are isoelectronic and have the same number and geometrical arrangement of nuclei—not merely for the conjugated system, but for any saturated substituents also.

The condition that a pair of molecules is merely *isoelectronic* is necessary and sufficient for a one-to-one correspondence to exist between all their energy levels. But it is not necessary or sufficient for the close resemblances in the visible and near ultraviolet which are given by the iso-π-electronic condition. Thus the toluene-benzene pair is spectrally similar but not isoelectronic; while many pairs of sterically hindered and unhindered molecules can be found which are isoleectronic but not spectrally similar.

* This work was assisted in part by the ONR under Task Order IX of Contract N6ori-20 with the University of Chicago.

[1] A. D. Walsh, Quart. Rev. Chem. Soc. II, 73 (1948); Proc. Roy. Soc. (London) A185, 176 (1946).

[2] A. D. Walsh, Trans. Faraday Soc. 41, 498 (1945); 42, 62 (1946).

[3] A. Burawoy, J. Chem. Soc. 1865 (1937); 1177 (1939).

[4] H. L. McMurry, J. Chem. Phys. 9, 231, 241 (1941); 10, 655 (1942).

[5] M. Kasha, "Characterization of electronic transitions in complex molecules," Faraday Society Discussion on Spectroscopy and Molecular Structure (September, 1950). M. Kasha and C. Reid, "π- and *n*-electron transitions in *N*-heterocyclics" (to be published).

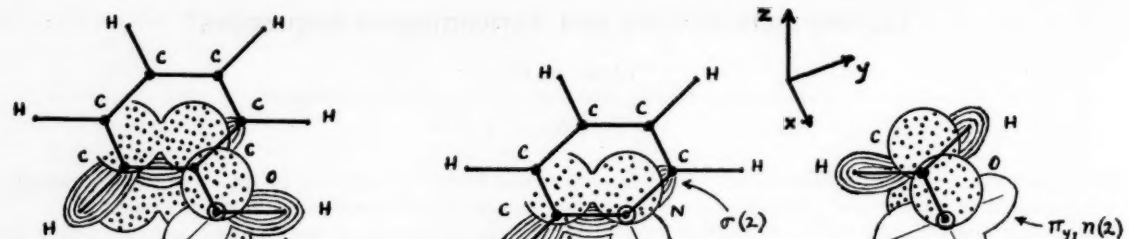

FIG. 1. Spatial arrangement of π- and n-orbitals.

Hereafter the term "isoconjugate" will be used loosely to include "iso-π-electronic" cases so as to avoid the more awkward term except where strict distinction is necessary.

The term isoconjugate is more general than the term *isoaromatic* coined by Longuet-Higgins,[6] since it can be applied also to polyene-type molecules. It implies approximate planarity; but in the plane it requires only a loose geometrical correspondence. Examination of spectral pairs differing slightly in geometry, such as aniline-styrene (Fig. 4), biphenyl-fluorene (Fig. 5), anthracene-phenanthrene,[7] naphthalene-azulene,[8] and *cis*- and *trans*-stilbene (Fig. 16), leads to the conclusion that the number and arrangement of low levels and the general spectral type are determined only by the *topology* of the conjugated system, while the selection rules, intensities, and polarizations are determined by its *symmetry*. Finer geometrical details have less effect on the spectrum.

Variconjugate Sequences

A series of approximately isoconjugate molecules in which the binding of some of the π-electrons changes steadily in the same direction is a *variconjugate sequence*. The spectra in such sequences also change regularly, as seen in the figures, though the accumulated changes may make the initial and final spectra of a sequence very different.

Sequences of neutral molecules with closed-shell ground states may be thought of as starting from a completely conjugated hydrocarbon without triple bonds. This "parent" molecule is not necessarily stable, though all the sequences presented in this paper have stable parents.

A sequence may then be produced in either of two ways: first, by *substitution* of formally *saturated* alkyl or heterogroups on the parent (Figs. 3–5, 8, 9); or second, by *replacement* of carbons in the parent by formally *conjugated or triple-bonded* acetylenic or heteroatoms (Figs. 12–18). Other ways of constructing sequences may be defined, but they seem less convenient. In these two ways of constructing sequences, π-electrons are either added to the parent, more and more loosely bound, or are "subtracted" from the parent by being more and more tightly bound; until in either case we arrive at molecules which are essentially iso-π-electronic with a conjugated hydrocarbon entirely different from the parent.

By substitution or replacement or both, any organic molecule which is not a parent can be built up from one. Sometimes if there are several heteroatoms it may be built up from several different parents and in several ways. We may therefore say that *the π-spectrum of every organic molecule with a closed-shell ground state lies on some variconjugate sequence between the π-spectra of two conjugated hydrocarbons*. These sequences form a "π-network" between all the possible conjugated hydrocarbons. Part of this network is shown in Fig. 10. Every organic spectrum has at least one place on this network. This principle may be useful in predicting unknown spectra, and in predicting the existence of hidden bands. It has been used for the latter purpose in several of the figures. It may therefore be subjected to experimental proof, for instance by a search for these bands at low temperatures or under small perturbations by substituents or solvents.

(In some variconjugate sequences, the position of a given band in the spectra may not move steadily in the same direction as we go down the sequence, in spite of the fact that the conjugation of the substituent π-electrons is changing monotonically down the sequence. The right sides of Figs. 3 and 4 show sequences where the lowest absorption bands move first to the blue and then to the red. An explanation of this behavior is given in Sec. II. It is therefore not always true that the spectrum of a molecule lies between the spectra of two conjugated hydrocarbons; but it does always lie on a smooth sequence connecting two such spectra.)

[6] H. C. Longuet-Higgins, J. Chem. Phys. **18**, 283 (1950).
[7] H. B. Klevens and J. R. Platt, J. Chem. Phys. **17**, 470 (1949).
[8] Mann, Platt, and Klevens, J. Chem. Phys. **17**, 481 (1949).

Besides its π-spectrum, a molecule may have long-wavelength n-electron transitions or n-bands, which are characteristic of the "n-type" of the molecules. Molecules of the same "n-type" are those which contain the same conjugated heteroatom or combination of heteroatoms. The positions of these n-bands are affected by the π-spectrum. Visible and near ultraviolet spectra are therefore determined by two factors: by the n-type, and by the location of the molecule in the π-network. This conclusion is well known, but deserves emphasis.

This classification of the electronic transitions is not complete for spectra at shorter wavelengths, where transitions from bound σ-electrons, Rydberg transitions, or other theoretically possible transitions may appear. In the vacuum ultraviolet, such foreign transitions may confuse the interpretation. They probably occur even at longer wavelengths than the π-transitions in some small conjugated systems such as the ethylene- and butadiene-type molecules of Figs. 12 and 13. But they seem to be mostly covered up when the π-transitions move to the red of 2000A. It seems improbable that they contribute at all to the visible colors of large molecules. In this respect the spectra of large molecules are simpler than those of small.

Substitution by Saturated Groups

In the first type of variconjugate sequence, substitution of formally saturated heteroatoms on a parent conjugated system adds new π-electrons to the system, more or less tightly bound. All π-orbitals are antisymmetric to the plane of the molecule; they have a node in that plane. The new π-electrons perturb the original π-electrons and may complicate the π-spectrum. This is conjugation. Alkyl substitution is similar to heterosubstitution in that it adds new electrons to the system in almost degenerate "σ"-orbitals in bonds out of the molecular plane; for such orbitals can be combined to have some π-character. The weaker interaction of these electrons with the original π-system is hyperconjugation.

Figure 1 shows the spatial arrangement of n- and π-orbitals for various n-types in the LCOA approximation. Table I shows the bookkeeping for the electrons in different n-types. It is assumed in Fig. 1 and in Table I that the substituent orbitals take the most conjugated and most stable configuration, with maximum π_z-orientation (perpendicular to the molecular plane). When steric hindrance disturbs this configuration, as in the molecules of Fig. 6, the bookkeeping changes.

The left side of Fig. 2 shows for saturated substitutions how to derive the changes in the π-spectra from molecular orbital theory. It shows that, as the binding of the added π-electrons (or σ-electrons with π-character) decreases up the variconjugate sequence, certain of the old π-levels may interact with the new. Low levels interact strongly, high ones weakly. Certain other π-levels may not interact, for symmetry reasons. (Their wave functions may have a node through the substituted carbon, perpendicular to the plane.) The longest wavelength transitions generally move to the red, but others may move to the violet; cross-overs may occur; and new bands may appear in a given region. As Fig. 2 suggests, the behavior of the observed

TABLE I. Classification of electrons of substituents in planar conjugated systems.

	Conjugated atoms				
No. valence electrons	4	5	6	7	—
Atomic types	C, Si B^-, B(H),[a] N^+	N, P C^-, O^+	O, S N^-	X O^-	C=C
I. Saturated sequence n-Type designation	{Saturated (hyperconj.)	Amine	Ether	Halide	Vinyl
Bonding σ (number of adjacent atoms)	4	3	2	1	4[d]
π (conjugated)	(2)[b]	2	2	2	2
Nonbonding n (σ?)	(4)[b]	—	2	4	—
II. Conjugated sequence n-type designation	{Aromatic, ethylenic[c]	Aza	Keto, Acid		
Bonding σ (number of adjacent atoms)	3	2	1		
Conjugated π	1	1	1		
Nonbonding n (σ?)	—	2	4		
III. Triple-bonded sequence n-type designation	Acetylenic[c]	Cyan			
Bonding σ (number of adjacent atoms)	2	1			
Conjugated π_z	1	1			
Conjugated π_y	1	1			
Nonbonding n (σ?)	—	2			

Note.—π- or π_z- orbitals antisymmetric to x, y plane. π_y, $n(\sigma)$-orbitals symmetric to plane.

[a] As in diborane.

[b] These figures give the number of bound σ-electrons which can be said to have some π- or n-character, including electrons not on the central substituent atom, as the H electrons in $-CH_3$.

[c] The bookkeeping on an *allenic* carbon, $=C=$, is the same as on an acetylenic carbon.

[d] Not counting the internal σ-bond in the group.

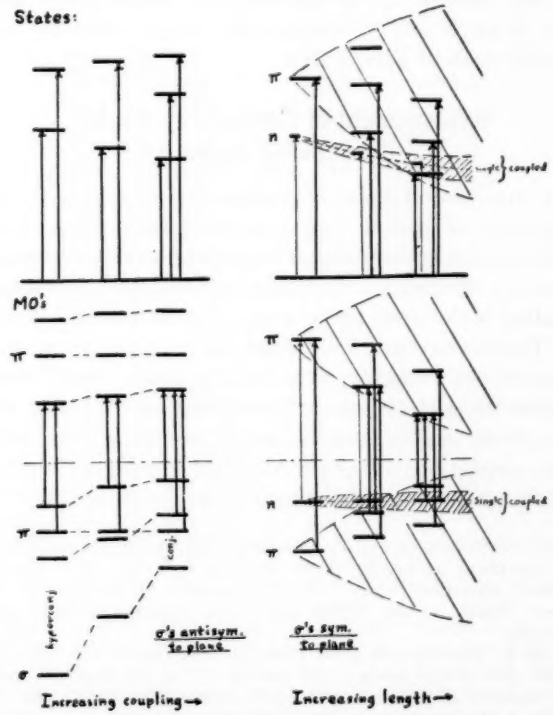

FIG. 2. Interpretation of spectral changes for formally saturated heterosubstitution and formally conjugated heteroreplacement.

transitions in the sequence will often permit a reliable prediction of their polarizations and of the symmetries of the molecular orbitals involved. Several of the sequences are shown in Figs. 3 to 5.

The *n*-electrons of the saturated ether and halide *n*-types (Table I) must be tightly bound, since no *n*-bands are observed in the spectra of Figs. 3 to 5. Even when steric twisting of the π-orbitals of aniline and thiophenol (Fig. 6) converts the substituent π-electrons into *n*-electrons, no *n*-bands are seen.

The conjugation of the π-electrons of the saturated heteroatoms in the phenyl sequence of Fig. 4 seem to get stronger in the order (CH_3), F, Cl, OH, NH_2, SH, ($-HC=CH_2$), which is approximately the order of decreasing ionization potential of these units.[9,10] The degree of conjugation depends not only on the binding of the added π-electrons (α in LCAO theory), but also on their overlap with the other π-electrons (β) and on whether the connection to the parent π-system is single (as in aniline) or multiple (as in pyrrole). The order of increasing conjugation is different in different variconjugate sequences, possibly because of these other factors. Braude and co-workers[11] and Robertson and Matsen[9] have discussed these problems in more detail.

Figure 7 shows the qualitative molecular orbital treatment of the complicated case where the substituent not only adds its levels to the parent levels but also couples parts of the parent hydrocarbon which were formerly uncoupled. (For comparison, the gradual coupling of two independent parents without any added substituent is also shown.) The interpretation of bands as they change up a variconjugate sequence of this type (Figs. 8 and 9) will be less certain than for the simpler cases of Figs. 2 to 6.

Replacement of Carbons by Other Conjugated Atoms

In the second type of variconjugate sequence, replacement of carbon atoms in the parent conjugated hydrocarbon by formally conjugated heteratoms brings no new π-electrons to the system, but brings new nonbonding *n*-electrons (*keto*, *aza*, and *cyan n*-types, Table I). These electrons are in orbitals symmetric to the plane of the molecule, or σ-orbitals, and cannot much disturb the π-electrons or the π-spectrum. But they are often more loosely bound than the π-electrons and may make transitions at long wavelengths to π-type excited states, giving *n*-bands. Transitions to other kinds of excited states seem to occur only at much shorter wavelengths.

The right side of Fig. 2 shows the molecular orbital interpretation of $n\rightarrow\pi$-transitions. With increasing size of the parent conjugated system, *n*-bands of a given type will move to the red only about half as fast as the longest-wavelength π-transitions (Fig. 11); and they are hidden by the latter transitions when the system is large enough (Fig. 15).

The *n*-bands are generally weaker than π-bands because the *n*-orbitals are local, while the π-orbitals are spread over the whole conjugated system. This makes the $n\rightarrow\pi$-transition matrix elements comparatively small. The best-known singlet-singlet *n*-bands, as in ketones and diazines, have extinction coefficients between 10 and 1000. Kasha has suggested that these limits correspond to forbidden ($^1A-{}^1U$) and allowed ($^1A-{}^1W$) transitions.[12] By contrast, the extinction coefficients of singlet-singlet π-bands run from 200 (forbidden) to 200,000 (allowed).

Judging by Figs. 12 to 18, the π-electrons on conjugated heteroatoms are coupled with the rest of the π-electrons more and more strongly in the approximate order $\equiv N$, $\equiv C$, $=O$, $=C$, $=N$. Again the order varies somewhat in different sequences, and the place of $=N$ and $=C$ may depend on whether the connection to the rest of the π-system is single or double. The tightness of binding of the *n*-electrons seems to decrease in the order $=N$, $\equiv N$, $=O$. Braude[11] and Bowen[13] have further discussion.

Interaction of n-orbitals

If two or more $=O$, $=N-$, or $\equiv N$ atoms are present close together in a molecule, their *n*-orbitals may interact to produce double or multiple *n*-bands. This may be the explanation of the double bands in glyoxal (Fig. 13) and of the double nitroso bands (Fig. 12). However, in glyoxal the interpretation is complicated by the probable existence of two geometrical forms, *s-cis-* and *s-trans-*, whose bands may lie at different places; and the second nitroso band may be a Rydberg or other foreign transition like those in other ethylenic types.

The doubling is perhaps more convincingly seen in cases where the *n*-bands from one heteroatom alone might be hidden, but the interaction of two heteroorbitals gives longer wavelength bands which are clearly visible. This happens in pyridazine and possibly phenazine (Fig. 15) and in the azobenzenes (Fig. 16).

[We may even look at O_2 from this point of view, and think of the low singlet-triplet *n*-band of the formaldehyde oxygen atom as being moved in O_2 so far to the red by the interaction that the upper state of this band actually becomes the (triplet) ground state of O_2 (Fig.

[9] W. W. Robertson and F. A. Matsen, "Molecular orbital theory and spectra of monosubstituted benzenes I. II. III. IV." Report of Navy Contract N8onr-70800 (September 30, 1949). The observed effects in the 2600A bands are interpreted very convincingly.

[10] H. B. Klevens and J. R. Platt, J. Am. Chem. Soc. **71**, 1714 (1949). For substituents in the second row of the periodic table, the intensity of the forbidden 2600A benzene transition also depends on the ionization potential of the substituent.

[11] Bowden, Braude, Jones, and Weedon, J. Chem. Soc. **45**, 948 (1946); E. A. Braude, Ann. Rep. Prog. Chem. **42**, 105 (1945).

[12] M. Kasha (private communication). The notation used is that of reference 19. The reader may note for himself that a preponderance of the *n*-bands of Figs. 11–18 fall close to one or the other of these limits.

[13] E. J. Bowen, Ann. Rep. Prog. Chem. **40**, 12 (1943).

12). In a similar way, low triplet states close to the ground state produced by interaction of n-orbitals may account for the instability and reactivity of many molecules containing two or more keto and aza atoms, when isoconjugate molecules containing only one such atom are comparatively stable and inert.]

The n-bands of heterogroups move to the red in the approximate order $-COOH$, $-C=N-$, $-N=C-C=N-$, $-NO_2$, $-C\equiv N$, $-C=O$, $-N=N-$, $-COCO-$, $-N=O$, when attached to π-systems of a given size, judging from Figs. 12 to 18. This order is useful to know in identifying compounds from their spectra. It is not necessarily the order of tightness of binding of the highest filled n-orbitals of these groups, since it depends also on the energy of the lowest unfilled π-orbital of the system. It is worth emphasizing that in this sequence the carboxyl and nitro transitions are 15,000 cm^{-1} higher than the carbonyl and nitroso transitions, respectively. Failure to realize this has fouled up many an interpretation of organic spectra now in the literature.

Acknowledgment

Most of the ideas presented in this section are old. Prominent users of the method of spectral comparisons are mentioned in Sec. III. The previous work most like this in its approach is that of Braude, Price, Walsh, Hausser, and Kuhn,[14] Smakula[14] and Daub and Vandenbelt.[15] Mulliken is of course principally responsible for the separation of spectra into types; McMurry, Kasha, and Burawoy have cleared up special points. I am especially indebted to Kasha, Longuet-Higgins, Matsen, Mulliken, Roothaan, and Price for stimulating discussions.

I have tried to gather these current ideas into a few minimum postulates for interpreting organic spectra. The postulates are bald and explicit enough to be susceptible of theoretical or experimental proof or disproof, or of challenge by opposing interpretations.

The graphical representations are mostly of sequences numerically described by other authors. They are extended to higher π-bands and to more molecules. The connections between bands in the figures are those that first strike the eye. They are intended to be suggestive rather than final. Many will need correction. These errors of individual "assignments" should not invalidate the general usefulness of the idea of isoconjugate spectra or of variconjugate sequences.

So far as I am aware, the classifications and sequences described here remain valid for triplet states, though the isohetero grouping takes on greater importance there, especially when low n-bands are present. However, detailed discussion of triplet states and singlet-triplet transitions must be left to those better qualified to undertake it.

[14] Bibliography in J. R. Platt and H. B. Klevens, Revs. Modern Phys. **16**, 182 (1944).

[15] L. Doub and J. M. Vandenbelt, J. Am. Chem. Soc. **69**, 2714 (1947); **71**, 2414 (1949).

II. PARTICULAR CASES

Discussion of Figures

Figure 1

The numbers in brackets give the population of the orbitals.

The orbitals marked "σ, n" in phenol and pyridine are sometimes assumed to be "$2s^2$," but this is only an approximation. In view of the near-trigonal angles between the other orbitals, these must have some "$sp^2\sigma$" character, partway toward the corresponding NH or CH σ-bond of the isoelectronic molecule. In pyridine, this will help account for the loose binding of these orbitals.

Similarly, in formaldehyde the "σ, n" orbital possibly has some digonal "$sp\sigma$" character. Or, to be more daring, it might mix with the "π_y, n" to have some trigonal "$sp^2\sigma$" character, with the lines of maximum electron density from the O atom pointing in almost the direction the isoelectronic CH bonds would take.[16] This would help account for the still looser binding of the keto n-electrons, which is actually hard to understand on the picture of pure "s^2" and pure "π_y" character for these orbitals.

Figures 3–6, 8, 9, 11–18

Height of horizontal lines indicates electronic levels as given by the long-wave "onset of absorption" for each observed electronic transition. All lower singlet states through the tentatively identified π-states are shown. Higher states are omitted. Vibrational structure is omitted for clarity; as a result, close electronic states may also be inadvertently omitted in some cases.

Length of horizontal lines indicates $\log\epsilon_{max}$ of absorption from ground state. Rounded-off numerical values are given where known. In several lighter molecules the extinction has not been measured but can be estimated from "appearance pressures" of the bands in the vapor to within a factor of perhaps 3. Intensities of some of the solution bands from unpublished work of Klevens and Platt (KP) have been estimated in the same way where photometry of the plates has not been completed. These estimated values are not shown, but have been used in drawing the horizontal lines. I am indebted to Dr. Klevens for permission to use some of these data in advance of full publication.

The "onset of absorption" is uncertain to ± 1500 cm^{-1} in many cases. It is plotted in the figures instead

[16] J. R. Platt, J. Chem. Phys. **18**, 932 (1950), has shown that the equilibrium position of the protons in simpler hydrides is almost exactly in the place predicted from the electron distribution for the united atom. The discussion in the text implies a reversal of this argument: if the CH_2 bonds of the hydride ethylene are trigonal, then the directions of maximum electron density near the oxygen "united atom" in formaldehyde must also be near-trigonal.

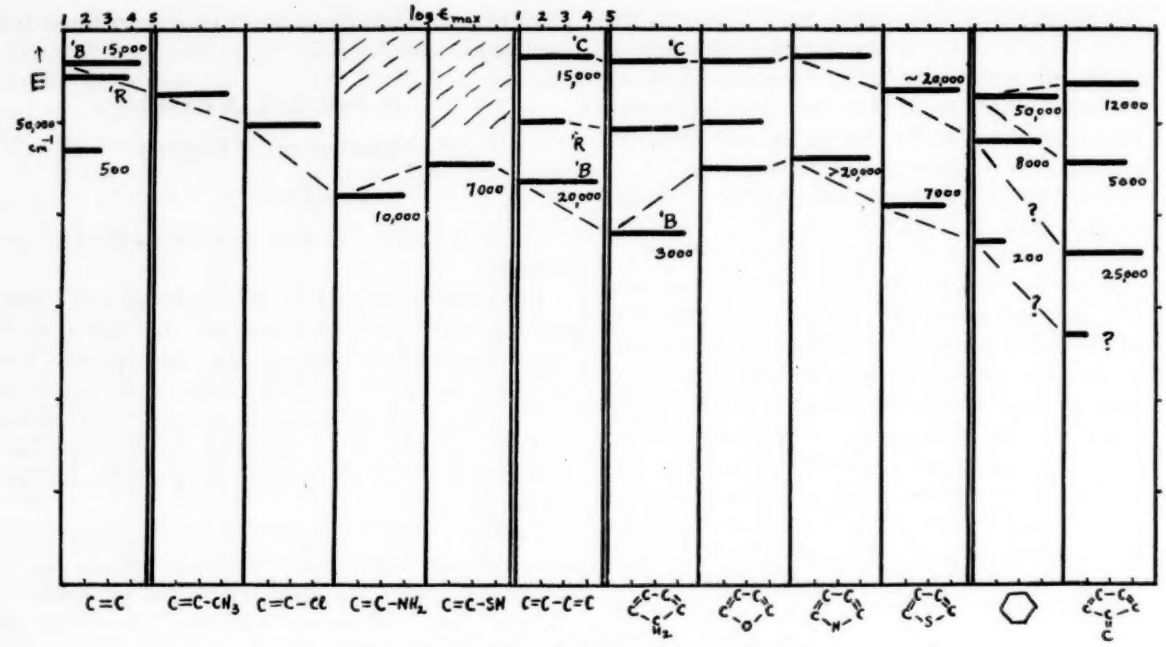

FIG. 3. The ethylene-butadiene-benzene sequence.

of "peak position" because it permits inclusion and comparison of many transitions whose peak position is even more uncertain: e.g., partly hidden *n*-bands; and transitions with peaks beyond the limit of observation, whose presence is indicated by strongly rising absorption at the limit. For diffuse transitions with observed peaks but no clear vibrational structure, the "onset" is arbitrarily taken near the position of one-third peak intensity.

The energies of the electronic states taken from absorption curves in this way still need to be corrected to some standard conditions for all the spectra. Solution measurements on the simple unsubstituted conjugated systems indicated in the legends were chosen as standard. Observed vapor transition frequencies were therefore corrected downward by 2000 cm^{-1}; and positions of transitions of alkyl derivatives were corrected upward 2000 cm^{-1} for each alkyl substituent.

In the figures, shading indicates short-wavelength regions where the spectra of some molecules have not been measured.

Figure 3

In vinyl amine and vinyl mercaptan, Braude's peak positions have been corrected downward by amounts estimated from the curves of octene[17] and butadiene, so as to give "onset of absorption."

The $N \rightarrow R$ (Rydberg) bands indicated in four compounds are sharp with much vibrational structure and relatively low integrated intensity. They are quite distinct from the π-bands in these molecules.

The large change of intensity of the first band from butadiene to cyclopentadiene is well understood. It is due to the symmetry change, from the *s-trans*-configuration to the *s-cis*.

The "blue shift" of the five-ring heterocyclics from cyclopentadiene is easily explained by both the "free-electron"[18] and the LCAO molecular orbital methods. It is principally due to the greater spacing of orbital energies in a ring system like cyclopentadienyl ion than in a linear system like butadiene, of about the same length. The blue shift from benzene is due to the greater spacing of the orbital energies in a five-ring than in a six-ring. Both methods predict the center-of-gravity of the first four singlets and triplets of pyrrole to lie near 73,000 cm^{-1}. This is on the assumption that the nitrogen and carbon bindings (α) are equal. The predicted center lies above the two known singlets, as it should. Similar blue shifts can be observed under similar circumstances in linear systems; as when four electrons are crowded into three orbitals in going from glyoxal to nitromethane (Fig. 18).

The benzene-fulvene correspondence is very speculative. But the third (degenerate) band of benzene must split. And in the similar case of naphthalene-azulene,[4] the transitions move to longer wavelengths in the five-ring isomer, in the same way suggested here. However, the first indicated transition of fulvene rests only on its brown color, and on the 40-yr.-old measurements of Stark. It would seem more reasonable for the first transition to be strong, as in thiophene, which also has low symmetry, instead of weak like the first (forbidden) transition of highly symmetrical benzene. This leads one to wonder whether the 36,000-cm^{-1} fulvene absorption

[17] Rusoff, Platt, Klevens, and Burr, J. Am. Chem. Soc. **67**, 673 (1945).

[18] J. R. Platt, J. Chem. Phys. **17**, 484 (1949).

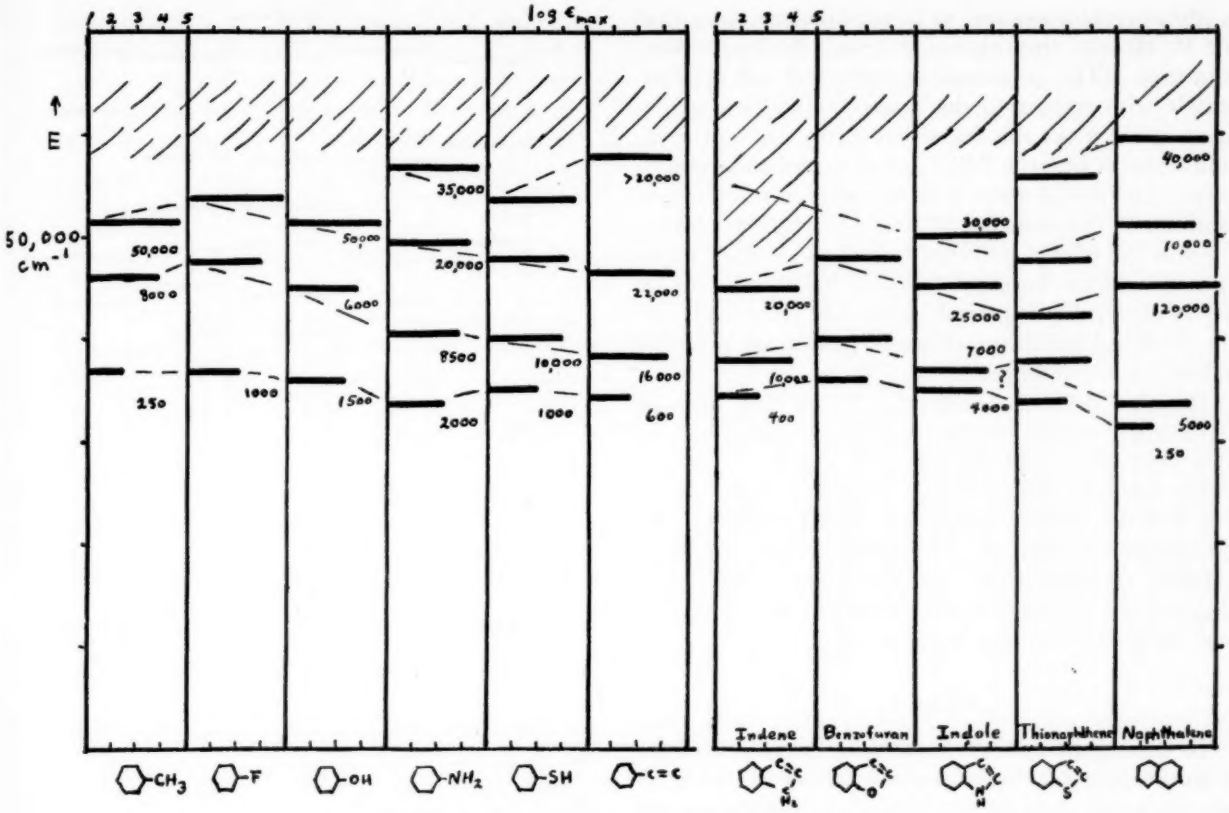

FIG. 4. The benzene-styrene-naphthalene sequence.

region is not really the lowest absorption, consisting of two strong overlapping transitions with a long absorption tail into the visible.**

Figure 4

See especially reference 9 for discussion of the $Ph-X$ variconjugate sequence.

Comparison with Fig. 3 shows that changes of binding of π-electrons affect spectral positions less strongly in large molecules than in small ones.

The position of the second transition in benzene is evidently more sensitive to perturbations than that of other transitions. This was true of all the similar (^1L_a) transitions in condensed-ring systems.[7] It strengthens the supposition that the total wave function of the upper state has an antinode rather than a node at the carbon positions in the ring, where substitutional perturbation is strongest. This would correspond to the $^1B_{1u}$ symmetry which has been assigned to this upper state in benzene.

From one point of view, the first effect of a perturbation on the ring is to remove the degeneracy of the third benzene transition (see also diphenyl methane, Fig. 9). The third and fourth transitions of aniline may be thought of as the components of this transition, with the perturbing "amine" transition hidden or lying higher. But actually any such separation of transitions is artificial; their properties mix. Moreover, the benzene spectrum may also be transformed gradually into the aniline spectrum by a different route (Fig. 6), with a different correspondence of transitions! This situation is familiar in atomic spectra, where there is a one-to-one correspondence between the energy states in an *LS* and a *jj* coupling scheme, but where the connection between the states depends on the route by which the transformation from one scheme to the other takes place. (The transformations of Fig. 4 correspond to the solid lines in Fig. 2 of Matsen I.[9] Those of Fig. 6 correspond to a change toward the dotted lines in his figure.)

The weakest transitions of ring systems always seem stronger for hetero *n*-types than for hydrocarbons, even when the symmetry is about equally low (thiophenol-styrene).

However, all the molecules of low symmetry in the center of Fig. 4 show more "long-field" character[19] in the near-equality of the intensities of different transitions than do the pure condensed-ring "round-field" systems at the left and right sides of the figure.

The molecular orbital polarization prediction for the first four transitions of styrene and the molecules next to styrene is *long, trans, trans, long* (Fig. 7), but there

** *Note added in proof:* Dr. B. Pullman, in a private communication, essentially confirms the fulvene levels and intensities as given in Fig. 3. This settles the question in the text above, but raises another: is there then a weak hidden transition in thiophene and in pyrrole?

[19] J. R. Platt, J. Chem. Phys. **18**, 1168 (1950).

is probably a cross-over, as in naphthalene, such that the 38,000-cm^{-1} transition of styrene is the longitudinal transition. (The polarizations indicated are approximately with respect to the longest axis.) This assignment would make this transition correspond to the ^1L_a transitions of benzene ($^1B_{1u}$) and of naphthalene (transverse); and would make it fit smoothly in position and intensity in the sequence of strong longitudinal transitions in the phenyl polyenes (where the weaker transverse transition becomes hidden). In styrene, as in naphthalene, this is probably the only cross-over, and the third and fourth transitions of styrene are probably indeed *trans* and *long*, respectively.

The blue shift after indene in Fig. 4 may have an explanation similar to that advanced above for the blue shift after cyclopentadiene in Fig. 3.

The correspondence indicated on the right side of Fig. 4 is not certain. Cross-overs could occur. Placing thionaphthene next to benzofuran would suggest a different correspondence. However, the styrene-naphthalene correspondences just mentioned lend some support, at least to the low assignments.

Figure 5

To the extent that the methylene group of fluorene is not conjugated, the conjugated part of this molecule has the same topology as biphenyl; to the degree that it is, the molecule has the same topology as carbazole and phenanthrene.

The hidden transition is suggested for biphenyl by the following arguments. First, the observed strong π-transition of biphenyl splits into two in the iso-π-electronic molecules fluorene and bipyridyl (Fig. 16). It seems unlikely that the new transition is one of the symmetry-forbidden transitions of biphenyl, because these should, and probably do, lie higher (see below). No other new transitions are expected; so the new transition is probably a weak hidden transition of biphenyl which is strengthened and shifted in the other molecules so as to be revealed.

Second, a long-wave weak transition appears in other ring systems; it is probably hidden in the same way in anthracene, which has the same symmetry and about the same size as biphenyl. Third, extending this argument, the molecular orbital polarization predictions are *long, trans, trans, long*, for the first four transitions of biphenyl. These correspond respectively to the ^1L_a, ^1L_b, ^1B_a, ^1B_b types in condensed-ring systems.[18] If the departure in diphenyl from the "round-field" intensity pattern were like that noted above for styrene, the second or *trans*-transition would still have enough ^1L_b character to have an extinction coefficient less than 1000 or 2000. Therefore, it is not the strong 49,000-cm^{-1} transition; this must be the third predicted transition, and the second transition must be hidden.

The connection implied in Fig. 5 between the hidden transition and the low fluorene transition also connects

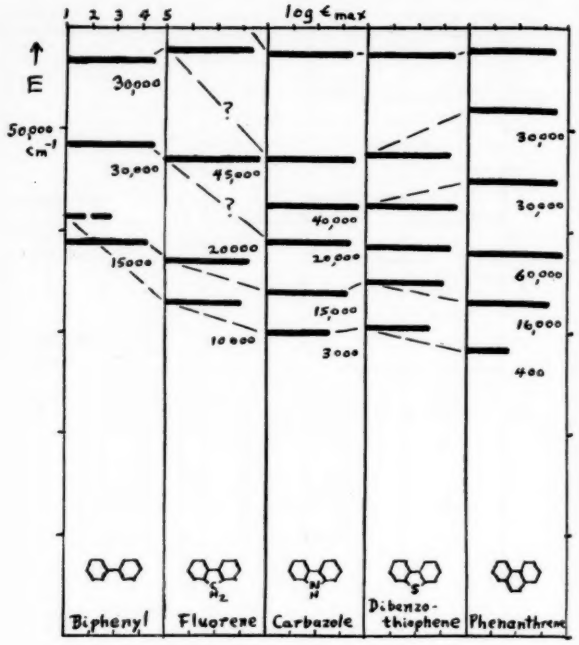

FIG. 5. The biphenyl-phenanthrene sequences.

the hidden transition up the variconjugate sequence to the ^1L_b phenanthrene transition.

This connection is further supported by another argument. A longitudinal transition, and a transition derived from ^1L_a, should be the stronger of the first two transitions in fluorene. From the intensity measurements the first biphenyl transition, which is presumed to have both these properties, should therefore go into the second fluorene transition, as shown.

A weak transition at 43,000 cm^{-1} was found on the KP plates for fluorene, but it may be an acenaphthene impurity since it is not in the ICT curve; it is omitted from Fig. 5. Another weak transition at 27,000 cm^{-1} in the ICT curve is not on the KP plates and has also been omitted. (Kasha was also unable to find this band.)

The changed appearance of the spectra between fluorene and carbazole suggest that some symmetry-forbidden transitions of biphenyl have become strongly allowed in carbazole with the loss of central symmetry, just as in the parallel anthracene-phenanthrene case.[7] Examination of intermediate spectra between fluorene and carbazole will be necessary to clear up the correspondence.

The 42,000-cm^{-1} transition shown for carbazole may be false. If so, the 39,000-cm^{-1} transition has peculiar vibrational structure. Comparison with dibenzothiophene suggests that the 42,000-cm^{-1} transition is real.

The 48,000-cm^{-1} band of dibenzothiophene has a peculiar vibrational envelope; there may be another band at 51,000 cm^{-1}. This spectrum, with six and perhaps seven π-transitions of about equal intensity and no obvious pattern, is the most complicated of any conjugated system I have so far examined. The fact that it may be plausibly understood from comparison

with the spectrum of phenanthrene, and that that spectrum may be understood in turn from comparison with anthracene, and that in turn from naphthalene and from benzene, shows the power of the comparative method. The polarization predictions for phenanthrene[7] should apply to dibenzothiophene and to carbazole if the connections shown in Fig. 5 are correct; the polarizations may be experimentally tested.

Phenanthrene is also iso-π-electronic with fluorenone (Fig. 11) and with benzazulene. The connection of its transitions with the low π-transitions of fluorenone is obvious. The presence of a single odd-carbon ring in the latter system spoils the distinction between ^1L_a and ^1L_b character. This may be related to the unusual equality of intensity of the two low π-transitions of fluorenone. A careful theoretical study would be necessary to predict their polarizations. The comparison between phenanthrene and benzazulene has been made elsewhere.[20]

Figure 6

The levels in columns 3, 4, 6, and 7 have been corrected upward for the red shifts due to the methyl groups on the ring so that all the aniline spectra will be comparable, and all the sulfides. The twisted dimethyl aniline in the third column is iso-π-electronic with benzene. The nonbonding orbitals on the nitrogen must be almost symmetric with respect to the benzene plane. Since no n-band appears, they are more tightly

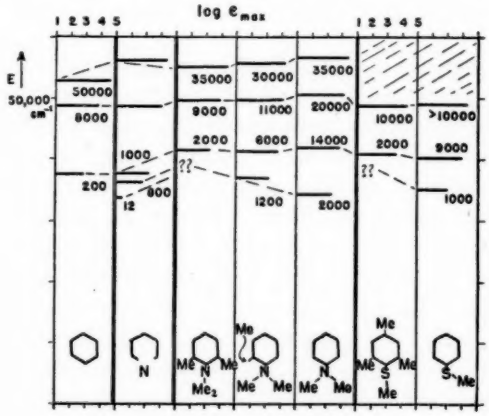

FIG. 6. Sterically twisted orbitals.

bound, as in all saturated heteroatoms, than the symmetric n-electrons of pyridine, which show two n-transitions below the π-transitions. Untwisting the aniline produces a new transition in column 5 from the interaction of the nonbonding electrons with the benzene π-system. Thus we carry the benzene transitions into aniline up a variconjugate sequence like that in Fig. 4, but the progressive perturbation here takes a different path from that in Fig. 4 and the transitions here have a different correspondence. In Fig. 4, the LCAO integral α for the loosely bound substituent electrons started large, decreasing up the sequence, with β almost constant; here α is almost constant, while β starts from zero and increases up the sequence.

The last two columns show the same changes in a similar sequence of phenyl methyl sulfides.

Figures 7, 8, 9

The left side of Fig. 7 shows how the weak coupling of two separate ethylenes through a CH_2 group or an oxygen atom produces conjugation in miniature. The N—V_1 and probably the N—V_4 transitions[14] of such molecules are shown in Fig. 8. One might look for intermediate N—V_2 and N—V_3 transitions of divinyl ether at low temperatures.

For coupling of two benzenes through a substituent, the theoretical pattern for the variconjugate sequence in the center of Fig. 7 is very complicated. As a result the interpretation and correspondence of the empirical transitions in Fig. 9 is obscure even though the spectra look comparatively simple. (The benzene states in Fig. 7 are shown first degenerate as in the simple LCAO picture, then multiple from the splitting produced by electron interaction.) Empirically, the first effect of a CH_2 link is to double the third benzene transitions. This effect could be either (a) the removal of the degeneracy of this transition in the two rings, with their spectra still superimposed, or (b) a coupling effect like that above in ethylene, with the degeneracy not conspicuously removed. Possibility (a) seems a little less plausible, since the simple removal of degeneracy is not obvious in the monosubstitutions of Fig. 4 where a comparable effect might have been expected.

The lowest transition of diphenyl amine would have one of the three components shown in Fig. 7 forbidden, if the molecule were centrally symmetric. The other two components would have opposite polarizations, corresponding to the two lowest transitions of the separated phenyl rings. This is no doubt the reason why the two lowest transitions of benzene come together to make the lowest transition of diphenyl amine as we go up the variconjugate sequence of Fig. 9. The other possible components must be weak and hidden in the intermediate molecules. Similarly, one component of the third transition of benzene must go into the second transition of diphenyl amine (Fig. 7), as shown in Fig. 9.†

The transverse component of the low diphenyl amine transition must go into the first transverse transition of iso-π-electronic stilbene; this band would be expected to be weak and to lie above the first strong longitudinal transition of stilbene by the same reasoning we used for the similar case of biphenyl in Fig. 5.

The right side of Fig. 7 shows the behavior of levels when two separate conjugated systems are slowly coupled without an intermediate saturated substituent. This might be the case if they are originally connected

[20] H. B. Klevens, J. Chem. Phys. 18, 1063 (1950).

† *Note:* The last column of Fig. 9 should be deleted, since the molecule is sterically hindered and nonplanar.

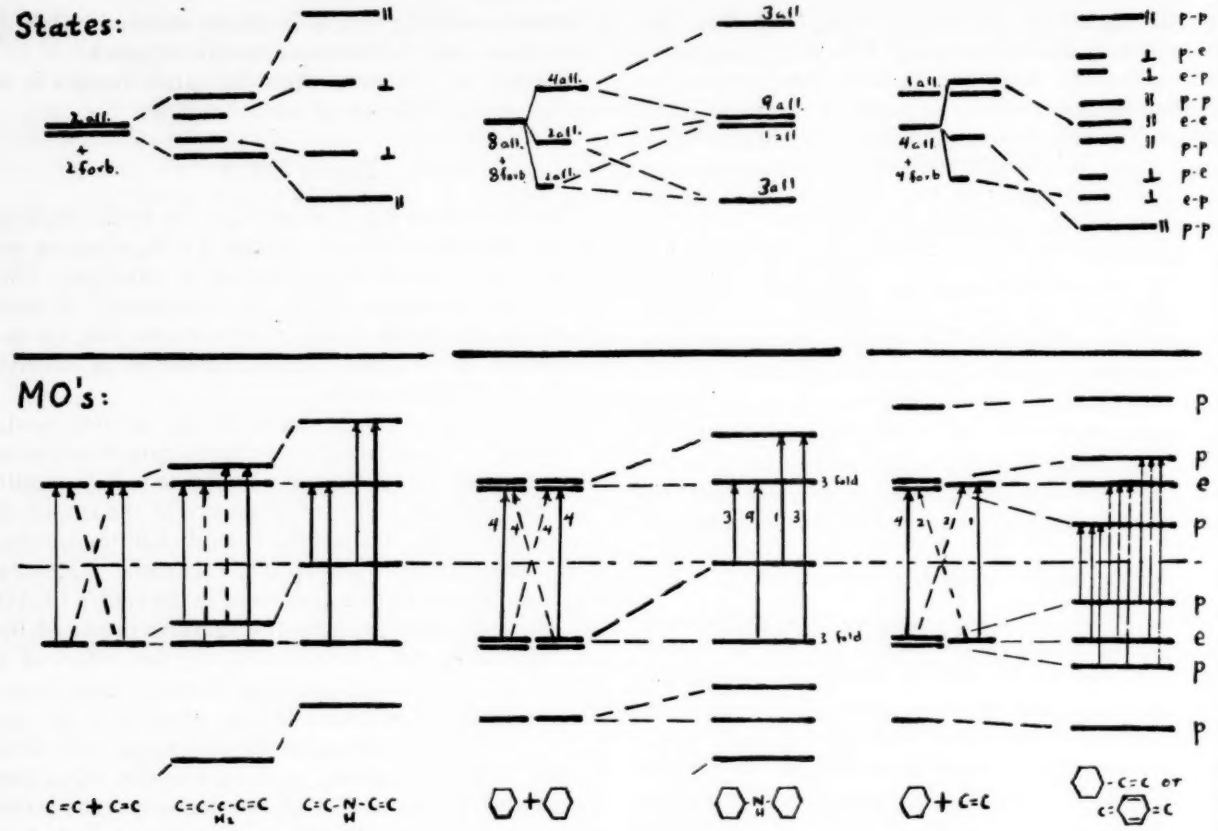

FIG. 7. Interpretation of spectral changes from coupling of separated π-systems.

by a single bond with their planes twisted perpendicular by steric hindrance and if the twisting is gradually reduced. The spectra will change continuously, but more analysis would be necessary to predict the direction of changes in particular transitions of particular molecules. For styrene, the transformation of this kind and the assignments are discussed under Figs. 4 and 6 (aniline).

The case of styrene illustrates two important points about phenyl-chain systems, including phenyl polyenes, diphenyl polyenes, *p*-polyphenyls, and molecules iso-π-electronic with them, such as the thiophene and pyrrole analogs.

The first point is that for every ring in such systems there is one filled orbital (two π-electrons) and one empty orbital, each with a longitudinal node (marked *e* in Fig. 7). These have about the same energy as the ethylene orbitals, or as the second and third benzene orbitals. For symmetry reasons, they do not mix with the transverse-node-orbitals (*p* in Fig. 7). *The transverse-node orbitals are therefore just the same in number as, and are similar in nodal properties, electron distributions and energies to, the total set of orbitals of a simple polyene of the same length.* In computing length for this purpose, each phenyl counts as four atoms. This orbital similarity accounts for the similarity of long-wave spectra of polyenes to those of phenyl-chains ($p-p$ in Fig. 7), which was one of the earliest important results of spectral comparisons.[14] The phenyl chains can be derived in principle from the polyenes by vinyl substitution on the "side" of the chain; this is then a case where substitution of one conjugated system on another does not much affect the long-wave spectra of the latter. The visible similarity of a phenyl-chain spectrum to that of the corresponding polyene of the same length does not hold for benzene because of electron interaction, nor yet for styrene, but it does for diphenyl, phenyl butadiene, and the longer molecules, where configuration interaction becomes relatively less significant.

The second, and less familiar, point about phenyl chains is the following. There must be additional transverse transitions ($e-p$ and $p-e$ in Fig. 7) from the ethylenic-type longitudinal-node orbitals, which have no counterpart in the polyenes. This is shown by the orbital diagram and confirmed by the spectrum of styrene. As chain length is increased, the first of these transverse transitions should move to the red about half as fast as the longest-wavelength longitudinal ($p-p$) band. This is why the first (transverse) transition of styrene becomes hidden in longer molecules. The transverse transitions ($e-p$ and $p-e$) in phenyl-chains will be weak, having small matrix elements like

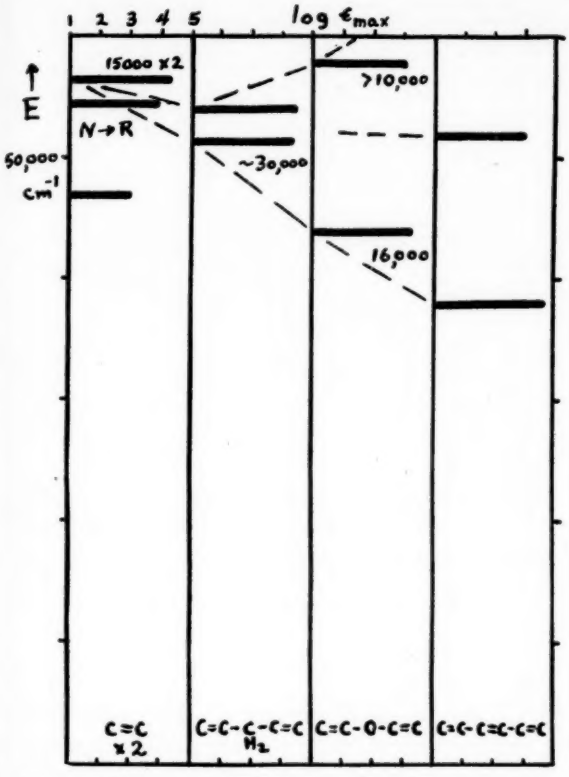

FIG. 8. The separated-ethylene-to-hexatriene sequence.

the n-bands discussed in the first section and for the same reason.

As a corollary of the second point, there must also be additional new longitudinal transitions in phenyl-chains at still shorter wavelengths. These are ethylenic-type transitions near 2000A ($e-e$ in Fig. 7) between one ethylenic-type orbital and another, and their position will be almost independent of the molecular length. These will be fairly strong transitions. Such transitions do seem to appear in those phenyl-chain spectra which have been examined to such short wavelengths[14] (Figs. 14, 16, and 18).

These various conclusions do not depend on the location of the rings along the chain. Thus, for instance,

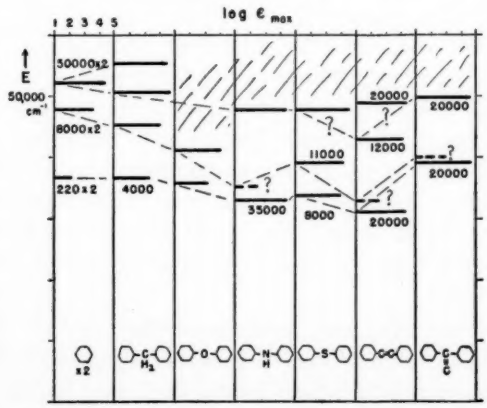

FIG. 9. The separated-benzene-to-stilbene sequence.

there is a close correspondence of the π-spectra of styrene and of quinone (not shown here), through the latter has additional n-bands. Their polarizations should also correspond. This is in spite of the fact that quinone and styrene have a different topology and so are not strictly iso-π-electronic.

There will be many other cases besides the phenyl-chains where substitution of a small conjugated system on a large one will produce little change in the long-wave spectra. These cases occur when the highest filled orbitals of the large system are well above those of the small, and the large system absorbs at much longer wavelengths. After coupling, the long-wave spectra will then still have properties predominantly those of the large system. This appears to be the reason for the stability of the spectra of large condensed-ring systems and of porphines under vinyl, keto, quinone, or other substitutions. The stability is more marked when the small system is substituted at the side of the large system rather than at the end, because the perturbation of the highest filled orbitals is then generally smaller.

Figure 10

This figure shows a section of the π-network of variconjugate sequences between conjugated hydrocarbons differing by two π-electrons. The number of π-electrons increases generally to the right. The length of a conjugated system increases going up the diagram; the first absorption transition then moves to the red. The width of a conjugated system increases going down the diagram; the first absorption transition then changes position very little, or may move to shorter wavelengths.[21]

Heavy dashed lines show the five variconjugate sequences of saturated substituents which were explored in Figs. 3 to 5. The two light dashed lines show the se-

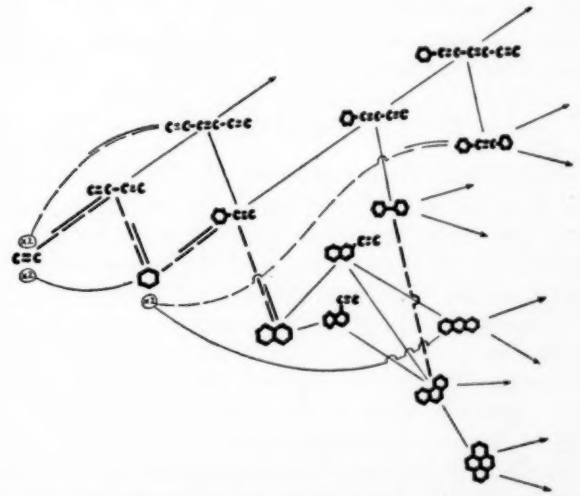

FIG. 10. Branching diagram for building up conjugated systems by successive addition of π-electrons.

[21] Longuet-Higgins, Rector, and Platt, J. Chem. Phys. 18, 1174 (1950).

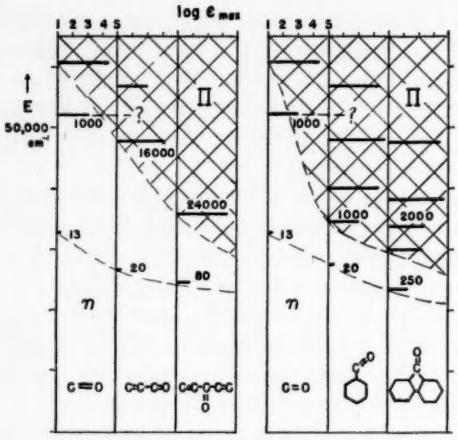

FIG. 11. Isohetero sequences: ketones.

quences made in Figs. 8 and 9 by connecting two separate systems by a saturated substituent. The short solid lines show the six variconjugate sequences produced by conjugated replacement in Figs. 12 to 16. The length of the solid lines suggests how far the character of the spectra changes toward that of the smaller conjugated system in these sequences.

The remaining light lines in the figures indicate variconjugate sequences which have not been examined here. Still other sequences are possible between these different hydrocarbons, but have been omitted from the figure to avoid confusion.

Figure 11

The cross-hatching indicates the energy band of the π-states. The formaldehyde absorption near 51,000 cm^{-1} is characteristic of the keto group. It is hidden by π-transitions in the longer molecules. It does not fit well into the Rydberg series. Perhaps it is from excitation of the second pair of more tightly bound nonbonding electrons of the oxygen atom.

See the discussion of Fig. 5 for comparison of fluorenone with phenanthrene.

Figure 12

Dashed lines connect the *n*-bands, and connect what are presumed to be transitions of π-type. The π-transitions lose their characteristic ethylenic appearance in the triple-bond systems as the electrons become more tightly bound. This figure shows the greatest number of transitions other than π- or *n*-bands. Individual examination would be necessary to interpret them. Their extinctions usually lie between 100 and 1000. They still appear in some of the triple-bond molecules of Fig. 13, but not in larger systems.

McClure pointed out that the red bands of HNO and PhNO (Fig. 14) must be singlet-singlet, because their intensities are too large for singlet-triplet bands. The fact that their position fits in well with our expectations, as discussed in Sec. I, supports this interpretation.

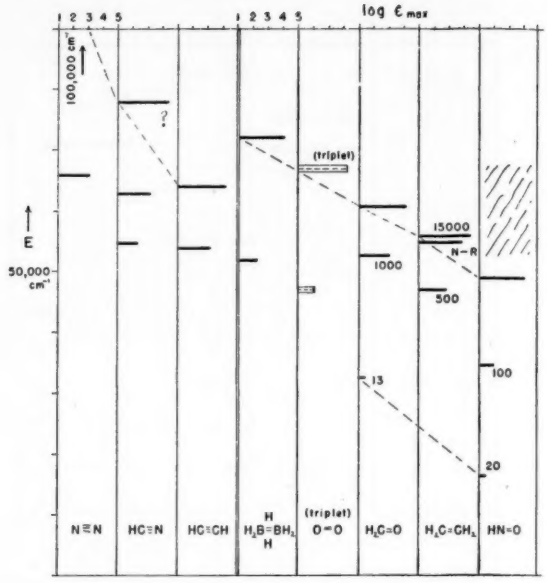

FIG. 12. Heteroreplacements in ethylene.

Figure 13

The blue shift or disappearance of the 51,000-cm^{-1} keto transition in glyoxal is strange. The transition at 60,000 cm^{-1} is suggested by strongly rising absorption at the limit of the KP plates; but the intensity, and so the transition type, is not known.

In propenal, the weakness of the second indicated π-transition is strange if it is a π-transition; no π-transitions of this molecule should be forbidden. A Rydberg transition nearby has been omitted from Fig. 13. The 8000-cm^{-1} red shift of the first π-transition of propenal on substitution of three methyls, as in mesityl oxide, is strangely large.

Braude's peak positions have been treated as in Fig. 3. The presence of an OH on some of his conjugated systems has been corrected for as though it were an alkyl group; empirically, this procedure is justifiable for most compounds.

Figure 14

The *red* shift of divinylacetylene from hexatriene is strange. The second band may be double.

Phenyl isocyanide has much ionic character in the C—N group. A theoretical analysis of the behavior of the *n*-electrons under these circumstances would be interesting; one would expect them to be less tightly bound than in phenyl cyanide. If so, the KP plates do not go to high enough concentrations to show the *n*-band.

It is surprising how closely the π-spectrum of phenyl cyanide approaches that of toluene or phenol. The CN π-electrons are so tightly bound that they hardly perturb the phenyl spectrum.

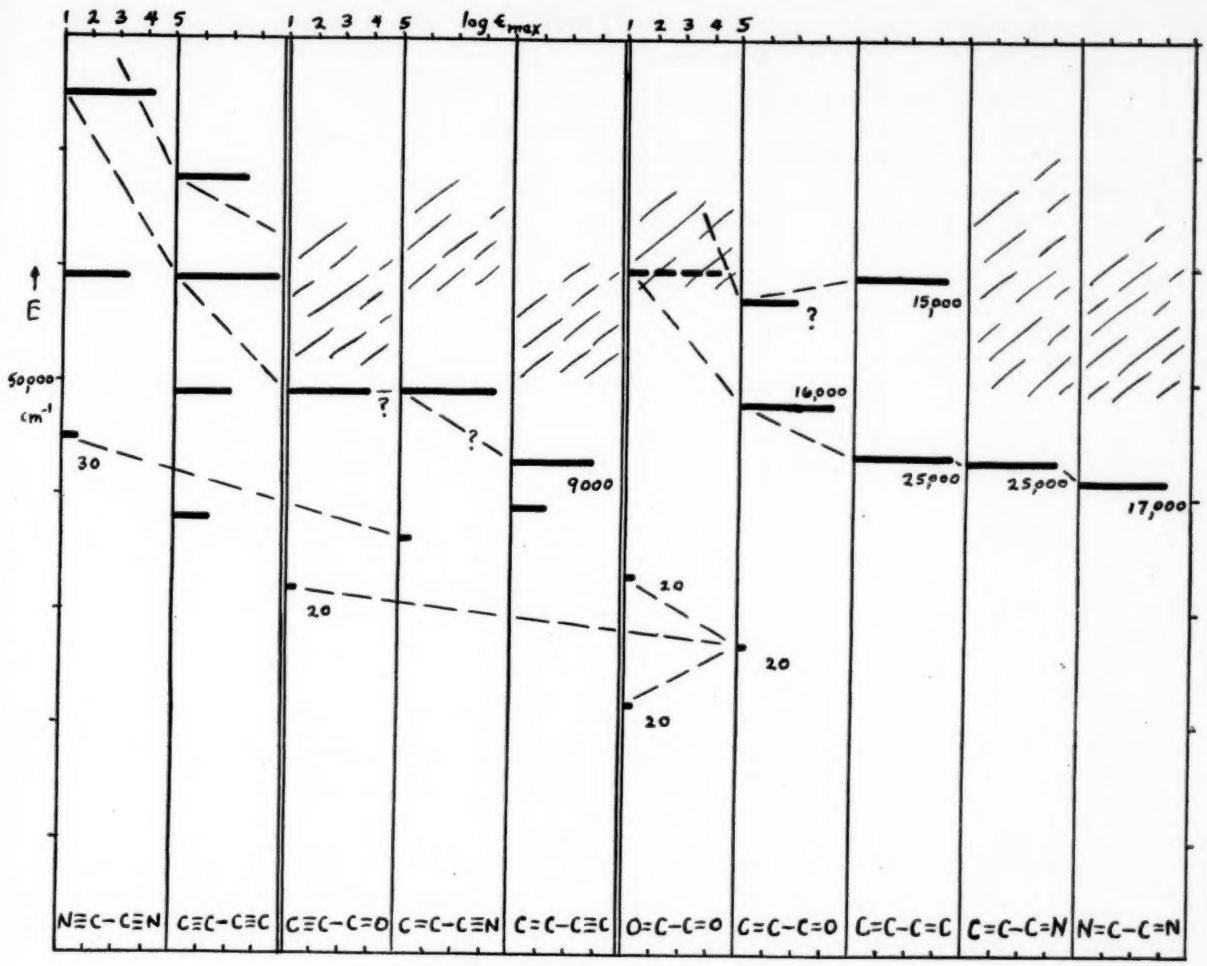

FIG. 13. Heteroreplacements in butadiene.

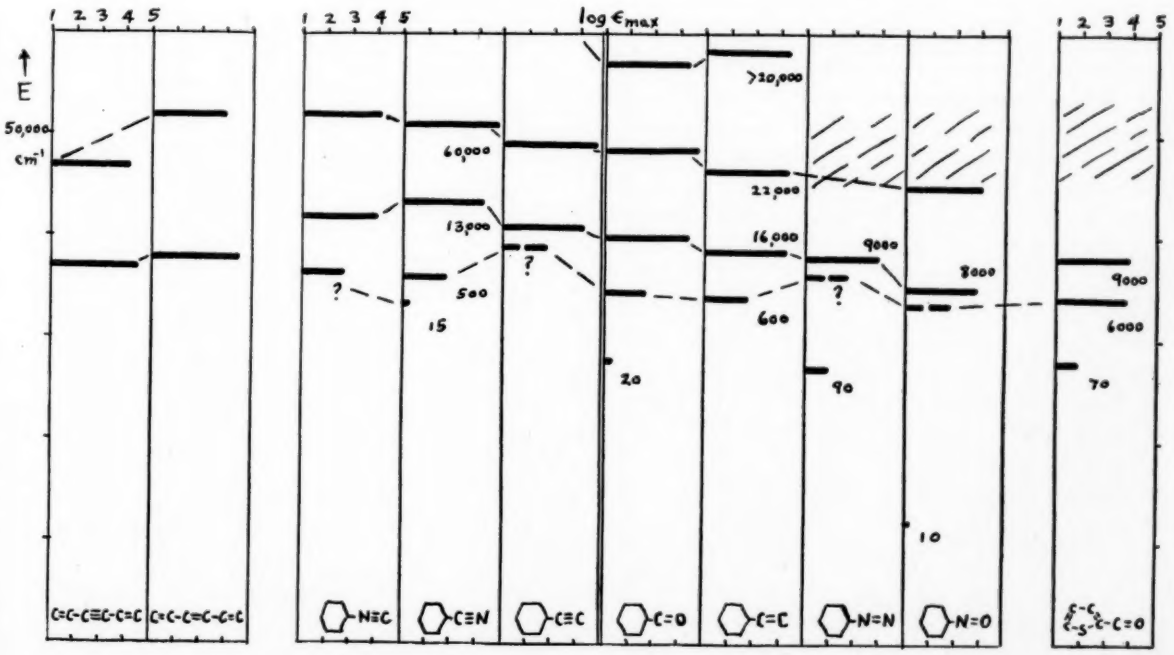

FIG. 14. Heteroreplacements in hexatriene and in styrene.

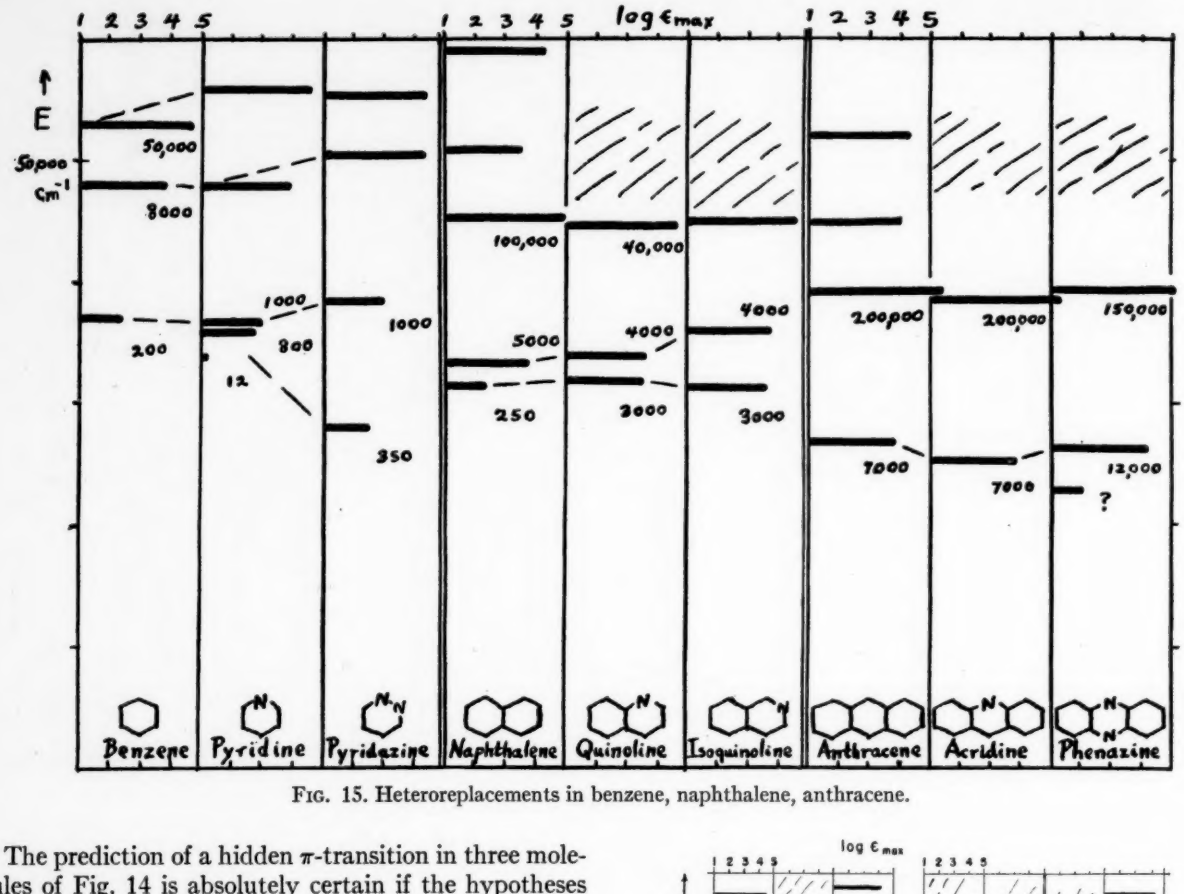

FIG. 15. Heteroreplacements in benzene, naphthalene, anthracene.

The prediction of a hidden π-transition in three molecules of Fig. 14 is absolutely certain if the hypotheses of this paper are correct.

The red band of nitrosobenzene was discussed under Fig. 12.

The last column of Fig. 14 shows how the spectrum of a molecule with both saturated and conjugated hetero atoms could be predicted from the simpler cases discussed in this paper. The spectrum of this molecule has a close correspondence to that of benzaldehyde, though the transverse transition is much stronger because of the permanent transverse asymmetry introduced by the saturated sulfur atom (as in Fig. 4).

The quinone spectrum also has a close correspondence to the spectra in Fig. 14, as discussed under Fig. 7.

Figure 15

The *n*-transitions are closer to the π-transitions for aza atoms than for keto, and so become hidden in molecules as large as naphthalene unless two heteroatoms are present to produce an interaction and red shift so that the *n*-bands can again be seen. So phenazine has an absorption tail as indicated, which is not present in acridine.

The heteroatoms again strengthen the weak (^1L_b) π-bands.

Figure 16

The biphenyl group and its interpretation was discussed under Fig. 5.

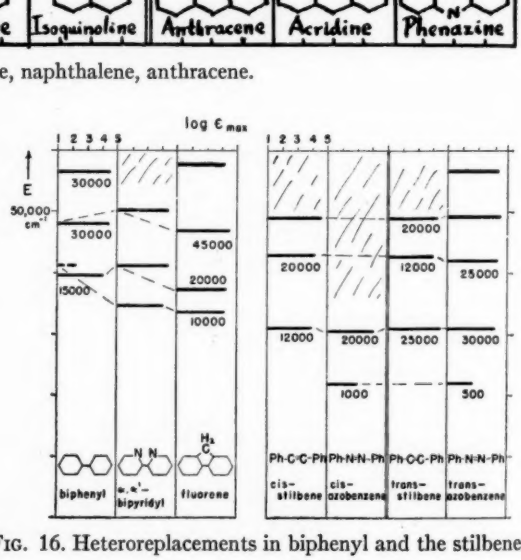

FIG. 16. Heteroreplacements in biphenyl and the stilbenes.

In the stilbenes and azobenzenes, the relative strength of the first π-transitions (longitudinal) in the *trans*-configuration and of the second π-transition in the *cis*-configuration is explained by the same reasoning as was applied to the similar difference between the *s-trans*- and *s-cis*-spectra of butadiene (Fig. 3). The first two observed strong π-transitions are essentially polyene bands but the 49,000-cm^{-1} band may be the stationary ethylenic-type band of phenyl-chains (see under Fig. 7).

Figure 17

The trisubstituted borazole spectra have been shifted upward 5000 cm^{-1} to correct for the simple red shifts

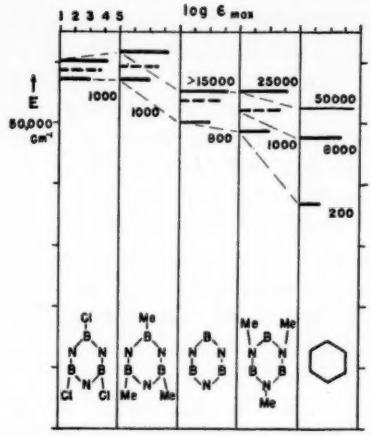

FIG. 17. Inductive variations in the borazoles.

produced by the substituents so that all the spectra will be comparable. In this variconjugate sequence of borazoles, the molecule on the left has so much electronic charge induced on the nitrogens and so little on the borons that it tends to have a saturated-amine, saturated-boron character and the spectrum perhaps approaches that of a perturbed cyclo-hexane. On the right, the π-electron charge distribution approaches uniformity (though the total charge distribution approaches 100 percent ionic character) and the spectrum approaches that of benzene. The dashed levels have been inserted to correspond to the molecular orbital prediction of an exact one-to-one correspondence in classification, sequence, and intensity of the borazole bands with benzene. Transitions to these levels are probably hidden by the adjacent allowed transition.

Figure 18

The acid and nitrospectra could be derived from the spectrum of vinyl alcohol (like vinyl chloride in Fig. 3) by replacement of ethylenic carbons by conjugated heteroatoms. Or they could be derived from glyoxal by replacing a C_2H_2 section by NH or CH_2, as in going from styrene to aniline or toluene (Fig. 4). The spectra are at shorter wave-lengths than for glyoxal both because the molecules are shorter (as discussed under Fig. 3) and because the electrons would be more tightly bound by the formally saturated C or N atoms. (The planarity of formic acid merely means that the conjugation of the two electrons contributed by the carbon is complete and is not mere hyperconjugation; i.e., these electrons are in true π-orbitals, and the carbon is C^-, iso-π-electronic with saturated N.)

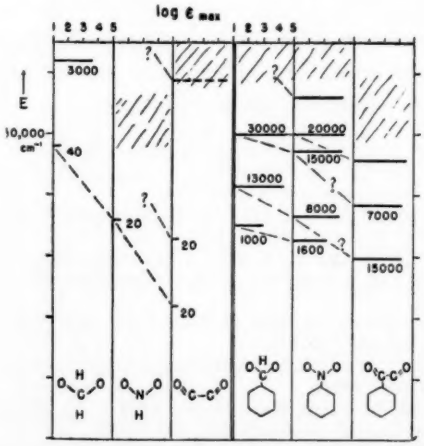

FIG. 18. Acid and nitro spectra.

The 61,000-cm^{-1} transition of formic acid does not seem to be strong enough or to lie at short enough wavelengths for a π-transition. Perhaps it is a Rydberg transition or another transition from the nonbonding electrons of the oxygens; it may be like the 51,000-cm^{-1} transitions of formaldehyde.

The π-electrons in the acid group are so tightly bound that they scarcely perturb the phenyl spectrum in benzoic acid; its π-spectrum resembles that of toluene or phenol just as did the spectrum of phenyl cyanide (Fig. 14) and for the same reason. The *n*-bands of benzoic acid and nitrobenzene are hidden.

The tempting interpretation of the nitrobenzene spectrum is that it is the benzene spectrum with the degeneracy removed and with one of the perturbing transitions visible. Examination of the molecular orbitals suggests that in this interesting case this obvious interpretation is substantially correct. The other transitions created by the coupling, which were so troublesome to deal with in Fig. 7, will be forbidden here.

Phenyl vinyl ketone is presumed to be the conjugated system of the *enol* form responsible for the spectrum given in the last column, since this should be the most stable form of the molecule in question.†† The spectrum has been corrected upward from that of benzoylacetone 2000 cm^{-1} for the OH red shift. This molecule should be iso-π-electronic with nitrobenzene. The correspondences have been suggested on the basis of corresponding intensities; and by analogy with the styrene-phenylbutadiene empirical correspondence, where a similar obliteration of the long-wave weak π-transition occurs; and because molecular orbital theory suggests that there should be a weak hidden transverse π-transition here of $e-p$ type (Fig. 7) corresponding to the first weak transverse phenyl π-transition of nitrobenzene. The *n*-band of the keto group is also hidden. The 46,000-cm^{-1} transition may be the longitudinal $e-e$ transition like the one in styrene and like the fourth transition of nitrobenzene.

III. THE ASSIGNMENT OF TRANSITIONS IN THE SPECTRA OF ORGANIC MOLECULES

The central problem of the theory of the spectra of organic molecules is to predict the observable properties of all electronic transitions for any molecule.

The problem of validating such predictions has two parts. First, we must be sure that observed transition *a* corresponds to predicted transition *A* and not to *B*.

†† *Note:* The right-hand oxygen atom in the formula should have been a carbon.

This is called *assignment* of the transition. Second, we can then examine whether transition *a* has the observable properties predicted for *A*. These parts of the problem are not independent. Commonly, we use some of the predicted properties in making the assignment, and then either confirm the assignment and the theory if the other properties are present, or repudiate the theory if they are not and if no rearrangement of assignments will improve the agreement.

In atomic spectra the predictable observable properties of a spectrum line are: (a) the frequency; (b) the intensity; (c) the spacing and properties of certain neighboring lines, as in a multiplet or a series; and (d) the effect of perturbations, such as the Zeeman effect.

The absolute frequency and intensity are usually too poorly predicted to be more than a rough guide in assignment. Assignment is more commonly made from properties of types (c) and (d) and confirmed by other properties of type (c) or (d).

In organic spectra the predictable observable properties of an electronic transition are: (a) the frequency; (b) the intensity and polarization (and decay time in emission); (c) the spacing and properties of certain neighboring transitions; (d) the effect of perturbations, such as immersion in solvents, or change of pH, or chemical substitutions or replacements at particular positions in the molecule; and (e) possibly the pattern and envelope of vibrational structure for the transition.

Here, unfortunately, properties (a), (b), (c), and (e) are all so poorly predictable in current theories that they are almost useless for assignment when there are several observed electronic transitions close together. An exception is polarization, which is accurately predictable for the theoretical transitions of a symmetrical molecule; but this property is hard to determine experimentally.

The type (d) effects then become of the utmost importance for the assignment of electronic transitions and for the validation of theory. These grosser perturbations may even play a more important role than the Zeeman effect plays in atomic assignments, since they are able to make up, by their number and variety and the great range of effects produced, for the crudeness of our other knowledge of organic spectra. The type (d) effects are also the properties of a transition which are of most importance to both analytical and fundamental chemistry, as shown by the extensive experimental literature on them.

The examination of variconjugate sequences is an examination of some of these perturbations. It could evidently be made into a major method for the assignment of transitions and for the testing of theory.

Need for Perturbation Theory

A few theoretical predictions have been made of the effect of substitution and replacement on electronic states, wavefunctions and transitions. In some cases, the perturbation point of view has been used. Recently, Longuet-Higgins has discussed the effects in the ground states of heteroaromatics.[6] Matsen and Robertson have treated the 2600A bands of benzene derivatives,[9] building on the earlier work of Sklar, of Förster, and of Herzfeld. Roothaan and Mulliken have compared the states and spectra of benzene and borazole.[22]

It is very important to the interpretation of organic spectra to extend and to generalize these studies. Undoubtedly the perturbation effects are implicit in the wave function of a theoretical electronic state, just as the Zeeman effect is implicit in an atomic wave function. The connection needs to be made explicit. At present many a molecule has several excited states and wave functions predicted from the theoretical side, and the perturbation effects are known for several observed transitions from the experimental side; but the additional theoretical guidance is lacking which would enable us to bridge the gap with certainty and to assign a particular observed transition having particular perturbation effects to a particular upper state wave function. Under these circumstances the theoretical predictions of states and of transitions float in a vacuum and can neither be confirmed nor refuted. This explains the disputatious character of most present assignments outside of the polyenes.

As a stopgap solution, semiclassical or elementary valence-bond arguments have been used with great ingenuity by many authors to infer the assignment of transitions from the perturbation effects—that is, from spectral comparisons. Notable studies are those of Scheibe,[23] Lewis and co-workers,[24] and Zechmeister and co-workers.[25] Clar carried the comparison method to a high point in his studies of homologous aromatic spectra.[26] Jones made polarization assignments from the behavior of aromatic spectra under various alkyl substitutions.[27] Braude confirmed polarization assignments by intensity calculations.[28] But some of the inferences based on these arguments are now known to be wrong or to be misapplied, and the others, except in the polyene-type molecules, lack quantum-mechanical justification.

The present paper and earlier ones[18,19] are attempts to apply elementary quantum-mechanical arguments to such comparisons. The conclusions are tentative and need strict theoretical examination.

---

[22] C. C. J. Roothaan and R. S. Mulliken, J. Chem. Phys. **16**, 118 (1948). See also R. S. Mulliken, J. Chem. Phys. **7**, 121, 339 (1939) and later papers, on alkyldienes.

[23] G. Scheibe, Kolloid-Z. **82**, 1 (1938); Z. angew. Chem. **42**, 631 (1939).

[24] G. N. Lewis and M. Calvin, Chem. Rev. **25**, 273 (1939); G. N. Lewis and J. Bigeleisen, J. Am. Chem. Soc. **65**, 520, 2102, 2107 (1943).

[25] L. Zechmeister *et al.*, Ber. **72**, 1350, 1678, 2039 (1939); J. Am. Chem. Soc. **65**, 1522 (1943).

[26] E. Clar, *Aromatische Kohlenwasserstoffe* (Verlag. Julius Springer, Berlin, 1941).

[27] R. N. Jones, Chem. Rev. **41**, 353 (1947); Y. Hirshberg and R. N. Jones, Can. J. Research **B27**, 437 (1949).

[28] E. A. Braude, J. Chem. Soc., 379 (1950).

It would evidently be valuable to direct into perturbation studies some of the theoretical man-hours which go into refined calculations of the energies of excited states. Energies are hard to predict exactly even in most atomic spectra and are of only minor importance for the confirmation of theory. Every prediction of an excited state wave function really needs to be accompanied by predictions of its changes under substitutions and replacements so that an experimental assignment and check is possible. Even more important would be the examination of the possibility of a general classification of all organic wave functions according to perturbation types. After some such general studies of the perturbation problem have been carried out, variconjugate sequences may begin to assume their full importance for the assignment of transitions and the confirmation of theory.

BIBLIOGRAPHY OF SPECTRA IN FIGURES

Abbreviations

RMP—See Bibliography in reference 14.
KP —H. B. Klevens and J. R. Platt (unpublished).
API —*American Petroleum Institute Catalog of Ultraviolet Spectrograms.*
ICT —V. Henri, *International Critical Tables* (McGraw-Hill Book Company, Inc., New York, 1929), Vol. V, p. 359 ff.

Figure 3

Ethylene—RMP; Platt, Klevens, and Price, J. Chem. Phys. **17**, 466 (1949); P. G. Wilkinson and H. L. Johnston, J. Chem. Phys. **18**, 190 (1950).
Propane—RMP.
Vinyl-Cl—A. D. Walsh, Trans. Faraday Soc. **41**, 35 (1945).
Vinyl-NH_2—Reference 11.
Vinyl-SH—Reference 11.
Butadiene—RMP; A. D. Walsh, Nature **157**, 768 (1946); L. E. Jacobs and J. R. Platt, J. Chem. Phys. **16**, 1137 (1948).
Cyclopentadiene—RMP; KP; API 53.
Furan—RMP, KP.
Pyrrole—RMP; KP; API 109.
Thiophene—RMP; KP; API 38, 136.
Benzene—J. R. Platt and H. B. Klevens, Chem. Rev. **41**, 301 (1947); API 1.
Fulvene—KP; J. Stark and W. Steubing, Physik. Z. **9**, 661 (1908).

Figure 4

Toluene—See especially reference 9; see benzene; API 2.
Fluorobenzene—H. B. Klevens and J. R. Platt, J. Am. Chem. Soc. **70**, 3526 (1948); API 296.
Phenol—KP; API 99.
Aniline—Reference 10.
Thiophenol—KP; E. A. Fehnel and M. Carmack, J. Am. Chem. Soc. **71**, 84 (1949).
Styrene—KP; API 168; A. D. Walsh, Proc. Roy. Soc. (London) **A191**, 32 (1947).
Indene—API 321.
Benzofuran—KP.
Indole—KP; ICT 26, 33, 56, 72.
Thionaphthene—KP.
Naphthalene—Reference 8.

Figure 5

Biphenyl—KP; ICT 78, 90.
Fluorene—KP; ICT 89.
Carbazole—KP; ICT 80; API 375.
Dibenzthiophene—KP.
Phenanthrene—Reference 7.

Figure 6

Benzene—See Fig. 3.
Pyridine—W. C. Price and A. D. Walsh, Proc. Roy. Soc. (London) **A191**, 22 (1947); M. Kasha (private communication).
Dimethylanilines—See aniline, Fig. 4.
Methyl phenyl sulfides—E. A. Fehnel and M. Carmack, J. Am. Chem. Soc. **71**, 2889 (1949).

Figure 8

Ethylene—see Fig. 3.
1,4-pentadiene—Estimated from linoleic acid, reference 17.
Divinyl ether—Harrison, Gaddis, and Coffin, J. Chem. Phys. **18**, 221 (1950).
Hexatriene—W. C. Price and A. D. Walsh, Proc. Roy. Soc. (London) **A185**, 182 (1946).

Figure 9

Benzene—See Fig. 3.
Diphenyl methane—KP.
Diphenyl ether—S. Kato and F. Someno, Inst. Phys. Chem. Research (Tokyo) **34**, 905 (1938).
Diphenyl amine—ICT 80; S. Kato and F. Someno, Inst. Phys. Chem. Research (Tokyo) **33**, 209, 729 (1937).
Diphenyl sulfide—E. A. Fehnel and M. Carmack, J. Am. Chem. Soc. **71**, 84 (1949).
Stilbene—ICT 90; A. Smakula and A. Wassermann, Z. physik. Chem. **A155**, 353 (1931).

Figure 11

Formaldehyde—API 96; Platt, Rusoff, and Klevens, J. Chem. Phys. **11**, 535 (1943); reference 1.
Propenal—API 100, 330; reference 2.
Phorone—G. Scheide, Ber. **58**, 587 (1925).
Benzaldehyde—KP; reference 2; H. Ley and H. Wingchen, Ber. **67**, 501 (1934).
Fluorenone—R. N. Jones, J. Am. Chem. Soc. **67**, 2127 (1945).

Figure 12

N_2—G. Herzberg, *Molecular Spectra and Molecular Structure. I. Diatomic Molecules* (Prentice-Hall, Inc., New York, 1939), p. 476.
HCN—J. A. Cutler, J. Chem. Phys. **16**, 136 (1948); W. C. Price and A. D. Walsh, Trans. Faraday Soc. **41**, 381 (1945).
Acetylene—Price and Walsh, *ibid.*; KP.
Diborane—W. C. Price, J. Chem. Phys. **16**, 894 (1948).
O_2—R. Ladenburg and C. C. Van Voorhis, Phys. Rev. **43**, 315 (1933); Herzberg, see N_2.
Formaldehyde—See Fig. 11.
Ethylene—See Fig. 3.
HNO—D. L. Hammick and M. W. Lister, J. Chem. Soc., 489 (1937); K. D. Anderson and D. L. Hammick, J. Chem. Soc., 30 (1935); G. N. Lewis and M. Kasha, J. Am. Chem. Soc. **67**, 994 (1945); D. S. McClure, J. Chem. Phys. **17**, 905 (1949).

Figure 13

Cyanogen—S. C. Woo and R. M. Badger, Phys. Rev. **39**, 932 (1932); W. C. Price and A. D. Walsh, Trans. Faraday Soc. **41**, 381 (1945).

Diacetylene—*ibid.*; S. C. Woo and T. C. Chu, J. Chem. Phys. **3**, 541 (1945).
Propynal—Reference 11.
Acrylonitrile—*ibid.*; KP.
Vinyl acetylene—Reference 11; API 320.
Glyoxal—KP; ICT 76, 85; Thompson, Trans. Faraday Soc. **36**, 988 (1940).
Propenal—See Fig. 11.
Butadiene—See Fig. 3.
C=C–C=N—Reference 11.
N=C–C=N—From glyoxime, reference 12.

Figure 14

Divinyl acetylene—A. D. Walsh, Proc. Roy. Soc. (London) **A191**, 32 (1947); W. C. Price and A. D. Walsh, Proc. Roy. Soc. (London) **A185**, 182 (1946).
Hexatriene—*ibid.*
Phenyl isocyanide—KP; Walsh, *loc. cit.*
Phenyl cyanide—KP; Walsh, *loc. cit.*
Phenyl acetylene—KP; Walsh, *loc. cit.*
Benzaldehyde—See Fig. 11.
Styrene—See Fig. 4.
Benzene azomethane—Reference 3.
Nitrosobenzene—S. H. Hastings and F. A. Matsen, J. Am. Chem. Soc. **70**, 3514 (1948); D. S. McClure, J. Chem. Phys. **17**, 905 (1949).
2-acetylthiophene—API 315.

Figure 15

Benzene—See Fig. 3.
Pyridine—See Fig. 6.
Pyridazine—KP; R. C. Evans and F. Y. Wiselogle, J. Am. Chem. Soc. **67**, 60 (1945).
Naphthalene—See Fig. 4.
Quinoline—ICT 26; G. W. Ewing and E. A. Steck, J. Am. Chem. Soc. **68**, 2181 (1946).
Isoquinoline—API 214; Ewing and Steck, *loc. cit.*
Anthracene—See phenanthrene, Fig. 5; API 170.
Acridine—D. P. Craig and L. N. Short, J. Chem. Phys., 419 (1945); D. Radulesen and G. Ostrogovich, Ber. **64**, 2233 (1931).
Phenazine—Radulescu and Ostrogovich, *loc. cit.*

Figure 16

Biphenyl—See Fig. 5.
Bipyridyl—KP.
Fluorene—See Fig. 5.
Stilbenes—See Fig. 9; also Lewis, Magel, and Lipkin, J. Am. Chem. Soc. **62**, 2973 (1940).
Azobenzenes—Cook, Jones, and Polya, J. Chem. Soc., 1315 (1939).
Trans-azobenzene—Also KP; reference 3.

Figure 17

Benzene—See Fig. 3.
Borazoles—Rector, Schaeffer, and Platt, J. Chem. Phys. **17**, 460 (1949).

Figure 18

Formic acid—W. C. Price and W. M. Evans, Proc. Roy. Soc. (London) **A162**, 110 (1937); See also 1,4-pentadiene, Fig. 8.
Nitrous acid—API 104.
Glyoxal—See Fig. 13.
Benzoic acid—KP; API 354–5–6, 376.
Nitrobenzene—KP; API 105; W. G. Brown and H. Reagan, J. Am. Chem. Soc. **69**, 1032 (1947).
Phenylvinylketone—From benzoylacetone, API 352 (probably *enol* form).

Substituted Methanes: V. Infrared Spectra and Calculated Thermodynamic Properties for Some Trichloromethanes*

JOHN R. MADIGAN** AND FORREST F. CLEVELAND
Spectroscopy Laboratory, Department of Physics, Illinois Institute of Technology, Chicago 16, Illinois
(Received September 19, 1950)

Wave numbers and estimated relative intensities for the infrared absorption bands of CCl_3H, CCl_4, and CCl_3Br and a percent transmission curve for CCl_3Br in the region 400–3500 cm^{-1} are given. Probable values of the infrared wave numbers are established and compared with previously obtained Raman and calculated values. Assignments of the observed bands are made. Thermodynamic properties—heat content, free energy, entropy, and heat capacity—have been calculated from the spectroscopic and molecular structure data to a rigid rotator, harmonic oscillator approximation for nine temperatures from 298.16° and 1000°K.

TRICHLOROMETHANES have been treated in two previous papers from this laboratory; in the first,[1] Raman spectral data were given for CCl_3H, CCl_3F, and CCl_3Br and calculated force constants for these three as well as CCl_3D and CCl_4; in the second,[2] Raman and infrared spectral data and calculated thermodynamic properties were given for CCl_3D. The present paper supplements this work by giving infrared spectral data and calculated thermodynamic properties for CCl_3H, CCl_4, and CCl_3Br.†

The infrared absorption spectra were obtained at 25°C with a Beckman IR-2 spectrophotometer equipped with KBr optics. The samples were the same as those used for the Raman spectra[1] and the cell thicknesses and other experimental details were the same as in *IV*.[2] The region scanned was 400–10,000 cm^{-1}.

INFRARED DATA AND ASSIGNMENTS

Trichloromethane (Chloroform, CCl_3H)

For CCl_3H, infrared bands were found in the region 660–3100 cm^{-1} for both liquid and vapor. The results

TABLE I. Comparison of the infrared spectral data for CCl_3H with the Raman data and with the calculated wave numbers.[a]

Infrared										Raman liquid			Theoretical	
Vapor					Liquid									
PR	N	ν PV	AD	I_e PR	PR	N	ν PV	AD	I_e PR	$\Delta\nu$	I	ν_c	Assignment	Type
						1	(135)					145	$\nu_2-2\nu_6$	A_1+E
						1	230					239	$\nu_5-2\nu_6$	A_1+A_2+2E
						2	260.5	0.5		261.1	100	**258.4**	ν_6	E
						1	303					301	$\nu_2-\nu_3$	A_1
						3	366.3	1.8		366.4	70	**371.8**	ν_3	A_1
						1	488			497	vw	500	$\nu_5-\nu_6$	A_1+A_2+E
						2	626.0	1.0		622	vw	627	$\nu_3+\nu_6$	E
681	1	681		m	667	3	665.0	2.7	m	667.4	80	**669.2**	ν_2	A_1
769	2	770.0	1.0	vs	761	4	762.3	1.8	vs	761.5	56	**772.0**	ν_5	E
						1	847		s			849	$\nu_4-\nu_3$	E
930	1	930		m	924	3	924.0	0.0	m			929	$\nu_2+\nu_6$	E
						1	980		w			994	$2\nu_3+\nu_6$	E
						2	1033.0	9.0	s	1027	vw	1034	$\nu_2+\nu_3$	A_1
1221	2	1220.0	1.0	vs	1217	2(5)	1216.7	0.2	vs	1215.6	15	**1210.0**	ν_4	E
					1390	2	1389.5	0.5	w			1400	$\nu_2+2\nu_3$	A_1
										1420	vw	1429	$\nu_2+\nu_5$	E
						1	1471		s			1477	$\nu_4+\nu_6$	A_1+A_2+E
										1501	2	1517	$\nu_2+\nu_4-\nu_3$	E
						1	1515			1518	2	1523	$2\nu_5$	A_1+E
						1	1695		w			1701	$2\nu_2+\nu_3$	A_1
						1	1786		w			1795	$\nu_2+\nu_3+\nu_5$	E
						1	2273		w			2285	$3\nu_5$	A_1+A_2+E
						2	2410.0	0.0				2431	$2\nu_4$	A_1+E
						1	2632		w			2644	$\nu_2+\nu_4+\nu_5$	A_1+A_2+E
	1	3034.4		m	3021	3(7)	3019.1	1.2	s	3018.2	30	**3017.2**	ν_1	A_1

[a] PR = present results; N = the number of times the band has been obtained in apparently reliable, separate investigations; PV = probable value (mean of the N values); AD = average deviation from the mean; ν is the wave number in cm^{-1}; I_e = estimated relative intensity (w = weak, m = medium, s = strong, v = very); $\Delta\nu$ = the observed Raman displacement (see reference 1); I = relative intensity; and ν_c = calculated wave number (see reference 1).

* Presented in part at the Chicago meeting of the American Physical Society, November, 1949; abstract in Phys. Rev. **77**, 740 (1950).

** Based on investigations carried out in partial fulfillment of the requirements for the degree of Master of Science. Present address: Department of Physics, Springfield Junior College, Springfield, Illinois.

[1] Zietlow, Cleveland, and Meister, J. Chem. Phys. **18**, 1076 (1950).

[2] Madigan, Cleveland, Boyer, and Bernstein, J. Chem. Phys. **18**, 1081 (1950).

† Circumstances made it impossible to include CCl_3F in the present investigation, but it is hoped that a similar study for this molecule can be carried out in the near future.

TABLE II. Comparison of the infrared spectral data for CCl_4 with the Raman data and with the calculated wave numbers.[a]

Infrared Vapor ν PR	Infrared Vapor I_e PR	Infrared Liquid PR	Infrared Liquid N	Infrared Liquid ν PV	Infrared Liquid AD	Infrared Liquid I_e PR	Raman liquid Δν	Raman liquid I	ν_c	Theoretical Assignment	Theoretical Type
							94	vw	96	$\nu_4-\nu_2$	F_1+F_2
							144	vw	145	$\nu_1-\nu_4$	F_2
							217.0	66	**217.0**	ν_2	E
			1	(217)						?	
			1	247					260	$\nu_3''-(\nu_2+\nu_4)$	$A_1+A_2+2E+2F_1+2F_2$
			4	309.0	4.5		313.5	88	**313.5**	ν_4	F_2
			1	328					331	$\nu_3''-\nu_1$	F_2
			1	370					363	$(\nu_1+\nu_2)-\nu_4$	F_1+F_2
							434	vw	434	$2\nu_2$	A_1+E
							458.7	100	**458.7**	ν_1	A_1
			1	490					477	$\nu_3''-\nu_4$	$A_1+E+F_1+F_2$
			2	533.5	4.5		536	vw	530	$\nu_2+\nu_4$	F_1+F_2
			1	572			587	vw	573	$\nu_3''-\nu_2$	F_1+F_2
			1	635			630	vw	627	$2\nu_4$	A_1+E+F_2
			1	662					666	$(\nu_2+\nu_3')-\nu_4$	$A_1+A_2+2E+2F_1+2F_2$
			2	670.0	2.0				694	$(\nu_2+\nu_3'')-\nu_4$	$A_1+A_2+2E+2F_1+2F_2$
							673	vw	676	$\nu_1+\nu_2$	E
768	vs	768	4	765.8	2.3	vs	761.7	37		ν_3'	F_2
									776.0		
789	vs	788	5	789.0	3.2	vs	790.4	37		ν_3''	F_2
							915	vw	917	$2\nu_1$	A_1
		980	4	979.7	1.2	m	989	vw	979	$\nu_2+\nu_3'$	F_1+F_2
1009	m	1004	4	1005.3	0.8	m			1007	$\nu_2+\nu_3''$	F_1+F_2
		1070	4	1071.5	2.5	w	1072	vw	1075	$\nu_3'+\nu_4$	$A_1+E+F_1+F_2$
		1106	4	1106.3	2.8	w	1110	vw	1104	$\nu_3''+\nu_4$	$A_1+E+F_1+F_2$
1217	m	1216	5	1216.0	2.4	m	1221	vw	1220	$\nu_1+\nu_3'$	F_2
1255	m	1247	5	1249.2	2.6	m	1250	vw	1249	$\nu_1+\nu_3''$	F_2

[a] The symbols have the same meaning as in Table I.

are given at the left in Table I. One or more bands in this region have been reported in 11 previous investigations.[3–13] For each band, the mean of all the apparently reliable values reported in separate investigations—including the present value—is listed in the table as the probable value (PV). The 1216.7-cm^{-1} band has, as indicated in the table, been obtained 5 times, but only 2 of the values seemed reliable; likewise, only 3 of the 7 values for the 3019.1-cm^{-1} band seemed reliable. Data for the gaseous state were obtained in only one of the previous investigations[6] and then only 3 bands were found.

Also given in Table I, for comparison, are the Raman displacements and the calculated frequencies from the previous paper.[1] Assignments for the observed bands are given at the right. Four of the foregoing investigations[10–13] and 8 additional investigations[14] yielded bands in the region above 3100 cm^{-1}, but no attempt was

TABLE III. Comparison of the infrared spectral data for CCl_3Br with the Raman data and with the calculated wave numbers.[a]

Infrared liquid PR	N	ν PV	AD	I_e PR	Raman liquid Δν	Raman liquid I	ν_c	Theoretical Assignment	Theoretical Type
					193.3	40	**193.3**	ν_6	E
					247.3	50	**247.3**	ν_3	A_1
	1	294			295.0	25	**295.0**	ν_5	E
	1	351					353	$\nu_4-\nu_2$	E
419	2	419.5	0.5	w	422.3	100	**422.3**	ν_2	A_1
444	1	444		w			441	$\nu_5+\nu_6$	E
487	1	487		w			488	$\nu_5+\nu_6$	A_1+A_2+E
494	1	494		w			495	$2\nu_3$	A_1
661	1	661		s			670	$\nu_2+\nu_3$	A_1
719	2	718.0	1.0	vs	716.3	15	**716.3**	ν_1	A_1
767	2	765.5	1.5	vs	775.3	5	**775.3**	ν_4	E
909	1	909		m			910	$\nu_1+\nu_6$	E
973	1	973		m			969	$\nu_4+\nu_6$	A_1+A_2+E
1078	1	1078		w			1070	$\nu_4+\nu_5$	A_1+A_2+E
1134	1	1134		s			1139	$\nu_1+\nu_2$	A_1
1429	1	1429		w	1438	vw	1433	$2\nu_1$	A_1
1538	1	1538		m	1542	vw	1551	$2\nu_4$	A_1+E

[a] See Table I for definition of the symbols.

TABLE IV. Bond distances and angles, and moments of inertia, for CCl_3H, CCl_4, and CCl_3Br.

Molecule	Bond distance C–X[a]	Bond distance C–Cl	Bond angle Cl–C–Cl	Moments of inertia $I_{zz}=I_{yy}$	Moments of inertia I_{xx}
CCl_3H	1.090A	1.761	112°0′	156(259)	302(501)[b]
CCl_4	1.76	1.76	109°28′	293(486)	293(486)
CCl_3Br	1.91	1.77	109°28′	436(724)	296(491)

[a] X = H, Cl, or Br. [b] Awu. $A^2(10^{-40}g\ cm^2)$.

[3] G. Emschwiller and J. Lecomte, J. phys. radium **8**, 130 (1937).
[4] Yeou Ta, Compt. rend. **206**, 1371 (1938).
[5] W. Gordy, J. Chem. Phys. **7**, 163 (1939).
[6] G. L. Jenkins and J. W. Staley, Phys. Rev. **68**, 99 (1945).
[7] J. Lecomte, Compt. rend. **196**, 1011 (1933).
[8] P. Barchewitz and M. Parodi, J. phys. radium **10**, 143 (1939).
[9] E. K. Plyler, J. Chem. Phys. **16**, 1008 (1948).
[10] W. W. Coblentz, *Investigations of Infra-Red Spectra* (Carnegie Institution of Washington, Pub. No. 35, 1905).
[11] B. Timm and R. Mecke, Z. Physik **98**, 363 (1935).
[12] A. Maione, Nuovo Cimento, **14**, 361 (1937).
[13] F. Daniels, J. Am. Chem. Soc. **47**, 2856 (1925).
[14] J. W. Ellis, Phys. Rev. **23**, 48 (1924); Easley, Fenner, and Spence, Astrophys. J. **67**, 185 (1928); R. Freymann and A. Naherniac, Compt. rend. **197**, 829 (1933); O. Vierling and R. Mecke, Z. Physik **99**, 204 (1935); C. Corin, Compt. rend. **202**, 747 (1936); E. Traubert and K. Schaum, Z. wiss. Phot. **35**, 153 (1936); K. Rumpf and R. Mecke, Z. physik Chem. **B44**, 299 (1939); M. V. Chulanovskaya, Izvest. Akad. Nauk, S.S.S.R., Ser. Fiz. **12**, 628 (1948).

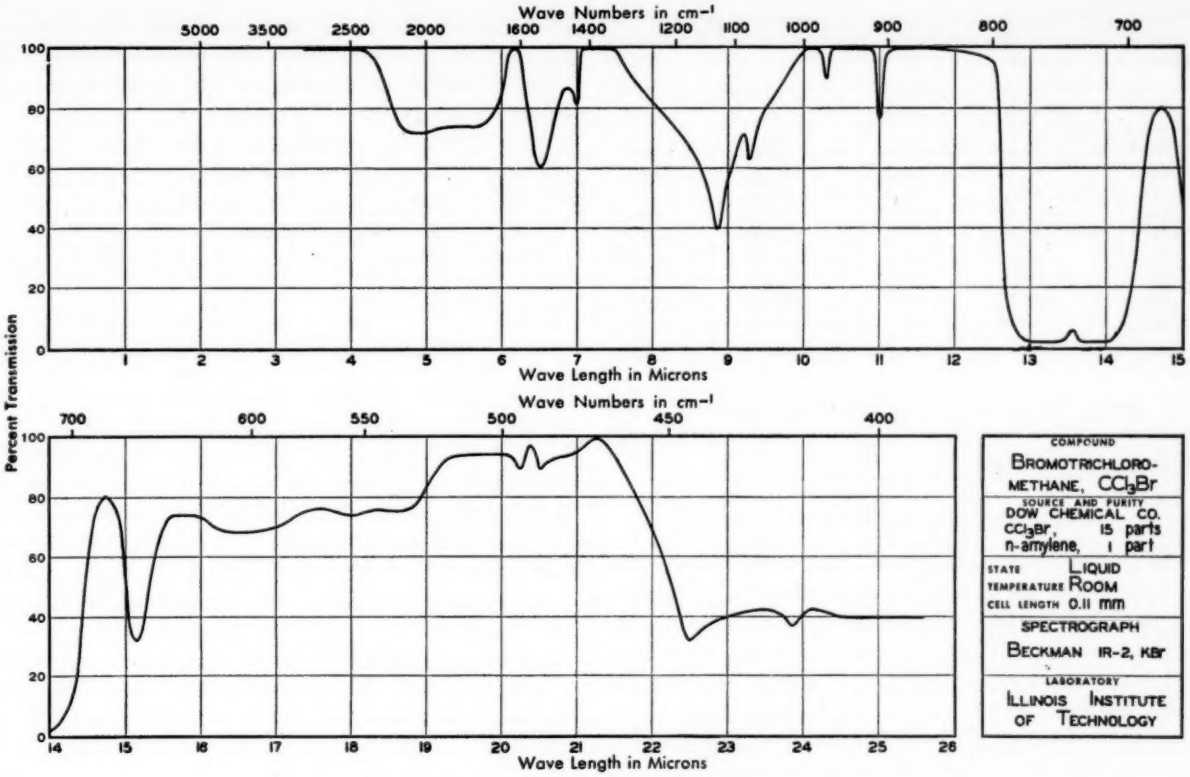

FIG. 1. Infrared absorption bands for bromotrichloromethane.

made to assign these bands because of the greater uncertainty as to the effect of the anharmonicity on the positions of the higher overtone and combination bands.

Tetrachloromethane (Carbon Tetrachloride, CCl_4)

For CCl_4, infrared bands were found in the region 700–1300 cm^{-1} for both liquid and vapor. The results are given in Table II. One or more bands below 1300 cm^{-1} have been reported in 9 previous investigations.[7–10,15–19] Probable values of the infrared wave numbers, the previous Raman displacements and calculated wave numbers,[1] and assignments of the observed bands are included in the table. Only one of the previous investigations was for the gaseous state and then only one band was obtained.[19]

Five of the foregoing investigations[10,13,15–17] and one additional investigation[20] yielded bands above 1300 cm^{-1}, but again—as for CCl_3H—no attempt was made to assign these bands because of uncertainty as to the effect of the anharmonicity for these higher wave numbers.

No assignment could be made for the uncertain infrared band at 217 cm^{-1}. It might correspond to the fundamental ν_2, occurring in the infrared because of a partial breakdown of the selection rules for the liquid state. However, the 217-, 247-, and 370-cm^{-1} bands

TABLE V. Wave numbers and degeneracies of the fundamentals of CCl_3H, CCl_3Br, and CCl_4.

Designation	Degeneracy	Wave number CCl_3H	Wave number CCl_3Br	Wave number CCl_4	Degeneracy	Designation
ν_1	1	[a]3034.4	716.3	458.7	1	ν_1
ν_2	1	[a]681	422.3	217.0	2	ν_2
ν_3	1	366.4	247.3	[a]778	3	ν_3
ν_4	2	[a]1218.9	775.3	313.5	3	ν_4
ν_5	2	[a]771	295.0			
ν_6	2	261.1	193.3			

[a] Gaseous state.

[15] H. H. Marvin, Phys. Rev. **33**, 952 (1922).
[16] W. W. Coblentz and R. Stair, Phys. Rev. **33**, 1092 (1922).
[17] C. Schaefer and R. Kern, Z. Physik **78**, 609 (1932).
[18] J. Strong, Phys. Rev. **38**, 1818 (1931).
[19] D. M. Gates, J. Chem. Phys. **17**, 393 (1949).

TABLE VI. Heat content, free energy, entropy, and heat capacity of CCl_3H for the ideal gaseous state at one atmosphere pressure.[a]

T	$(H^0-H_0^0)/T$	$-(F^0-H_0^0)/T$	S^0	C_p^0
298.16	11.34	59.29	70.62	15.63
300	11.37	59.36	70.72	15.67
400	12.71	62.81	75.53	17.75
500	13.88	65.78	79.66	19.27
600	14.87	68.40	83.28	20.37
700	15.73	70.76	86.49	21.22
800	16.45	72.91	89.37	21.87
900	17.09	74.89	91.97	22.40
1000	17.64	76.72	94.36	22.83

[a] In this and subsequent tables, T is in °K and the other four quantities are in cal deg^{-1} $mole^{-1}$.

[20] W. W. Coblentz, *Investigations of Infra-Red Spectra* (Carnegie Institution of Washington, Pub. No. 41, 1906).

TABLE VII. Heat content, free energy, entropy, and heat capacity of CCl_4 for the ideal gaseous state at one atmosphere pressure.

T	$(H^0-H_0^0)/T$	$-(F^0-F_0^0)/T$	S^0	C_p^0
298.16	13.83	60.20	74.03	19.94
300	13.86	60.29	74.15	19.98
400	15.65	64.53	80.18	21.92
500	17.03	68.18	85.21	23.09
600	18.10	71.37	89.48	23.82
700	18.96	74.24	93.20	24.30
800	19.65	76.82	96.47	24.63
900	20.22	79.21	99.43	24.87
1000	20.69	81.31	102.00	25.04

have been obtained in only one investigation[8] and Gates in a more recent study[19] could find no evidence for these 3 bands and doubts their existence.

Bromotrichloromethane (CCl_3Br)

For CCl_3Br, bands were found in the region 400–1600 cm^{-1}, but only for the liquid since the vapor pressure was so small at 25°C that no bands could be obtained for the vapor. The sample used was the one previously used in the Raman spectral investigation,[1] to which 1 part of *n*-amylene to 15 parts of CCl_3Br had been added to prevent coloring of the liquid under exposure to the Hg arcs. The results are given in Table III and the percent transmission curve is shown in Fig. 1. Probable values, the previous Raman data and calculated values,[1] and assignments also are listed in the table.

Infrared data have been reported in only 2 previous investigations,[21,22] in both of which the spectrum was incomplete. For this molecule, all the observed bands could be assigned as fundamentals, first overtones, or binary combinations.

THERMODYNAMIC PROPERTIES

Present Results

Since several of the frequencies were now available for the gaseous state, and since more recent values of the physical constants,[23] and in some cases of the bond angles and distances, were available than those used in earlier thermodynamical calculations,[24–26] it seemed worth while to calculate the heat content, free energy, entropy, and heat capacity for the 3 molecules. The calculations are for the rigid rotator, harmonic oscillator approximation, and nuclear spins and the effect of isotopic mixing are neglected.

The moments of inertia of CCl_3H were calculated from the recent microwave data[27] and those of CCl_4 and CCl_3Br from the electron diffraction data used previously[1] in calculating the force constants. The bond distances and angles and the resulting moments of inertia are given in Table IV.

The symmetry numbers for CCl_3H, CCl_3Br, and CCl_4 are 3, 3, and 12, respectively. The values used for the fundamentals and their degeneracies are given in Table V. The values obtained for the thermodynamic properties of CCl_3H, CCl_4, and CCl_3Br are given in Tables VI–VIII.

Comparison with Previous Results

For CCl_3H, calculated values were given by Vold[24] for the heat capacity at 14 temperatures from 273° to 773°K and for the heat content at 7 temperatures in the same range. His results are compared with the present values, obtained from the results in Table VI by graphical interpolation, in Table IX. Vold used for the fundamentals the values: 260.8, 365.9, 760.4, 667.1, 1215.6, and 3018.7 cm^{-1}, all of which are smaller than the present values, the mean difference being 7.4 cm^{-1}. Consequently, his thermodynamic values are all slightly greater than the present values; the mean difference—as shown in Table IX—is 0.14 and 0.09 cal deg^{-1} M^{-1} for the heat capacity and the heat content, respectively. Although this difference is not too great, the present results should be slightly closer to the actual values; in fact, even the present values are probably a little too large (by about 0.02 or 0.03 unit) because two of the frequencies are still for the liquid rather than the gaseous state.

No calculated values for the free energy of entropy and no experimental values for any of the four functions, for the gaseous state, were found in the literature.

For CCl_4, calculated values also were given by Vold[24] for the heat capacity and the heat content at the same temperatures as for CCl_3H. His results are compared with the present values at the left in Table X. The wave numbers used by him were: 217.9, 314.0, 458.9, and 776.3 cm^{-1}. Two of these are smaller and two are slightly greater than the present values; on the average, Vold's are only 0.5 cm^{-1} smaller, whence his thermodynamic properties are a little larger than the present ones, but not so much as for CCl_3H. For the heat

TABLE VIII. Heat content, free energy, entropy, and heat capacity of CCl_3Br for the ideal gaseous state at one atmosphere pressure.

T	$(H^0-H_0^0)/T$	$-(F^0-F_0^0)/T$	S^0	C_p^0
298.16	14.37	65.18	79.55	20.38
300	14.41	65.26	79.67	20.43
400	16.16	69.66	85.81	22.22
500	17.48	73.41	90.89	23.30
600	18.52	76.69	95.21	23.98
700	19.33	79.62	98.95	24.43
800	19.99	82.27	102.26	24.73
900	20.53	84.62	105.15	24.95
1000	20.98	86.83	107.81	25.11

[21] Lecomte, Volkringer, and Tchakerian, Compt. rend. **204**, 1927 (1937).
[22] E. K. Plyler, J. Chem. Phys. **17**, 218 (1949).
[23] R. T. Birge, Revs. Modern Phys. **13**, 233 (1941).
[24] R. D. Vold, J. Am. Chem. Soc. **57**, 1192 (1935).
[25] R. C. Lord, Jr., and E. R. Blanchard, J. Chem. Phys. **4**, 707 (1936).
[26] D. M. Yost, Proc. Indian Acad. Sci. **8A**, 333 (1938).
[27] Unterberger, Trambarulo, and Smith, J. Chem. Phys. **18**, 565 (1950).

capacity the mean difference was 0.08; for the heat content it was 0.06 cal deg^{-1} M^{-1}.

The entropy at 298°K was calculated by Yost,[26] using 214, 311, 450, and 775 cm^{-1} for the fundamentals and 1.755A for the C—Cl distance. All these wave numbers are less than the present ones, the average difference being 4.8 cm^{-1}; hence, his entropy value is larger than the present one by 0.08 cal deg^{-1} M^{-1}.

Lord and Blanchard[25] also calculated the entropy at 298°K, as well as at 348.5°K, using the Raman displacements reported by Langseth[28] for some of the isotopes and calculating frequencies for the other isotopes from the equations of Rosenthal.[29] Their entropy value at 298°K is only 0.03 greater than the present value, but their value at 348.5°K is 0.26 greater.

Experimental entropy values were obtained at 298°K and at 348.5°K by Lord and Blanchard[25] and at 298.19°K by Hicks, Hooley, and Stephenson.[30] The experimental and calculated values are given at the right in Table X and the mean differences with the present values are listed at the bottom.

For CCl_3Br, no previous calculated or experimental values were found in the literature.

TABLE IX. Comparison of present and previous calculated values for the heat capacity and heat content of CCl_3H.

T (°K)	C_p^0 Present	C_p^0 Vold[24]	$(H^0-H_0^0)/T$ Present	$(H^0-H_0^0)/T$ Vold[24]
273		15.11		11.03
283		15.36		
293		15.62		
298	15.63	15.73	11.34	11.40
303	15.73	15.85		
313	15.94	16.09		
323	16.15	16.32		
333	16.36	16.54		
353	16.77	16.96		
373	17.19	17.36	12.35	12.44
473	18.86	19.00	13.56	13.67
573	20.07	20.19	14.60	14.71
673	20.99	21.08	15.50	15.59
773	21.69	21.77	16.26	16.35
Mean difference	0.14		0.09	

[28] A. Langseth, Z. Physik **72**, 350 (1931).
[29] J. Rosenthal, Phys. Rev. **46**, 760 (1934).

TABLE X. Comparison of present and previous calculated values for the heat capacity, heat content, and entropy of CCl_4.

T (°K)	C_p^0 Present	C_p^0 Vold[a]	$(H^0-H_0^0)/T$ Present	$(H^0-H_0^0)/T$ Vold[a]	S^0 Present	S^0 Lord and Blanchard[b]	S^0 and Yost[c]	S^0 Experimental
273		19.30		13.33				
283		19.57						
293		19.84						
298	19.94	19.96	13.83	13.86	74.02	74.05	74.1	74.35 ±0.8[d]
303	20.04	20.09						
313	20.23	20.33						
323	20.43	20.55						
333	20.62	20.76						
348.5					77.07	77.33		77.69 ±0.8[d]
353	21.01	21.16						
373	21.40	21.52	15.17	15.25				
473	22.77	22.84	16.66	16.73				
573	23.62	23.67	17.81	17.88				
673	24.17	24.20	18.73	18.78				
773	24.54	24.56	19.46	19.51				
Mean difference	0.08		0.06			0.15	0.08	0.48

[a] See reference 24.
[b] See reference 25.
[c] See reference 26.
[d] Lord and Blanchard (see reference 25) and Hicks, Hooley, and Stephenson (see reference 30) obtained an experimental value of 73.7 ±0.3 cal deg^{-1} M^{-1} at 298.19°K.

ACKNOWLEDGMENT

The authors wish to express their thanks to the Dow Chemical Company, Midland, Michigan, for furnishing the sample of bromotrichloromethane used in this investigation.

[30] Hicks, Hooley, and Stephenson, J. Am. Chem. Soc. **66**, 1064 (1944).

Estimated Bond Energies in Carbon, Nitrogen, Oxygen, and Hydrogen Compounds

GEORGE GLOCKLER
Department of Chemistry and Chemical Engineering, The State University of Iowa, Iowa City, Iowa*
(Received October 25, 1950)

Estimates of bond energies of CC, CN, CO, NO, OO, NN, CH, NH, and OH bonds are made on the basis of the heat of sublimation of carbon (L(C)) being 7.36 ev and the heat of dissociation of nitrogen ($D(N_2)$ = 11.80 ev).

AN earlier study[1] on carbon-carbon and carbon-hydrogen bond energies has been extended to include carbon-nitrogen, carbon-oxygen, nitrogen-oxygen, nitrogen-nitrogen, oxygen-oxygen, nitrogen-hydrogen, and oxygen-hydrogen bonds. Two values of the heat of sublimation of carbon[2] (L(C) = 5.888 ev and 7.36 ev)[3–6] and three values of the heat of dissociation of nitrogen ($D(N_2)$ = 7.384 or 9.764 or 11.80 ev)[7,8] are considered. The heat of dissociation of oxygen is well known.[9] It is found that the set L(C) = 7.36 ev and $D(N_2)$ = 11.80 ev yields a family of bond energy-distance curves (Fig. 1) which corresponds to a similar family of curves relating force constants to internuclear distance (Fig. 2) in the sense that the sequence CC, CN, CO, NO, OO, and NN is the same for both types of curve at a given internuclear distance. The corresponding XH curves are shown in Fig. 3. Bond energies based on the other five combinations of L(C) and $D(N_2)$ exhibit a different sequence. This finding can be used as an argument in favor of L(C) = 7.36 ev and $D(N_2)$ = 11.80 ev.

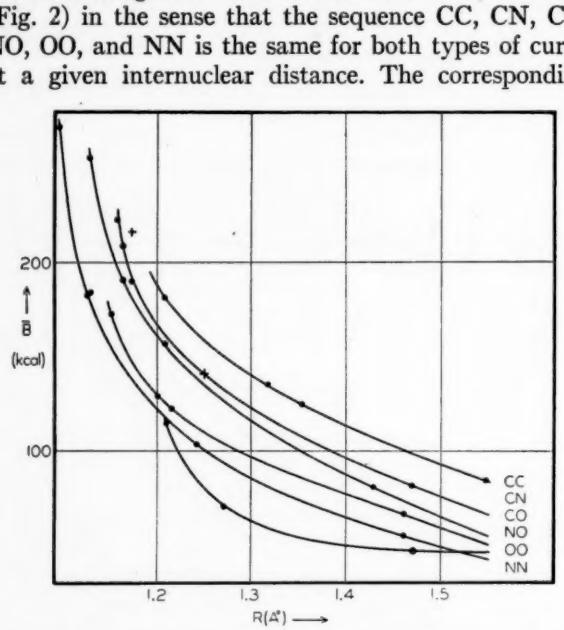

FIG. 1. Estimates of average CC, CN, CO, NO, OO, and NN bond energies ($\bar{B}$) as a function of internuclear distance (R).

The estimated bond energies and other needed data[9–11] are given in Tables I and II. This information substantiates the belief that bonds with large force constants have large bond energies and small bond distances. The similar relation would not be found in the case of dissociation energies or removal energies of some atom or radical and bond distances. In the last case the reorganization energy of the resulting structures must be taken into consideration. Bond energies are ascribed to bonds as the latter *exist in the molecule* in its normal state. The division of the total heat of atomization of a molecule into bond energies is to a certain extent arbitrary.[12] They are needed, however, in order to calculate resonance energies.

The graphs presented here are useful for detecting erroneous values. For example, the force constants of NO_2 (0.91 md/cm at 1.215A) and of the NN-bond in HN_3 (2.04 md/cm at 1.128A) do not fall on the curves and they may be in error. In the case of CN radical the bond energy-distance curves indicate that D(CN)

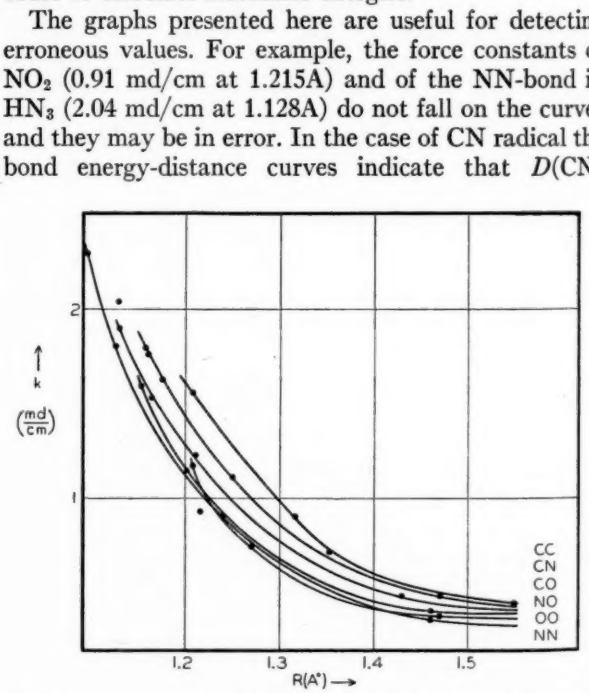

FIG. 2. Force constants of CC, CN, CO, NO, OO, and NN bonds [k(md/cm)] as a function of internuclear distance (R).

* Financial support was received from ONR contract N-8onr-79400.

[1] G. Glockler, J. Chem. Phys. **16**, 842 (1948).
[2] H. D. Hagstrum, Phys. Rev. **72**, 947 (1947).
[3] Brewer, Gilles, and Jenkins, J. Chem. Phys. **16**, 797 (1948).
[4] Simpson, Thorn, and Winslow, AEC General Chemistry Report ANL-4264, Argonne Nat. Lab. (1949).
[5] A. L. Marshall and F. J. Norton, J. Am. Chem. Soc. **72**, 2166 (1950).
[6] H. D. Springall, Research **3**, 260 (1950).
[7] A. G. Gaydon, *Dissociation Energies and Spectra of Diatomic Molecules* (John Wiley and Sons, Inc., New York, 1947).
[8] G. Glockler, J. Chem. Phys. **18**, 1518 (1950).
[9] G. Herzberg, *Molecular Spectra and Molecular Structure, I, Spectra of Diatomic Molecules* (D. Van Nostrand Company, Inc., New York, 1950), second edition.
[10] K. W. F. Kohlrausch, *Der Smekal-Raman Effect*, Erg. Band (Verlag. Julius Springer, Berlin, 1938).
[11] F. R. Bichowsky and F. D. Rossini, *The Thermochemistry of the Chemical Substances* (Reinhold Publishing Corporation, New York, 1936).
[12] M. Szwarc and M. G. Evans, J. Chem. Phys. **18**, 618 (1950).

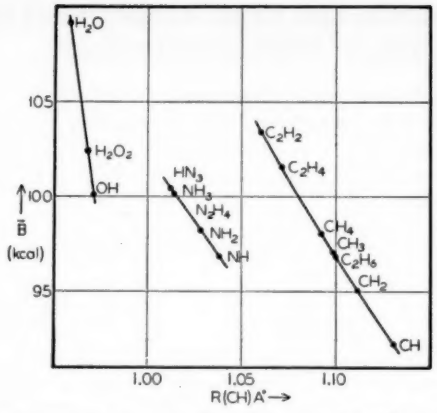

FIG. 3. Estimates of average XH bond energies ($\bar{B}$) as a function of internuclear distance ($\bar{R}$).

= 189.8 kcal rather than 215.9 kcal (cross in upper left-hand corner of Fig. 1). In the case of methyl isocyanate, the C=N distance can be estimated to be 1.25A since Qa is known (cross on CN curve). The CH bond energy is assumed to be as in ethane, the C−N bond energy is from CH_3NH_2 and the CO bond energy is taken from CO_2. In the present system ($L(C)=7.36$ ev and $D(N_2)=11.80$ ev) the bond energy of the CH radical is 92.2 kcal, which differs from 80 kcal given by Shidei.[13] The

TABLE I. Internuclear distances, force constants, atomic heats of formation, and estimated average bond energies of CC, CN, CO, NO, NN, and OO bonds. $L(C)=169.7$ kcal; $D(N_2)=272.1$ kcal.

Bond	Gas	R(A)	k(md/cm)	Qa(kcal)	$\bar{B}$(kcal)
C≡C	C_2H_2	1.207	1.56	388.4	181.5
C=C	$C_2(^3\Pi_u)$	1.316	0.91	135.4	135.4
C=C	C_2H_4	1.353	0.72	531.4	125.0
C−C	Diamond	1.545		169.7	84.9
C−C	C_2H_6	1.547	0.45	665.7	84.6
C≡N	HCN	1.157	1.79	326.3	222.8
C≡N	C_2N_2	1.16	1.76	537.8	208.7
C≡N	$CN(^2\Sigma^+)$	1.172	1.62	189.8	189.8
				215.9	215.9
C=N	$CN(A^2\Pi_i)$	1.233	1.25		
C=N	$CH_3\cdot NCO$	(1.25)	(1.11)	704.1	141.1
C−N	$CH_3\cdot NH_2$	1.469	0.49	187.4	81.9
C≡O	$CO(^1\Sigma^+)$	1.128	1.89	255.5	255.5
C=O	CO_2	1.163	1.53	380.9	190.5
C=O	H_2CO	1.21	1.23	360.2	157.1
C−O	CH_3OH	1.428	0.49	480.6	80.9
N≡O	$NO(^2\Pi_i)$	1.151	1.59	173.0	173.0
N=O	N_2O	1.20	1.14	311.1	128.9
N=O	NO_2	1.215	0.91?	245.2	122.6
N−O	NH_2OH	1.46	0.41	367.8	66.7
N≡N	$N_2(^1\Sigma_g^+)$	1.095	2.29	272.1	272.1
N≡N	N_2O	1.125	1.80	311.1	182.2
N≡N	HN_3	1.128	2.04?	387.9	183.8
N=N	HN_3	1.241	0.91	467.4	103.8
N−N	N_2H_4	1.46	0.36	452.6	55.1
O=O	$O_2(^3\Sigma_g^-)$	1.207	1.17	117.2	117.2
O=O	O_3	1.27	0.75	141.2	70.6
O−O	H_2O_2	1.47	0.38	251.7	47.0

[13] T. Shidei, Japan. J. Phys. **11**, 23 (1936).

latter value depends on the interpretation of a feature of the spectrum as a predissociation, but it may be a perturbation. Similarly, $D(C_2)=135.4$ kcal rather than 80 kcal as given by Herzberg[10] is nearer to 115 kcal obtained from the intensity of variation of the Swan bands with temperature in a carbon tube furnace.[3] The heat of dissociation of NO (173.0 kcal) is of course higher than values given in the literature, since it depends on the heat of dissociation of nitrogen. The bond energies given for hydrogen peroxide are not very satisfactory as yet, since only meagre data exist in this case.

When the present values are used to make comparisons with appearance potentials of ions in oxygen, nitrogen, nitric oxide, and carbon monoxide,[14] it is, of course, found that the present system ($L(C)=7.36$ ev and $D(N_2)=11.80$ ev) leads to different values of the kinetic energy of the resulting ions, atoms, and radicals. For example, the first appearance of N^+ ions in N_2 should occur at 26.2 ev if the neutral atom is not excited. N^+ ions are found[14] at 24.3 ev. If it is assumed that the reaction is $N_2 \rightarrow N^+ + N^-$ and that the electron affinity of nitrogen atom[15] is 1.6 ev, then N^+ ions should appear at 24.6 ev. Workers in the field of appearance potentials have always assumed convenient excited states and negative ions in order to interpret their experiments.

TABLE II. Internuclear distances, force constants, atomic heats of formation, and estimated average bond energies of CH, NH, and OH bonds. $L(C)=169.7$ kcal; $D(N_2)=272.1$ kcal.

XH	Gas	R(A)	k(md/cm)	Qa(kcal)	$\bar{B}$(kcal)
	C_2H_2	1.060	0.59	388.4	103.4
	C_2H_4	1.071	0.53	531.4	101.6
	C_2H_6	1.0995	0.48	665.7	96.9
CH	CH_4	1.092	0.50	392.2	98.1
	CH_3	1.0984		291.2	97.1
	CH_2	1.1112		190.2	95.1
	CH	1.1305	0.43	92.2	92.2
	HN_3	1.012		387.9	100.5
	NH_3	1.014	0.64	467.4	100.2
NH	N_2H_4	1.02		452.6	99.4
	NH_2	1.028		196.5	98.2
	NH	1.038	0.60	96.9	96.9
	H_2O	0.958	0.78	218.3	109.2
OH	H_2O_2	(0.968)	0.65?	251.7	102.4
	OH	0.971	0.77	100.1	100.1

The interesting result of these calculations lies in the fact that both bond energy-distance curves and force constant-distance curves follow the same sequence at a given internuclear distance for the nine bonds considered if $L(C)=7.36$ ev and $D(N_2)=11.80$ ev. The resonance energy of benzene is 80 kcal on the present basis.

[14] H. D. Hagstrum and J. T. Tate, Phys. Rev. **59**, 354 (1941).
[15] G. Glockler and J. W. Sausville, J. Electrochem. Soc. **95**, 292 (1949).

Critical Constants, Boiling Points, Triple Point Constants, and Vapor Pressures of the Six Isotopic Hydrogen Molecules, Based on a Simple Mass Relationship*

ABRAHAM SOLOMON FRIEDMAN, DAVID WHITE, AND HERRICK L. JOHNSTON
The Cryogenic Laboratory and The Department of Chemistry, The Ohio State University, Columbus, Ohio
(Received November 13, 1950)

INTRODUCTION

RECENTLY we[1] have completed the experimental determination of the vapor pressure and critical constants of deuterium. This work showed that there was a considerable discrepancy between the values of the critical constants predicted by Hammel[2] based on the DeBoer correction for quantum effects and our experimentally determined values. However, it is quite evident in the case of the hydrogen isotopes that the DeBoer modification of the law of corresponding states based on semi-emperic quantum corrections and the Lennard-Jones potential function is not sufficient for the prediction of their properties. Orientation effects, as one would expect, become quite important in non-spherical molecules, and thus a comparison of the hydrogen isotopes with the inert gases is invalid in the prediction of the various thermodynamic properties. However, if one assumes that the orientation effects

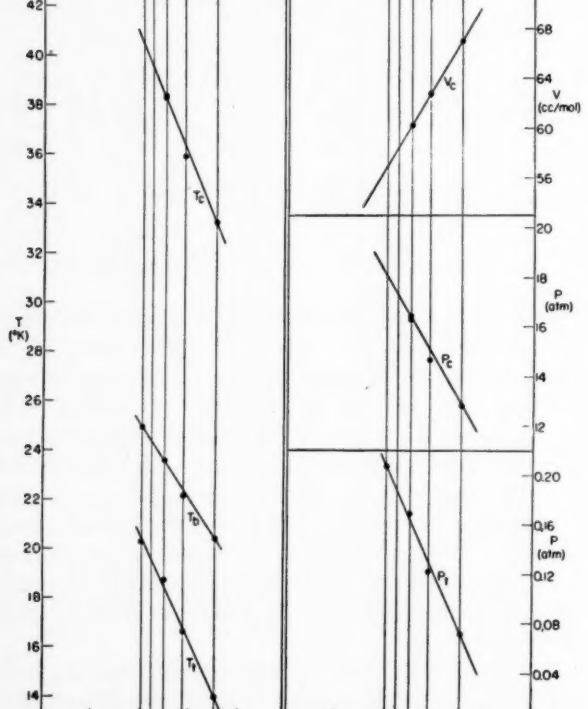

FIG. 1. Critical, boiling point, and triple point constants of the hydrogen isotopes as function of mass.

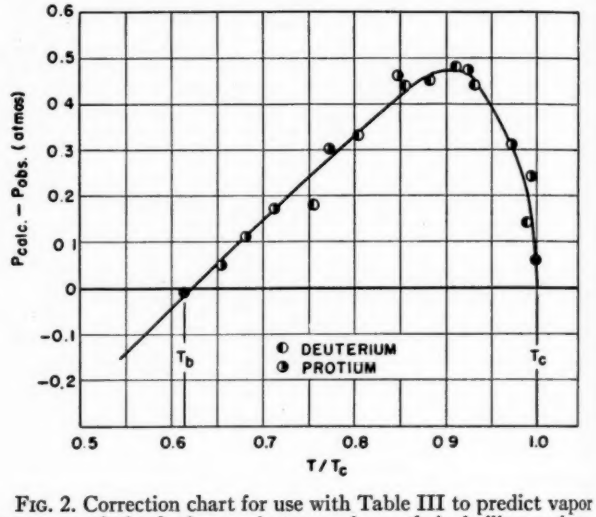

FIG. 2. Correction chart for use with Table III to predict vapor pressures of the hydrogen isotopes above their boiling points, based on experimental vapor pressure curves for H_2 and D_2.

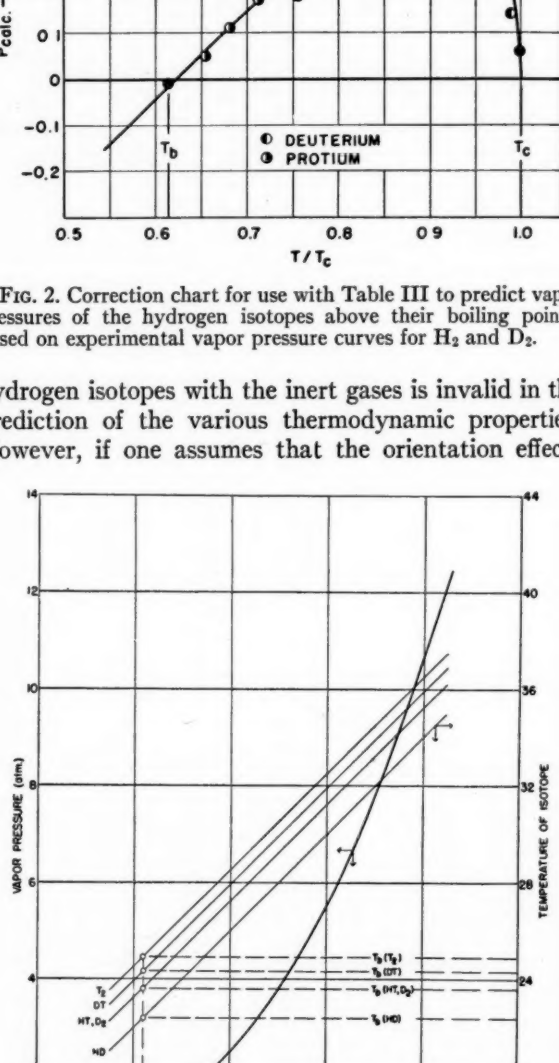

FIG. 3. Dühring chart for the hydrogen isotopes, with H_2 as reference.

* This work was supported in part by the ONR, under contract with The Ohio State University Research Foundation.
[1] A. S. Friedman, D. White, and H. L. Johnston, J. Am. Chem. Soc. (to be published).
[2] E. F. Hammel, J. Chem. Phys. 18, 228 (1950).

TABLE I. Critical, boiling point, and triple point constants predicted graphically for the hydrogen isotopes. Comparisons of predicted values with available experimental values.

	Boiling point T_b(°K)		Critical constants T_c(°K)		P_c(atmos)		V_c(cc/mole)		Triple point T_t(°K)		P_t(atmos)	
	expt	graph	expt	graph	expt	graph	expt	graph	expt	graph	expt	graph
H_2	20.39[a]	20.4	33.24[c]	33.2	12.797[c]	12.8	66.95[a]	67.0	13.96[a]	14.0	0.071[a]	0.071
HD	22.13[a]	22.4	35.91[d]	36.4	14.64[d]	15.1	62.8[d]	62.8	16.60[a]	16.8	0.122[a]	0.130
			38.35[e]		16.432[e]							
D_2	23.57[a]	23.6		38.3		16.4	60.3[d]	60.3	18.72[a]	18.5	0.169[a]	0.164
			38.26[d]	(41.1)[f]	16.28[d]	(18.9)[f]		(56.7)[f]				
HT		23.6		38.3		16.4		60.3		18.5		0.164
DT		24.3		39.5		17.3		58.5		19.7		0.188
T_2	24.92[b]	24.9		40.6		18.1		57.1	20.27[b]	20.5	0.207[b]	0.207
				(43.7)[f]		(20.8)[f]		(53.7)[f]		(21.65)[f]		(0.248)[f]

[a] Wooley, Scott, and Brickwedde, J. Research Natl. Bur. Standards **41**, 379 (1948).
[b] E. R. Grilly, J. Am. Chem. Soc. (to be published).
[c] White, Friedman, and Johnston, J. Am. Chem. Soc. **72**, 3565 (1950).
[d] R. D. Arnold and H. J. Hoge, J. Chem. Phys. **18**, 1295 (1950).
[e] See reference 1.
[f] See reference 2.

TABLE II. Predicted vapor pressures for the hydrogen isotopes from their triple points to approximately four degrees above their boiling points.

	H_2	HD	D_2, HT	DT	T_2
a	2.513	2.658	2.849	3.108	3.187
b	−51.26	−59.55	−67.23	−75.53	−79.35
	Vapor pressure (atmospheres)				
T(°K)					
14	0.071				
15	0.125				
16	0.204				
17	0.315	0.143			
18	0.462	0.224			
19	0.654	0.334	0.205		
20	0.891	0.479	0.307	0.214	
21	1.18	0.664	0.445	0.324	0.256
22	1.52	0.893	0.621	0.473	0.380
23	1.92	1.17	0.843	0.667	0.546
24	2.44	1.50	1.12	0.914	0.761
25		1.89	1.45	1.22	1.03
26		2.33	1.83	1.60	1.36
27			2.29	2.05	1.77
28				2.57	2.25
29					2.82

are the same in all the isotopic forms of a molecule, and one relates the various properties of these isotopes to the mass, a prediction of these properties becomes possible.

In Fig. 1 we have plotted the boiling points, triple points, and critical constants of the hydrogens *versus* the reciprocal of the square root of their molecular weights. We can utilize these graphs to predict constants for those isotopes for which experimental data are not available. This plot appears to justify the assumption that these properties vary linearly with $1/(m)^{\frac{1}{2}}$.

In Table I the triple points, boiling points, and critical constants predicted graphically are tabulated and compared with experimental values, where they are known. We have also included in Table I the values computed by Hammel from DeBoer's modified law of corresponding states.

From the predicted triple point and boiling point constants, equations of the form $\log p = a + b/T$ can be obtained for the vapor pressures of the hydrogen isotopes. These equations represent the vapor pressures reasonably well from the triple points to a few degrees above the boiling points of the hydrogens. The constants of the vapor pressure equations and the vapor pressures computed therefrom are given in Table II. It can be seen in this table that the constants of the vapor pressure equations of HT and D_2 are identical. That the vapor pressures of these substances should be the same, was first predicted, and experimentally verified, by Libby and Barter.[3]

TABLE III. Predicted vapor pressure constants for the hydrogen isotopes for the region between their boiling and critical points.

	a'	b'
H_2	2.872	−58.59
HD	3.066	−68.67
D_2, HT	3.165	−74.70
DT	3.217	−78.18
T_2	3.252	−80.98

Using the boiling point and critical point constants, similar two-constant equations can be obtained to give the vapor pressures in the region above the boiling points of the hydrogen isotopes. However, the logarithm of the vapor pressure is not a linear function of the reciprocal temperature in this temperature range and the deviation plot of Fig. 2 should be used to correct the vapor pressures for this non-linearity. The constants a' and b' in the equation $\log p = a' + b'/T (T_b < T < T_c)$ are given in Table III.

The vapor pressure curves of protium, deuterium, and, it is presumed, of the other hydrogens are, to a first approximation, superimposable by a simple shift of the temperature scale. This permits the construction of a Dühring chart using the protium vapor pressure as the reference curve. The Dühring lines of the heavy hydrogens are constructed by drawing straight lines with slopes of unity through their boiling points. Such a chart is illustrated in Fig. 3.

[3] W. F. Libby and C. A. Barter, J. Chem. Phys. **10**, 184 (1942).

Letters to the Editor

THIS section will accept reports of new work, provided these are terse and contain few figures, and especially few half-tone cuts. The Editorial Board will not hold itself responsible for opinions expressed by the correspondents. Contributions to this section should not exceed 600 words in length and must reach the office of the Managing Editor not later than the first of the month preceding that of the issue in which the letter is to appear. No proof will be sent to the authors. The usual publication charge ($8.00 per page) will not be made and no reprints will be furnished free.

On the Ultraviolet Absorption of Cyanogen Chloride

D. P. STEVENSON, D. D. TUNNICLIFF, AND C. D. WAGNER
Shell Development Company, Emeryville, California
November 20, 1950

IN connection with a recent investigation of the ionization and dissociation of cyanogen chloride by electron impact[1] it was of interest to attempt to fix more closely the long wavelength limit to the continuous absorption band of this substance than was done by Badger and Woo,[2] who gave $\lambda_c > 2270$A. A sample of cyanogen chloride containing 0.90 percent M CCl_4 and 0.40 percent M $(CN)_2$ as the only mass spectrometrically detectable impurities was prepared, and its absorption was measured for $\lambda < 3000$A in a 5.0-cm cell at 730-mm Hg pressure (25°C). Measurements with a Cary recording spectrophotometer and a Beckman D.U. instrument were in complete agreement.

Data for correcting the observed absorption for that due to the carbon tetrachloride impurity were obtained from a mixture of carbon tetrachloride vapor (22 mm) and air at atmospheric pressure. In the region $2500 \geqslant \lambda \geqslant 2100$A cyanogen was shown to be essentially transparent except for its very sharp characteristic bands. These bands appeared superimposed on the continuous absorption of the cyanogen chloride, and correction for this cyanogen absorption was obtained simply by drawing a smooth curve below the bands.

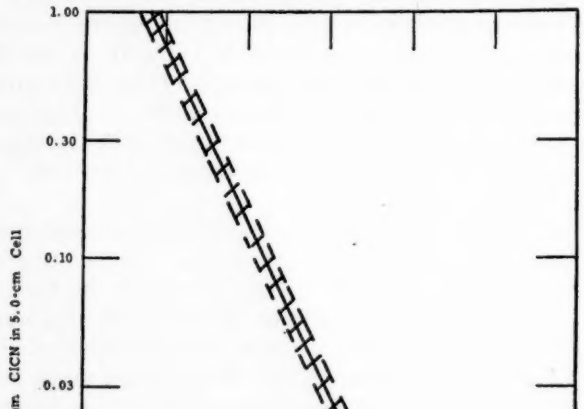

FIG. 1. The ultraviolet absorption of cyanogen chloride.

The final absorption curve obtained for cyanogen chloride, as the average of three series of measurements, is shown in Fig. 1. In this figure the shaded area shows the maximum range of uncertainty of the absorption coefficient. It may be concluded from these data that the long wavelength limit to this continuous absorption band of cyanogen chloride, λ_c, is greater than 2450±20A.

The relation of this value of λ_c to the heats of dissociation of cyanogen and cyanogen chloride has been discussed in reference 1.

[1] D. P. Stevenson, J. Chem. Phys. 19, 17 (1951).
[2] R. M. Badger and S. C. Woo, J. Am. Chem. Soc. 52, 2572 (1931).

On the Thermal Conductivity of Liquids and Polymers and its Relation to the Pressure Coefficient of Viscosity

A. BONDI
Shell Development Company, Emeryville, California
October 28, 1950

THE thermal conductivity K of "simple" liquids is well described by a formula developed on the basis of independent theories by Bridgman[1] and by Kincaid and Eyring[2]:

$$K = (0.931)3ku_s/\gamma^{\frac{1}{2}}v^{\frac{1}{3}}, \quad (1)$$

where $\gamma = C_p/C_v$, k = Boltzmann constant, u_s = sound velocity in the liquid, and v = molecular volume. This equation becomes quite invalid, however, if applied to higher molecular weight liquids, such as mineral lubricating oils, higher triglycerides, siloxane polymers, and the like, as is shown by the data in Table I. Viscosity[3] and thermodynamic[4] properties of such substances suggested that their molecules are flexible and act as if they were composed of independently moving segments. If one calculates the volume per molecule effective in momentum transfer, by solving Eq. (1) for v with the observed values of u_s and K, one obtains the values given in column 5 of Table I. These are obviously smaller than the chemical molecular volume. The data presented here indicate that thermal conduction in liquids composed of large molecules likewise is effected by segmental motion, rather than by motion of the entire molecule.

TABLE I. Thermal conductivity and molal volume effective in momentum transfer of various liquids and polymers.

Substance	Thermal conductivity ×10⁻⁴ Calculated	Thermal conductivity ×10⁻⁴ Observed[a]	Effective volume V_x	V_x/V
Benzene	3.4	3.56	84	0.94
Glycerol	6.6	6.8	70	0.96
n-Hexane	2.9	3.3	107	0.82
n-Decane	2.3	3.5	101	0.52
Olive oil	0.94	3.9	112	0.12
Castor oil	0.9	4.3	83	0.084
Rubber	···	4.7	96	···
Polyisobutylene	···	3.9	110	···

[a] From Chemical Engineering Handbook and Manual and J. F. Downie-Smith, Trans. ASME 58, 719 (1936).

The relatively narrow range of calculated segment sizes suggests that they are determined by the uniformity of orientability of the skeletal C−C bond common to the oils and polymers studied.[5] The dimethylsiloxane polymers emphasize this point. Independent evidence points to exceptional mobility around the Si−O bond, such that the alkyl silicone group is freely rotating.[6] Consequently, one should expect that the effective volume of the first member of the series $(CH_3)_3SiOSi(CH_3)_3$, being that of the trimethylsilane group, should be larger—and its thermal conductivity smaller—than that of the higher members of the series, for which the

TABLE II. Thermal conductivity and molal volume effective in momentum transfer in dimethylsiloxane polymers.

Degree of polymerization	Thermal conductivity ×10⁻⁴ Calculated[a]	Observed[b]	Effective volume V_x	V_x/V
2	1.2	2.36	86	0.39
7	0.86	2.55	89	0.195
20	0.47	3.17	72	0.055
115	0.11	3.68	61	0.009
455	0.062	3.81	58	···

Volume of trimethylsilane group in above dimer, 100 cm³
Volume of dimethylsilane group in above higher polymers, 61 cm³

[a] Calculated by means of Eq. (1) using the sound velocity data by A. Weisler, J. Am. Chem. Soc. **71**, 93 (1949).
[b] From O. K. Bates, Ind. Eng. Chem. **41**, 1966 (1949).

average segment is the dimethylsilane. The data in Table II show that this expectation is verified surprisingly well.

The close connection between segment size and the pressure coefficient of viscosity, expressed by Eyring's theory as

$$\Delta V_{\neq} = RT(\partial \ln \nu/\partial p)_T = \text{size of the hole required for flow} \quad (2)$$

(where ν = kinematic viscosity of liquid), suggested relating the volume effective in thermal conduction to the flow volume $\Delta V_{\neq}$. The relative volumes V_x/V and $\Delta V_{\neq}/V$ are compared in Fig. 1.

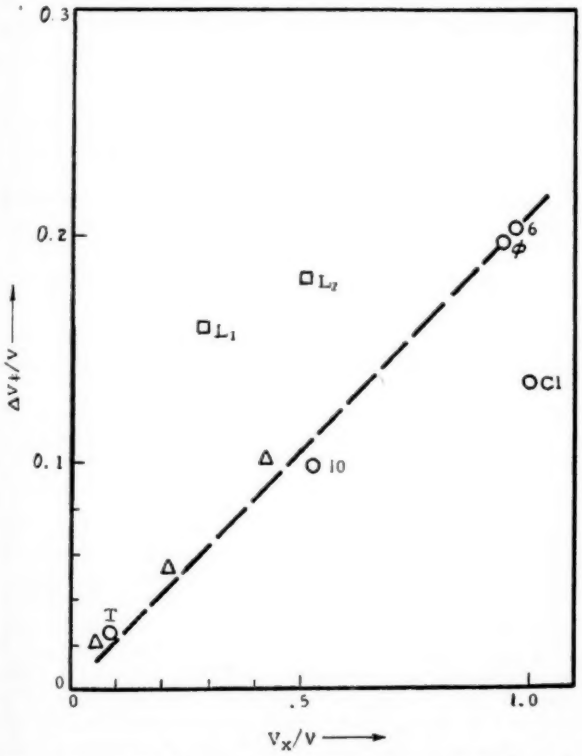

FIG. 1. Correlation between viscosimetric and thermal (conductivity) segment size. For straight-chain compounds the curve $\Delta V_{\neq}/V \sim 0.2 V_x/V$ seems to be valid. T = C_{18} triglycerides, 10 = *n*-decane, 6 = *n*-nexane, φ = benzene, Cl = chlorobenzene, *L* = lube oils, Δ = dimethylsiloxane polymers ($\Delta V_{\neq}$ calculated from data of P. W. Bridgman, Am. Acad. Arts Sci. **77**, 115 (1949).

All of the linear compounds are found to straddle a line $\Delta V_{\neq}/V \cong 0.2 V_x/V$. Cyclic and spherically symmetrical compounds do not fit into this scheme. There being no means to predict V_x and $\Delta V_{\neq}$ from first principles, this discrepancy remains unexplained.

The applicability of free-volume theory in its present form to large flexible molecules—those for which $V_x \neq V$—is rather questionable. The first consequence drawn from the observations described above may be to substitute V_x and the "effective molecular weight" M_x (corresponding to V_x) for the chemical molecular

TABLE III. Comparison of free-volume V_f (and corresponding "free-liberation radius" *a*) data of flexible molecules calculated from chemical molecule size with those calculated from thermal segment size.

Substance	V_f cm³	a A	$V_f(x)$ cm³	$a(x)$ A
n-Decane	0.26	0.48	0.30	0.49
Triolein	0.052	0.28	0.154	0.40
Methylsiloxane dimer	0.54	0.60	1.28	0.81
Methylsiloxane polymer (degree of polym. = 82)	0.074	0.31	0.75	0.68

V_f calculated from Eq. (3); $a = (V_f/4)^{\frac{1}{3}}$; $V_f(x)$ and $a(x)$ calculated using V_x from Tables I and II.

volume V and weight M in the formula for the calculation of the free volume V_f,

$$(V/V_f)^{\frac{1}{3}} = u_0(M/RT\gamma)^{\frac{1}{2}}, \quad (3)$$

which forms the basis of Eq. (1) above.

This substitution may lead to a more plausible value for the average liberation amplitude or free path between collisions of molecule segments rather than the use of the chemical molecular weight. Examples are given in Table III. More doubtful yet is the meaning of the concept "free-angle ratio" δ_2 when applied to large flexible molecules.

The described differences in segmental mobility suggest that the diffusion of small molecules through high molecular weight liquids may not be predictable from the Stokes-Einstein equation. The diffusion rate through a polysiloxane liquid, e.g., should be faster than through the isoviscous *n*-paraffin, etc. The correctness of this prediction will be subjected to test by experiment.

[1] P. W. Bridgman, *Physics of High Pressure* (New York, 1932).
[2] J. F. Kincaid and H. Eyring, J. Chem. Phys. **6**, 620 (1938).
[3] W. Kauzman and H. Eyring, J. Am. Chem. Soc. **62**, 3113 (1940).
[4] R. E. Powell and H. Eyring, Advances in Colloid Sci. **1**, 183 (1942).
[5] Contrary to the view expressed by J. Rehner, J. Polymer Sci. **2**, 263 (1947), there is thus no basic difference in the mechanism of thermal conductivity between amorphous liquid and solid organic compounds.
[6] W. L. Roth, J. Am. Chem. Soc. **69**, 474 (1947); Acta Cryst. **1**, 34 (1948).

The Thermodynamic Properties of Gaseous Titanium

PAUL W. GILLES AND QUENTIN DE L. WHEATLEY
Department of Chemistry, University of Kansas, Lawrence, Kansas
October 30, 1950

THE recent widespread interest in titanium and its compounds and alloys has increased the need for accurate thermodynamic data on all forms of the element and its compounds. Sufficient energy levels of neutral titanium have been tabulated[1] to permit the calculation of the thermodynamic properties of the ideal monatomic gas in the temperature range 0 to 5000°K. The methods of calculation employed have been described by Giauque.[2] The values of the constants used are those recommended by the National Bureau of Standards;[3] *viz.*, $R = 1.98719 \pm 0.00013$ cal/deg mole, $hc/k = c_2 = 1.43847 \pm 0.00045$ cm deg, $N = (6.02283 \pm 0.00220) \times 10^{23}$/mole and 1 wave No. (cm⁻¹) = 2.85851 cal/mole. The atomic weight of titanium was taken as 47.90 ± 0.005 g/mole.[4]

The results of these calculations are given in Table I and include the translational and electronic contributions, but omit that due to nuclear spin. At each temperature enough terms were used so that the contribution of higher terms was negligible. At three of the temperatures only the free energy function was calculated. Tabular differences were used to check the free energy function and heat content.

Figure 1 shows a plot of the calculated heat capacity *versus* temperature. The rapid rise of the heat capacity to a maximum of 6.578 cal/deg mole at 135°K is occasioned by the existence in gaseous titanium of two low lying excited energy levels that are respectively only 486 and 1106 cal/mole above the ground state. Since all other excited states have energies considerably higher,

TABLE I. The thermodynamic properties of gaseous titanium.

T deg K	$-(F_T^0-H_0^0)/T$ cal/deg mole	$H_T^0-H_0^0$ cal/mole	S_T^0 cal/deg mole	C_p^0 cal/deg mole
10	18.888	49.680	23.856	4.9680
20	22.332	99.363	27.300	4.9700
30	24.347	149.234	29.322	5.0210
40	25.782	200.22	30.787	5.1965
50	26.903	253.47	31.972	5.4630
100	30.567	555.78	36.125	6.4471
125	31.829	718.90	37.580	6.5727
140	32.486	817.56	38.326	6.5749
150	32.891	883.23	38.779	6.5555
160	33.272	948.63	39.201	6.5238
175	33.806	1046.03	39.783	6.4600
200	34.607	1205.9	40.637	6.3302
250	35.958	1515.6	42.020	6.0597
298.16	37.025	1801.9	43.068	5.8386
300	37.062	1812.7	43.104	5.8312
350	37.990	2099.6	43.989	5.6548
400	38.788	2378.9	44.735	5.5218
450	39.485	2652.3	45.379	5.4211
500	40.104	2921.4	45.946	5.3441
550	40.658	3187.0	46.453	5.2843
600	41.160	3450.0	46.910	5.2373
650	41.619	3710.9	47.328	5.2000
700	42.041	3970.1	47.712	5.1701
750	42.431	4228.0	48.068	5.1463
800	42.794	4484.8	48.400	5.1276
850	43.133	4740.8	48.710	5.1134
900	43.451	4996.3	49.002	5.1036
950	43.750	5251.3	49.278	5.0978
1000	44.033	5506.1	49.539	5.0963
1050	44.301	5761.0	49.788	5.0989
1100	44.556	6016.1	50.025	5.1057
1150	44.799	6271.6	50.253	5.1169
1200	45.031	6527.8	50.471	5.1324
1250	45.253	6784.9	50.681	5.1522
1300	45.465	7043.1	50.883	5.1763
1350	45.670	7302.6	51.079	5.2046
1400	45.866	7563.6	51.269	5.2369
1450	46.056	7826.4	51.453	5.2730
1500	46.239	8091.0	51.633	5.3129
1550	46.415	8357.7	51.807	5.3562
1600	46.587	8626.7	51.978	5.4027
1650	46.753	8898.0	52.145	5.4523
1700	46.914	9172.0	52.309	5.5045
1750	47.070	9448.5	52.469	5.5593
1800	47.222	9727.9	52.627	5.6164
1850	47.370	10010.8	52.782	5.6771
1900	47.515	10295	52.933	5.7364
1950	47.656	10584	53.083	5.7990
2000	47.793	10875	53.231	5.8630
2250	48.437	...	...	...
2500	49.021	...	...	...
2750	49.559	...	...	...
3000	50.059	17435	55.871	7.2801
4000	51.804	25424	58.160	8.6666
5000	53.284	34650	60.214	9.7085

above 18,743 cal/mole, the heat capacity decreases from the maximum, passes through a minimum of 5.096 cal/deg mole at 990°K and then increases as the temperature increases. This type of behavior has been noted also with gaseous iron.[5]

Previous calculations of the thermodynamic properties of titanium gas include that of the free energy function at 1000-degree intervals between 2000 and 5000°K by Latimer,[6] that of the free energy function, entropy, and heat content at 298, 1000, and 2000°K by Brewer,[7] and that of the entropy at 298°K by Kelley.[8]

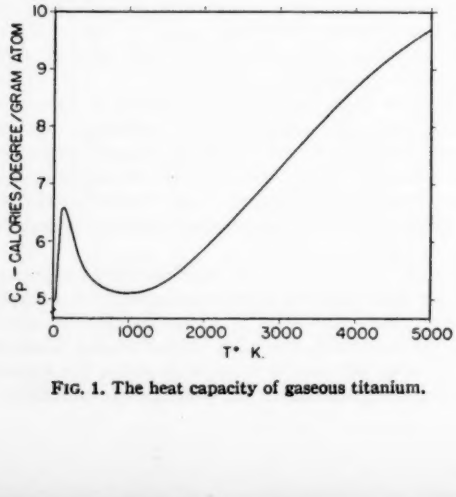

FIG. 1. The heat capacity of gaseous titanium.

The present tabulation is in excellent agreement with these previous data, with the exception of the value of $H^0-H_0^0$ at 2000°K, where a difference of 1.5 percent exists.

Similar data for condensed titanium have been given by Brewer,[7] Kelley,[8,9] and the National Bureau of Standards.[3] Data on the vapor pressure of the metal have been obtained by Carpenter and Reavell[10] and Blocher and Campbell.[11]

The authors wish to acknowledge the financial support of the Atomic Energy Commission and the technical assistance of Mr. Lester Leifer.

[1] Charlotte E. Moore, "Atomic energy levels," Nat. Bur. Standards Circ. **467**, 273–277 (1949).
[2] W. F. Giauque, J. Am. Chem. Soc. **52**, 4808 (1930).
[3] National Bureau of Standards, *Selected Values of Chemical Thermodynamic Properties*, December 31, 1947.
[4] International Atomic Weights (1949), J. Am. Chem. Soc. **72**, 1431 (1950).
[5] K. K. Kelley, "Calculation of the Specific heats and entropies of metal vapors from spectroscopic data, with special reference to gaseous iron and copper," Bureau of Mines Rept. of Investigations 3341, 1937.
[6] W. M. Latimer, *Tables of Free Energy Functions for Elements and Compounds in the Temperature Range 2000 to 5000°K* (MDDC-1462, U. S. Atomic Energy Commission, September 10, 1947), p. 4.
[7] L. Brewer, "Thermodynamic and physical properties of the elements," *National Nuclear Energy Series, Div. IV, Vol. 19B, Chemistry and Metallurgy of Miscellaneous Materials* (McGraw-Hill Book Company, Inc., New York, 1950), pp. 13–39.
[8] K. K. Kelley, "Contributions to the data on theoretical metallurgy. XI. Entropies of inorganic substances," Bureau of Mines Bull. **477**, 92 (1950).
[9] K. K. Kelley, "X. High-temperature heat-content, heat-capacity, and entropy data for inorganic compounds. Bureau of Mines Bull. **476**, 192 (1949).
[10] L. G. Carpenter and F. R. Reavell, private communication, January 25, 1950.
[11] J. M. Blocher and I. E. Campbell, J. Am. Chem. Soc. **71**, 4040 (1949).

The Surface Energy of Small Nuclei

G. C. BENSON
Division of Chemistry, National Research Council, Ottawa, Canada
AND
R. SHUTTLEWORTH
Physics Department, University of Illinois, Urbana, Illinois
October 30, 1950

GIBBS,[1] Tolman,[2] Koenig,[3] and Buff and Kirkwood[4] have developed thermodynamic and statistical mechanical treatments of surfaces in which the surface tension is permitted to depend on the curvature of the surface. In this letter elementary molecular arguments are used to show why the surface energy depends on the curvature and to make a rough estimate of the dependence; this treatment is appropriate to small nuclei for which the earlier treatments were not valid.

Since all surface effects are due to short-range interatomic forces, it is clear that when a surface has a radius of curvature that is large compared to the interatomic distance, it will behave has a plane surface: no anomalies will be found in capillary experiments. However, nucleation phenomena depend upon the properties of small clusters of molecules,[5,6] and it is important to know how different the surface energy of a nucleus is from the surface energy of a plane surface. For simplicity the calculations will be made at 0°K and additive central forces between the molecules will be assumed.

The principles are well illustrated by discussion of a two-dimensional close-packed cluster (Fig. 1). The total surface energy of the cluster is half the energy necessary to remove the cluster from the infinite lattice (the other half is the surface energy of the hole in the lattice); the energy can be estimated by counting the number of bonds that must be broken. The nearest-neighbor bonds are perpendicular to the sides of the hexagons, and the number of these that must be broken is proportional to the zig-zag distance $AB, BC, CD, \cdots ZA$; but if the dashed line is taken as the surface of the cluster, the length of the surface is proportional to the zig-zag distance. (Apart from a negligible correction (shaded corners in Fig. 1), the area enclosed by the dashed line is equal to the area of the molecules in the cluster.) Hence, on a nearest-neighbor interaction approximation the surface energy per unit

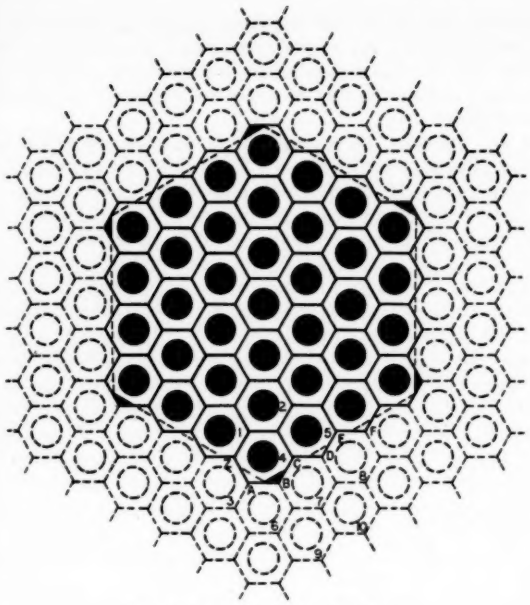

FIG. 1. A two-dimensional nucleus.

length (this corresponds to surface energy per unit *area* in the three-dimensional case) is independent of cluster size. Of course, the average surface energy per *surface molecule* will increase with decrease of cluster size; this is the first-order effect responsible for the greater vapor pressure of small clusters.

When next-nearest neighbor bonds are considered (these are the sides of the hexagons, e.g., bonds between the molecules 2–7, 5–10, 4–8), it is seen that to form the surface two must be broken for each edge length, *BC*, *CD*, *DE*, *EF*, etc.; but only one bond need be broken for the 6 corner lengths such as *AB*, since the bond 3–7 will not be broken. Therefore, owing to interactions between non-nearest neighbor molecules, the corners contribute a negative energy; and the average surface energy per unit length will decrease with decrease in size of the cluster.

Similarly, for a three-dimensional crystal of area A, the total surface energy AU' will depend on three terms, proportional respectively to the area, the edge length, and the number of corners. So that the average surface energy per unit area will have the form:

$$U'=U[(1-k_1/N^{\frac{1}{2}})-(k_2/N^{\frac{1}{2}})], \quad k_2\ll k_1, \tag{1}$$

where N is the number of molecules in the cluster, k_1 and k_2 are positive constants whose values depend on non-nearest neighbor interactions. It should be noted that the value of U' will be the same for the cluster and the corresponding hole in the lattice.

The smallest three-dimensional cluster, for which the concept of surface energy is useful, is that of a central molecule surrounded by twelve others. The total energies of such clusters have been calculated on the assumption that all pairs of molecules interact according to a potential $\lambda r^{-12}-\mu r^{-6}$. Then, if the thirteen molecules are arranged as are a molecule and its twelve nearest neighbors in a close-packed cubic lattice, the heat of evaporation per molecule ϵ' is given by

$$-2\epsilon'=D_{12}''\lambda a'^{-12}-D_6''\mu a'^{-6},$$

where $\sqrt{2}a'$ is the distance between nearest-neighbor molecules, and

$$D_s''=(12/13)[(6/2^{s/2})+(2/4^{s/2})+(4/6^{s/2})+(1/8^{s/2})],$$

since in the cluster there are 6×6 bonds of length $\sqrt{2}a'$, 6×2 bonds of length $4^{\frac{1}{2}}a'$, and so on. The equilibrium condition that $d\epsilon'/da'$ vanish gives

$$2\lambda D_{12}''a'^{-12}=D_6''\mu a'^{-6}.$$

Two similar equations can be written for the infinite close-packed crystal, and the relevant lattice sums have been evaluated by Lennard-Jones and Ingham.[7] From the four equations the ratios ϵ'/ϵ and a'/a can be calculated (Table I), where ϵ and $\sqrt{2}a$ are the heat of evaporation per molecule and the nearest-neighbor distance in the infinite crystals.

The density of the cluster is 6 percent less than that of the infinite crystal; this is because non-nearest-neighbor interaction always produces a decrease in density of the surface layer, and here this effect extends throughout the volume of the cluster. Thus, for small clusters, the concept of a surface tension γ producing a pressure $2\gamma/R$ inside the drop is not useful. It should also be remembered that only for a plane liquid surface is the surface tension equal to the surface free energy.[8]

The surface energy per unit area U' of a cluster of thirteen molecules will be defined by the relation

$$-13\epsilon'=-13\epsilon+AU',$$

where $A=42.44a^2$ is the area of a sphere whose volume is equal to that of 13 molecules in the infinite crystal. It is found that $U'=0.194\epsilon/a^2$, as compared with $0.216\ \epsilon/a^2$, the surface energy per unit area of a (111) face of the infinite crystal;[9] the (111) face is the face with the minimum surface energy.

The arrangement of the thirteen molecules as in a close-packed cubic lattice is not unique, they could be arranged as in a close-packed hexagonal lattice, or in a pentagonal structure in which one molecule is in the center and the other twelve surround it, and the structure has six pentagonal axes, ten trigonal axes, and a center of inversion (Schonflies group P_i). Computations for all three arrangements are given in Table I, for the pentagonal

TABLE I. Energies of three arrangements of thirteen molecules.

Arrangement	ϵ'/ϵ	a'/a	$U'a^2/\epsilon$
Close-packed cubic	0.36526	1.01928	0.194
Close-packed hexagonal	0.36545	1.01924	0.194
Pentagonal	0.39601	$a_1'/a=0.99235$ $a_2'/a=1.04342$	0.185
(111) face of crystal			0.216

structure; $\sqrt{2}a_1'$ is the distance between the atom at the center and one at the surface; $\sqrt{2}a_2''$ is the distance between two adjacent surface atoms. The greater stability of the pentagonal structure has been pointed out by Wefelmeier[10] in connection with the α-particle model of the atomic nucleus.

We conclude that, even for clusters of thirteen molecules, surface energy will have decreased less than 15 percent from the value for a plane surface. Using this value, estimates of the surface energy of larger nuclei can be obtained by Eq. (1) if it is supposed that $k_2\simeq 0$, so that $k_1\sim\frac{1}{3}$.

The authors are grateful to Dr. R. S. Bradley (Leeds University, England) for discussion of the problem.

[1] J. W. Gibbs, *Collected Works* (Longmans, Green and Company, New York, 1928), Vol. I, 219.
[2] R. C. Tolman, J. Chem. Phys. **16**, 758 (1948); **17**, 118 (1949); *ibid.* **17**, 333 (1949).
[3] F. O. Koenig, J. Chem. Phys. **18**, 449 (1950).
[4] F. P. Buff and J. G. Kirkwood, J. Chem. Phys. **17**, 338 (1949).
[5] V. K. Lamer and G. M. Pound, J. Chem. Phys. **17**, 1337 (1949).
[6] F. P. Buff and J. G. Kirkwood, J. Chem. Phys. **18**, 991 (1950).
[7] J. E. Lennard-Jones and A. E. Ingham, Proc. Roy. Soc. (London) **A107**, 636 (1925).
[8] R. Shuttleworth, Proc. Phys. Soc. (London) **A63**, 44 (1950).
[9] R. Shuttleworth, Proc. Phys. Soc. (London) **A62**, 167 (1949).
[10] W. Wefelmeier, Z. Physik **107**, 332 (1937).

Effect of Pressure on Thermal Diffusion in Gases

E. W. BECKER
Physics Institute, University of Marburg, Marburg, Germany
September 25, 1950

WITH respect to some recent papers concerning the behavior of thermal diffusion columns,[1–3] it seems worth while to make the following remarks:

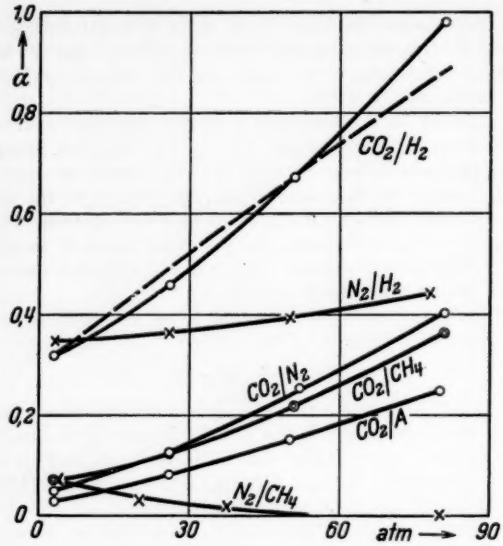

FIG. 1. Pressure dependence of the thermal diffusion factor α. $T=287°$, $T'=427°$ abs. Average mole fraction of the components$\approx$0,5.

The thermal diffusion factor α of a gas mixture is not independent of pressure as predicted by the Enskog-Chapman Theory of quasi-ideal gases and as it apparently might be derived from low pressure experience. Over a region from 3 to 80 atmos (Fig. 1), α increases for CO_2/H_2 by a factor of 3, for CO_2/N_2 and CO_2/A by a factor of 8, and for CO_2/CH_4 by a factor of 5. An N_2/H_2 mixture shows only small pressure dependence of α, while for N_2/CH_4, α even decreases with increasing pressure. We found these results observing the elementary thermal separation in a two-bulb system.[4]

Theoretically, it was shown that an essential part of the pressure dependence of α is due to the reality of the gases, and may be described in terms of the equation of state.[4,5] In case of small separations, for the rather simple mixture of a real and a quasi-ideal gas, there results the formula[4]

$$\alpha \approx \alpha_i + \alpha_r, \tag{1}$$

where α_i means the thermal diffusion factor in the sense of Enskog and Chapman, and α_r may be obtained in first approximation from van der Waals' equation:

$$\alpha_r = \frac{1}{\gamma \ln T'/T}\left(\frac{1+\beta/T^2}{1+\beta/T'^2}-1\right), \tag{2}$$
$$\beta = \gamma^2 pa/R^2.$$

Here, T and T' are the absolute temperatures of the hot and the cold wall, γ is the average mole fraction of the real component, a the coefficient of attraction in van der Waals' equation, p the pressure, and R the gas constant.

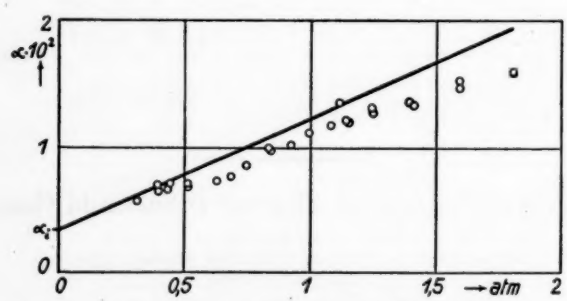

FIG. 2. Plot of α for CO_2/C_3H_8 calculated from Eqs. (1) and (2). Circles = α-values measured by Drickamer, O'Brien, Bresee, and Ockert (reference 1).

A curve, calculated from formulas (1) and (2) for the H_2/CO_2 mixture, assuming H_2 to be quasi-ideal, is plotted in Fig. 1 (dotted line). Comparison with the experimental curve shows an agreement as good as may be expected regarding the simplifications of the theory.

In our opinion, the special effects observed by Drickamer, O'Brien, Bresee, and Ockert[1] in a thermal diffusion column working with CO_2/C_3H_8 may also be due to the reality of gases. In Fig. 2 the uncorrected α-values measured by Drickamer, *et al.*, have been plotted and compared with a curve calculated from Eqs. (1) and (2), assuming CO_2 to be the quasi-ideal component. As a matter of fact, this assumption is not completely justified, as the van der Waals' constants of the two components, derived from the critical data, are in a ratio of 1:2,4 only. Taking into account the reality of CO_2, the theoretical curve would become less steep and the agreement of both curves even better. The additive constant α_i was obtained by an extrapolation to zero pressure from the measurements of Drickamer, *et al.*, yielding a value of $\alpha_i=0.0035$. When the molecular interaction is described by a repulsive force model $F=-K_{12}/r^\nu$, this renders a value close to 5 for the exponent ν. As CO_2 and C_3H_8 have about the same exponents and as, on the other hand, the pair $C^{12}O_2^{16}/C^{13}O_2^{16}$ at 300° abs changes the sign of the thermal separation,[6] our result seems to be rather reasonable.

From the preceding considerations we may conclude that the corrections of column theory,[7] as applied by Drickamer and coworkers,[3] are not necessary for *laminar* gas flow. The results which they obtain for *turbulent* convection are in qualitative agreement with our own experiments.[8]

[1] Drickamer, O'Brien, Bresee, and Ockert, J. Chem. Phys. **16**, 122 (1948).
[2] H. G. Drickamer and J. R. Hofto, J. Chem. Phys. **17**, 1165 (1949).
[3] Drickamer, Mellow, and Tung, J. Chem. Phys. **18**, 945 (1950).
[4] E. W. Becker and A. Schulzeff, Naturwissenschaften **35**, 218 (1948); E. W. Becker, Habilitationsschrift, Marburg/Lahn, (1949); E. W. Becker, Z. Naturforsch. **5a**, (1950), to be published.
[5] R. Haase, Z. Physik **127**, 1 (1950).
[6] E. W. Becker and E. Dörnenburg, Naturwissenschaften **37**, 165 (1950).
[7] Furry, Jones, and Onsager, Phys. Rev. **55**, 1083 (1939).
[8] E. W. Becker, Z. Naturforsch. **2a**, 447 (1947).

Spectroscopic Evidence for the Proton Conductivity through Solid Alcohols

YOSHINOBU KAKIUCHI, HACHIRO KOMATSU, AND SUSUMU KYOYA
Institute of Science and Technology, University of Tokyo, Tokyo, Japan
November 14, 1950

IT is well known that certain normal alcohols have anomalous dielectric constant and electric conductivity between the transformation and the melting points. The rotation of molecules around their long axis in the solid phase above the transformation temperature was concluded by Baker and Smyth[1] from dielectric studies, as well as from x-ray measurements by Ott[2] and independently by one of the authors and his collaborators.[3] Specific heat measurements in our laboratory have also confirmed the above conclusion.[4]

Anomalous conductivity was attributed to the large mobility of protons forming hydrogen bonds,[5] and Hoffman and Smyth[6] considered it to be due to the mechanism which is similar to that discussed by Hückel[7] in explaining the anomalous proton conductivity through water. It may be of some value, therefore, to verify that protons are really the carrier of the electric charge.

A cylindrical condensor filled with normal hexadecyl alcohol (cetyl alcohol) was placed in a glass vessel. After it was wholly evacuated, stopcock S_1 in Fig. 1 was closed, the sample being kept at the temperature between the transformation and the melting points, where the conductivity is anomalously large. After being left for two hours, the cock S_1 was opened and S_2 closed; and the electrodeless discharge through the gas in the discharge tube D was observed by a quartz spectrograph.

When no voltage was applied to the electrodes, the color of the discharge was extremely faint and somewhat bluish (Fig. 2a). When the voltage was on and the current was flowing through the

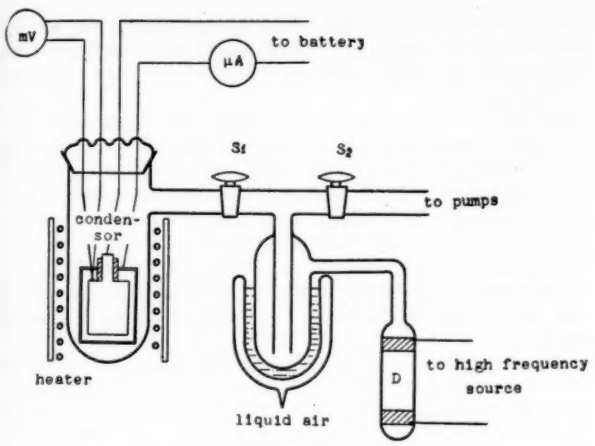

FIG. 1.

crystal, the color of the discharge was bright reddish white; and its spectrum was easily identified with that of the hydrogen (Fig. 2b). The charge carried and the quantity of hydrogen evolved by electrolysis was estimated; and as a result, the greater part of the charge was found to be carried by protons. In the temperature region where the conductivity is small, the hydrogen evolved was also found to be small in quantity, although the same voltage

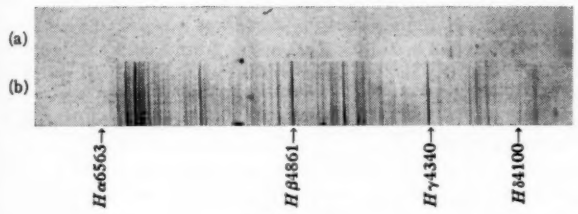

FIG. 2.

was applied to the electrodes as before. Therefore, it may safely be concluded that the conduction of electricity through cetyl alcohol is due mainly to protons.

Further results and discussions will shortly be published in the *Journal of the Physical Society of Japan.*

[1] Baker and Smyth, J. Am. Chem. Soc. **60**, 1229 (1938); Higasi and Kubo, Sci. Papers Inst. Phys. Chem. Research (Tokyo) **36**, 286 (1939).
[2] Ott, Z. physik. Chem. **193**, 218 (1944), original not available.
[3] Sano and Kakiuchi, J. Phys. Soc. Japan **4**, 178 (1949).
[4] Kakiuchi, Sakurai, and Suzuki, J. Phys. Soc. Soc. Japan **4**, 365 (1949); **5**, 369 (1950). Y. Kakiuchi, to be published.
[5] Y. Kakiuchi, Proc. Jap. Acad. **23**, 65 (1947).
[6] Hoffman and Smyth, J. Am. Chem. Soc. **71**, 431 (1950).
[7] Hückel, Z. Elektrochem. **34**, 546 (1928).

Some Newer Experimental Results on the Osmosis in Alternating Electric Fields

Z. LÁSZLÓ
Budapest, Hungary
July 24, 1950

IN previous papers[1] we have discussed the effect of an ac field on the process of osmosis. In our experiments a U-shaped vessel was divided into two compartments by soldering either a Jena glass filter "G3" or a glass plate with a 0.4-mm diameter hold in its middle. When a platinum electrode was placed in each of the sections of the vessel and the two sides were filled with two different polar liquids, and when applying a few thousand volts/cm 50 cc ac were applied, the liquid level rose on one side and sank in the other. Owing to the mixing of the liquids after a period of 60 to 180 minutes, the level difference disappeared.

Table I contains the pairs of liquids we have tested. The rise of level was observed on the liquid standing left of the dash.

TABLE I.

Using a glass filter diaphragm	Using a glass plate with a hole diaphragm
ethylalcohol —methylalcohol	ethylalcohol —methylalcohol
propylalcohol —methylalcohol	propylalcohol—methylalcohol
propylalcohol —ethylalcohol	ethylalcohol —propylalcohol
amylalcohol —methylalcohol	amylalcohol —methylalcohol
amylalcohol —ethylalcohol	amylalcohol —ethylalcohol
amylalcohol —propylalcohol	amylalcohol —propylalcohol
methylalcohol—acetone	acetone —methylalcohol
ethylalcohol —acetone	acetone —ethylalcohol
propylalcohol —acetone	acetone —propylalcohol
amylalcohol —acetone	acetone —amylalcohol
methylalcohol—nitrobenzene	nitrobenzene —methylalcohol
ethylalcohol —nitrobenzene	nitrobenzene —ethylalcohol
propylalcohol —nitrobenzene	nitrobenzene —propylalcohol
amylalcohol —nitrobenzene	nitrobenzene —amylalcohol
acetone —nitrobenzene	nitrobenzene —acetone
water —methylalcohol	water —methylalcohol
water —ethylalcohol	ethylalcohol —water
propylalcohol —water	propylalcohol—water
water —acetone	acetone —water

These experiments show that in the case of glass filter diaphragm the liquid with higher degree of association rose, while in the test with pierced glass diaphragm the liquid of less conductivity rose. The acetone—amylalcohol pair is an exception, as the acetone—though of higher conductivity—rose.

We have repeated our measurements with 1100 cc. The observed phenomena were quite different from those at 50 ccs, as when any kind of alcohol was paired with nitrobenzene, the nitrobenzene rose (Fig. 1). In the case of water and ethylalcohol the ethylalcohol rose. We could not carry out our measurements at 1100 cc in the case of water-methylalcohol and propylalcohol—water, as the audiofrequency source we used was not capable of supplying sufficient current for these liquids. With other pairs of liquids and with the pierced diaphragm no dependence on frequency has been observed.

We also examined the effect of ions (especially of K^+ and J^- ions) on the osmosis in an ac field. Such measurements were performed in the vessel with the sintered glass diaphragm for the

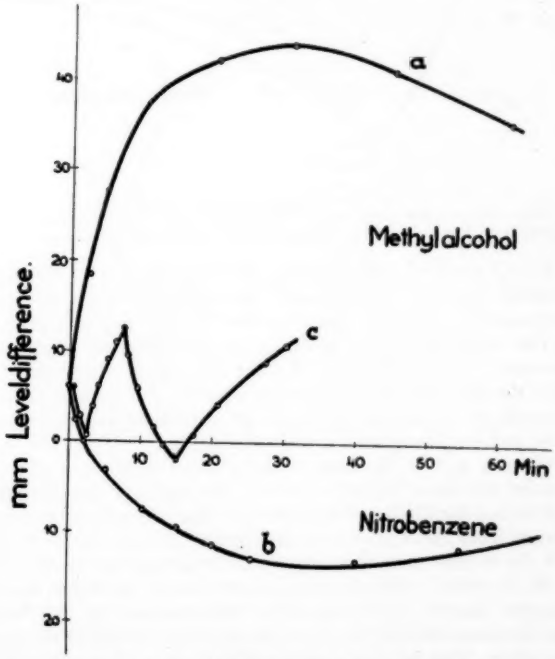

FIG. 1. (a) Osmosis in the case of a glass filter diaphragm with methylalcohol—nitrobenzene in an electrical field of a 4000 v 50 cc, (b) 4000 v 1100 cc, (c) alternating 1100 and 50 cc.

following liquid pairs: ethylalcohol—acetone, ethylalcohol—methylalcohol, and methylalcohol—acetone. When *KJ* is dissolved in that one of the two liquids which without the addition of *KJ* would rise under the influence of ac, the rise will be higher. When the iodide is added to the sinking liquid, the sinking will be less.

If we dissolve *KJ* on the rising side, then above a certain concentration the direction of the rise changes (Fig. 2). The reverse takes place before the conductivity of the ethylalcohol solution of *KJ* equals that of the methylalcohol (Fig. 2d).

When a glass filter was used and both sides were filled with the same liquid, but *KJ* was dissolved in one of the compartments, only then on application of an ac field was it observed that, in the case of methylalcohol, ethylalcohol, acetone, and water, the level of the *KJ* solution rises, while with propyl-, amyl-, and isobutylalcohol the level of the compartment without *KJ* rises. When a pierced glass plate is used, the level of the liquid without iodide always rises.

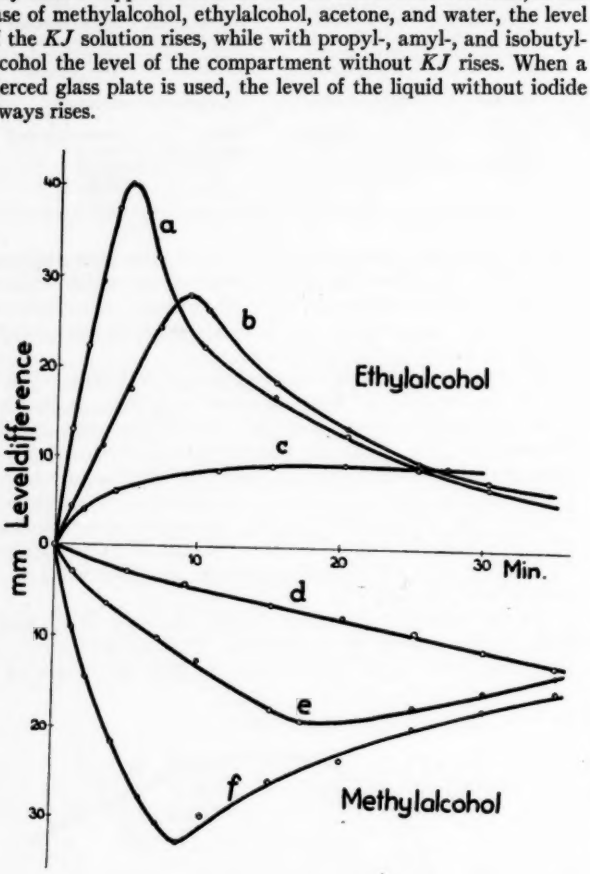

FIG. 2. (a) Osmosis in case of pierced glass plate diaphragm in an ac field of 4000 v 50 cc with ethylalcohol—methylalcohol, (b)–(f) the same as (a) but with increasing concentrations of *KJ* solved in ethylalcohol.

In our series of measurements the concentration of *KJ* varied between 0.01 and 0.001 percent. Without application of electric field no level difference could be recorded with any pair of fluids.

The following considerations seem to explain the above phenomena: when both sides—divided by a glass filter—are filled with the same described liquid, the number of molecules diffusing through the diaphragm in the ac field will be equal in both directions and no difference of levels will appear.

When a salt is dissolved in one compartment only, the ions become solvated. The diffusion velocity through the diaphragm will be less for the more solvated ions than that of the molecules coming from the other side. Consequently, in an ac field the level will rise in that compartment to which the ions had been added.

The degree of molecule-association is high in the higher alcohols (propyl-, amyl-, isobutylalcohol). The presence of the foreign ions decreases the degree of the association by means of the solvation effect. This fact may explain why in an ac field the solution with smaller associated groups diffuses towards the pure solvent having undiminished associated groups.

When both sides are filled with different liquids, the solvation rather than the associated molecules will play the decisive role. The rise will take place on that side in which the degree of association is higher.

In the case of pierced-hole diaphragm, the diffusion of ions is only slightly hindered. In an ac field the ions diffuse to the other side, carrying their solvatation shells with them, so the diffusion of the liquid with greater conductivity is easily explained. In the case, however, when a liquid with a lower conductivity diffuses into the liquid with a greater conductivity, the difference of conductivities is small. If the solvatation diameter of the ions of the diffusing liquid is larger than that of the ions of the other liquid, the diffusion of the liquid with smaller conductivity becomes evident.

The dependence on frequency is to be explained by supposing that with higher frequencies the size of the molecule groups of some kinds of liquids decreases more rapidly than that of other liquids.

[1] Z. László, Hung. Acta Phys. 1, 44 (1949); J. Chem. Phys. 17, 507 (1949), and 18, 567 (1950); Kolloid Z. 114, 151 (1949).

Cathode Luminescence of Crystalline Quartz

D. D. SAKSENA AND L. M. PANT
Department of Physics, University of Allahabad, Allahabad, India
November 1, 1950

THE luminescence in quartz appears to be very feeble. The cathode luminescence in quartz was investigated by Northrup[1] who found a broad band extending from 5280A to 2410A with a maximum at 4300A. Peters[2] observed red-phosphorescence in pure quartz and glass under the action of cathode rays of low voltage, and he considered that the Si—O group is responsible for this luminescence. According to Leverenz,[3] pure $Si-O_2$ possesses appreciable cathode luminescence extending from 4900 to 3000A which is quite different from the spectra of silicates excited by manganese. The manganese activator is believed to be associated with cation lattice positions whereas pure crystal emission centers are the Si—O radicals. Webb[4] noticed a luminescence of short duration in fused quartz in the region 3700–4750A when excited by a wavelength less than 2270A which is not seen in crystalline quartz. Perrine[5] found that quartz shows no trace of luminescence when exposed to x-rays, and according to Lyman[6] the ultraviolet luminescence is so feeble that it is doubtful whether it exists at all. Nichols and Howes[7] report that quartz does not visibly fluoresce at room temperature with ultraviolet light, but with metallic impurities it gives rise to definite emission.

We have investigated the cathode luminescence spectra of amethyst quartz, colorless crystalline quartz, and glass and also

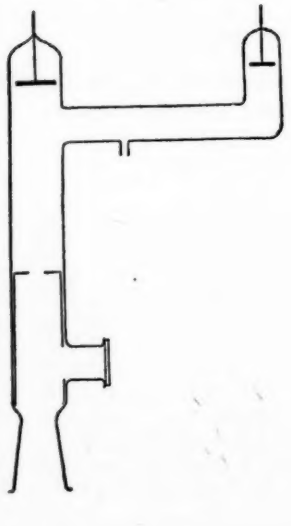

FIG. 1.

of fluorite and barium chloride. A Pyrex-glass discharge tube having a quartz window shown in Fig. 1 was used for investigation. A suitably ground anti-cathode fits in the ground-glass cone of the discharge tube, and a small piece of the crystal was mounted on the sloping edge of the anti-cathode. The tube was evacuated to the fluorescent stage by means of two Warren- mercury-diffusion pumps in series backed by a Cenco-hyvac pump. The cathode luminescence in quartz is so feeble that cathode rays had to be generated by a large induction coil which gave 70,000 volts across the secondary terminals, and exposures running to six hours were given by a constant deviation type baby quartz spectrograph. Because of long exposures a number of lines appear on the plates which may be identified with the bands of mercury, Co^+, OH, N_2, and oxygen. The intensity of these lines differs considerably in different spectrograms, and this is most likely due to the conditions prevailing in the discharge tube. In order to separate the luminescence effects and to identify the lines, a spectrum was recorded with light reflected from a polished metal plate in place of the crystal. The results are shown in Table I.

TABLE I.

Spectr. no.	Description of crystal	Voltage used	Time of exposure	Nature of the spectrum
(1)	Metal surface	70,000	6 hr	No continuum.
(2)	Amethyst quartz	70,000	6 hr	A strong continuum in the region 6550 to 5650A. Another strong but slightly weaker continuum from 4900 to 3000A with a minimum intensity in the region 3700 to 3200A. The surface turns orange and finally brown on prolonged exposure.
(3)	Colorless transparent natural quartz	70,000	6 hr	The continuum between 4900 and 3000A is very faint but there is a prominent continuum in the region 6550 to 5650A.
(4)	Colorless glass	70,000	6 hr	A very faint continuum in the region 4900 to 3000A.
(5)	$BaCl_2$	70,000	10 min	A strong and broad diffuse band from 5000 to 3100A with a maximum in the range 4300 to 3800. Northrup (see reference 1) also found a continuum in the region 5280 to 2320A.
(6)	Colorless transparent fluorite	4000	45 min	A strong continuum extending from 4500 to 2300A. The intensity shows a slight increase in the region 3550 to 3300A and then decreases towards shorter wavelengths. Another weak maximum occurs between 3000 and 2650. The crystal fluoresces with blue light. With 70,000 volts the surface of the crystal turned violet.

The first four spectra are reproduced in Fig. 2. It may be seen that both amethyst and colorless quartz give a continuum in the region 5650–6550A which is very weak in the case of glass. This band has not been reported by earlier workers and J. de Ment[8] states that amethyst quartz rarely shows visible fluorescence. This suggests two possibilities that either the amethyst and the colorless quartz used by us have the same impurity or the band 6550–5650A is a characteristic emission of crystalline quartz. The former view appears to be less probable in view of the fact that the amethyst was colored deep violet and the other quartz piece was colorless, and the two quartz pieces did not belong to the same locality. On the other hand it is possible that this band may correspond to the red-phosphorescence band observed by Peters in pure quartz and glass. Since these bands are present in the amethyst and the colorless quartz, and also perhaps in glass, they may in some way be associated with the SiO bonds in quartz, but on this view it is not clear why the intensity of the continuum is so small in the case of the glass and so large in the case of the amethyst. According to Pringsheim,[9] the luminescence in fluorites

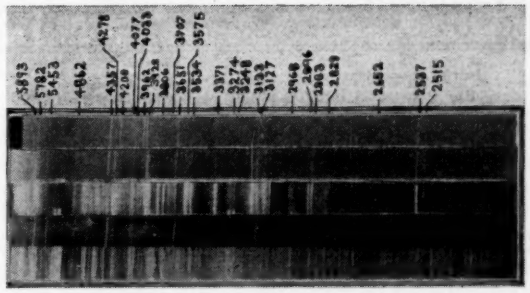

FIG. 2. Cathode luminescence spectra of (a) colorless glass (b) colorless crystalline quartz (c) violet-colored amethyst quartz (d) light reflected from a metal plate from the interior of the cathode tube.

is due to the impurities and the production of F centers by irradiation. It is therefore possible that the 5650–6550 band in quartz may be due to the production of some F centers on account of the intense excitation by the cathode rays.

We are thankful to the Council of Scientific and Industrial Research for a research grant and a fellowship to one of us (L. M. P.).

[1] Nichols, Howes, and Wilbur, *Northrup cathode-luminescence and the luminescence of incandescent solids*, p. 106.
[2] H. Peters, Phys. Rev. **36**, 1631 (1930).
[3] H. W. Leverenz, *Luminescence of Solids*, p. 220.
[4] H. W. Webb and H. A. Messenger, Phys. Rev. **34**, 1463 (1929).
[5] J. O. Perrine, Phys. Rev. **22**, 48 (1923).
[6] T. Lyman, Phys. Rev. **40**, 578 (1932).
[7] E. L. Nichols and H. L. Howes, J. Opt. Soc. Am. **6**, 42 (1922).
[8] J. de Ment, *FluoroChemistry* (Chemical Publishing Company, New York), p. 466.
[9] P. Pringsheim, *Fluorescence and Phosphorescence* (Interscience Publishers, New York).

Bromination of Hydrocarbons. III. Photo-Bromination of Toluene

E. W. SWEGLER, H. A. SCHERAGA, AND E. R. VANARTSDALEN
Department of Chemistry, Cornell University, Ithaca, New York
November 20, 1950

CARBON–HYDROGEN bond strengths in simple alkanes have been determined from kinetic studies of photo-bromination of these hydrocarbons.[1] Also pyrolysis experiments have given corresponding values for carbon-hydrogen bonds in the alkyl side chains of aromatic hydrocarbons.[2] It appeared desirable to extend the photo-chemical method to the alkyl side chain cases in aromatic compounds.

We should like to report here some preliminary results on the photo-bromination of toluene which indicate a similarity in reaction mechanism to that previously reported for the alkanes.

Using experimental techniques to be described in detail later, the photo-bromination of toluene in the gas phase at 110.3°C was found to proceed according to the following rate laws for the initial part of the reaction, without taking into account inhibition by the products of the reaction:

$$-\frac{d(Br_2)}{dt}=k_I(Br_2)^{\frac{1}{2}}(C_6H_5CH_3)P^{-\frac{1}{2}}, \quad (1)$$

or

$$-\frac{d(Br_2)}{dt}=k_{II}(Br_2)^{\frac{1}{2}}(C_6H_5CH_3)^{\frac{1}{2}}, \quad (2)$$

where P is the total pressure and k_I and k_{II} are products of specific rate constants and apparatus factors including light intensity. It is evident that these two rate laws are essentially identical when the concentration of bromine is small compared with that of toluene. This is the situation in our experiments. Some of the data, involving approximately a twofold variation in the initial bromine concentration and over a threefold variation in the initial toluene concentration, are shown in Table I.

The bromination appears to be inhibited by the products of the reaction and by oxygen.

TABLE I. Photo-bromination of toluene at 110.3°C at constant light intensity. (Wavelength 4890A.)

Initial concentrations Br_2	$C_6H_5CH_3$	$k_I \times 10^4$	$k_{II} \times 10^4$
37.6 mm	313 mm	5.7 sec^{-1}	5.5 sec^{-1}
26.0	370	5.6	5.4
20.8	141	5.3	4.9
18.6	471	5.5	5.4

On this basis it appears that photo-chemical dissociation of bromine molecules is followed by a chain reaction involving formation of benzyl radicals, with a chain termination step of recombination of bromine atoms by three-body collisions in the gas phase as has been found in the case of the alkanes. The difference in rate laws (1) and (2) is ascribable to the nature of the third body in the homogeneous recombination but both rate laws correspond to the same chain mechanism for bromination. Molecules with many degrees of freedom, such as toluene, would be expected to be very efficient third bodies and when present in high concentration would make distinction between the two rate laws difficult. A similar situation has been found in the photo-chemical bromination of neopentane.[3] It is also suggested that HBr may serve an inhibiting role leading to regeneration of bromine atoms by removal of benzyl radicals.

This problem is being investigated further.

[1] Andersen, Kistiakowsky, and VanArtsdalen, J. Chem. Phys. **10**, 305 (1942); G. B. Kistiakowsky and E. R. VanArtsdalen, *ibid.* **12**, 469 (1944); H. C. Andersen and E. R. VanArtsdalen, *ibid.* 479 (1944).
[2] M. Szwarc, Nature **160**, 403 (1947); J. Chem. Phys. **16**, 128 (1948) and erratum **16**, 637 (1948); **16**, 609 (1948); **17**, 431 (1949).
[3] Hormats and E. R. VanArtsdalen, manuscript in preparation.

Erratum: The Infra-Red Spectrum of Acetylene

[J. Chem. Phys. **18**, 1382 (1950)]
E. E. BELL AND H. H. NIELSEN
Ohio State University, Columbus, Ohio

THE band $\nu_2 - \nu_5^1$, with a frequency of 1243.3 cm^{-1}, has been improperly labeled as $\nu_1 - \nu_5^1$ in Table XI, in the title of Fig. 3, and in the paragraph about this band on p. 1386.

Concerning the Steric Factor of Free Radical Reactions

ROBERT GOMER
Institute for the Study of Metals, The University of Chicago, Chicago, Illinois
AND
LEON M. DORFMAN
Knolls Atomic Power Laboratory, The General Electric Company, Schenectady, New York
November 8, 1950

IN a recent paper M. Szwarc[1] repeats the statement made previously[2] that reactions of free radicals in general have steric factors close to unity. In particular, the reaction (using the numbering of Szwarc[1]),

$$CH_3 + \phi CH_3 \rightarrow CH_4 + \phi CH_2, \qquad (2)$$

is discussed; and the conclusion is drawn that this reaction has a steric factor of about 0.3. This figure is arrived at by considering the pyrolysis in a flow system of ϕC_2H_5, $Hg(CH_3)_2$, and di-tert-butyl peroxide. The last is also investigated in a static system. The calculations are made for s_2^2/s_4 by assuming that the collision numbers of reaction (2) and reaction (4):

$$CH_3 + CH_3 \rightarrow C_2H_6 \qquad (4)$$

are given by 10^{12} (mole/cc)$^{-1}$ sec^{-1} in each case. It may readily be verified that assignment of this collision number to reaction (2) implies a collision diameter of about 0.3A. If the much more probable diameter of 5A is used, the collision number becomes 5×10^{14} for reaction (2). The rate constant of reaction (4) has recently been evaluated[3] $k_4 = 5 \times 10^{13}$ (mole/cc)$^{-1}$ sec^{-1}, which is also larger than 10^{12}.

If no *a priori* assumptions are made about the "normal" collision numbers of reactions (2) and (4) and if the value of $k_4 = 5 \times 10^{13}$ is used (which is more favorable to Szwarc's argument than 10^{12}), and E_2 is taken to be 11 kcal/mole, as Szwarc indicates,[1] it is possible to calculate from the data given[1] the values of $s_2\sigma_2^2$ at the various temperatures:

T°K	$s_2\sigma_2^2$ cm^2	s_2 (for $\sigma = 5$A)	s_2 (for $\sigma = 10$A)
403	6.8×10^{-18}	2.7×10^{-3}	6.8×10^{-4}
503	1.2×10^{-17}	4.8×10^{-3}	1.2×10^{-3}
793	1.0×10^{-17}	4.0×10^{-3}	1.0×10^{-3}
983	8.4×10^{-18}	3.4×10^{-3}	8.4×10^{-4}.

It is seen that any reasonable assignment of collision diameter for reaction (2) leads to a steric factor of the order of 10^{-3} from Szwarc's own data.[1] An uncertainty of 2 kcal/mole in E_2 can change these results by a factor of 10 at the lowest and 2.8 at the highest temperature considered.

The method used by Szwarc to calculate $k_2/k_4^{\frac{1}{2}}$ unfortunately involves assumptions about the steady-state concentration of CH_3 radicals, which are at best approximate. It is assumed that the rate of disappearance of CH_3 radicals can be sufficiently approximated by the rate of that reaction which is predominant in any given case, namely, by either CH_4 or C_2H_6 formation. This assumption is certainly valid when $C_2H_6/CH_4 = 0.01$ or 100, but becomes questionable when the ratio takes values of 0.25 or 3.0. Since Szwarc lists only the ratio of ethane to methane, it is impossible to improve on the calculations. Had the separate values of CH_4 and C_2H_6 been given, it would have been possible to apply the more rigorous expression,

$$k_2/k_4^{\frac{1}{2}} = R_{CH_4}/(R^{\frac{1}{2}}_{C_2H_6} \times \phi_{CH_3}),$$

which, in its various forms, has been used by several authors,[4,5] with the advantage that a knowledge of the rate of the methyl generating reaction is not needed, as in Szwarc's method.

In view of the foregoing it is concluded that it is not justifiable to draw the conclusion of normal steric factors for radical reactions from the data cited.[1] There have recently appeared papers[3,5] in which reactions of type (2) with several compounds were studied photo-chemically in static systems, leading to the conclusion that such reactions have steric factors of the order of 10^{-3} to 10^{-4}. It is quite true, however, that radical recombinations (at least reaction (4)) do show normal efficiencies.

[1] M. Szwarc and J. S. Roberts, Trans. Farad. Soc. **46**, 625 (1950).
[2] M. G. Evans and M. Szwarc, Trans. Farad. Soc. **45**, 940 (1949).
[3] R. Gomer, J. Chem. Phys. **18**, 998 (1950); R. Gomer and G. B. Kistiakowsky, J. Chem. Phys. **18**, 85 (1951).
[4] A. F. Trotman-Dickenson and E. W. R. Steacie, J. Am. Chem. Soc. **72**, 2310 (1950).
[5] L. M. Dorfman and R. Gomer, Chem. Rev. **46**, 499 (1950).

The Photographic Infrared Spectrum of CD_3CCH and the Structure of Methyl Acetylene

G. HERZBERG, A. VALLANCE JONES, AND L. C. LEITCH
National Research Council of Canada, Ottawa, Canada
November 22, 1950

THE photographic infrared spectrum of ordinary methyl acetylene (CH_3CCH) has been investigated by Herzberg, Patat, and Verleger.[1] They showed that the moment of inertia derived from this spectrum leads to an abnormally small value for the carbon-carbon single bond distance if all other bond lengths and angles were assumed to be normal. This result was confirmed by Badger and Bauer[2] using the same photographic infrared band, and later by Pauling, Springall, and Palmer[3] on the basis of electron diffraction work. As pointed out by HPV, it would be desirable to determine the moment of inertia of CD_3CCH in order to obtain a check on the assumption made.

Recently one of us[4] developed a synthesis of heavy methyl acetylene which made it possible to prepare a quantity of CD_3CCH

sufficient for an investigation of its photographic infrared spectrum. Using an absorbing path of 120 m, two strong || bands were found at 10308 and 7852A and two very weak bands at 8467 and 7902A. The two strong bands are without doubt the second and third overtones of the ≡C−H stretching mode ($3\nu_1$ and $4\nu_1$). The strongest band, at 10308A, is the analog of the CH_3CCH band studied by HPV.

The fine structure of the two bands 10308 and 7852A was clearly resolved in the first and second order, respectively, of a 21-ft grating. By standard methods the following values for the rotational constants B of CD_3CCH were obtained:

$$B_0=0.2456_6,\quad B_3=0.2438_3,\quad B_4=0.2433_5\ \text{cm}^{-1}.$$

The $\Delta_2F''(J)$ values from which B_0 was determined do not show clearly the effect of the rotational constant D_J. But an approximate value, $D_J\approx 5\times10^{-7}$ cm^{-1}, was obtained from the lines of high J of the P branch (for which corresponding lines in the R branch are not resolved and which can, therefore, not be used for the $\Delta_2F''(J)$ curve); and this D_J value was used in determining B_0 from the $\Delta_2F''(J)$ values. When the same correction is applied to the values of HPV, a corrected B_0 value of CH_3CCH is obtained:

$$B_0=0.2847_5\ \text{cm}^{-1}.$$

The uncertainty of the B values is estimated to be ±0.00020 for CD_3CCH and ±0.00040 for CH_3CCH. The accuracy is somewhat less than customary for photographic infrared work because the unresolved K structure makes the lines broad.

Using $I_B=27.98_{30}\times10^{-40}/B$, the moments of inertia in the lowest vibrational level are:

$$\text{for } CD_3CH,\quad I_B^{[0]}=113.91\times10^{-40}\ \text{g cm}^2,$$
$$\text{for } CH_3CCH,\quad I_B^{[0]}=98.27\times10^{-40}\ \text{g cm}^2.$$

These two moments of inertia are still not sufficient to determine all the geometrical data. But if the C≡C and C−H distance in the acetylene group are assumed to be the same as in C_2H_2 (i.e., 1.207 and 1.059A, respectively[5]) and if the C−H distance in the methyl group is assumed to be the same as in methane (1.093A), then the two remaining parameters, the C−C distance and the HCH angle, can be determined. The result is

$$r(C-C)=1.461\pm0.006A,\quad \sphericalangle HCH=108°6'\pm1°.$$

During the preparation of these results we obtained, through the courtesy of Professor Gordy, the manuscript of a paper by Trambarulo and Gordy[6] on the microwave spectrum and structure of methyl acetylene. They observed the microwave spectrum for a sufficient number of isotopic species to make it possible to determine all geometric parameters independently of any assumption about bond lengths. Their value for I_B^0 of CH_3CCH is $98.17_{23}\times10^{-40}$ g cm^2, which agrees well with the (less accurate) value of HPV. They did not obtain the spectrum of CD_3CCH here described. The assumptions made above for the C≡C and C−H distances are confirmed by Trambarulo and Gordy within ±0.003A and the values for r(C−C) and ∢HCH given above agree with theirs within 1/5 of the uncertainty assigned to our values.

It must be emphasized that both Trambarulo and Gordy's and our bond distances and angles depend on the assumption that the effect of zero-point vibrational motion can be neglected. To be free of this assumption, one will have to determine all the rotational constants α_i. Our data allow only the determination of α_1 which is found to be 0.00060 cm^{-1}.

Further work on the infrared spectra of CD_3CCH, CD_3CCD, and CH_3CCH, both in the region of the fundamentals and the overtones, is in progress.

[1] Herzberg, Patat, and Verleger, J. Chem. Phys. 41, 123 (1937), in future referred to as HPV.
[2] R. M. Badger and S. H. Bauer, J. Chem. Phys. 5, 599 (1937).
[3] Pauling, Springall, and Palmer, J. Am. Chem. Soc. 61, 2922 (1939).
[4] L. C. Leitch and R. Renaud (to be published).
[5] See G. Herzberg, *Infrared and Raman Spectra of Polyatomic Molecules* (D. Van Nostrand and Company, Inc., New York, 1945).
[6] R. Trambarulo and W. Gordy, J. Chem. Phys. 18, 1613 (1950).

Infrared Absorption Spectrum of $H_2C=CHD$

C. Courtoy, M. de Hemptinne, and M. V. Migeotte
Institut de Physique, Parc d'Aremberg, Louvain, France
November 22, 1950

In preceding works[1] it has not been possible to assign all the fundamental frequencies of $H_2C=CHD$. We have hoped that the study of the rotational fine structure of the unassigned experimental frequencies lower than 1200 cm^{-1} using the grating spectrograph of the Institut d'Astrophysique de l'Université de Liège[2] might solve the question definitely.

Although we are not yet able to present the complete solution, we think that the results of our measurements may be of some use.

The infrared spectrum shows:

(1) At 1121 cm^{-1} an absorption band of medium intensity and of the parallel type. The corresponding line in the Raman spectrum is strong and polarized; this makes the assignment of the line very difficult.

(2) At 1000.44 cm^{-1} a strong absorption band of perpendicular type. The Q bands may be found using a formula based on the model proposed by W. S. Gallaway and E. F. Barker for ethylene:

$$\nu=1000.44+3.13K'^2-3.2K''^2-0.0005K'^4+0.0003K''^4.$$

(3) At 943.68 cm^{-1}, a strong absorption band of a perpendicular type, the Q bands being very accurately given by the formula:

$$\nu=943.68+3.12K'^2-3.2K''^2-0.0003(K'^4-K''^4).$$

(4) At 807.88 cm^{-1} a strong perpendicular band, the Q band being given by

$$\nu=807.88+3.25K'^2-3.2K''^2+0.0003K''^4.$$

A second, but weaker, maximum appears at 809.68 cm^{-1}; it is possible that two bands superpose in this region, but we were unable to find a reasonable formula taking all the lines into account.

(5) Around 765.02 cm^{-1} a somewhat complicated absorption spectrum.

[1] M. de Hemptinne, 7ième conseil de Chimie Solvay, p. 161 (1948). M. de Hemptinne and C. Courtoy, Ann. Soc. Sci. Série I 63, 98 (1949). W. S. Gallaway and E. F. Barker, J. Chem. Phys. 7, 96 (1942).
[2] M. Migeotte, Mem. soc. roy. sci. Liège, Tome I, Fasc. 3 (1945).

On the Viscosity of Liquid Hydrocarbon Mixtures

Fausto W. Lima
Escola Politécnica, Department of Chemistry, University of São Paulo, São Paulo, Brazil
October 23, 1950

Trevoy and Drickamer[1] presented data on the viscosity of binary mixtures of normal paraffins, benzene, and 2.4 dimethyl pentane in 50 mole percent concentration. It was shown that Roegiers and Roegiers' formula[2] best correlated the viscosity data on those mixtures and that the use of the mentioned formula to calculated viscosities of the mixtures yielded values subject to an average error of about 5 percent and a maximum error of 14 percent.

Recently Lima[3] showed that the application of Souders' Viscosity Constant[4] to mixtures would give the following relation between the viscosity of the mixture η and the viscosities of pure components

$$\log\log\eta=(x_1I_1+x_2I_2)(d-k)/(x_1M_1+x_2M_2), \qquad (1)$$

where x_i ($i=1, 2$) is the mole fraction of component i, M_i its molecular weight, I_i its Souders Viscosity Constants,[4] d the density of the mixture in g/cc, and k is a constant. The value of k depends only on the type of mixture and not on concentration or temperature, and so it can be determined by the knowledge of the viscosity of the mixture at one concentration and temperature and be used for other concentrations and temperatures. For the values determined by Trevoy and Drickamer, $x_1=x_2=0.5$, and so

$$\log\log\eta=(I_1+I_2)(d-k)/(M_1+M_2). \qquad (2)$$

TABLE I.[a] Observed and calculated viscosities of 50 mole percent liquid mixtures.

Mixtures	T°K	k	η_{calc}	η_{obs}[b]	$\Delta\eta/\eta$%
Ph$-n$C$_7$	298.0	2.928	...	4.167	...
	318.0		3.38	3.407	−0.9
	335.8		2.87	2.850	+0.6
Ph$-n$C$_{10}$	298.0	2.935	...	6.712	...
	318.0		5.18	5.262	−1.5
	335.8		4.26	4.272	−0.3
Ph$-n$C$_{12}$	298.0	2.921	...	9.053	...
	318.0		6.73	6.904	−2.6
	335.8		5.34	5.494	−2.81
Ph$-n$C$_{14}$	298.0	2.920	...	12.394	...
	318.0		9.15	9.217	−0.7
	335.8		7.00	7.175	−2.4
Ph$-n$C$_{16}$	298.0	2.925	...	16.502	...
	318.0		11.9	11.919	+0.1
	335.0		8.79	9.081	−3.2
	298.0		16.5	16.515	−0.1
	318.0		11.9	11.928	0.0
	335.8		8.79	9.100	−3.3
Ph$-n$C$_{18}$	298.0	2.916	...	21.226	...
	318.0		15.3	15.012	+2.2
	335.8		11.0	11.284	−2.1
nC$_7-n$C$_{12}$	298.0	2.888	...	7.873	...
	318.0		6.00	6.058	−1.8
	335.8		4.74	4.859	−2.4
	298.0		7.87	7.868	+0.1
	318.0		6.00	6.054	−1.7
	335.8		4.74	4.849	−2.2
nC$_7-n$C$_{14}$	298.0	2.887	...	10.314	...
	318.0		7.50	7.754	−3.3
	335.8		5.90	6.149	−4.1
nC$_7-n$C$_{16}$	298.0	2.885	...	13.766	...
	318.0		9.90	10.046	−1.5
	335.8		7.64	7.765	−1.6
nC$_7-n$C$_{18}$	298.0	2.879	...	17.300	...
	318.0		12.6	12.412	+1.2
	335.8		9.49	9.416	+0.8
iC$_7-n$C$_{12}$	298.0	2.882	...	7.489	...
	318.0		5.71	5.809	−1.6
	335.8		4.58	4.682	−2.2
iC$_7-n$C$_{16}$	298.0	2.885	...	13.144	...
	318.0		9.30	9.631	−3.5
	335.8		7.23	7.510	−3.8
Ph$-i$C$_7$	298.0	2.935	...	3.825	...
	318.0		3.17	3.140	+1.0
	335.8		2.72	2.641	+3.0

[a] T = temperature °K; k = constant, Eq. (1); η_{calc} = calculated viscosity in millipoise; η_{obs} = observed viscosity in millipoise; $\Delta\eta/\eta$ = deviation in percent.
[b] Taken from Trevoy and Drickamer (reference 1).

Equation (2) was applied to the data of Trevoy and Drickamer,[1] giving an average error of 1.8 percent and a maximum error of 4.1 percent. The values of the constant k were calculated with the data at 298.0°K for every mixture. Values of I_i were taken from Souders'[4] work for every component of the mixtures. No results are shown for η at 298.0°K, since the deviation would be zero, obviously. The results are shown in Table I.

[1] D. G. Trevoy and H. G. Drickamer, J. Chem. Phys. 17, 582 (1949).
[2] M. Roegiers and K. Roegiers, *The Viscosity of Normal Fluids* [Societé des Huiles de Cavel e Roegiers (Electron Oil Works) Conpure 197, Ghent, 1945].
[3] F. W. Lima, "On the viscosity of binary liquid mixtures," Thesis, University of Wisconsin, 1950; Anais Acad. Bras. Cienc., to be published.
[4] M. Souders, Jr., J. Am. Chem. Soc. 60, 154 (1938).

Vibration-Rotation Spectrum and Structure of Monochlorosilane

ANDRÉ MONFILS
University of Liège, Liège, Belgium
November 10, 1950

UP to the present, a great deal of work in infrared spectroscopy has been devoted to molecules having C_{3v} symmetry, with special emphasis on the CH_3X (X=halogen) compounds.[1] In contrast to the many studies of organic compounds, silicon compounds of the same symmetry have received little attention; and, in particular, the SiH_3X molecules have not been investigated in spite of their considerable importance. The purpose of this note is to report briefly on some results which we have obtained for SiH_3Cl.

Infrared spectra of SiH_3Cl vapor were recorded with a Perkin-Elmer model 12C spectrometer in the region 650 cm^{-1} to 2200 cm^{-1} and with the prism-grating spectrometer described elsewhere by M. V. Migeotte.[2] The spectra were obtained at pressures ranging from 5 to 0.3 mm Hg, by means of gas cells having optical thicknesses of 17 and 10 cm. The following fundamental frequencies (cm^{-1}) were found:

770 952 1090 2150 2195.

Only three of the bands have been observed at high dispersion (952, 2150, 2195) and for them the origins have been located with accuracy. For the remaining two the figures given correspond to the middle of the band.

If the molecule is assumed to have a C_{3v} symmetry, it follows that the six normal modes are divided into three totally symmetric and three doubly degenerate vibrations, giving rise respectively to parallel and perpendicular bands. The bands observed at 952 and 2150 cm^{-1} are perpendicular, whereas the band at 2195 cm^{-1} is parallel. The only possibility left for the bands at 770 and 1090 cm^{-1}, taking into account their contours and magnitudes, is to identify them as respectively perpendicular and parallel. The following assignment of the bands to the normal modes is given (Dennison's notation):

$$\nu_1=2195 \qquad \nu_2=2150$$
$$\nu_3=1090 \qquad \nu_4=\ 952$$
$$\nu_5\cong\ 460 \qquad \nu_6=\ 770.$$

The question as to what is the value of ν_5, which has not been observed, is solved by analogy with the value measured in similar compounds.[3] For the ν_5 frequency, corresponding to the SiCl vibration, a value of 460 cm^{-1} is proposed.

The structure of the bands at 2150 and 952 cm^{-1} indicates the presence of a threefold symmetry axis, every third Q branch being enhanced. The infrared evidence is therefore in favor of a C_{3v} symmetry, in agreement with the microwave results.[4] The spacing between the zero branch lines is reduced to 5.48 cm^{-1} for the 2150 cm^{-1} band and to 6.18 cm^{-1} for the other if one takes into account a slight convergence observed for the latter band. The variation in the spacings is due to a coupling between the rotation and the internal angular momentum of vibrational origin. One is struck by the appearance of a rather regular fine structure between the Q branches of the 952 cm^{-1} band. This must be due to the lines of the P and R branches, which nearly exactly overlap one another. The average spacing between these lines in the best parts of the band is 0.449 cm^{-1}. From this result we can therefore deduce $I_A=124.52\times10^{-40}$ g-cm^2, where I_A is the moment of inertia about an axis perpendicular to the symmetry axis of the molecule. This result compares favorably with the microwave data,[4] which give $I_A=125.6815\times10^{-40}$ g-cm^2. Since the perpendicular band at 770 cm^{-1} has not yet been resolved, it is not possible to draw any precise conclusion about I_c, the other moment of inertia.

However, if we assume the spacing between the Q branches to be 4.1 cm^{-1}, by analogy with what occurs in CH_3Cl,[5] we can deduce $I_c=9.7\times10^{-40}$ g-cm^2 for SiH_3Cl, instead of 9.33×10^{-40} g-cm^2 obtained by Trindal, Straley, and Nielsen for SiH_4.[6] Future measurements on ν_6, which are now planned, will allow us to determine I_c with much greater accuracy. A detailed account of this work will appear in the near future.

We are particularly indebted to Dr. Jules Duchesne, who suggested the problem, for his constant interest and many helpful discussions. Our thanks are also due to Professor L. D'Or for advice in connection with the preparation of SiH_3Cl, and to Dr. M. V. Migeotte for much help during the course of the spectroscopic experiments.

The sample of $SiHCl_3$ used in the preparation of SiH_3Cl was generously supplied by Professor E. G. Rochow, to whom we wish to express our gratitude. This research has been made possible thanks to the financial aid of the Fonds National Belge de la Recherche Scientifique.

[1] G. Herzberg, *Infrared and Raman Spectra* (D. Van Nostrand Company, Inc., New York, 1945).
[2] M. V. Migeotte, Mém. soc. roy. sci. Liège, 1è Série, Fasc. 3, Tome I (1945).
[3] A. Anspach and J. Duchesne, J. Chem. Phys. **16**, 1106 (1948); *ibid.* **17**, 1101 (1949); Goubeau, Siebert, and Winterwerb, Z. anorg. Chem. **259**, 240 (1949); Shimanouchi, Tsuchiya, and Mikawa, J. Chem. Phys. **18**, 1306 (1950).
[4] Dailey, Mays, and Townes, Phys. Rev. **76**, 136 (1949).
[5] A. H. Nielsen and H. H. Nielsen, Revs. Modern Phys. **16**, 241 (1944).
[6] Tindal, Straley, and Nielsen, Phys. Rev. **62**, 151 (1942).

Erratum: The Vibrational Spectra and Structure of Inorganic Molecules. II. Sulfur S_8, Sulfur Chloride S_2Cl_2, Phosphorous P_4

[J. Chem. Phys. **18**, 1018 (1950)]

H. J. Bernstein and J. Powling
Division of Chemistry, National Research Council, Ottawa, Canada

CLEVELAND has pointed out[1] that difference bands cannot be involved in Fermi resonance with a fundamental of nearly the same frequency because the energy states of the upper levels in the two cases are too different. The bands at 150 cm^{-1} and 200–250 cm^{-1} in the infrared spectrum of sulfur (Table I) cannot be interpreted then as arising from resonance splitting as was done in this paper.

When all interpretations involving Fermi resonance with difference bands are deleted, there is no plausible interpretation of the band at 150 cm^{-1}, whereas the explanation of the band at 200–250 cm^{-1} is still satisfactory. This throws some doubt only on the assignment of $\nu_6=190$ cm^{-1}, since the assignment of the other fundamentals is not involved in this revision. Best arithmetic agreement between observed and calculated combination tones is obtained for $\nu_6=190$ cm^{-1} instead of the other possible choice of $\nu_6=150$ cm^{-1}. For this reason it seems preferable to retain the assignment for ν_6 suggested in the above paper and leave the band at 150 cm^{-1} unexplained.

A similar error has been made also in assigning a few of the weaker bands in "Vibration spectra of *cis* and *trans* $C_2H_2Cl_2$ and $C_2D_2Cl_2$."[2] The weak bands at 985 cm^{-1} in Table II, at 1179 and 1314 cm^{-1} in Table III, and 826 cm^{-1} in Table IV require a different interpretation from that given in this paper. These minor changes will not effect the results and assignments obtained in that work. Possible interpretations of these weak bands are

$$985=349+2\times192=998(B_u)$$
$$1179=2\times(761-171)=1180A_1$$
$$1314=368+558+406=1332B_2$$
$$826=658-346+784-265=831A_u.$$

[1] F. F. Cleveland (private communication).
[2] H. J. Bernstein and D. A. Ramsey, J. Chem. Phys. **17**, 556 (1949).

Erratum: Kinetics of OH Radicals from Flame Emission Spectra. I

[J. Chem. Phys. **18**, 1221 (1950)]

K. E. Shuler
Applied Physics Laboratory, The Johns Hopkins University, Silver Spring, Maryland

OWING to an arithmetical error, some of the quantities referring to the 2→3 transition of OH in Table III are incorrect. For $|M_{2-3}|^2$ (with $\rho=-0.754$) now read 0.002 instead of 0.686, for A_{2-3} read 0.001 instead of 0.442. The curve for the 2→3 transition in Fig. 3 should be deleted. The relative lifetime τ_{rel} for $v'=2$ is now 1.13 instead of 0.76, and $\tau_{abs}\cdot10^6$ sec is now 4.3 rather than 2.9. The statement that the lifetime of OH^* in the $v'=2$ level may be somewhat shorter than in the other vibrational levels is now incorrect. These corrected results are in better agreement with the experimental observations on the very weak 2→3 band. The above corrections do not affect the conclusions of this paper or the one subsequent to it (Part II).

The Superposition Approximation in Statistical Mechanics of Compressed Gases

R. W. Hart, R. Wallis, and L. Pode
The Catholic University of America, Washington, D. C.
November 2, 1950

THE "superposition approximation" suggested by Kirkwood[1] provides a convenient approach to approximate determination of the distribution of pairs of molecules, $n_2(\mathbf{r}_1, \mathbf{r}_2)$. (For a system of N molecules, $n_2(\mathbf{r}_1, \mathbf{r}_2)\,d\mathbf{r}_1 d\mathbf{r}_2$ specifies the probability that two molecules have their centers in volume elements $d\mathbf{r}_1$ at $\mathbf{r}_1$ and $d\mathbf{r}_2$ at $\mathbf{r}_2$, and is normalized to $N(N-1)\simeq N^2$.) The quantitative effect of the superposition approximation is, in general, very difficult to determine because most problems which may be solved with its use are not solvable without this approximation.

One estimate of the reliability of superposition may be obtained by calculating virial coefficients of a hard sphere gas and comparing the values with those derived without approximation by Boltzmann and Happel.[2] We have carried out calculation of the first four virial coefficients with the aid of the Born-Green[3] integro-differential equations.

The equation of state may be expressed in terms of the pair distribution function in the following way:[4]

$$PV=NkT\left\{1-(V/6NkT)\int\eta_2(r)\phi^1(r)4\pi r^3dr\right\}, \tag{1}$$

where $\phi(r)$ is the potential energy of a pair of molecules whose centers are a distance r apart and k is Boltzmann's constant. This equation is simplified by defining a new function $f(r)$ by the relation:

$$n_2(r)=N^2/V^2[1+f(r)]\exp(-\phi(r)/kT). \tag{2}$$

We use the hard sphere interaction potential function

$$\phi(r)=\begin{cases}0 & \text{when } 0\le r<1\\ \infty & \text{when } 1\le r\end{cases}$$

(where the sphere diameter is taken as the unit of length) with Eq. (2) to write the equation of state as:

$$PV=NkT\{1+(Nb/V)(1+f(1))\}, \tag{3}$$

where $b=2\pi/3=4$ times the volume of one molecule. If $f(r)$ is expanded in powers of the density according to

$$f(r)=\sum_{n=1}^{\infty}\left(\frac{N}{V}\right)^n f_n(r)\quad n=1, 2, 3, \cdots, \tag{4}$$

the virial coefficients are found to be expressed in terms of $f(r)$ as:

$$\nu_1=1$$
$$\nu_2=b$$
$$\nu_i=bf_{i-2}(1)\quad i=3, 4, 5, \cdots. \tag{5}$$

The function $f(r)$ is determined with the aid of the superposition approximation as follows. Born and Green express N simultaneous integro-differential equations, each relating one distribution function to the one of next higher order. In particular,

$$0=kTn_2^1(r)+n_2\phi^1(r)$$
$$+\int_0^{\infty}\int_0^{\pi}\int_0^{2\pi}n_3(r_{13}, r_{12}, R)\phi^1(r_{13})d\phi\cos\theta\sin\theta d\theta r_{13}^2dr_{13}, \tag{6}$$

where $R^2=r_{13}^2+r_{12}^2-2r_{12}r_{13}\cos\theta$, and θ is the angle between r_{12} and r_{13}.

A method capable of yielding solutions of these equations has not yet been found, but Eq. (6) reduces to a single nonlinear

integro-differential equation for $n_2(r)$ when the approximation of superposition is made. The superposition approximation is written by Born and Green in terms of the distribution functions as:

$$n_3=\frac{n_2(r_{13})n_2(r_{12})n_2(R)}{n_1^3}.$$

Substituting this approximate form for n_3 into Eq. (4) and expressing the "n" functions in terms of the "f" functions, we obtain after two integrations:

$$\frac{d}{dr}\{\ln[1+f(r)]\}=\frac{2\pi N}{V}[1+f(1)]\int_0^\pi [1+f(R_1)]\times\exp\left[\frac{-\phi(R_1)}{kT}\right]\cos\theta\sin\theta d\theta, \quad (7)$$

where R_1 is the value of R for r_{13}=unity. Utilizing Eq. (4), and equating coefficients of corresponding powers of the density, we obtained from (7) the equations:

$$\frac{df_1(r)}{dr}=2\pi\int_0^\pi \exp\left[\frac{-\phi(R_1)}{kT}\right]\sin\theta\cos\theta d\theta, \quad (7a)$$

$$\frac{df_2(r)}{dr}=2\pi\int_0^\pi [f_1(R_1)+f_1(1)+f_1(r)]\times\exp\left[\frac{-\phi(R_1)}{kT}\right]\sin\theta\cos\theta d\theta. \quad (7b)$$

Using the boundary conditions $f(r)\to 0$ as $r\to\infty$, the following values for the virial coefficients are obtained:

third virial coefficient$=(5/8)b^2$,
fourth virial coefficient$=0.2252b^3$.

The (exact) values are $(5/8)b^2$ and $0.2869b^3$, respectively.

A low value of the fourth virial coefficient is to be expected by the physical interpretation of superposition. Evaluation of higher virial coefficients can be carried out by this method, but the calculation is lengthy.

It is of some interest to note that if terms of order $f^2(r)$ are neglected—to obtain an equation linear in $f(r)$—(approximations equivalent to this have been made by Green[4] and Rodriguez[5])—the third and fourth virial coefficients are found to be $(5/8)b^2$ and $0.0299b^3$, respectively. It appears that linearization approximations are likely to yield unreliable equations of state even for gases.

[1] J. G. Kirkwood, J. Chem. Phys. **3**, 300 (1935).
[2] See Happel, Ann. Physik **21**, 342 (1906); or R. Fowler and E. Guggenheim, *Statistical Thermodynamics* (Cambridge University Press), p. 289.
[3] M. Born and H. S. Green, Proc. Roy. Soc. (London) **A188**, 10 (1946).
[4] See, for example, H. S. Green, Proc. Roy. Soc. (London) **A189**, 103 (1947).
[5] A. E. Rodriguez, Proc. Roy. Soc. (London) **A196**, 73 (1949).

The Hydrogen Sulfide Band at 1180 cm^{-1}*

HARRY C. ALLEN, JR. AND PAUL C. CROSS
Department of Chemistry and Chemical Engineering, University of Washington, Seattle, Washington
October 27, 1950

ONE of the principal factors retarding the completion of a satisfactory interpretation of the hydrogen sulfide vibrational band system has been the lack of a determination, from a rotational analysis, of the band center and the band type ("A" or "B") of the bending fundamental.

A consideration of the differences[1] (101)−(100)=1164 cm^{-1} and (111)−(110)=1144 cm^{-1} leads to the conclusion that the center of the $(n_\sigma n_\pi n_\delta)=(001)$ band must be in the region of 1180 cm^{-1}, fully 100 cm^{-1} lower than the generally accepted value.[2] Further confirmation of this deduction comes from the low temperature spectrum of the solid,[3] in which this band is found at 1170 cm^{-1}. In ice, because of the strong hydrogen bonding, the analogous band is found about 60 cm^{-1} higher than in water vapor.[4] The magnitude and direction of the solid-vapor shift in H_2S cannot be determined *a priori*, but it may safely be estimated to be small.

Mecke[5] quoted this band center at 1180 cm^{-1}. This is in agreement with the early work of Mischke[6] which shows absorption extending nearly to 1000 cm^{-1}, about 150 cm^{-1} lower than does any recent work. His data exhibit well-defined P and R branches with a definite gap at the center indicating a B-type band. There has been some objection to his work since his sample was contaminated with H_2O and CO_2. Neither of these compounds absorb strongly between 1000 cm^{-1} and 1340 cm^{-1}; hence his data in this region should be quite reliable.

According to this evidence for the location of the band center, the existing data of sufficient resolution to allow a rotational analysis[7–10] represents, in each instance, only the high frequency half of the band. It has been analyzed as such by the method successfully applied in the analysis of the 6290 cm^{-1} band.[11] An excellent fit of the observed absorption between 1180 cm^{-1} and 1280 cm^{-1} is obtained with the following parameters:

$$A^*=10.71\text{ cm}^{-1}\quad B^*=9.18\text{ cm}^{-1}\quad C^*=4.67\text{ cm}^{-1}$$
$$\nu_0=1183\text{ cm}^{-1}.$$

From 1280 cm^{-1} to 1370 cm^{-1} most of the principal features of the absorption are accounted for, except that the calculated intensities appear to be too low. The measurements of the different investigators are in agreement on the peak positions in this region, but the relative peak intensities show considerable variation. This suggests that the different samples may have contained varying amounts of some contaminant. Absorption by water vapor also becomes a factor at frequencies higher than 1340 cm^{-1}.

A check on the excited state moments of inertia is furnished by the value of $\Delta=I_C-I_A-I_B$, which is 0.333 10^{-40} g cm^2, in agreement with that predicted theoretically from the zero frequencies.

Several minor factors are believed to account for the relatively high intensity of absorption in the R-branch region as compared to the P-branch region. First, the main wings of R transitions between low τ-levels are converging as J increases, and hence the lines are more closely spaced over a given slit-width of the spectrum to produce a greater effective background than in the P branch. Second, the values of A^* and B^*, being larger than in the ground state, cause a shift of high τ-transitions of both the R and Q branches toward higher frequencies of the R region. This accounts for some of the strong absorption very far out in the R branch, for example, at 1290 cm^{-1} and 1340 cm^{-1} where several transitions nearly coincide. Third, the frequency dependence of the intensity increases by about 20 percent from the middle of the P-branch region to the middle of the R-branch region. Fourth, the population factor in the intensity equation yields somewhat stronger transitions for $\Delta J=+1$ than for $\Delta J=-1$.

* The work herein reported was supported in part by the ONR under Contract N8onr 52010.
[1] Allen, Cross, and King, J. Chem. Phys. **18**, 1412 (1950).
[2] G. Herzberg, *Infrared and Raman Spectra of Polyatomic Molecules* (D. Van Nostrand Company, Inc., New York, 1945), p. 283.
[3] D. F. Hornig (private communication).
[4] Cross, Burnham, and Leighton, J. Am. Chem. Soc. **59**, 1134 (1937).
[5] R. Mecke, Z. physik. Chem. **B16**, 431 (1932).
[6] W. Mischke, Z. Physik **67**, 106 (1931).
[7] A. H. Rollefson, Phys. Rev. **34**, 604 (1929).
[8] A. D. Sprague and H. H. Nielsen, J. Chem. Phys. **5**, 85 (1937).
[9] R. H. Noble, thesis (Ohio State University, 1946).
[10] E. A. Wilson, thesis, (Brown University, 1947).
[11] Allen, Cross, and Wilson, J. Chem. Phys. **18**, 691 (1950).

The Central Force Model for Additive Molecular Properties

H. J. BERNSTEIN
Division of Chemistry, National Research Council, Ottawa, Canada
October 23, 1950

THE simple additivity scheme[1] has been particularly useful for estimating heats of atomization but has recognized shortcomings. This simple additivity scheme corresponds to a valence

force model for the molecule and as such gives a good approximation to the additive molecular property. Recently this model has been extended[2] to include all the interactions between bonds, and satisfying relations for heats of atomization of the acyclic paraffins were obtained. All contributions arising from interactions between bonds separated by the same number of bonds were considered the same in this work,[2] so fine details such as rotational isomerism were neglected. Further, several empirical quadratic terms were introduced to obtain a better fit with the data. The additive properties of these paraffins have been considered also in terms of the number of C atoms which are 3 bonds apart and the sum of all the CC distances in the molecule.[3] The agreement between observed and calculated properties obtained by this more empirical method is quite good. Both of the methods mentioned above are approximations of considerable accuracy.

It is more significant perhaps from a physical point of view and certainly more rigorous quantitatively to consider the interactions between all nuclei, corresponding to a central force field. It is the purpose of this note to give some of the results obtained for the substituted methanes $CA_{4-n}B_n$ with the central force model in which all internuclear interactions are considered.

Let p_{CA}, p_{CB}, p_{AA}, p_{BB}, and p_{AB} associated with the internuclear distances CA, CB, AA, BB, and AB, respectively, be considered strictly additive. The physical property P_n for the nth substituted methane is readily seen to be

$$P_n=(4-n)p_{CA}+np_{CB}+\frac{(4-n)(3-n)}{2}p_{AA}+\frac{n(n-1)}{2}p_{BB}+n(4-n)p_{AB}, \quad (1)$$

where $n=0$, 1, 2, 3, and 4. The five equations represented by (1) are not independent and are related in the following ways:

$$2P_1-(P_0+P_2)=2P_2-(P_1+P_3)=2P_3-(P_2+P_4)=-p_{AA}-p_{BB}+2p_{AB}=\Delta(\text{say}). \quad (2)$$

Thus if values of a physical property for any 3 of the molecules are known, those of all 5 can be calculated. This may be compared with the simple additivity scheme where only p_{CA} and p_{CB} are used to describe the physical property and where from any 2 values of the physical property the others can be evaluated.

Equation (1) may be rewritten in the form

$$P_n=P_0+n/4(P_4-P_0+8\Delta)(-n^2\cdot\Delta/2), \quad (3)$$

where Δ has been defined in (2). This indicates that the additive physical property is a parabolic function of the number of substituents instead of the linear function usually obtained in practice. It is apparent from Eq. (3) that a necessary and sufficient condition that a linear relation be obtained is that

$$\Delta=-p_{AA}-p_{BB}+2p_{AB}=0. \quad (4)$$

Indeed, if Eq. (4) is true, the relation based on the simple additivity scheme is obtained.

Tests for strict additivity and/or calculations of physical properties may be made for P=density, molecular volume, refractive index, molecular refraction, boiling point, heat of atomization (Q), and heat of formation (ΔH_f).

If the contributions to the physical properties of radicals also be assumed strictly additive, then bond dissociation energies may also be calculated. Thus if D_n is the bond dissociation energy of the CA bond in $CA_{4-n}B_n$ and equal to $Q_{CA_{4-n}B_n}-Q_{CA_{3-n}B_n}-Q_A$ then

$$2D_1-(D_0+D_2)=2D_2-(D_1+D_3). \quad (5)$$

Also, if d_n is the bond dissociation energy of CB in $CA_{4-n}B_n$, then

$$2d_2-(d_2+d_4)=2d_2-(d_1+d_3). \quad (6)$$

Relations between the physical properties of the substituted ethylenes, ethanes, and benzenes have also been calculated on the basis of this model. These calculations and those for the substituted cyclohexanes and the acyclic hydrocarbons where internuclear interactions were neglected when the atoms were considered far enough apart will be given in forthcoming publications.

The foregoing treatment is based on the assumption of strict additivity. If this assumption is not made and only the second-order interactions between nonbonded atoms are considered strictly additive, and if a bond energy/bond distance relation exists, it is possible to obtain relations between the bond distances in homologous series and heats of formation and/or atomization of the corresponding molecules. Bond distances among the substituted methanes, ethanes, ethylenes, benzenes, and cyclohexanes and also the acyclic hydrocarbons have been related to the corresponding thermochemical properties of these molecules.

[1] See L. Pauling, *Nature of the Chemical Bond* (Cornell University Press, Ithaca, 1942), p. 47 *et seq.*
[2] J. R. Platt, J. Chem. Phys. **15**, 419 (1947).
[3] H. Weiner, J. Chem. Phys. **15**, 766 (1947); J. Am. Chem. Soc. **69**, 17, 2636 (1947).

The Determination of Normal Coordinates*

BRYCE L. CRAWFORD, JR. AND WILLIAM H. FLETCHER
University of Minnesota, Minneapolis, Minnesota
November 6, 1950

THE actual determination of normal coordinates is at best a laborious process if one is dealing with symmetry species containing more than three or four frequencies. The following method reduces this process to one of simple matrix multiplication and is easily applicable to any size symmetry block.

We begin with the usual relation between the symmetry coordinates, S, and the normal coordinates, Q; in customary matrix-vector notation,

$$S=LQ,$$

and the expressions for the kinetic and potential energy are

$$2T=\dot{S}'G^{-1}\dot{S},$$
$$2V=S'FS,$$

where the prime indicates the transpose of a matrix, and the F and G matrices are those introduced by Wilson.[1] From these the following expression is easily obtained,

$$GFL_r=\lambda_r L_r,$$

where L_r is the rth column of L and λ_r is the frequency parameter for the rth normal vibration.

If λ_r is the largest root of GF, its value can be found by an iterative process[2] which yields at the same time a column matrix $\bar{L}_r$, which is related to L_r by a trivial constant. In general, λ_r will be known already, but the iteration must be carried out in order to find $\bar{L}_r$.

In order to find the next largest root and its corresponding modal column $\bar{L}_r$, it is necessary to reduce GF by the method described in the preceding reference. This requires the rth *row* of $\bar{L}^{-1}$, which is easily found from the relation,

$$(L_r)'F=\lambda_r(L^{-1})^r.$$

The superscript r indicates a row instead of a column. Since constants are unimportant here, we may get the desired row $(\bar{L}^{-1})^r$ by multiplying $(\bar{L}_r)'$ into F. After annihilating the rth column of GF, the null column is retained in order to determine all of the elements of the next modal column of L. The process of iteration and reduction is continued until all of the modal columns have been found.

The modal columns found in this way are put together in the proper order to form a matrix $\bar{L}=LD$, where D is a diagonal matrix of trivial constants. D is easily found from the relation

$$\bar{L}'F\bar{L}=DL'FLD=D\Delta D\sim D_r^2\lambda_r\delta_{rs}.$$

After L has been found, a convenient check is provided by

$$LL'=G.$$

The matrix relating the Q's to the Cartesian coordinates is desired, so we need the usual relations[1] involving valence-bond coordinates R,

$$R=Bx \quad \text{and} \quad S=UR,$$

where U is an orthogonal transformation. We find,†

$$x=(B^{-1}U'L)Q.$$

B^{-1} can be found most easily from the kinetic energy expression,

$$2T=\dot{S}'G^{-1}\dot{S}=\dot{S}'U(B^{-1})'MB^{-1}U'\dot{S},$$

in which M is the diagonal matrix of atomic masses. From this we find

$$(B^{-1})'=U'G^{-1}UBM^{-1}; \quad B^{-1}=M^{-1}B'U'G^{-1}U;$$

and finally

$$(B^{-1}U'L)=M^{-1}B'U'G^{-1}L.$$

All the matrices on the right are known except G^{-1} which can easily be found from the rows of L^{-1}, determined in the iteration process:

$$(L^{-1})'L^{-1}=G^{-1}.$$

If one is interested in the normal coordinates belonging to a single symmetry species, it is only necessary to use the appropriate rows of U, B, and M^{-1}, for the others do not contribute to the final result.

* This study is part of a research program which receives support from the ONR through contract N5ori-147, T.O.2.

[1] E. B. Wilson, Jr., J. Chem. Phys. **7**, 1047 (1939); **9**, 76 (1941). Our notation follows Wilson's reasonably closely, but not exactly.

[2] Frazer, Duncan, and Collar, *Elementary Matrices* (The Macmillan Company, New York, 1947), pp. 142–145.

† Strictly speaking B must be a square matrix in order to have an inverse, and therefore should contain the translations and rotations. However, in the method used to compute B^{-1}, these rows of B can be ignored since they affect only the corresponding columns of $B^{-1}U'L$ and we are not interested in them.